Option Pricing and Market Risk Management in the Presence of Jump Risk

Dissertation submitted to the
Faculty of Business, Economics and Informatics
of the University of Zurich

to obtain the degree of
Doktor der Wirtschaftswissenschaften, Dr. oec.
(corresponds to Doctor of Philosophy, PhD)

presented by

Nikola Vasiljević

from Serbia

approved in July 2016 at the request of

Prof. Dr. Markus Leippold

Prof. Dr. Marc Chesney

Prof. Dr. Erich Walter Farkas

Prof. Dr. Loriano Mancini

The Faculty of Business, Economics and Informatics of the University of Zurich hereby authorizes the printing of this dissertation, without indicating an opinion on the views expressed in the work.

Zurich, 20.07.2016

The Chairman of the Doctoral Board: Prof. Dr. Steven Ongena.

Acknowledgements

"We are all standing on the shoulders of our parents."

— *Espen Gaarder Haug*

I dedicate this thesis to my beloved family.

First and foremost, I want to express my deepest gratitude to Prof. Dr. Markus Leippold, my Ph.D. thesis supervisor, for his constant support and patience, enthusiastic encouragement, and excellent guidance. I am very grateful for being given the chance to be part of the wonderful world of science under his supervision. Further, I have had a privilege to teach the Financial Engineering lecture and to supervise numerous bachelor and master theses during my Ph.D. studies. Indeed, I have immensely benefited from my teaching experience, which complemented my research activities over the past 4 years.

Second, I would like to thank Prof. Dr. Marc Chesney from the University of Zurich for giving me the opportunity to work with him on a very interesting topic. I have truly enjoyed our collaboration, and I am thankful for his insightful suggestions and comments, as well as for his kindness and support. Moreover, our discussions about finance, economics and their impact on our society were truly invaluable for me. I would like to point out that my research interest in American options and Lévy processes was kindled by his remarkable lectures in Mathematical Finance during the first year of my Ph.D. studies at the University of Zurich.

I am very grateful to Prof. Dr. Loriano Mancini from Swiss Finance Institute (SFI) and EPFL for generously accepting to be on my Ph.D. thesis committee. I would also like to sincerely thank to Prof. Dr. Walter Farkas from the University of Zurich for his persistent support and encouragement during my doctoral studies, and for being part of my thesis committee.

I am deeply indebted also to Prof. Dr. Michel Habib from the University of Zurich for his teaching and financial support in the first year of the second phase of my Ph.D. studies. I am truly thankful for his kindness and helpfulness. Moreover, I benefited intellectually from our discussions, and impressive breadth of his knowledge inspired me to study various topics in economics, sociology, and politics in my spare time, which are well beyond the boundaries of my research field and specialization. Additionally, I would like to thank Prof. Dr. Marc Paolella and Prof. Dr. Per Östberg from the University of Zurich for their firm support and many useful advises regarding my Ph.D. studies and academic research in general.

Special thanks to Prof. Dr. Jérôme Detemple from Boston University for his detailed and insightful comments, critique and advices regarding my research papers. During my Ph.D. studies I have also received valuable comments and benefited from discussions with Prof. Dr. Carol Alexander, Prof. Dr.

Stefano Battiston, Prof. Dr. Peter Christoffersen, Prof. Dr. Jakša Cvitanić, Prof. Dr. Mia Hubert, Prof. Dr. Antonio Mele, Prof. Dr. Alain Monfort, Prof. Dr. João Pedro Vidal Nunes, Prof. Dr. Jean-Charles Rochet, Prof. Dr. Peter Rousseeuw, Prof. Dr. George Skiadopoulos, Prof. Dr. Branko Urošević, Prof. Dr. Alexander Wagner, and PD Dr. Alexandre Ziegler.

Furthermore, I would like to express my profound gratitude to Dr. Michael Markovich, who supervised my part-time work in the Quantitative Analysis team at Credit Suisse for more than two years, and from whom I have learnt much about econometrics and practical applications of the financial theory. I am sincerely thankful for his excellent guidance and leadership, ceaseless support and understanding, and great collaboration. Additionally, I would like to thank my team colleague Rasmus Rousing for his valuable comments about my academic research, as well as for his constant support and readiness to help.

Next, I would like to thank all the faculty members and Ph.D. students at the Department of Banking and Finance at the University of Zurich for their valuable feedback and for providing such an inspiring research environment throughout my entire Ph.D. program. Therefore, I would like to express my special thanks to my dear colleagues and friends: Chris Bardgett, Nilüfer Caliskan, Pascal Caversaccio, Sabine Elmiger, Felix Fattinger, Fulvia Fringuellotti, Nicoletta Gabrielli, Marco Gambacciani, Elise Gourier, Ethem Ibrahim Güney, Manish Gupta, Regina Hammerschmid, Robert Huitema, Meriton Ibraimi, Manuel Kannenberg, Victoria Keller, Felix Matthys, Elisabeth Megally, Kevin Meyer, Florian Müller-Reiter, Cosimo Munari, Magnus Nyboe, Caroline Oehri, Diego Ostinelli, Anca Pana, Ivan Petzev, Pawel Polak, Tatjana-Xenia Puhan, Thomas Richter, Jakub Rojček, Cornelia Rösler, Kim Schartz, Anastasiia Sokko, Felix Stang, Jacob Strömberg, Lujing Su, Adriano Tosi, Bruno Troja, Hanlin Yang, and Ally Quan Zhang. I should not forget my fellow SFI Ph.D. students from Léman and Lugano centers: Thomas Geelen, Nataliya Gerasimova, Piotr Orlowski, Paola Pederzoli, András Sali, Jovan Stojković and Davide Tedeschini, whom I met at various SFI events, workshops and Ph.D. courses. I am grateful to all of them for their comments and suggestions regarding my research projects, for inspiring scientific discussions, as well as for their friendship. Finally, I would also like to thank Eckart Jäger, Mira Jovanović, Michelle Rüegg, and Franziska Spycher for their indispensable help with administrative and organizational matters.

Special thanks to all the students who wrote their semester projects, bachelor and masters theses under my supervision, and/or who attended my lectures and exercise sessions. Indeed they helped me discover how much I enjoy teaching. Moreover, their keen interest in financial engineering and many challenging questions and insightful comments they have eagerly shared with me were truly inspirational and helpful.

Last but not least, I wish to express my eternal gratitude to my family for their selfless support, love and encouragement. I am deeply grateful to my wife Ivana for her boundless love and understanding, for her precious support in my professional endeavors, and for putting up with me and my attachment to work. I am forever indebted to my family for being such an incredible support and utmost inspiration for me in good and bad times alike.

Zurich, July 2016 Nikola Vasiljević

Contents

List of Figures

List of Tables

Part I

Introduction

Chapter 1

Introduction and Summary of Research Results

This dissertation is entitled "Option pricing and market risk management in the presence of jump risk", and it considers the valuation of American-style options, and an application of option pricing techniques and option data in market risk management. In addition to options, the common denominator of the three papers comprising this dissertation are jump processes. The main goal of this chapter is to briefly motivate the research questions studied in this dissertation, and to provide a summary of the main theoretical and empirical findings for each of the papers.

First, sudden and adverse market moves during the the recent financial and economic turmoil and the Global financial crisis of 2007–08 have reiterated the importance of jump risk for modelling of asset returns. Indeed, in times of increased uncertainty, mathematical models of financial markets have to account for possibility of large and swift changes in asset prices. Lévy models represent particularly interesting and attractive framework because they can capture asset price dynamics that include jumps. This dissertation focuses on a flexible and analytically tractable class of Lévy processes, i.e., the hyper-exponential models and their generalizations.

Second, American-style options are among the most traded derivative financial instruments, and their pricing and hedging is of great practical importance. However, even for standard (vanilla) American option contracts in the Black-Scholes setting, a closed-form solution to the pricing problem has not been found yet (after almost 50 years of active research in this field). From mathematical point of view, an American option price is a function of an unknown early exercise boundary, and the solution to the pricing problem requires joint computation of the option price and the early exercise boundary. Although the vast literature on American-style derivatives offers a rich spectrum of numerical pricing techniques to deal with this problem, effectiveness and insightfulness of a given approach depend on

modelling assumptions and intended application. One of the main contributions of this dissertation is that it provides a fast and accurate pricing engine for American-style options in a flexible jump-diffusion setting based on the Laplace transform methods. Moreover, the proposed theoretical framework allows us to study the contribution and the impact of jumps and diffusion to the American early exercise premium. Finally, the theoretical results on option pricing derived in this dissertation are further applied in market risk management applications. The individual contribution of each papers in this dissertation can be summarized as follows.

Chapter 2 represents my first paper (joint work with Prof. Dr. Markus Leippold), which is entitled "Pricing and disentanglement of American puts in the hyper-exponential jump-diffusion model". Using a maturity randomization approach—which can be interpreted as a Laplace-Carson transform of the option price function with respect to the time to maturity—we transform the partial integro-differential equation (PIDE) describing an American put price dynamics in a hyper-exponential jump-diffusion model into an ordinary integro-differential equation (OIDE) which can be solved analytically. After applying a Laplace inversion algorithm we obtain the final result, which represents a tight lower bound for the American option price. In the second step, we analytically disentangle the contributions of jump and diffusion components to the American early exercise premium. To the best of our knowledge, this is the first paper to provide theoretical results for the jump-diffusion disentanglement for American options. To understand better the implications of our results, we conduct an empirical study using American options on S&P 100 index from 2007 until 2013. Our findings indicate that jump risk is the main driver of the early exercise premium, especially in the post-crisis period.

The second paper (joint work with Prof. Dr. Marc Chesney), entitled "Québécoisation method for the pricing of Parisian options with jump risk", is presented in Chapter 3. We study the pricing of European and American Parisian options in hyper-exponential jump-diffusion model. To this end, we introduce a new pricing technique called québécoisation method. Our approach is based on the double Laplace-Carson transform with respect to the time to maturity and the time to expiration of the Parisian window. Québécoised option prices, deltas and gammas are computed in a closed form by solving a system of OIDEs, and the final results are obtained via a two-dimensional Laplace inversion algorithm. Additionally, we provide numerical examples for the pricing of Parisian options with the québécoisation method, as well as for the effects of jumps on the option prices. This paper is the first study that considers the pricing of American Parisian options with jump risk.

My single-authored paper "Option-implied intra-horizon risk and first-passage disentanglement" studies the intra-horizon value at risk (iVaR). This paper is presented in Chapter 4. First, a new model of asset returns called displaced mixed-exponential model (D-MEM) is introduced. The D-MEM class of models is particularly interesting because it can arbitrarily closely approximate both finite-activity jump-diffusions and completely monotone Lévy processes of infinite-activity. By adopting the D-MEM framework, and using the relationship between the iVaR and one-touch digital options, we obtain analytical results for the Laplace-Carson transform of the iVaR with respect to the monitoring period. Similarly to the first paper presented in this dissertation, we analytically disentangle the contributions of jumps and diffusion to the iVaR. In the next step, using two different S&P 100 index data sets, i.e., the historical returns and the American options spanning the period 2001–2014, we estimate the iVaR for several popular jump models. We find that, on average, jumps account for about 90 percent of the intra-horizon risk. The backtesting results strongly indicate the option-implied estimates are more responsive to market moves in comparison to their historical counterparts. Therefore, we conclude that the option-based estimation approach represents an important source of information due to its forward-looking nature.

Finally, the proofs and the supplementary theoretical results and figures are given in the appendix. The last chapter of the dissertation represents the cumulative bibliography of all three research papers.

Part II

Research Papers

Chapter 2

Pricing and Disentanglement of American Puts in the Hyper-Exponential Jump-Diffusion Model

Markus Leippold and Nikola Vasiljević[1]

This paper is published in *Journal of Banking & Finance*, 2017, Volume 77, pp. 78–94. Copyright by Elsevier B.V. DOI: https://doi.org/10.1016/j.jbankfin.2017.01.014

Abstract

We analyze American put options in a hyper-exponential jump-diffusion model. Our contribution is threefold. Firstly, by following a maturity randomization approach, we solve the partial integro-differential equation and obtain a tight lower bound for the American option price. Secondly, our method allows to disentangle the contributions of jumps and diffusion for the early exercise premium. Finally, using American-style options on the S&P 100 index from January 2007 until December 2012, we estimate various hyper-exponential specifications and investigate the implications for option pricing and jump-diffusion disentanglement. We find that jump risk accounts for a large part of the early exercise premium.

Keywords: American options, early exercise premium, hyper-exponential jump-diffusion model, maturity randomization, jump-diffusion disentanglement.

JEL classification: G01 · G12 · G13 · C51 · C52 · C61.

[1]We thank Carol Alexander (the editor) and two anonymous reviewers for their constructive comments. We also thank Chris Bardgett, Marc Chesney, Peter Christoffersen, Jakša Cvitanić, Jérôme Detemple, Antonio Mele, András Sali, George Skiadopoulos, and the seminar participants of the Brown Bag Lunch Seminar at the Department of Banking and Finance Institute at the University of Zürich, the Gerzensee Swiss Finance Institute PhD workshop, the Bachelier 2012 Finance Conference, and the University of Zürich and ETH Zürich joint Fin & Math Doc seminar. We gratefully acknowledge financial support from the Swiss Finance Institute (SFI) and Bank Vontobel.

2.1 Introduction

The valuation of American options has been one of the most important topics in mathematical finance for almost five decades. A fully analytic solution to the problem, even in the simplest setting, has not yet been obtained whatsoever. The main difficulty stems from the fact that American options allow for an early exercise feature, which requires solving for the option price as a function of a free boundary that is not known a priori. A common approach is to use numerical procedures.[2] However, numerical methods are generally devoid of financial intuition and meaningful interpretations. Moreover, their implementation is often computationally expensive, even more so when we leave the classical Black and Scholes (1973) setting.

A huge part of the literature on analytic pricing of American options in non-Gaussian settings deals with perpetual American options, which can be solved in closed-form under certain assumptions regarding the jumps of the underlying process, and because the early exercise boundary is flat.[3] Moreover, they very often exclude the possibility of overshooting a predefined constant barrier by confining jumps to be always in the opposite direction from the barrier. Hence, many models are based on spectrally one-sided Lévy processes in order to utilize renewal-type integral equations or fluctuation identities. The possibility of an overshoot of the exercise boundary poses several mathematical problems. We need not only an exact distribution of the overshoot, but also the dependency structure between the overshoot and the first passage time. Moreover, for finite-maturity American options, the optimal stopping time is actually a first passage time of an unknown non-uniform space-time boundary.

Our first goal in this paper is the valuation of finite-maturity American put options in the hyper-exponential jump-diffusion model (HEJD) introduced by Lipton (2002). The logarithm of the asset price is assumed to follow a process, which is a mixture of a drifted Brownian motion and a compound Poisson process with an arbitrary number of positive and negative types of exponentially distributed jumps of finite activity.[4] We choose to work in this particular framework, because it is flexible enough

[2] Broadie and Detemple (2004) and Detemple (2005) provide a comprehensive overview of different pricing methods for American-style options.

[3] See, e.g., Boyarchenko and Levendorskiĭ (2002), Mordecki (2002), Chesney and Jeanblanc (2004), Alili and Kyprianou (2005) and references therein.

[4] General properties of the HEJD model are thoroughly analyzed and discussed in Cai (2009).

to capture the main empirical features of asset returns and option prices.[5] Furthermore, due to the memorylessness of the exponential distribution, analytic pricing and hedging of vanilla and certain exotic options in a HEJD framework is feasible, hence making this model a plausible candidate for our purpose.

To derive the price of an American put, we adopt a maturity randomization approach. We study the Laplace-Carson transform with respect to the time to maturity of the partial integro-differential equation (PIDE) and the corresponding initial and boundary conditions describing the dynamics of the American option price. Instead of using a sequence of Erlangian random variables suggested in Carr (1998), we rely on a different sequence of random variables following a distribution suggested in queueing theory literature by Gaver (1966). Both approaches converge pointwise to Dirac's delta function centered at the residual maturity. However, while Carr's maturity randomization requires to solve recursively a set of differential equations, the alternative randomization approach relies on the computation of the Gaver's functionals, resulting in a much simpler and faster computational procedure. For option pricing applications, the alternative randomization approach was studied in, e.g., Kou and Wang (2003), Sepp (2004), Kimura (2010), and Hofer and Mayer (2013). However, American options have not yet been priced using this method. Hence, our results represent a genuine contribution to the existing literature on maturity randomization.[6] We support our theoretical results with numerical examples and demonstrate that our approach represents a fast and accurate pricing engine.

Our second contribution is concerned with analyzing the importance of jump risk for American options. Although we borrow the syntax "disentanglement of diffusion from jumps" from Aït-Sahalia (2004), the semantics is quite different in our study. While Aït-Sahalia (2004) takes an econometric perspective and studies the effect of jumps on the estimation of the diffusion component in asset returns using high-frequency data, we study the implications of a possible overshoot for the early exercise premium. By combining the martingale approach and the PIDE method in the Laplace transform

[5] Jeannin and Pistorius (2010) and Crosby, Le Saux and Mijatović (2010) show that any Lévy process with completely monotone Lévy density can be approximated by a HEJD process. Such Lévy models include, e.g., the Variance-Gamma, the Normal-Inverse-Gaussian, the Carr-Geman-Madan-Yor model.

[6] American option pricing in double-exponential and hyper-exponential jump-diffusion setting has been studied Kou and Wang (2004) and Cai and Sun (2014). These papers are based on the quadratic approximation of Barone-Adesi and Whaley (1987). Avram, Chan and Usabel (2002) consider fluctuation theory approach in a spectrally one-sided (positive or negative) Lévy model. Levendorskiĭ (2004a,b) analyze regular Lévy processes of exponential type using the Wiener-Hopf factorization formula embedded in the dynamic programming approach.

framework, we can disentangle the contribution of jumps and diffusion for the American early exercise premium. Our disentanglement result pertains to the risk-neutral world and is model-dependent in the sense that it relies on the assumption that the underlying process has both diffusion and finite activity jump components. However, unlike econometric approaches, it holds irrespectively of the data frequency.

The impact of jumps on American option prices has been recently considered in Chiarella and Ziogas (2009). They examine jump effects by comparing the shape of the early exercise boundary with and without jumps, keeping the overall volatility constant. In contrast, we consider the disentanglement of jumps and diffusion directly by analytically decomposing the early exercise premium into the respective contributions. Hence, we do not need to rely on a moment-based condition. More importantly, our approach does not require the use of different models, which may distort the inference due to model misspecification. In our setting, we can disentangle jumps from the diffusion component within the same model. Therefore, to the best of our knowledge, our disentanglement idea for American options has not been previously studied in the literature.

Finally, as our third contribution, we estimate a range of HEJD models using American options on the S&P 100 index to provide more intuition and to demonstrate the disentanglement of jumps from diffusion on real data. We focus on short-term options with time to maturity of up to two months and perform sequential (weekly) calibration via penalized weighted nonlinear least squares. The chosen data set and the sequential calibration allow us to study the time variation in the model parameters. Since our sample includes the recent financial crisis, we can study the importance of diffusion and jumps during calm and turbulent periods.

The reminder of the paper is organized as follows. Section 2.2 introduces the hyper-exponential jump-diffusion model and presents our theoretical contributions regarding the pricing of European and American put options, and the early exercise jump-diffusion disentanglement. In Section 2.3, we present and discuss our calibration results as well as the implications for the disentanglement. Section 2.4 concludes the paper. All proofs, tables, and graphs can be found in the appendix.

2.2 Option pricing and disentanglement in the HEJD model

2.2.1 Model formulation

We consider a filtered probability space $(\Omega, \mathcal{F}, \mathbb{F} = \{\mathcal{F}_t, t \geq 0\}, \mathbb{Q})$ satisfying the usual assumptions. The asset price dynamics under the fixed risk-neutral probability measure $\mathbb{Q}$ follows a hyper-exponential jump-diffusion process

$$\frac{dS_t}{S_{t^-}} = (r - \delta - \lambda\zeta)dt + \sigma dW_t + d\left(\sum_{i=1}^{N_t}(V_i - 1)\right), \tag{2.1}$$

where $\{W_t, t \geq 0\}$ is a standard Brownian motion under $\mathbb{Q}$. The interest rate $r \in \mathbb{R}_+$, the dividend yield $\delta \in \mathbb{R}_+$, and the volatility $\sigma \in \mathbb{R}_+$ are constants.[7] The Poisson process $\{N_t, t \geq 0\}$ is characterized by the jump intensity parameter $\lambda \in \mathbb{R}_+$ and $\{Y_i := \log(V_i) : i = 1, 2, ...\}$ is a sequence of independent and identically distributed hyper-exponential random variables with probability density function

$$\varphi_Y(y) = \sum_{i=1}^{m} p_i \eta_i e^{-\eta_i y} \mathbb{1}_{\{y \geq 0\}} + \sum_{j=1}^{n} q_j \theta_j e^{\theta_j y} \mathbb{1}_{\{y < 0\}}, \tag{2.2}$$

where $m, n \in \mathbb{N}$. The coefficients $p_i > 0$ for all $i = 1, ..., m$ and $q_j > 0$ for all $j = 1, ..., n$ are probabilities of different kinds of positive and negative jumps, respectively, satisfying $\sum_{i=1}^{m} p_i + \sum_{j=1}^{n} q_j = 1$. Similarly, the parameters $\eta_i > 1$ for all $i = 1, ..., m$ and $\theta_j > 0$ for all $j = 1, ..., n$ are magnitude parameters of different kinds of random upward and downward jumps, respectively. Furthermore, $\mathcal{F}_t = \sigma(W_s, N_s; s \leq t, \{V_j\})$.[8] For ease of notation, we denote by HEJD(m, n) an HEJD model with m different types of positive and n different types of negative jumps. The average (percentage) jump size is given by

$$\zeta := \mathbb{E}\left[e^{Y_1} - 1\right] = \sum_{i=1}^{m} \frac{p_i \eta_i}{\eta_i - 1} + \sum_{j=1}^{n} \frac{q_j \theta_j}{\theta_j + 1} - 1. \tag{2.3}$$

For our purpose, it is convenient to introduce the log-return process

$$X_t := \log(S_t/S_0) = \mu t + \sigma W_t + \sum_{i=1}^{N_t} Y_i, \tag{2.4}$$

[7] We remark that the assumption of positive interest rates is, under reasonable parameter specifications, not restrictive for our analysis and implementation using the Gaver-Stehfest canadization method. However, for this numerical method, we require dividends to be continuous and deterministic.

[8] Given a jump type, the magnitude parameter is the inverse of the corresponding average jump size, e.g., a magnitude parameter of 50 corresponds to the average jump of 2 percent.

with risk-neutral drift $\mu = r - \delta - \lambda\zeta - \frac{\sigma^2}{2}$. The log-return process has a cumulant generating function given by

$$\Psi(u) := \frac{1}{t}\log \mathbb{E}\left[e^{uX_t}\right] = \frac{\sigma^2}{2}u^2 + \mu u + \lambda\left(\sum_{i=1}^{m}\frac{p_i\eta_i}{\eta_i - u} + \sum_{j=1}^{n}\frac{q_j\theta_j}{\theta_j + u} - 1\right), \tag{2.5}$$

for any $u \in (-\theta_1, \eta_1)$. Cai (2009) proved that the characteristic equation $\Psi(u) = \kappa$ for $\kappa \in \mathbb{R}_+$ has exactly $(n + m + 2)$ different real roots and showed that there is no analytical solution in the general case. In fact, the only candidates of analytically tractable root-finding problems within the broad class of HEJD processes are: *a)* Pure geometric Brownian motion models, i.e., HEJD(0,0), *b)* jump-diffusions with only one type of jumps, either positive or negative, i.e., HEJD(1,0) and HEJD(0,1), or *c)* double-exponential jump-diffusion models, i.e., HEJD(1,1).[9]

2.2.2 Option Pricing

Our approach is closely related to the maturity randomization method introduced in finance by Carr (1998), which has its mathematical roots in the Post-Widder inversion formula. To provide a brief sketch of the randomization method, consider an ordinary European put on the stock S with strike K and residual maturity, $\tau := T - t$. Under the measure $\mathbb{Q}$, the time-t price of the put is

$$p(S,\tau) = \mathbb{E}\left[e^{-r\tau}\left(K - S_T\right)^+ | S_t = S\right]. \tag{2.6}$$

The first step of the randomization method is the derivation of so-called "Canadized" version of European and American options, where the maturity of the contract is random. To obtain the Canadized version of (2.6), we assume the residual maturity to be exponentially distributed with mean τ, i.e., we consider the randomized residual maturity $\tilde{\tau} \sim \exp(\alpha)$, where $\alpha := \tau^{-1}$. Denoting by $p^*(S,\alpha)$ the Canadized European put value at time t with random time to maturity $\tilde{\tau}$, we have

$$\begin{aligned} p^*(S,\alpha) &= \mathbb{E}\left[e^{-r\tilde{\tau}}\left(K - S_{t+\tilde{\tau}}\right)^+ | S_t = S\right] \\ &= \mathbb{E}\left[\mathbb{E}\left[e^{-r\tau}\left(K - S_T\right)^+ | S_t = S, \tilde{\tau} = \tau\right]\right] \\ &= \mathbb{E}\left[p(S,\tilde{\tau})\right] = \int_0^\infty \alpha e^{-\alpha\tau} p(S,\tau)d\tau =: \mathcal{LC}(p(S,\tau)), \end{aligned} \tag{2.7}$$

where $\mathcal{LC}(p(S,\tau))$ is the Laplace-Carson transform of the European put price $p(S,\tau)$. Once we have calculated the Canadized version $p^*(S,\alpha)$, we can use an inversion method to determine the price of the

[9] Including additional jump types gives rise to a mathematical problem of solving quintic, sextic, or even higher order equations which are not analytically solvable, and one has to revert to numerical procedures in such cases.

ordinary European put price $p(S,\tau)$. While the assumption of an exponentially distributed maturity leads to simple approximations, they generate large numerical errors.[10] To improve the approximation, we instead assume that the time to maturity may be subdivided into N subperiods, for which Carr (1998) assumes the Erlang-N distribution. As $N \to \infty$, the Erlang distribution converges to a point mass concentrated at the mean. Hence, for large N, the value of an option with random maturity approximates the value of the option with the original maturity.

Contrary to Carr's randomization where the Erlangian assumption requires us to solve a time-consuming dynamic programming problem, we adopt an alternative randomization technique, which allows us to derive analytic expressions for option prices in the hyper-exponential jump-diffusion setting.[11] The original idea stems from queuing theory. Gaver (1966) introduced a three-parameter family of density functions (henceforth Gaver distribution) corresponding to the (k_1+1)-st smallest member of the (k_1+k_2)-sized sample $(k_1, k_2 \in \mathbb{N})$ of independent and identically distributed exponential random variables,

$$f_{k_1,k_2}(\tau;\nu) = \frac{(k_1+k_2)!}{k_1!(k_2-1)!}\left(1-e^{-\nu\tau}\right)^{k_1}\nu e^{-k_2\nu\tau}, \quad \tau \geq 0. \tag{2.8}$$

The asymptotic convergence of a Gaver distribution to a Dirac delta function means that for a continuous function $g(\cdot)$ defined on $\mathbb{R}_+$, it holds that

$$g(\tau) = \lim_{k_1,k_2\to\infty} g^*_{k_1,k_2}, \tag{2.9}$$

where

$$g^*_{k_1,k_2} := \int_0^\infty f_{k_1,k_2}(\tau;\nu)g(\tau)d\tau. \tag{2.10}$$

Moreover, the Gaver distribution has a special computational advantage over the Erlang distribution used in Carr (1998), since the sequence of approximations $(g^*_{k_1,k_2})_{k_1,k_2\geq 1}$ satisfies the recursive relationship:

$$g^*_{0,k_2}(\nu) = \int_0^\infty g(\tau)k_2\nu e^{-k_2\nu\tau}d\tau, \tag{2.11}$$

$$g^*_{k_1,k_2} = \frac{k_1+k_2}{k_1}g^*_{k_1-1,k_2} - \frac{k_2}{k_1}g^*_{k_1-1,k_2+1}. \tag{2.12}$$

This relationship substantially simplifies calculations, because we need to solve analytically only equation (2.11), i.e., we need to compute the analytic expression for the Laplace-Carson transform of the

[10] See, Carr (1998), Table 1.
[11] See, e.g., Kou and Wang (2003), Sepp (2004), Kimura (2010), and Hofer and Mayer (2013).

original function $g(\cdot)$. Therefore, if we would have analytical solutions for the Canadized options, the Gaver-Stehfest inversion algorithm in equations (2.11) and (2.12) allows for an efficient computation of the original option prices.[12] The parameter ν depends on the chosen statistic of the Gaver distribution to which the sequence of random times to maturity asymptotically converges. We decide to use the mode-matching approach, i.e., $\nu := \log(2)/\tau$. Additionally, for computational convenience we consider the case $k_1 = k_2 = k \in \mathbb{N}$. Therefore, from equations (2.7) and (2.11) we obtain the Laplace-Carson parameter α in the form $\alpha = k'\nu = k' \log(2)/\tau$, for $k' = 1, 2, ..., 2k$. For the numerical implementation we use $k = 4$, because it provides accurate and robust numerical results in the HEJD framework. We refer to Kimura (2010) for more details.

Equipped with an efficient randomization methodology, we can address the problem of deriving Canadized variants of European and American options.[13] Indeed, we get the following result for European options. All proofs are delegated to the appendix.

Theorem 2.2.1. *Under the hyper-exponential jump-diffusion model (2.1)–(2.4), the price of a Canadized European put option with strike K and time to maturity τ given the underlying spot price S_t is*

$$p^*(S_t, \alpha) = \begin{cases} \sum_{i=1}^{m+1} \underline{w}_i \left(\frac{S_t}{K}\right)^{\beta_{i,r+\alpha}} + \frac{\alpha K}{\alpha + r} - \frac{\alpha S_t}{\alpha + \delta} & \text{if } S_t < K, \\ \sum_{j=1}^{n+1} \overline{w}_j \left(\frac{S_t}{K}\right)^{\gamma_{j,r+\alpha}} & \text{if } S_t \geq K. \end{cases} \tag{2.13}$$

The coefficients $\beta_{1,r+\alpha}, ..., \beta_{m+1,r+\alpha}$ and $\gamma_{1,r+\alpha}, ..., \gamma_{n+1,r+\alpha}$ are positive and negative roots of the characteristic equation $\Psi(u) = r + \alpha$. The Lévy exponent $\Psi(\cdot)$ is defined in (2.5) and the coefficients $\underline{w}_1, ..., \underline{w}_{m+1}, \overline{w}_1, ..., \overline{w}_{n+1}$ solve the system of equations (A.17) *of Appendix A.1.*

For American options, the same procedure as for European options applies. Considering the American put

$$P(S, \tau) = \operatorname*{ess\,sup}_{\tau_{B_p} \in [0, T-t]} \mathbb{E}\left[e^{-r\tau_{B_p}} \left(K - S_{t+\tau_{B_p}}\right)^+ | S = S_t \right], \tag{2.14}$$

[12] For and overview of the Gaver-Stehfest algorithm and other Laplace inversion techiques, we refer to Valkó and Abate (2004), Abate and Whitt (2006) and Kuznetsov (2013).

[13] Note that we only give the results for put options. The corresponding values for call options follow from the symmetry relation of Schroder (1999).

where τ_{B_p} is the first hitting time of the early exercise boundary B_p of the process (2.1), we can write the Laplace-Carson transform of the American put price as

$$P^*(S,\alpha) = \mathcal{LC}(P(S,\tau)). \tag{2.15}$$

Hence, given an analytical expression for its Canadized variant which we present in the theorem below, we can use the Gaver-Stehfest inversion algorithm outlined above to efficiently calculate the prices of American put options with finite maturity.

Theorem 2.2.2. *Under the hyper-exponential jump-diffusion model (2.1)–(2.4), the price of a Canadized American put option with strike K and time to maturity τ given the underlying spot price S_t is*

$$P^*(S_t,\alpha) = \begin{cases} p^*(S_t,\alpha) + e_p^*(S_t,\alpha) & \text{if } S_t > B_p^*, \\ K - S_t & \text{if } S_t \leq B_p^*, \end{cases} \tag{2.16}$$

where B_p^* is the time-independent early exercise boundary, $p^*(\cdot)$ is the Canadized European put option price (2.13), and $e_p^*(\cdot)$ is the early exercise premium given by

$$e_p^*(S_t,\alpha) = \begin{cases} \sum_{j=1}^{n+1} v_j \left(\frac{S_t}{B_p^*}\right)^{\gamma_{j,r+\alpha}} & \text{if } S_t > B_p^*, \\ K - S_t - p^*(S_t,\alpha) & \text{if } S_t \leq B_p^*, \end{cases} \tag{2.17}$$

using the same notation as in Theorem 2.2.1. The coefficients $v_1,...,v_{n+1}$ solve the matrix equation (A.34) and the early exercise boundary B_p^* can be obtained by numerically solving the equation (A.39) of Appendix A.2.

The two theorems generalize the results of Kimura (2010), who analyzed European and American options in the Black-Scholes model. Moreover, the above result on European options generalizes Sepp (2004), who applied the same technique in the special case of a double-exponential jump-diffusion model.[14] However, we emphasize that American options have not yet been priced in a jump-diffusion setting using the Gaver-Stehfest canadization (GSC) technique outlined above.

[14] Sepp (2004) considers pricing of European-style vanilla and barrier options in a double-exponential jump-diffusion model.

2.2.3 Disentangling jumps and diffusion

Generally, an American option is exercised in a jump-diffusion model, if the stock price either exactly hits the early exercise boundary or the price jumps into the interior of the exercise region. Paths of the diffusion process are almost surely continuous, hence an early exercise at the boundary is due to the pure diffusion. However, conditional on stopping of the process, continuously distributed jumps will almost surely overshoot the critical price and trigger the early exercise inside of the stopping region.

Given this property, a natural question arises. Can we disentangle the contribution of jumps and diffusion on the early exercise premium of American options? By combining our adoption of the Gaver-Stehfest Canadization approach with the martingale method for option pricing and some recent results on the Laplace transform of the first hitting time to a lower flat boundary developed in Yin, Shen and Wen (2013), we obtain the following result on the decomposition of the early exercise premium for the Canadized American put.

Theorem 2.2.3. *In the continuation region, the early exercise premium for the Canadized American put can be orthogonally decomposed as*

$$e_p^*(S_t, \alpha) = e_{p,d}^*(S_t, \alpha) + e_{p,j}^*(S_t, \alpha), \tag{2.18}$$

where $e_{p,d}^*(S_t, \alpha)$ represents the fraction of the early exercise premium due to the diffusion of the process, and $e_{p,j}^*(S_t, \alpha)$ is the contribution of jumps to the early exercise premium. The overall contribution of jumps can be further orthogonally decomposed into components associated with each type of negative jumps, i.e.,

$$e_{p,j}^*(S_t, \alpha) = \sum_{l=1}^{n} e_{p,j,l}^*(S_t, \alpha), \tag{2.19}$$

where $e_{p,j,l}^*(S_t, \alpha)$ corresponds to the negative jump of kind $l = 1, 2, ..., n$. Analytic expressions for the diffusion and jump components are given in (A.49) and (A.51) of Appendix A.3.

Given the above result for the Canadized American options, we can invert the Laplace-Carson transform to obtain the early exercise premium disentanglement in the original space.

2.2.4 Numerical examples

To demonstrate the pricing accuracy of the GSC method in a HEJD model, we compute European and American put option prices and benchmark the results against the Fourier space time-stepping

technique (FST) of Jackson, Jaimungal and Surkov (2008).[15] In particular, European option prices are obtained using a grid of 65,536 points and American option prices are computed using the 4-step Richardson extrapolation based on (four) Bermudan option prices with 16,384 space steps each, and 256, 512, 1,024, and 2,048 time steps, respectively. Furthermore, we report numerical results for the GSC method that relies on the mode-matching approach with a 4-step recursive scheme.

We assume that the current underlying asset price is 100, the risk-free rate is 4 percent, and the dividend yield is 2 percent. Without loss of generality, we focus on the double-exponential jump-diffusion model of Kou (2002), i.e., HEJD(1,1). The volatility is set to either 15 or 30 percent, the jump intensity takes values of either 5 or 10 (jumps per annum), the conditional probability of a negative jump is fixed at 70 percent, the positive jump parameter (average positive jump size) is either 100 (1 percent) or 200 (0.5 percent), and the negative jump parameter (average negative jump size) is either 25 (4 percent) or 50 (2 percent). We compute prices of OTM and ATM European and American put options, because these are most frequently traded options in the market. The performance of the GSC method is measured by the relative pricing error with respect to the benchmark method (FST).

Table 2.1 provides results for options with 3 months to maturity. Table 2.2 summarizes the results for options with 1 year to maturity. We conclude that European options are accurately priced with the GSC method in all cases, with absolute relative error not exceeding 0.3 percent, and being less than 0.001 percent in many cases. On the other hand, American options have larger absolute relative errors, which are in the range between 0.2 and 1.4 percent. However, American options with shorter time to maturity, i.e., 3 months, are more accurately priced. This is important because jump-diffusion dynamics are generally plausible for pricing of short term options, and our example demonstrates that GSC method performs well for such options. The absolute relative error increases with moneyness and varies between 0.3 and 0.8 percent for ATM options, and between 0.2 and 0.5 percent for OTM options. These errors are lower than the typically observed bid-ask spread for ATM and OTM options. Hence, we conclude that the proposed method works well.

Next, we compute the contribution of diffusion and jump components to the early exercise premium for OTM and ATM American put options. Table 2.3 summarizes our disentanglement results for options with 3 months and 1 year maturity. Early exercise premium, expressed as a percentage of the

[15]For pricing American options in the HEJD framework our numerical tests, which we do not report here, suggest that the FST exhibits superior speed-accuracy characteristics than the convolution method of Lord et al. (2008) and the cosine method of Fang and Oosterlee (2009).

Table 2.1: **Pricing performance of the Gaver-Stehfest canadization method (GSC) for OTM and ATM put options with time to maturity $\tau = 3$ months.** European and American put option prices are computed via the GSC method for a range of double-exponential jump-diffusion models. The underlying asset price is set to $S_t = 100$, the risk-free rate is $r = 0.04$, the dividend yield is fixed at $\delta = 0.02$, and the conditional probability of a negative jump is $q = 0.7$. Variable input parameters are strike, volatility σ, jump intensity λ, positive jump parameter η, and negative jump parameter θ. We compare the results of our approach to the benchmark (Fourier space time-stepping method), and report the relative pricing errors in percentages.

	Parameters				Benchmark		GSC Method		Rel. Error (%)	
Strike	σ	λ	η	θ	European	American	European	American	European	American
100	0.15	5	100	25	3.3150	3.3642	3.3150	3.3409	-0.0006	-0.6933
100	0.15	5	100	50	2.9135	2.9559	2.9135	2.9333	-0.0004	-0.7676
100	0.15	5	200	25	3.3027	3.3523	3.3026	3.3288	-0.0006	-0.7025
100	0.15	5	200	50	2.8997	2.9426	2.8997	2.9196	-0.0005	-0.7802
100	0.15	10	100	25	3.8487	3.9041	3.8486	3.8780	-0.0017	-0.6688
100	0.15	10	100	50	3.0910	3.1350	3.0910	3.1116	-0.0004	-0.7447
100	0.15	10	200	25	3.8274	3.8836	3.8273	3.8571	-0.0017	-0.6837
100	0.15	10	200	50	3.0648	3.1097	3.0648	3.0858	-0.0004	-0.7673
100	0.30	5	100	25	6.0219	6.0650	6.0219	6.0379	0.0003	-0.4467
100	0.30	5	100	50	5.7865	5.8272	5.7865	5.8010	0.0004	-0.4497
100	0.30	5	200	25	6.0148	6.0579	6.0148	6.0308	0.0003	-0.4480
100	0.30	5	200	50	5.7792	5.8199	5.7792	5.7937	0.0004	-0.4510
100	0.30	10	100	25	6.3415	6.3871	6.3415	6.3588	0.0003	-0.4430
100	0.30	10	100	50	5.8825	5.9237	5.8826	5.8972	0.0004	-0.4471
100	0.30	10	200	25	6.3280	6.3737	6.3280	6.3453	0.0003	-0.4453
100	0.30	10	200	50	5.8681	5.9094	5.8681	5.8828	0.0004	-0.4497
95	0.15	5	100	25	1.5092	1.5284	1.5093	1.5195	0.0075	-0.5804
95	0.15	5	100	50	1.1098	1.1220	1.1099	1.1152	0.0109	-0.6108
95	0.15	5	200	25	1.5009	1.5202	1.5010	1.5113	0.0076	-0.5897
95	0.15	5	200	50	1.1004	1.1128	1.1005	1.1058	0.0113	-0.6243
95	0.15	10	100	25	1.9942	2.0196	1.9943	2.0078	0.0048	-0.5847
95	0.15	10	100	50	1.2614	1.2754	1.2615	1.2677	0.0090	-0.6036
95	0.15	10	200	25	1.9792	2.0050	1.9793	1.9930	0.0050	-0.5998
95	0.15	10	200	50	1.2432	1.2575	1.2433	1.2496	0.0094	-0.6275
95	0.30	5	100	25	3.7908	3.8142	3.7908	3.7991	0.0013	-0.3966
95	0.30	5	100	50	3.5565	3.5777	3.5566	3.5636	0.0014	-0.3945
95	0.30	5	200	25	3.7845	3.8080	3.7845	3.7928	0.0013	-0.3979
95	0.30	5	200	50	3.5500	3.5713	3.5500	3.5571	0.0014	-0.3959
95	0.30	10	100	25	4.1014	4.1273	4.1014	4.1109	0.0012	-0.3974
95	0.30	10	100	50	3.6471	3.6689	3.6472	3.6544	0.0013	-0.3934
95	0.30	10	200	25	4.0894	4.1154	4.0895	4.0990	0.0012	-0.3997
95	0.30	10	200	50	3.6343	3.6561	3.6343	3.6416	0.0013	-0.3960
90	0.15	5	100	25	0.5920	0.5988	0.5926	0.5963	0.1110	-0.4103
90	0.15	5	100	50	0.3080	0.3107	0.3087	0.3098	0.2196	-0.2952
90	0.15	5	200	25	0.5879	0.5947	0.5885	0.5922	0.1106	-0.4204
90	0.15	5	200	50	0.3039	0.3067	0.3046	0.3057	0.2193	-0.3104
90	0.15	10	100	25	0.9285	0.9392	0.9291	0.9348	0.0690	-0.4634
90	0.15	10	100	50	0.3951	0.3987	0.3958	0.3973	0.1749	-0.3401
90	0.15	10	200	25	0.9199	0.9308	0.9205	0.9263	0.0687	-0.4793
90	0.15	10	200	50	0.3865	0.3902	0.3872	0.3887	0.1746	-0.3665
90	0.30	5	100	25	2.1808	2.1925	2.1811	2.1851	0.0142	-0.3408
90	0.30	5	100	50	1.9723	1.9823	1.9726	1.9757	0.0161	-0.3321
90	0.30	5	200	25	2.1759	2.1876	2.1762	2.1801	0.0143	-0.3421
90	0.30	5	200	50	1.9672	1.9772	1.9675	1.9706	0.0162	-0.3334
90	0.30	10	100	25	2.4525	2.4662	2.4528	2.4576	0.0120	-0.3476
90	0.30	10	100	50	2.0480	2.0584	2.0483	2.0515	0.0152	-0.3330
90	0.30	10	200	25	2.4430	2.4567	2.4433	2.4482	0.0121	-0.3499
90	0.30	10	200	50	2.0379	2.0483	2.0382	2.0415	0.0154	-0.3355

Table 2.2: **Pricing performance of the Gaver-Stehfest canadization method (GSC) for OTM and ATM put options with time to maturity $\tau = 1$ year.** European and American put option prices are computed via the GSC method for a range of double-exponential jump-diffusion models. The underlying asset price is set to $S_t = 100$, the risk-free rate is $r = 0.04$, the dividend yield is fixed at $\delta = 0.02$, and the conditional probability of a negative jump is $q = 0.7$. Variable input parameters are strike, volatility σ, jump intensity λ, positive jump parameter η, and negative jump parameter θ. We compare the results of our approach to the benchmark (Fourier space time-stepping method), and report the relative pricing errors in percentages.

	Parameters				Benchmark		GSC Method		Rel. Error (%)	
Strike	σ	λ	η	θ	European	American	European	American	European	American
100	0.15	5	100	25	6.1209	6.3733	6.1209	6.2888	-0.0007	-1.3273
100	0.15	5	100	50	5.2566	5.4783	5.2566	5.4025	-0.0005	-1.3834
100	0.15	5	200	25	6.0972	6.3504	6.0972	6.2656	-0.0008	-1.3347
100	0.15	5	200	50	5.2295	5.4519	5.2295	5.3759	-0.0005	-1.3927
100	0.15	10	100	25	7.1837	7.4587	7.1837	7.3620	-0.0005	-1.2970
100	0.15	10	100	50	5.6092	5.8374	5.6092	5.7581	-0.0005	-1.3583
100	0.15	10	200	25	7.1426	7.4190	7.1426	7.3219	-0.0005	-1.3097
100	0.15	10	200	50	5.5579	5.7873	5.5579	5.7077	-0.0005	-1.3752
100	0.30	5	100	25	11.2944	11.5435	11.2943	11.4378	-0.0007	-0.9154
100	0.30	5	100	50	10.8175	11.0562	10.8175	10.9545	-0.0006	-0.9205
100	0.30	5	200	25	11.2806	11.5298	11.2806	11.4242	-0.0007	-0.9165
100	0.30	5	200	50	10.8033	11.0420	10.8032	10.9402	-0.0006	-0.9217
100	0.30	10	100	25	11.9280	12.1881	11.9279	12.0777	-0.0007	-0.9061
100	0.30	10	100	50	11.0052	11.2462	11.0051	11.1432	-0.0006	-0.9155
100	0.30	10	200	25	11.9019	12.1622	11.9018	12.0517	-0.0007	-0.9083
100	0.30	10	200	50	10.9771	11.2182	10.9770	11.1152	-0.0006	-0.9179
95	0.15	5	100	25	4.0802	4.2299	4.0802	4.1776	-0.0002	-1.2372
95	0.15	5	100	50	3.2533	3.3699	3.2533	3.3271	0.0001	-1.2710
95	0.15	5	200	25	4.0597	4.2096	4.0597	4.1572	-0.0001	-1.2448
95	0.15	5	200	50	3.2300	3.3467	3.2300	3.3038	0.0001	-1.2805
95	0.15	10	100	25	5.0751	5.2516	5.0751	5.1874	-0.0002	-1.2223
95	0.15	10	100	50	3.5764	3.7017	3.5764	3.6552	-0.0000	-1.2540
95	0.15	10	200	25	5.0388	5.2160	5.0388	5.1516	-0.0002	-1.2351
95	0.15	10	200	50	3.5317	3.6573	3.5317	3.6108	0.0000	-1.2713
95	0.30	5	100	25	8.8743	9.0538	8.8743	8.9752	-0.0006	-0.8685
95	0.30	5	100	50	8.4104	8.5794	8.4104	8.5047	-0.0006	-0.8704
95	0.30	5	200	25	8.8614	9.0409	8.8613	8.9622	-0.0006	-0.8697
95	0.30	5	200	50	8.3970	8.5659	8.3969	8.4912	-0.0005	-0.8716
95	0.30	10	100	25	9.4870	9.6780	9.4870	9.5945	-0.0006	-0.8628
95	0.30	10	100	50	8.5904	8.7620	8.5903	8.6861	-0.0006	-0.8666
95	0.30	10	200	25	9.4624	9.6534	9.4624	9.5699	-0.0006	-0.8650
95	0.30	10	200	50	8.5638	8.7354	8.5638	8.6595	-0.0006	-0.8689
90	0.15	5	100	25	2.5507	2.6343	2.5509	2.6041	0.0079	-1.1443
90	0.15	5	100	50	1.8318	1.8876	1.8320	1.8659	0.0132	-1.1507
90	0.15	5	200	25	2.5344	2.6180	2.5346	2.5879	0.0081	-1.1519
90	0.15	5	200	50	1.8139	1.8696	1.8141	1.8479	0.0136	-1.1602
90	0.15	10	100	25	3.4151	3.5232	3.4152	3.4828	0.0044	-1.1463
90	0.15	10	100	50	2.0974	2.1608	2.0977	2.1361	0.0101	-1.1442
90	0.15	10	200	25	3.3851	3.4935	3.3853	3.4530	0.0046	-1.1591
90	0.15	10	200	50	2.0624	2.1257	2.0627	2.1011	0.0107	-1.1614
90	0.30	5	100	25	6.7698	6.8951	6.7698	6.8385	-0.0002	-0.8217
90	0.30	5	100	50	6.3321	6.4476	6.3321	6.3947	-0.0001	-0.8203
90	0.30	5	200	25	6.7580	6.8832	6.7580	6.8266	-0.0002	-0.8228
90	0.30	5	200	50	6.3198	6.4352	6.3198	6.3824	-0.0001	-0.8214
90	0.30	10	100	25	7.3458	7.4820	7.3457	7.4207	-0.0003	-0.8196
90	0.30	10	100	50	6.4992	6.6173	6.4992	6.5632	-0.0001	-0.8176
90	0.30	10	200	25	7.3232	7.4594	7.3232	7.3981	-0.0002	-0.8216
90	0.30	10	200	50	6.4749	6.5929	6.4749	6.5389	-0.0001	-0.8198

Table 2.3: **Early exercise disentanglement of jumps from diffusion for OTM and ATM American put options.** We compute early exercise disentanglement for options with $\tau = 3$ months and $\tau = 1$ year to maturity for a range of double-exponential jump-diffusion models. Early exercise premium (EEP) is represented as a percentage of the American put option price. Contributions of the diffusion component (DC) and the jump component (JC) to the early exercise are represented as percentages of the EEP, hence summing up to unity. The underlying asset price is set to $S_t = 100$, the risk-free rate is $r = 0.04$, the dividend yield is fixed at $\delta = 0.02$, and the conditional probability of a negative jump is $q = 0.7$. Variable input parameters are strike, volatility σ, jump intensity λ, positive jump parameter η, and negative jump parameter θ.

	Parameters				$\tau = 3$ months			$\tau = 1$ year		
Strike	σ	λ	η	θ	EEP (%)	DC (%)	JC(%)	EEP(%)	DC(%)	JC(%)
100	0.15	5	100	25	0.78	48.64	51.36	2.67	57.73	42.27
100	0.15	5	100	50	0.67	83.45	16.55	2.70	86.43	13.57
100	0.15	5	200	25	0.79	48.45	51.55	2.69	57.54	42.46
100	0.15	5	200	50	0.68	83.36	16.64	2.72	86.35	13.65
100	0.15	10	100	25	0.76	35.24	64.76	2.42	42.53	57.47
100	0.15	10	100	50	0.66	72.55	27.45	2.59	76.56	23.44
100	0.15	10	200	25	0.77	34.94	65.06	2.45	42.20	57.80
100	0.15	10	200	50	0.68	72.30	27.70	2.63	76.33	23.67
100	0.30	5	100	25	0.26	83.77	16.23	1.26	86.81	13.19
100	0.30	5	100	50	0.25	96.25	3.75	1.25	96.66	3.34
100	0.30	5	200	25	0.27	83.76	16.24	1.26	86.79	13.21
100	0.30	5	200	50	0.25	96.24	3.76	1.25	96.65	3.35
100	0.30	10	100	25	0.27	73.00	27.00	1.24	77.01	22.99
100	0.30	10	100	50	0.25	92.81	7.19	1.24	93.56	6.44
100	0.30	10	200	25	0.27	72.92	27.08	1.24	76.94	23.06
100	0.30	10	200	50	0.25	92.79	7.21	1.24	93.54	6.46
95	0.15	5	100	25	0.67	46.15	53.85	2.33	57.14	42.86
95	0.15	5	100	50	0.48	82.18	17.82	2.22	86.18	13.82
95	0.15	5	200	25	0.68	45.96	54.04	2.35	56.95	43.05
95	0.15	5	200	50	0.48	82.08	17.92	2.24	86.10	13.90
95	0.15	10	100	25	0.67	34.29	65.71	2.17	42.10	57.90
95	0.15	10	100	50	0.49	71.14	28.86	2.16	76.23	23.77
95	0.15	10	200	25	0.68	34.00	66.00	2.19	41.77	58.23
95	0.15	10	200	50	0.51	70.89	29.11	2.19	76.00	24.00
95	0.30	5	100	25	0.22	83.22	16.78	1.12	86.69	13.31
95	0.30	5	100	50	0.20	96.16	3.84	1.11	96.64	3.36
95	0.30	5	200	25	0.22	83.19	16.81	1.13	86.67	13.33
95	0.30	5	200	50	0.20	96.15	3.85	1.11	96.63	3.37
95	0.30	10	100	25	0.23	72.30	27.70	1.12	76.85	23.15
95	0.30	10	100	50	0.20	92.66	7.34	1.10	93.52	6.48
95	0.30	10	200	25	0.23	72.21	27.79	1.12	76.78	23.22
95	0.30	10	200	50	0.20	92.63	7.37	1.10	93.50	6.50
90	0.15	5	100	25	0.62	43.82	56.18	2.04	56.46	43.54
90	0.15	5	100	50	0.35	80.41	19.59	1.82	85.89	14.11
90	0.15	5	200	25	0.62	43.64	56.36	2.06	56.26	43.74
90	0.15	5	200	50	0.36	80.29	19.71	1.83	85.81	14.19
90	0.15	10	100	25	0.61	33.21	66.79	1.94	41.64	58.36
90	0.15	10	100	50	0.38	69.43	30.57	1.80	75.87	24.13
90	0.15	10	200	25	0.62	32.94	67.06	1.96	41.31	58.69
90	0.15	10	200	50	0.39	69.16	30.84	1.83	75.63	24.37
90	0.30	5	100	25	0.18	82.49	17.51	1.00	86.56	13.44
90	0.30	5	100	50	0.16	96.06	3.94	0.98	96.62	3.38
90	0.30	5	200	25	0.18	82.45	17.55	1.00	86.54	13.46
90	0.30	5	200	50	0.16	96.05	3.95	0.98	96.61	3.39
90	0.30	10	100	25	0.20	71.50	28.50	1.01	76.68	23.32
90	0.30	10	100	50	0.16	92.48	7.52	0.98	93.49	6.51
90	0.30	10	200	25	0.20	71.41	28.59	1.01	76.61	23.39
90	0.30	10	200	50	0.16	92.46	7.54	0.98	93.47	6.53

American put option, increases with moneyness and time to maturity and varies between 0.1 and 2.7 percent. The contribution of jumps can be as low as 3 percent or as high as 66 percent of the early exercise premium, depending on the model and the option contract.

From Table 2.3 we see that the diffusion (jump) contribution increases (decreases) in strike. Intuitively, this observation makes sense, since the probability that early exercise occurs due to the diffusion decreases for options that are deeper OTM. The jump contribution also increases with jump intensity and average negative jump size, while it decreases with volatility. The effect of average positive jump size on the jump contribution is negative but negligible.

2.3 Empirical analysis

We next explore empirically the disentanglement of jumps from diffusion for the early exercise premium. By calibrating different HEJD models to American options on the S&P 100 index, we analyze whether jumps play an important role for the early exercise of American put options.

2.3.1 Data and calibration procedure

We use six years of weekly (Wednesdays) S&P 100 index American options data (ticker symbol OEX), spanning the period from January 3, 2007 until December 31, 2012. Thus, the sample encompasses the recent financial crisis.[16] Since we are interested in the calibration of a jump-diffusion model, we focus on short-term options with less than 60 days to maturity. We define moneyness M as the ratio of the strike K and the futures price $F_{t,T} := S_t e^{(r-\delta)(T-t)}$, i.e., $M := K/F_{t,T}$.

We eliminate illiquid in-the-money options (ITM), i.e., calls with moneyness less than 0.97 and puts with moneyness greater than 1.03. Hence, our sample contains only liquid near-the-money (NTM) and out-of-the-money (OTM) options. We use mid-prices, which are computed as averages of the bid and ask market quotes, as a proxy for our market prices. We also eliminate all the options whose prices are lower than 0.125 units due to the minimum tick limitations. Finally, we eliminate all the options for which the volume or the open interest are zero.

Descriptive statistics of our sample of options are given in Table 2.4. The total number of options in the dataset is 23,169 distributed over 313 days, or approximately 74 option quotes per observation

[16] S&P 100 index quotes, American options data (bid and ask prices, strikes and maturities), zero-coupon curve, and dividend yields are obtained from OptionMetrics.

Table 2.4: **S&P 100 index options data, January 3, 2007–December 31, 2012.** We report descriptive statistics of ATM and OTM American options on the S&P 100 index. The data is obtained from OptionMetrics and filtered as described in the Section 2.3.1. The dataset comprises closing quotes for call and put options traded on Wednesdays for the given time period. There are 313 days of observations in total. We report the number of option contracts traded, the average quoted price and the average implied volatility. Each statistic is computed for four different maturity bins and six different moneyness bins, as well as for collective observations across given maturity and moneyness buckets. DTM stands for days-to-maturity, and $M := K/F_{t,T}$ denotes moneyness.

Panel A: Number of contracts across moneyness and maturity

Moneyness	DTM < 7	7≤DTM<14	14≤DTM<30	30≤DTM<60	All
K/F < 0.94	271	593	1,842	3,902	6,608
0.94<K/F<0.97	525	244	485	1,002	2,256
0.97<K/F<1.00	1,702	494	964	1,921	5,081
1.00<K/F<1.03	1,476	480	958	1,909	4,823
1.03<K/F<1.06	177	188	453	1,011	1,829
1.06<K/F	84	150	513	1,825	2,572
All	4,235	2,149	5,215	11,570	23,169

Panel B: Average quoted price across moneyness and maturity

Moneyness	DTM < 7	7≤DTM<14	14≤DTM<30	30≤DTM<60	All
K/F < 0.94	0.39	0.68	1.19	2.92	2.14
0.94<K/F<0.97	0.54	1.83	3.76	7.70	4.55
0.97<K/F<1.00	5.02	8.75	11.50	15.79	10.69
1.00<K/F<1.03	5.04	7.93	10.52	14.48	10.15
1.03<K/F<1.06	0.66	1.24	1.97	4.73	3.30
1.06<K/F	0.58	0.82	0.92	2.00	1.67
All	3.91	4.35	5.09	7.39	5.96

Panel C: Average implied volatility across moneyness and maturity

Moneyness	DTM < 7	7≤DTM<14	14≤DTM<30	30≤DTM<60	All
K/F < 0.94	0.8058	0.4177	0.3734	0.3384	0.3745
0.94<K/F<0.97	0.4866	0.2681	0.2439	0.2359	0.2991
0.97<K/F<1.00	0.3385	0.2294	0.2145	0.2128	0.2557
1.00<K/F<1.03	0.3141	0.2058	0.1924	0.1944	0.2307
1.03<K/F<1.06	0.4682	0.2138	0.1760	0.1745	0.2073
1.06<K/F	0.9103	0.4012	0.2554	0.2196	0.2600
All	0.3971	0.2912	0.2700	0.2519	0.2855

day on average. NTM options, i.e., options for which $M \in (0.97, 1.03)$, include both calls and puts, and they account for almost 43 percent of the sample. OTM puts ($M < 0.97$) constitute around 38 percent of the dataset, and OTM calls ($M > 1.03$) account for the remaining 19 percent of all considered option quotes.

We re-calibrate parameters of a HEJD(m, n) model for each observation date in the sample by minimizing a loss function in the form of penalized weighted non-linear least squares (WNLLS). In particular, we consider a weighted Euclidian distance between market quotes and corresponding model option prices.[17] Nevertheless, it is well known that any framework involving re-calibration of the model parameters inherently suffers from instability and the non-convexity of the multidimensional loss function implies the existence of local minima. Therefore, we add a positive and locally convex penalty term to the loss function and recast the original problem into a sequential regularized weighted non-linear least squares setting. We follow Hellmich, Kassberger and Schmidt (2013) and define the penalty function as the Kulback-Leibler divergence between the probability distributions on two successive points in time.[18] The probability density function of the HEJD process is not known in closed form, but we are able to numerically compute the Kullback-Leibler divergence by using the Fourier cosine method of Fang and Oosterlee (2008).[19]

2.3.2 Model selection

The HEJD(m, n) offers the flexibility to choose any number of distinct positive and negative jump types. To keep the analysis tractable, we consider a set of HEJD(m, n) models for which the total number of different jump types is such that $m + n \leq 4$, which gives us 15 different models with up to nine parameters.[20] This choice includes some special cases such as, e.g., HEJD$(0, 0)$ is the no-jump ca-

[17] We follow Lindström et al. (2008) and define the weights as the inverse of the squared bid-ask spreads.

[18] Others, like Cont and Tankov (2004), opt for the relative entropy as an alternative to ensure positivity. However, the relative entropy approach is based on the Kullback-Leibler divergence with respect to the prior model on the path space. It implies that the volatility parameter would remain constant in order to have non-singular (equivalent) probabilities. In fact, the choice of the penalty term defined as the relative entropy function would make it impossible to obtain dynamic diffusion parameters.

[19] A detailed description of the calibration procedure can be obtained from the authors.

[20] Further in text, we use interchangeably the notation HEJD(m, n) and (m, n). We also note that it is necessary to introduce a constraint on the total number of different positive and negative jump types in the model. Generally, the HEJD class of models admits a (countably) infinite number of jumps. However, in practical applications we have to limit the number of parameters to keep our analysis tractable and to avoid overfitting. Our particular choice of $m + n \leq 4$ is motivated by two facts. First, this set contains the most popular HEJD model specifications which are studied in the literature. Second, the total number of calibration parameters when $n + m = 4$ is nine, which is already quite high for a single-asset option pricing model.

Table 2.5: **Model selection.** Entries report the value of negative regularized log-likelihood (ℓ_{reg}), i.e., the MAP, Akaike (AIC), corrected Akaike (AICc), and Bayesian (BIC) information criteria, as well the corresponding AIC, AICc, and BIC weights for 15 different calibrated HEJD models for weekly OEX observations in the period January 3, 2007–December 31, 2012. Models are calibrated using the regularized weighted non-linear least squares. The jump structure (m, n), for $m, n \in \mathbb{N}$, denotes a HEJD model with m distinct positive and n distinct negative jump types. Models with better data fit exhibit lower values for negative log-MAP, AIC, AICc, and BIC, and higher values for the AIC, AICc, and BIC weights.

Model (m, n)	ℓ_{reg}	AIC	AICc	BIC	AIC Weights	AICc Weights	BIC Weights
(0,0)	327.30	656.59	656.65	658.88	1.95e-30	4.60e-30	8.27e-28
(0,1)	261.71	529.42	529.78	536.28	0.00803	0.01630	0.34708
(1,0)	332.82	671.63	671.99	678.49	1.05e-33	2.14e-33	4.56e-32
(0,2)	265.16	540.33	541.25	551.75	0.00003	0.00005	0.00015
(1,1)	257.68	525.36	526.28	536.79	0.06116	0.09353	0.26891
(2,0)	333.80	677.61	678.53	689.03	5.32e-35	8.14e-35	2.34e-34
(0,3)	267.62	549.23	551.02	565.23	4.00e-07	3.98e-07	1.79e-07
(1,2)	253.05	520.11	521.89	536.10	0.84538	0.84111	0.37816
(2,1)	258.29	530.57	532.36	546.57	0.00451	0.00448	0.00202
(3,0)	334.62	683.23	685.02	699.23	3.19e-36	3.17e-36	1.43e-36
(0,4)	261.36	540.72	543.69	561.28	0.00003	0.00002	1.29e-06
(1,3)	253.40	524.80	527.76	545.37	0.08086	0.04450	0.00368
(2,2)	270.81	559.63	562.60	580.20	2.21e-09	1.22e-09	1.01e-10
(3,1)	268.93	555.85	558.82	576.42	1.46e-08	8.04e-09	6.65e-10
(4,0)	334.47	686.73	689.70	707.30	5.55e-37	3.06e-37	2.53e-38

Table 2.6: **In-sample Diebold-Mariano test.** We compute the in-sample weighted root mean squared errors (RMSEs) for weekly OEX observations in the period January 3, 2007–December 31, 2012. The jump structure (m, n) denotes a HEJD model with m distinct positive and n distinct negative jump types. Panel A summarizes the mean and the standard deviation estimates of the series of weighted RMSEs. Panel B reports the pairwise Diebold-Mariano statistics for the calibrated models. Standard errors are obtained using the Newey-West estimator with optimal number of lags based on Andrews (1991) and AR(1) process. A value greater than 1.645 implies that the test model (column) outperforms the benchmark (row) at a 95% confidence interval. A value less than -1.645 implies the opposite.

Panel A: Mean and standard deviation of the the in-sample weighted RMSEs

Model	(0,0)	(0,1)	(1,0)	(0,2)	(1,1)	(2,0)	(0,3)	(1,2)	(2,1)	(3,0)	(0,4)	(1,3)	(2,2)	(3,1)	(4,0)
Mean	3.76	1.51	3.74	1.49	1.45	3.75	1.66	1.38	1.45	3.74	1.52	1.35	1.75	1.56	3.74
	(1.13)	(0.58)	(1.12)	(0.58)	(0.59)	(1.12)	(0.87)	(0.51)	(0.58)	(1.12)	(0.71)	(0.50)	(1.09)	(0.84)	(1.12)

Panel B: Diebold-Mariano in-sample statistics of the weighted RMSEs

Model	(0,0)	(0,1)	(1,0)	(0,2)	(1,1)	(2,0)	(0,3)	(1,2)	(2,1)	(3,0)	(0,4)	(1,3)	(2,2)	(3,1)	(4,0)
(0,0)		27.04	11.52	27.07	27.14	9.41	23.70	5.36	27.69	27.25	12.46	23.25	27.81	25.33	12.52
(0,1)			-27.06	2.75	3.05	-27.08	-4.35	5.76	4.42	-27.04	-0.97	6.80	-5.24	-2.49	-27.04
(1,0)				27.08	27.14	-5.70	23.68	27.71	27.26	3.56	23.22	27.83	21.77	25.33	4.62
(0,2)					2.02	-27.10	-4.57	5.12	3.10	-27.07	-1.19	6.15	-5.37	-2.72	-27.07
(1,1)						-27.16	-5.02	3.58	0.26	-27.13	-1.65	4.59	-5.78	-3.22	-27.13
(2,0)							23.69	27.72	27.28	8.12	23.24	27.84	21.79	25.34	9.37
(0,3)								6.08	5.13	-23.66	2.26	6.48	-2.48	1.63	-23.66
(1,2)									-3.84	-27.69	-2.75	3.10	-6.52	-4.44	-27.70
(2,1)										-27.25	-1.68	4.86	-5.86	-3.30	-27.25
(3,0)											23.21	27.82	21.76	25.32	1.24
(0,4)												3.10	-3.68	-1.01	-23.21
(1,3)													-6.78	-4.87	-27.82
(2,2)														3.86	-21.76
(3,1)															-25.32
(4,0)															

Table 2.7: **Out-of-sample Diebold-Mariano test.** We compute the out-of-sample weighted root mean squared errors (RMSEs) for weekly OEX observations in the period January 3, 2007–December 31, 2012. The jump structure (m, n) denotes a HEJD model with m distinct positive and n distinct negative jump types. Panel A summarizes the mean and the standard deviation estimates of the series of weighted RMSEs. Panel B reports the pairwise Diebold-Mariano statistics for the calibrated models. Standard errors are obtained using the Newey-West estimator with optimal number of lags based on Andrews (1991) and AR(1) process. A value greater than 1.645 implies that the test model (column) outperforms the benchmark (row) at a 95% confidence interval. A value less than -1.645 implies the opposite.

Mean and standard deviation of the the out-of-sample weighted RMSEs

Model	(0,0)	(0,1)	(1,0)	(0,2)	(1,1)	(2,0)	(0,3)	(1,2)	(2,1)	(3,0)	(0,4)	(1,3)	(2,2)	(3,1)	(4,0)
Mean	4.39	2.84	4.41	2.85	2.84	4.43	2.97	2.85	2.84	4.44	2.90	2.82	3.05	2.92	4.45
	(1.69)	(1.92)	(1.72)	(1.93)	(1.94)	(1.72)	(1.87)	(2.19)	(1.93)	(1.73)	(1.99)	(1.94)	(1.97)	(1.87)	(1.74)

Panel B: Diebold-Mariano out-of-sample statistics of the weighted RMSEs

Model	(0,0)	(0,1)	(1,0)	(0,2)	(1,1)	(2,0)	(0,3)	(1,2)	(2,1)	(3,0)	(0,4)	(1,3)	(2,2)	(3,1)	(4,0)
(0,0)		11.56	-1.97	11.30	11.32	-3.07	13.21	5.36	11.25	-3.46	10.25	11.31	11.38	14.74	-4.41
(0,1)			-13.27	-2.55	-0.93	-13.26	-1.19	-0.82	-0.98	-13.74	-2.93	0.20	-2.70	-0.61	-13.74
(1,0)				12.98	13.02	-4.18	15.05	5.68	12.93	-7.65	11.69	12.88	13.12	16.99	-9.31
(0,2)					0.47	-12.96	-0.79	-0.69	1.34	-13.24	-1.43	1.54	-2.12	-0.09	-13.06
(1,1)						-13.00	-1.03	-0.77	-0.10	-13.47	-2.09	0.50	-2.55	-0.48	-13.48
(2,0)							15.23	5.77	12.91	-2.77	11.71	12.88	13.27	17.15	-6.44
(0,3)								-0.39	1.01	-15.56	-0.07	1.20	-2.83	1.10	-15.79
(1,2)									0.78	-5.85	0.38	0.85	-0.17	0.58	-5.92
(2,1)										-13.37	-1.84	0.54	-2.51	-0.46	-13.38
(3,0)											12.12	13.32	13.59	17.49	-4.07
(0,4)												2.03	-1.38	0.58	-12.16
(1,3)													-2.62	-0.65	-13.33
(2,2)														3.80	-13.83
(3,1)															-17.73
(4,0)															

se of Black and Scholes (1973), HEJD$(1,1)$ is the double-exponential model of Kou (2002), and HEJD$(0,1)$ is the spectrally one-sided (negative) exponential Lévy model of Avram, Chan and Usabel (2002).

Given the Bayesian nature of the sequential regularized WNLLS procedure due to the penalty function, we can transform our calibration exercise into a series of maximum a posteriori problems (MAP), which can be considered as a regularized maximum likelihood approach.[21] In addition to the MAP objective function, we compare the models' in-sample performance in terms of the Akaike (AIC), the corrected Akaike (AICc) and the Bayesian (BIC) information criterion. The corresponding weights based on the relative likelihood of the models are also computed. Finally, we compute the pairwise evidence ratios.

Table 2.5 summarizes the average in-sample information criteria. In terms of the average negative log-maximum a posteriori loss function (neg. log-MAP), we conclude that the model $(1,2)$ has the best score, and it is closely followed by the models $(1,3)$ and $(1,1)$. The same results are obtained for AIC and AICc statistics. Using BIC we conclude that $(1,1)$ shows better performance than $(1,3)$, but the model $(1,2)$ still remains the selected one. As expected, models that completely exclude the possibility for negative jumps in the underlying asset perform very poorly.

To determine the significance of the difference between models' option pricing errors, we also consider the Diebold and Mariano (1995) test. For the in-sample (out-of-sample) exercise, the model prices are obtained by using the set of calibrated parameters on a date, which coincides with (precedes) the observation date of the quoted market option prices. The test is computed for the series of average weighted root mean square errors. For the in-sample test, given in Table 2.6, the hyper-exponential jump-diffusion models with jump structures (1,3) and (1,2) have the smallest mean and standard deviation estimates, respectively. The Diebold-Mariano test indicates that the HEJD(1,3) outperforms all calibrated models at all significance levels. The HEJD(1,2) significantly outperform all model, except the HEJD(1,3). However, in the case of the out-of-sample test in Table 2.7, results are less clear. Models with only positive jumps are clearly rejected in favor of models including negative jumps. Models with both negative and positive jumps fail to significantly outperform models with only negative jumps. The HEJD(1,3) no longer significantly outperforms the HEJD(1,2) model.

[21] The results on the equivalence between the MAP and the regularized maximum likelihood, and the computation of the information criteria for model selection are available upon request.

2.3.3 Exploring the HEJD(1,2) model

To obtain some intuition about the parameter values and their time variation in the sequential calibration, we explore graphically the properties of the the HEJD$(1, 2)$ model. Figure 2.1, Panel A, shows the time series of conditional volatility. The average calibrated volatility σ for the whole time span from January 3, 2007 until December 31, 2012 is 14.94 percent. We observe a sharp increase in the volatility around September 2008 reaching 65 percent. A similar behavior can be observed for the jump intensity parameter λ in Panel B of Figure 2.1. The average jump intensity is approximately 10.5 jumps per year, but varies quite a lot depending on the calibration day.

In the HEJD(1,2) model, jumps can be divided into one positive and two types of negative jumps (see Figure 2.1, Panel C). The average positive jump size equals 0.22 percent, the absolute average magnitude of small negative jumps is approximately 0.40 percent, and the absolute average size of large negative jumps is 6.26 percent. Hence, negative jumps strongly dominate positive ones. Figure 2.1, Panel D, represent the probabilities p, q_1, and q_2 of positive, small negative, and large negative jumps. These are conditional probabilities given that a jump occurs. Over the whole sample period, they average 0.40, 42.00 and 57.60 percent, respectively. Therefore, the positive jumps are not only small in magnitude, but they also have very low conditional probability of occurrence. Hence, from a practical viewpoint, they might be even negligible. In contrast, the conditional probabilities for small and large negative jumps are substantial and similar in magnitude. For large negative jump sizes, we observe a gradual increase in their conditional probability until September 2008. In the subsequent period, this probability seems to decrease again, while the probability for small negative jumps becomes large. Nevertheless, the probability for large jumps seems to be persistently high from 2010 onwards, with additional peaks around May 2010 and August 2011.

We further explore in a regression analysis how the time series of calibrated model parameters such as the volatility parameter σ, the jump intensity λ, and the average jump size ζ depend on observable market variables, such as the implied volatility, implied skewness, and implied convexity. To this end, we use as implied volatility the 1 month ATM implied volatility. For the implied skewness, we use the difference between the 10% OTM call and put implied volatilities for options with maturity of 1 month, divided by the moneyness differential ($\Delta M = 0.2$), i.e., the so-called 90/110 skewness. The implied skewness represents a measure of the asymmetry of OEX 1-month implied volatility smile. Finally, we

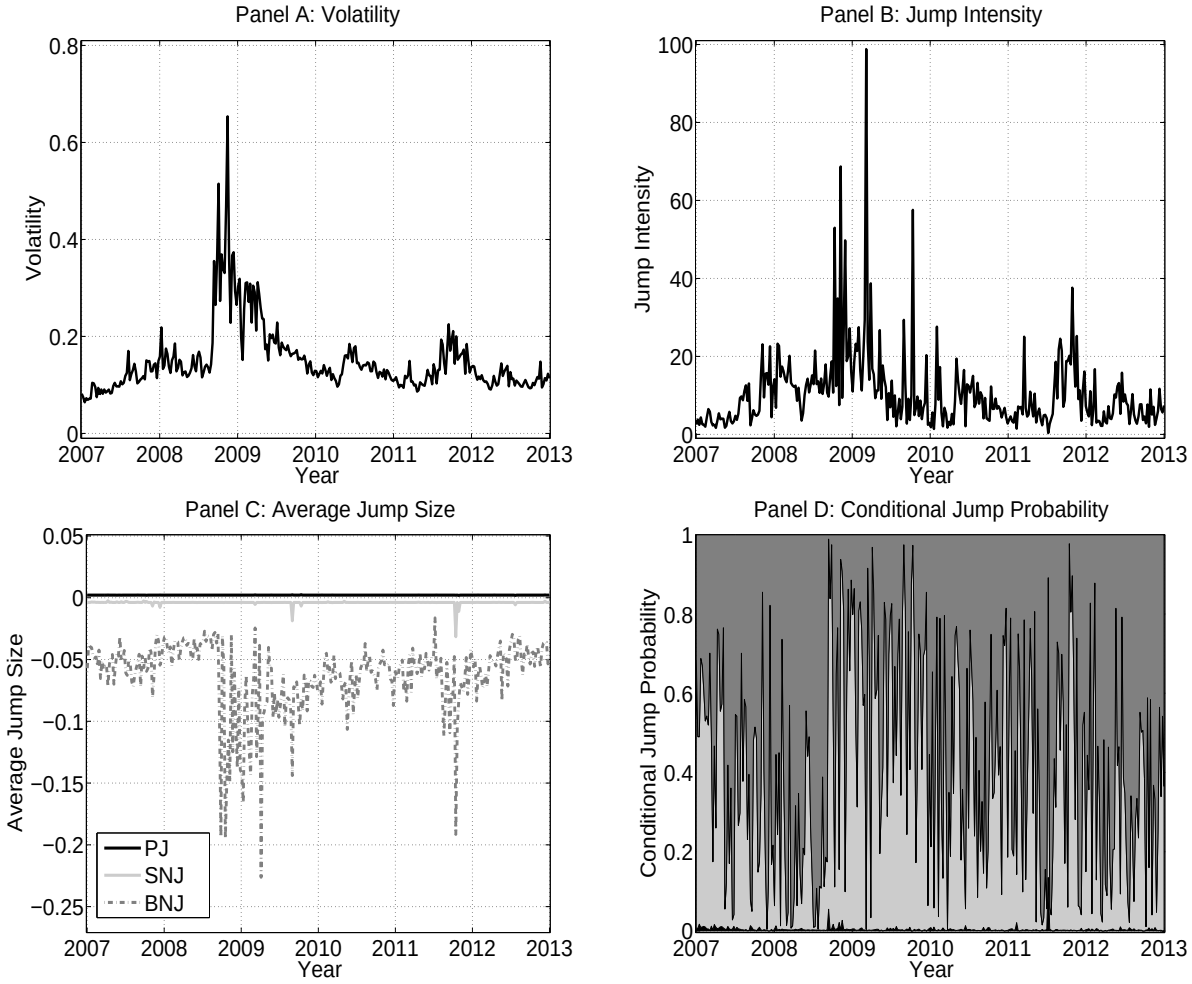

Figure 2.1: **Calibrated parameters for HEJD(1,2).** Panels A and B represent the dynamics of the volatility parameter σ and the jump intensity parameter λ. Panel C gives the dynamics of the average sizes of different jump types. Positive jumps (PJ) are represented by the solid black line, negative jump of the first kind (big negative jumps BNJ) by the dash-dot line, and the negative jump of the second kind (small negative jumps SNJ) by the solid gray line. Panel D shows an area plot for the dynamics of the conditional jump probability parameters. The black area at the bottom of the graph represents the probability for PJ, the gray area in the middle represents the probability for SNJ, and the remaining area for BNJ.

Table 2.8: **Regression of changes in model parameters on changes in observable market parameters**. We regress the volatility σ, the jump intensity λ, and the unconditional and conditional jump sizes $\lambda\zeta$ and ζ of the HEJD(1,2) model given in equations (2.1)–(2.4) on ATM implied volatility (IV), 90/110 implied skewness (Skew), and 90/110 implied convexity (Conv), respectively, for OEX options with 1 month to maturity. We base our analysis on robust linear regression using differences and the Huber weighting function (see Huber 1981). We report t-statistics in brackets.

	Volatility (σ)			Jump intensity (λ)			Unconditional jump ($\lambda\zeta$)			Conditional jump (ζ)		
const.	0.000	0.000	0.001	0.125	0.103	0.096	-0.000	-0.000	-0.000	0.000	0.000	0.000
	(0.342)	(0.352)	(0.524)	(0.389)	(0.301)	(0.273)	(-0.349)	(-0.323)	(-0.278)	(0.272)	(0.275)	(0.297)
IV	0.450	0.481	0.706	37.898	26.711	24.740	-0.182	-0.160	-0.147	-0.084	-0.084	-0.037
	(16.960)	(17.170)	(21.373)	(4.092)	(2.625)	(2.049)	(-15.140)	(-11.939)	(-8.557)	(-2.832)	(-2.750)	(-1.010)
Skew	–	0.022	0.060	–	-13.141	-13.662	–	0.017	0.019	–	-0.000	0.013
		(2.122)	(5.058)		(-3.441)	(-3.145)		(3.334)	(3.135)		(-0.033)	(0.995)
Conv	–	–	0.004	–	–	-0.034	–	–	0.000	–	–	0.001
			(9.969)			(-0.254)			(1.293)			(2.281)
Adj. R^2	0.234	0.245	0.348	0.007	0.034	0.033	0.038	0.059	0.057	0.004	0.003	0.021

define the implied convexity as a measure of the curvature of the implied volatility smile. We calculate the implied convexity as the second-order central difference of implied volatility curve using ATM, and 10% OTM call and put implied volatilities, divided by the squared moneyness differential.

In Table 2.8, we report the results from our linear regression.[22] As expected, the changes in the volatility parameter σ are prominently driven by the changes in the implied volatility. Changes in implied skewness and convexity do have less but still a statistically significant impact. Using all three variables, we end up with an R^2 of more than 34 percent. The jump intensity parameter λ is mostly driven by implied volatility and (negative) skewness. Convexity has an insignificant impact and the R^2 value, using all three variables, is below four percent. When we look at the conditional jump size ζ, however, we find that implied convexity is the only significant variable that has a positive impact on the jump size. In contrast, unconditional jump sizes ($\lambda\zeta$) are mainly driven by implied volatility and skewness.

As an additional exercise, we also perform a maximum likelihood estimation of the HEJD model under the physical measure using the time series of the S&P 100 returns. We calculate the log-likelihood function for each of the candidate HEJD models by summing up the logarithms of the respective probability density functions evaluated at the observed S&P 100 returns. For a given point in time, we compute the probability density function numerically by Fourier-inverting the respective characteristic function. Based on the log-likelihood function and the Akaike information criteria, we find that the HEJD (2,2) model provides the best fit.[23] Hence, our estimation exercise under the historical measure corroborates previous findings in the literature regarding the model selection in the HEJD framework. For instance, Sepp (2012) finds that jumps are symmetric and have two values, a small and a large jump, for both negative and positive returns. Comparing with our calibration results under the risk-neutral measure, we find that the absolute average size of negative small (large) jumps is 0.63 (2.28) percent under the historical measure. Under the risk-neutral measure, the absolute average magnitude of small negative jumps is approximately 0.40 percent, and the absolute average size of large negative jumps is 6.26 percent. Also, under the historical measure, the average size of positive small (large) jumps is 0.49 (1.98) percent. The average jump size under the risk-neutral measure for

[22] We note that we first take differences of the relevant variables and we use robust regression based on the Huber weighting function, see Huber (1981). The reason to do so is that the errors of ordinary least-square regressions fail the Jarque-Bera test for normality.

[23] However, using the BIC we find that the preferred mode is HEJD(0,2).

positive jumps averages only 0.22 percent. These findings reflect the concern of risk-averse investors by putting less weight on positive jumps and more weight on negative jumps.[24]

2.3.4 Early exercise premium and disentanglement

To analyze the evolution of the early exercise premium (EEP) and its decomposition into diffusion and jump components we proceed in two steps. First, we compare the differences between the EEP implied by the HEJD(1,2) and the standard Black-Scholes-Merton model (BSM). While this comparison of the EEP across two different models, we exploit in a second step our theoretical result of the jump disentanglement in Theorem 2.2.3 and analyze the EEP impact of small and large jumps within the same model, in particular within the HEJD(1,2) model.

Using the calibrated parameters from the previous section, we compute prices of both European and American options for the HEJD(1,2) model. By doing so, we obtain a time series of the HEJD(1,2)-implied EEP. Similarly, to obtain the BSM-implied EEP, we first calculate BSM implied volatilities from the market prices of ATM American put options.[25] We then use these BSM implied volatilities to obtain the corresponding BSM ATM European put option prices, which allow us then to calculate the BSM-implied EEP.

In Figure 2.2, we plot the dynamics of the absolute difference (Panel A) and the relative difference (Panel B) between the HEJD(1,2) and BSM-implied EEP for ATM options. We observe that both absolute and relative EEP differences are almost always positive, except for several observation dates at the beginning of the sample, in the case of options with shortest time to maturity. Hence, the model with jumps exhibits a higher EEP. Furthermore, the EEP difference tends to increase with maturity. However, this pattern seems to completely fade away from the end of 2008 onwards.

The above analysis uses two different models to quantify the impact of jumps. In contrast, our orthogonal decomposition of the EEP in Theorem Theorem 2.2.3 allows us to perform a similar analysis within the same model. In Figure 2.3, we plot the EEP dynamics implied by the HEJD(1,2) model for different maturities. For each maturity, we plot the portion of the EEP which is due to diffusion (solid gray line), to the small jump component (solid black line), and to the large jump component (dash-dot

[24] More results on the maximum likelihood estimation of the different HEJD models can be obtained from the authors on request.

[25] To achieve this goal, we rely on Fourier space time-stepping approach developed in Jackson, Jaimungal and Surkov (2008).

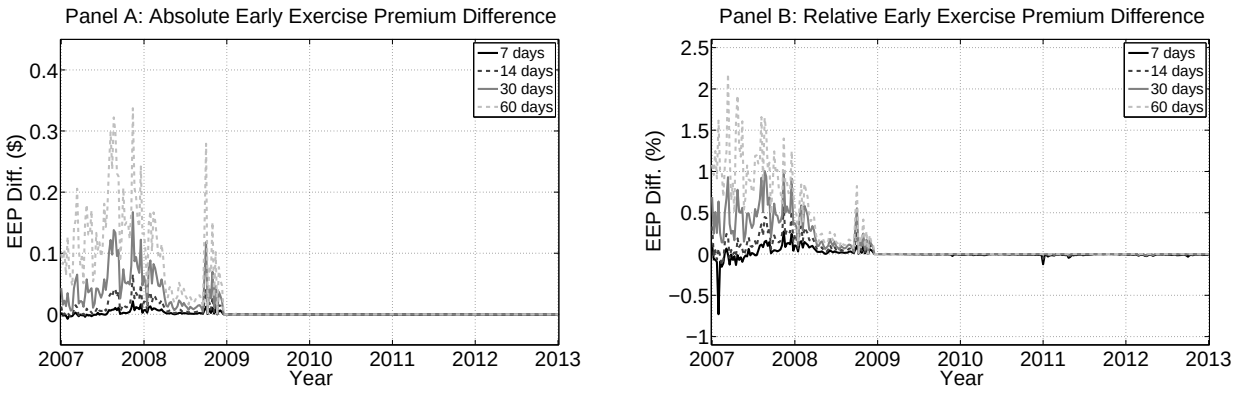

Figure 2.2: **Difference between HEJD(1,2) and BSM early exercise premiums.** Panel A represents the absolute (dollar) difference between the HEJD(1,2) and the BSM-implied early exercise premium (EEP) for ATM American put options with different maturities (7, 14, 30, or 60 days). In Panel B, we plot the relative (percentage) EEP difference between the HEJD(1,2) and the BSM-implied EEP with respect to the corresponding American put option price computed using the HEJD(1,2) model. The difference (absolute and relative) is almost always positive, except for only couple of instances in the case of options with shortest maturity. The difference between the two EEPs becomes more pronounced for options with longer time to maturity.

black line). We observe similar patterns across different maturities. Small jumps have a negligible contribution except at very few isolated points in time. Again, a striking feature of the data is a structural break shortly after the start of the financial crisis in 2008. While large jumps dominate the diffusion contribution most of the time before, the early exercise premium is predominantly determined by the contribution of large jumps.

Clearly, we observe a structural change in both Figure 2.2 and Figure 2.3. This abrupt change is driven by extraordinarily low interest rates.[26] Starting from the end of 2008, the continuing decrease in interest rates led to a substantial reduction in the EEP. Having interest rates close to zero pushes the early exercise boundary for American put options down, which in turn significantly lowers the probability of an early exercise. The reason for absolute domination of jumps over diffusion in the post-crisis period is the following. In a relatively short period of time, which is exactly the case in our data set that consists of short-term options, the diffusion is unlikely to reach a distant early exercise boundary. On the other hand, by definition, (negative) jumps move by leaps and bounds. Hence, they have a better chance of reaching the exercise region. While the early exercise premium is close to zero

[26] We recall the American put-call symmetry of Carr and Chesney (1996), which implies that an American put would not be exercised when the riskless interest rate is zero. However, their results holds only in a diffusion setting. Generalizations would require some symmetry properties for the return volatility.

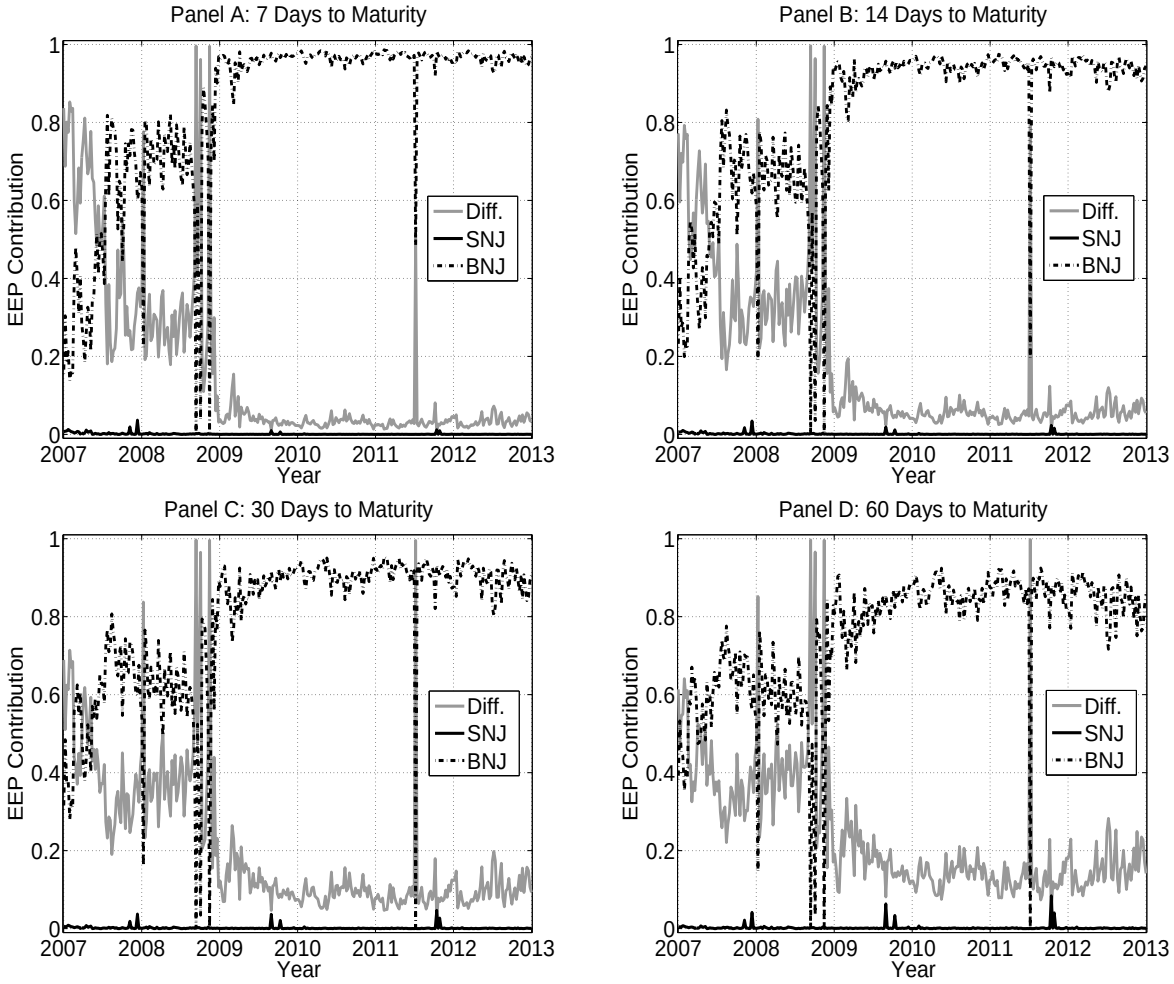

Figure 2.3: **Empirical early exercise premium disentanglement.** Dynamics of the analytic disentanglement approach is presented for ATM OEX options ($M := K/F_{t,T} = 1$) given the calibrated HEJD(1,2) model parameters. In each plot solid gray line describes the portion of the early exercise premium due to the diffusion (Diff.). Solid and dash-dot black line correspond to the small (SNJ) and large (LNJ) negative jumps, respectively. Each panel corresponds to a different maturity of the ATM OEX option (7, 14, 30, or 60 days). For a given date, the contributions of diffusion, small and big jumps sum up to unity.

in the post-crisis period, it is nevertheless possible to extract information about the importance of each process in the underlying asset price dynamics. We find that large negative jumps are by far the most important component, as they account for between 80 and 95 percent in the period from December 2008 to December 2012. The pre-crisis time window conveys different disentanglement structure and the contribution of large negative jumps varies between 20 and 80 percent. Finally, irrespectively of the time period considered, increasing time to maturity implies more importance attached to the diffusion component.

2.4 Conclusion

We price American put options in a hyper-exponential jump-diffusion framework using a maturity randomization approach. We obtain the prices of Canadized European and American options in closed form. We also obtain an analytic disentanglement of jumps and diffusion for the American early exercise premium. Given the wide spectrum of jump-diffusion models that can be accommodated within the HEJD setting, we conduct a calibration and model selection exercise using six years of data of American options on the S&P 100 index. We find that jumps play a dominant role for the early exercise of American put options by accounting on average for more than half of the early exercise premium prior to the financial crisis and more than 90 percent from December 2008 onwards.

Chapter 3

Québécoisation Method for the Pricing of Parisian Options with Jump Risk

Marc Chesney and Nikola Vasiljević[27]

Abstract

This paper introduces a new, analytically tractable technique—called québécoisation method—for the pricing of European and American Parisian options in a flexible jump–diffusion model. Our contribution is threefold. First, using a double Laplace–Carson transform with respect to the option maturity and the Parisian (excursion) time, we obtain closed-form solutions for different types of Parisian contracts. Second, we provide numerical examples and quantify the impact of jumps on the option price and the greeks. Finally, we study the non-monotonic effects of volatility and jump intensity close to the excursion barrier, which are important for shareholders' investment policy decisions in a levered firm.

Keywords: Parisian options, Québécoisation method, Gaver-Stehfest inversion algorithm, Hyper-exponential jump-diffusion model.

JEL classification: G13 · C02 · C65.

[27]We would like to thank Jérôme Detemple, João Pedro Vidal Nunes, Paola Pederzoli, and Felix Stang for their valuable comments. We are also grateful to the participants at the Gerzensee Research Days 2014, and at the Bachelier Finance Conference 2014 in Brussels, Belgium. We gratefully acknowledge financial support from the Swiss Finance Institute (SFI) and the Department for Banking and Finance (DBF) at the University of Zurich (UZH). The previous version of this paper was entitled "European and American Parisian options in a jump-diffusion model".

3.1 Introduction

In the last couple of decades, proliferate research in quantitative finance provided the necessary mathematical tools for pricing and hedging of a wide range of financial products. It is now generally recognized that standard put and call options do not perfectly match all risk profiles and do not provide universal means of hedging. In addition to vanilla European and American options, many different types of exotic options are traded on organized exchanges and over-the-counter (OTC).

Standard (one-touch) barrier options are among the most popular derivative contracts. Their value depends on whether or not the underlying asset process reaches a certain prespecified region before option expiry. An option that is cancelled (activated) when the barrier is breached for the first time is referred to as a knock-out (knock-in) option. By construction, barrier options are particularly suitable for investors who have a directional view on the market. They provide the same upside potential as the corresponding vanilla options but are less expensive due to the knock-out (knock-in) provision. Barrier options are also attractive to market participants seeking a protection against adverse market moves above or below a certain threshold level(s). However, due to the one-touch feature, influential market participants might be incentivized to manipulate the underlying asset price close to the knock-out (knock-in) threshold, hence triggering the cancellation (activation) of certain barrier options. This issue is particularly pronounced in illiquid markets.

To mitigate this problem, Chesney, Jeanblanc and Yor (1997) stipulated a class of occupation-time derivatives called Parisian (barrier) options. These derivatives introduce the notion of excursion time, i.e. the time that the underlying asset price spends (with or without interruption) in a prespecified region. Therefore, a Parisian option is not cancelled or activated immediately upon the occurence of a barrier event. The underlying asset price process has to spend a certain amount of time—referred to as the Parisian window—in the excursion domain. Consequently, Parisian options provide a remedy for potential price manipulations. Since it is more difficult to maintain control over the underlying asset price for an extended period of time, Parisian option holders are better protected from potential adverse actions of their counterparties, and vice versa. Moreover, in contrast to the standard barrier options, the greeks of Parisian options are not discontinuous at the barrier, which is critical from a hedging perspective.

Continuous monitoring of the underlying asset price process naturally introduces the notion of a 'clock' or a 'stopwatch' that is triggered or stopped depending on the barrier event(s) and measures the time spent in the excursion region. More specifically, one can distinguish between two different types of Parisian-style options. A standard Parisian option, or simply a Parisian option, is characterized by a clock which records the duration of uninterrupted excursions. The Parisian clock is activated (reset to zero) each time the underlying process crosses the barrier and enters (exits) the excursion region. On the other hand, a cumulative Parisian option, which is also known as a Par*asian* option, is characterized by a clock that is never reset to zero. Therefore, the Par*asian* clock measures the total time that the underlying process spends in the excursion region.

In this paper, we study the pricing of European and American Parisian options in a flexible jump–diffusion model. Discontinuities in asset returns are most prominent in times of crises when financial markets exhibit sudden and large price moves. Most recently, the Financial crisis of 2007–08 has reiterated the importance of the jump risk for asset return dynamics. Our modelling framework is based on a class of Lévy processes called hyper-exponential jump–diffusion models (HEM), which are introduced in Lipton (2002). There are two reasons for this particular choice. First, any Lévy process with completely monotone Lévy density can be approximated by a HEM model (e.g., see Crosby, Le Saux and Mijatović 2010, Hackmann and Kuznetsov 2016, Jeannin and Pistorius 2010). Popular examples include the Variance–Gamma (VG), Normal–Inverse–Gaussian (NIG), Generalized Hyperbolic (GH), and Carr–Madan–Geman–Yor (CGMY) processes. Second, the option pricing in a HEM setting is analytically tractable, which makes these models particularly interesting for financial engineering applications (e.g., see Cai, Chen and Wan 2009, Cai 2011, Cai and Kou 2012, Hofer and Mayer 2013, Leippold and Vasiljević 2017, in addition to the aforementioned papers).

Our contribution is threefold. First, using the double Laplace–Carson transform of the system of partial integro-differential equations (PIDEs) describing the dynamics of a European or American Parisian option price with respect to the option maturity and the Parisian (excursion) time, we obtain a system of ordinary integro-differential equations (OIDEs) that can be solved in a closed form. Subsequently, the Parisian option price, delta and gamma are computed via a two-dimensional Gaver–Stehfest inversion algorithm. The proposed solution procedure can be interpreted as a two-dimensional generalization of Carr (1998)'s canadization method, hence we call it québécoisation method.[28] Sec-

[28] First, we note that our 'double canadization' approach is motivated by the Parisian option pricing problem, hence we intermingle the two geographic terms and christen our method *québécoisation*, deriving its name from the term *Québécois*

ond, to quantify the impact of jumps on the Parisian option prices and greeks, we provide several numerical examples and discuss the main implications. Finally, we consider a special case in which the underlying asset price is close to the threshold level, and study the conditions under which the standard barrier and Parisian option prices become non-monotonic functions of volatility and jump intensity.

Substantial progress has been already made in Parisian option pricing literature.[29] By and large, European-style Parisian options have attracted the most attention. The pricing of American Parisian options has been studied in only a few papers only (e.g., see Chesney and Gauthier 2006, Haber, Schönbucher and Wilmott 1999, Zhu et al. 2015). From a modelling perspective, the vast majority of the literature assumes a Black–Scholes setting. The only paper which studies Parisian options in a jump–diffusion framework is Albrecher, Kortschak and Zhou (2012). However, they focus on European-style payoffs and consider only Kou (2002)'s double-exponential jump–diffusion model (DEM).[30] To the best of our knowledge, the pricing of American Parisian options with jumps has not been considered in the literature.

The rest of the paper is organized as follows. An overview of the HEM model and the parity/symmetry relations for Parisian options are presented in Section 3.2. The PIDE systems for European and American Parisian up-and-out put options are introduced in Section 3.3. Our main theoretical results for the pricing and disentanglement of randomized European and American Parisian options are presented in Section 3.4. We provide a numerical study of the jump effects on Parisian options in Section 3.6. Finally, we conclude in Section 3.7.

---

that refers to a French-speaking person of the Canadian province of Québéc. Second, we stress that Carr (1998) relied on the Post–Widder inversion, whereas our implementation rests on the Gaver–Stehfest inversion. For further discussion and technical details regarding the two approaches we refer an interested reader to Kimura (2010) and Leippold and Vasiljević (2017).

[29] E.g., see Albrecher, Kortschak and Zhou (2012), Anderluh (2008), Anderluh and van der Weide (2009), Avellaneda and Wu (1999), Bernard, Le Courtois and Quitard-Pinon (2005), Boyarchenko and Boyarchenko (2011), Chesney et al. (1997), Chesney and Gauthier (2006), Costabile (2002), Czarna and Palmowski (2011), Dassios and Wu (2010, 2011), Dassios and Lim (2013), Fujita and Miura (2002), Haber, Schönbucher and Wilmott (1999), Hugonnier (1999), Labart and Lelong (2009), Landriault, Renaud and Zhou (2011), Li and Zhao (2009), Loeffen, Renaud and Zhou (2014), Schröder (2003), Vetzal and Forsyth (1999), Zhu and Stokes (1998), Zhu and Chen (2013).

[30] Some other types of occupation-time derivatives are analyzed in the presence of jump risk Ait Aoudia and Renaud (2016), Cai, Chen and Wan (2010), Wu and Zhu (2016).

3.2 Preliminaries

3.2.1 Hyper-exponential jump-diffusion model

We introduce a filtered probability space $(\Omega, \mathcal{F}, \mathbb{F} = \{\mathcal{F}_t, t \geq 0\}, \mathbb{Q})$ which satisfies the usual assumptions. Since we are interested in option pricing, our starting point is the risk-neutral dynamics of the underlying asset which are given by a hyper-exponential jump-diffusion process

$$\frac{dS_t}{S_{t^-}} = (r - \delta - \lambda\zeta)dt + \sigma dW_t + d\left(\sum_{i=1}^{N_t}(V_i - 1)\right). \tag{3.1}$$

Therefore, the filtration is defined as $\mathcal{F}_t = \sigma(W_s, N_s; s \leq t, \{V_j\})$. The process $\{W_t, t \geq 0\}$ represents a standard Brownian motion under the risk-neutral measure $\mathbb{Q}$. The (domestic) risk-free interest rate is denoted by $r \in \mathbb{R}^+$, the dividend yield is $\delta \in \mathbb{R}_0^+$, and the volatility parameter is $\sigma \in \mathbb{R}^+$.[31] Jumps are modelled by a Poisson process $\{N_t, t \geq 0\}$ with jump intensity parameter $\lambda \in \mathbb{R}^+$. The probability density function (p.d.f.) characterizing the sequence of independent and identically distributed (i.i.d.) hyper-exponential random variables $\{Y_i := \log(V_i) : i = 1, 2, ...\}$ is given by

$$\varphi_Y(y) = \sum_{i=1}^{m} p_i \eta_i e^{-\eta_i y} \mathbb{1}_{\{y \geq 0\}} + \sum_{j=1}^{n} q_j \theta_j e^{\theta_j y} \mathbb{1}_{\{y < 0\}}, \tag{3.2}$$

where probabilities of different kinds of positive and negative jumps are given by $p_i > 0$ for $i = 1, ..., m$ and $q_j > 0$ for $j = 1, ..., n$, respectively.[32] Jump size parameters $\eta_i > 1$ for $i = 1, ..., m$ and $\theta_j > 0$ for $j = 1, ..., n$ correspond to different kinds of discontinuous upward and downward movements, respectively. The symbol $\mathbb{1}_{\{\cdot\}}$ denotes an indicator function.

The dynamics of the log-price process $X_t := \log S_t$ is obtained by applying the Itô lemma,i.e.,

$$X_t := X_0 + \mu t + \sigma W_t + \sum_{i=1}^{N_t} Y_i, \quad X_0 := \log S_0. \tag{3.3}$$

The drift of the log-price process is defined as

$$\mu = r - \delta - \lambda\zeta - \frac{\sigma^2}{2}, \tag{3.4}$$

and the average size of a return jump is given by

$$\zeta := \mathbb{E}\left[e^{Y_1} - 1\right] = \sum_{i=1}^{m} \frac{p_i \eta_i}{\eta_i - 1} + \sum_{j=1}^{n} \frac{q_j \theta_j}{\theta_j + 1} - 1. \tag{3.5}$$

[31] In the case of foreign exchange options, r and δ represent a domestic and a foreign risk-free interest rate, respectively.
[32] The conditional probabilities sum up to unity, i.e., $\sum_{i=1}^{m} p_i + \sum_{j=1}^{n} q_j = 1$.

A very important mathematical object for our analysis is the cumulant generating function (c.g.f.). In the case of an HEM process, the c.g.f. is given by

$$\begin{aligned}\Psi(a) :&= \frac{1}{t}\log\mathbb{E}\left[e^{aX_t}|X_0=0\right] \\ &= \frac{\sigma^2a^2}{2}+\mu a+\lambda\left(\sum_{i=1}^{m}\frac{p_i\eta_i}{\eta_i-a}+\sum_{j=1}^{n}\frac{q_j\theta_j}{\theta_j+a}-1\right),\end{aligned} \tag{3.6}$$

for any $a\in(-\theta_1,\eta_1)$. Without loss of generality we assume that $\eta_1<\eta_2<\cdots<\eta_m$ and $\theta_1<\theta_2<\cdots<\theta_n$. The characteristic equation, which is defined as

$$\Psi(x)=\alpha,\quad \text{for } \alpha>0, \tag{3.7}$$

has exactly $(m+1)$ positive real roots $\{\beta_{i,\alpha}\}_{i=1,\ldots,m+1}$ and $(n+1)$ negative real roots $\{\gamma_{j,\alpha}\}_{j=1,\ldots,n+1}$ such that $-\infty<\gamma_{n+1,\alpha}<-\theta_n<\gamma_{n,\alpha}<-\theta_{n-1}<\cdots<\gamma_{2,n}<-\theta_1<\gamma_{1,\alpha}<0<\beta_{1,\alpha}<\eta_1<\beta_{2,\alpha}<\cdots<\eta_{m-1}<\beta_{m,\alpha}<\eta_m<\beta_{m+1,\alpha}<+\infty$ (e.g., see Lemma 2.1 in Cai (2009), pp. 128–129). The special cases of *(a)* geometric Brownian motion of Black and Scholes (1973), *(b)* spectrally one-sided Lévy models considered in Avram, Chan and Usabel (2002), and *(c)* double-exponential jump-diffusion model of Kou (2002), allow for computation of the respective characteristic roots in a closed-form. More involved HEM models require solving higher order polynomial equations, which can be attained only numerically.

Last but not least, the infinitesimal generator of the Markovian process X_t introduced in equation (3.3) is defined as

$$\begin{aligned}(\mathcal{L}v)(x) :&= \lim_{t\downarrow0}\frac{\mathbb{E}[v(X_t)|X_0=x]-v(x)}{t} \\ &= \frac{\sigma^2}{2}\frac{\partial^2v}{\partial x^2}(x)+\mu\frac{\partial v}{\partial x}(x)+\lambda\int_{-\infty}^{+\infty}[v(x+y)-v(x)]\varphi_Y(y)dy,\end{aligned} \tag{3.8}$$

where $v(\cdot)$ is any twice continuously differentiable function.

3.2.2 Symmetry and parity relations in the presence of jumps

Parisian options come in many flavors. Depending on the exercise style, there exist European and American Parisian call and put options. Furthermore, we distinguish between 'knock-in' and 'knock-out' options, as well as between 'up' and 'down' features. Based on these characteristics, it is possible to construct 32 different combinations in total. Clearly, our goal is not to present results for all existing types of Parisian options. We leverage on the fact that several studies have already demonstrated that

certain symmetry and parity relations hold between different option types. For example, Chesney, Jeanblanc and Yor (1997), Section 6 and Section 7, pp. 176–179, and Chesney and Gauthier (2006), Section 2.1, p. 478, show that there exist symmetry and parity relations between different option types, hence it is enough to consider only several cases to span the entire list of Parisian option contracts. However, their results hold only in the Black-Scholes setting. We generalize these findings and provide the symmetry and parity relations for Parisian options in a hyper-exponential jump-diffusion model.

To motivate our discussion, we begin with an example of symmetry relations for USD/EUR foreign exchange European and American options. The crucial observation is that holding a USD/EUR put option is equivalent to a long position in an appropriately chosen number of EUR/USD calls. This statement holds for vanilla options as well as for standard barrier and Parisian options irrespective of the exercise style (e.g., see Chesney, Jeanblanc and Yor 1997, Schroder 1999, Chesney and Gauthier 2006). Let's assume that the risk-neutral dynamics of the spot exchange rate S_t follows the hyper-exponential jump–diffusion process (3.1). The strike price is K, the barrier level is H, the option contract matures at time T, and the Parisian window is given by D. If we denote European (American) call and put by c and p (C and P), respectively, the following symmetry relations hold:

$$\begin{aligned} p(S_t, K, r, \delta, T; \sigma, \nu) &= S_t K \cdot c(1/S_t, 1/K, \delta, r, T; \sigma, \tilde{\nu}), \\ P(S_t, K, r, \delta, T; \sigma, \nu) &= S_t K \cdot C(1/S_t, 1/K, \delta, r, T; \sigma, \tilde{\nu}). \end{aligned} \tag{3.9}$$

The set of parameters $\nu := \{\lambda, \{p_i, \eta_i\}_{i=1,\ldots,m}, \{q_j, \theta_j\}_{j=1,\ldots,n}\}$ describes a compensated compound Poisson process with hyper-exponential jumps under the risk-neutral measure $\mathbb{Q}$. On the other hand, the set of jump parameters $\tilde{\nu} := \{\tilde{\lambda}, \{\tilde{p}_i, \tilde{\eta}_i\}_{i=1,\ldots,m}, \{\tilde{q}_j, \tilde{\theta}_j\}_{j=1,\ldots,n}\}$ is computed under the equivalent martingale measure $\tilde{\mathbb{Q}}$ which ensures that the discounted and reinvested price process $\{e^{-(r-\delta)t}S_t, t \geq 0\}$ is a martingale. The change of measure for a hyper-exponential jump-diffusion model is based on the Esscher transform. The explicit expressions for the model parameters under the equivalent martingale measure $\tilde{\mathbb{Q}}$ are provided in Cai (2011), Appendix B, pp. 652–653.

Put-call symmetry relations for European and American Parisian options in the HEM model are therefore obtained by putting together the symmetry results for Parisian options in the Black-Scholes

setting presented in Chesney and Gauthier (2006), p.478, and the equation (3.9):

$$\begin{aligned}
\mathcal{O}^p_{do}(S_t, K, H, r, \delta, T, D; \sigma, \nu) &= S_t K \cdot \mathcal{O}^c_{uo}(1/S_t, 1/K, 1/H, \delta, r, T, D; \sigma, \tilde{\nu}), \\
\mathcal{O}^p_{di}(S_t, K, H, r, \delta, T, D; \sigma, \nu) &= S_t K \cdot \mathcal{O}^c_{ui}(1/S_t, 1/K, 1/H, \delta, r, T, D; \sigma, \tilde{\nu}), \\
\mathcal{O}^p_{uo}(S_t, K, H, r, \delta, T, D; \sigma, \nu) &= S_t K \cdot \mathcal{O}^c_{do}(1/S_t, 1/K, 1/H, \delta, r, T, D; \sigma, \tilde{\nu}), \\
\mathcal{O}^p_{ui}(S_t, K, H, r, \delta, T, D; \sigma, \nu) &= S_t K \cdot \mathcal{O}^c_{di}(1/S_t, 1/K, 1/H, \delta, r, T, D; \sigma, \tilde{\nu}).
\end{aligned} \tag{3.10}$$

The option type is denoted by $\mathcal{O} \in \{\pi, \Pi\}$. The letter π designates a European Parisian option contract, and the letter Π stands for an American Parisian option. The first letter in the subscript is either d or u, and it corresponds to a 'down' or 'up' barrier feature, respectively. The second letter in the subscript can be either i ('knock-in') or o ('knock-out'). Finally, the superscript provides information about the exercise style of the option and we use the letter c for calls and the letter p for puts. For example, π^p_{do} stands for a European Parisian down-and-out put option.

Last but not least, European-style Parisian options satisfy 'in–out parity' relations. The sum of a knock-in and knock-out European Parisian option price (with otherwise identical contractual specifications) is equal to their vanilla European counterpart. Therefore, for European Parisian put options, it holds that

$$\begin{aligned}
\pi^p_{do}(S_t, K, H, r, \delta, T, D; \sigma, \nu) + \pi^p_{di}(S_t, K, H, r, \delta, T, D; \sigma, \nu) &= p(S_t, K, r, \delta, T; \sigma, \nu), \\
\pi^p_{uo}(S_t, K, H, r, \delta, T, D; \sigma, \nu) + \pi^p_{ui}(S_t, K, H, r, \delta, T, D; \sigma, \nu) &= p(S_t, K, r, \delta, T; \sigma, \nu).
\end{aligned} \tag{3.11}$$

Similar in-out parity relations hold also for European Parisian call options.

3.3 PIDE systems for Parisian options

In this section, we introduce the systems of partial integro-differential equations describing the evolution of European and American Parisian options. Our approach closely follows the work of Haber, Schönbucher and Wilmott (1999) and Zhu and Chen (2013). However, the exposition in this section is specifically tailored to the québécoisation method which represents the main contribution of our paper. To keep the analysis parsimonious, we focus on up-and-out put options. Results for other option types can be derived with the help of symmetry and parity relations introduced in Section 3.2.2.

The notation used in the rest of the paper is summarized as follows. The option contract expires at time T, the calendar time is given by $t (0 \leq t \leq T)$, and the Parisian window is given by D. The

strike price is K, and the barrier level is H.[33] At time t, the price of the underlying asset is S_t, and the early exercise price (for an American Parisian option) is B_t. The logarithm of the price, strike, barrier and early exercise level are given by $x := \log S$, $\kappa := \log K$, $h := \log H$, and $b := \log B$, respectively. Without loss of generality, we assume that the rebate is equal to zero.

3.3.1 European Parisian up-and-out put

European Parisian up-and-out put (EPUOP) price is a function of log-price x, calendar time t, and Parisian time t_p. The state variable t_p measures the time that the underlying process spends consecutively above the boundary, i.e., the duration of an uninterrupted excursion in the region $x \geq h$. The Parisian time is therefore characterized by

$$\begin{cases} t_p = 0, \quad dt_p = 0, & \text{for} \quad x < h, \\ dt_p = dt, & \text{for} \quad x \geq h. \end{cases} \tag{3.12}$$

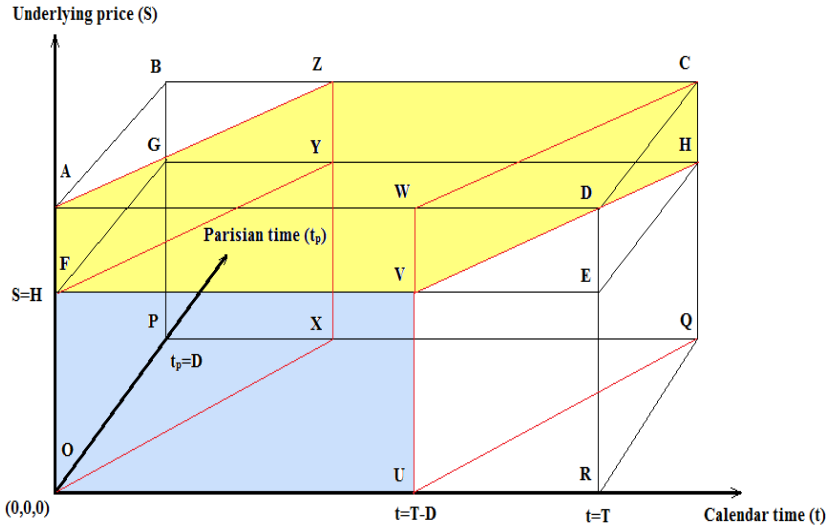

Figure 3.1: **An illustration of the pricing domains.** The blue rectangular area OUVF represents the standard region, and the yellow parellelepiped AWCZYFVH represents the excursion region of a European Parisian up-and-out put option.

First, we consider the *excursion domain*—the region in which the Parisian clock is activated. Following Haber, Schönbucher and Wilmott (1999), we initially define the pricing domain as the

[33] We arbitrarily choose the barrier level to be above the strike price, i.e., $H > K$.

parallelepiped ADCBPORQ in Figure 3.1. By construction, excursion time t_p is always less or equal to calendar time t, hence we exclude the prism AZBGFY from the pricing domain. Furthermore, the Parisian provision matters only if the remaining time to maturity $\tau := T - t$ is greater than the residual Parisian time $\tau_p := D - t_p$. When $\tau \leq \tau_p$, the occupation time condition becomes void and the price of an EPUOP option becomes equal to the price of its vanilla counterpart. Thus, the prism WDCHVE should also be excluded.[34] Therefore, the excursion domain is represented by the parallelepiped AWCZYFVH:

$$\mathscr{E} := \big\{(x,t,t_p) \in \mathbb{R}^3 : h \leq x < \infty, \quad t_p \leq t \leq t_p + T - D, \quad 0 \leq t_p \leq D\big\}. \tag{3.13}$$

Second, we define the *standard region* as the region in which the Parisian clock is inactive and the option price depends only on the calendar time (rectangle OUVF):

$$\mathscr{S} := \big\{(x,t,t_p) \in \mathbb{R}^3 : -\infty < x < h, \quad 0 \leq t \leq T - D, \quad t_p = 0\big\}. \tag{3.14}$$

The standard domain can be further decomposed into two subdomains:

(a) The *payoff domain* is the subspace of the standard domain in which the option is in-the-money:

$$\mathscr{S}_p := \big\{(x,t,t_p) \in \mathbb{R}^3 : -\infty < x < \kappa, \quad 0 \leq t \leq T - D, \quad t_p = 0\big\}, \tag{3.15}$$

(b) The *corridor domain* represents the subspace of the standard domain in which the option is out-of-the-money:

$$\mathscr{S}_c := \big\{(x,t,t_p) \in \mathbb{R}^3 : \kappa \leq x < h, \quad 0 \leq t \leq T - D, \quad t_p = 0\big\}. \tag{3.16}$$

Based on the above definitions of the pricing domains, EPUOP price can be expressed as

$$\pi_{uo}(x,t,t_p) = \begin{cases} \pi^e_{uo}(x,t,t_p), & \text{if } (x,t,t_p) \in \mathscr{E}, \\ \pi^s_{uo}(x,t), & \text{if } (x,t,t_p) \in \mathscr{S}. \end{cases} \tag{3.17}$$

In the excursion domain, the option price satisfies the PIDE

$$\frac{\partial \pi^e_{uo}}{\partial t}(x,t,t_p) + \frac{\partial \pi^e_{uo}}{\partial t_p}(x,t,t_p) + \mathcal{L}\pi^e_{uo}(x,t,t_p) = r\pi^e_{uo}(x,t,t_p). \tag{3.18}$$

[34] Both modifications of the original pricing domain are thoroughly discussed in Zhu and Chen (2013), Section 2, pp. 876–880.

The operator $\mathcal{L}$ is defined in (3.8). The terminal and the boundary condition in the excursion region are, respectively,

$$\begin{aligned} \lim_{t_p \uparrow D} \pi^e_{uo}(x,t,t_p) &= 0, \\ \lim_{x \uparrow +\infty} \pi^e_{uo}(x,t,t_p) &= 0. \end{aligned} \tag{3.19}$$

In the standard domain $\mathscr{S}$, the option price satisfies the PIDE

$$\frac{\partial \pi^s_{uo}}{\partial t}(x,t,t_p) + \mathcal{L}\pi^s_{uo}(x,t,t_p) = r\pi^s_{uo}(x,t,t_p). \tag{3.20}$$

The terminal and the boundary condition in the standard region are, respectively,

$$\begin{aligned} \lim_{t \uparrow T-D} \pi^s_{uo}(x,t) &= \lim_{t \uparrow T-D} p(x,t;\kappa,T) = p(x,0;\kappa,D), \\ \lim_{x \downarrow -\infty} \pi^s_{uo}(x,t) &= e^{\kappa - r(T-t)}. \end{aligned} \tag{3.21}$$

The function $p : \mathbb{R} \times \mathbb{R}^+ \mapsto \mathbb{R}^+$ represents the price of a vanilla European put option. The value-matching and a smooth-pasting conditions at the boundary between the payoff domain $\mathscr{S}_p$ and the corridor domain $\mathscr{S}_c$ are, respectively,

$$\begin{aligned} \lim_{x \uparrow \kappa} \pi^s_{uo}(x,t) &= \lim_{x \downarrow \kappa} \pi^s_{uo}(x,t), \\ \lim_{x \uparrow \kappa} \frac{\partial \pi^s_{uo}}{\partial x}(x,t) &= \lim_{x \downarrow \kappa} \frac{\partial \pi^s_{uo}}{\partial x}(x,t). \end{aligned} \tag{3.22}$$

Finally, to close the system of equations, we impose a value-matching and a smooth-pasting condition at the boundary between the standard domain $\mathscr{S}$ and the excursion domain $\mathscr{E}$:

$$\begin{aligned} \lim_{x \uparrow h} \pi^s_{uo}(x,t) &= \lim_{x \downarrow h} \pi^e_{uo}(x,t,0), \\ \lim_{x \uparrow h} \frac{\partial \pi^s_{uo}}{\partial x}(x,t) &= \lim_{x \downarrow h} \frac{\partial \pi^e_{uo}}{\partial x}(x,t,0). \end{aligned} \tag{3.23}$$

We note that the excursion time t_p is set to zero in the equation above because we do not consider the case of an 'already started excursion'.

The introduced PIDE system is difficult to solve analytically. However, we are able to simplify our problem and effectively reduce the dimensionality of the PIDE in the excursion domain by applying the rotational transform of the time-coordinate system proposed by Zhu and Chen (2013), Section 3.1, pp. 881–882. Leveraging the fact that the calendar and Parisian clocks are ticking at the same rate in the excursion domain, the partial derivatives of the option price with respect to the calendar time

t and Parisian time t_p in (3.18) can be replaced by a directional derivative

$$\mathcal{T}_e : \quad \frac{\partial}{\partial t} + \frac{\partial}{\partial t_p} \;\longrightarrow\; \sqrt{2}\,\frac{\partial}{\partial t_h}. \tag{3.24}$$

The new excursion clock t_h is ticking at a rate which is $\sqrt{2}$ times higher than the rate associated with the calendar clock t and the Parisian clock t_p. To normalize the time flow, we rescale the new excursion clock by substituting t_h with $t'_h := t_h/\sqrt{2}$. Therefore, the time dependence in the excursion domain is now fully captured by a single time variable

$$t_e := t'_h \mathbb{1}_{\{X_t \geq h\}}, \tag{3.25}$$

which we call hybrid excursion time. Furthermore, the transformation $\mathcal{T}_e$ introduces a new clock in the standard domain—standard time t_s—which is given by

$$t_s := t\mathbb{1}_{\{X_t < h\}} + t_l \mathbb{1}_{\{X_t \geq h\}}, \tag{3.26}$$

where t_l represents the last exit time from the standard domain:

$$t_l := \begin{cases} 0, & \text{if } \big\{0 \leq u \leq t \big| X_u < h\big\} = \emptyset, \\ \sup\limits_{0 \leq u \leq t} \big\{u \big| X_u < h\big\}, & \text{otherwise.} \end{cases} \tag{3.27}$$

The standard time t_s and the calendar time t are identical in the standard domain. The standard clock is paused as soon as the underlying process enters the excursion domain, and is equal to the last exit time t_l from the standard domain. Therefore, the standard time is merely a parameter in the excursion domain. If the process re-enters the standard domain, the standard clock counter immediately jumps to the calendar time and starts ticking again. Simultaneously, the hybrid excursion clock is set to zero and paused until the next excursion is activated.

We adjust the notation in equations (3.14)–(3.23) accordingly. First, the (hybrid) excursion domain and the two standard subdomains are now defined as

$$\begin{cases} \tilde{\mathscr{E}} & := \big\{(x, t_s, t_e) \in \mathbb{R}^3 : h \leq x < \infty, \;\; t_s = t_l, \;\; 0 \leq t_e \leq D\big\}, \\ \tilde{\mathscr{S}_c} & := \big\{(x, t_s, t_e) \in \mathbb{R}^3 : \kappa \leq x < h, \;\; 0 \leq t_s \leq T - D, \;\; t_e = 0\big\}, \\ \tilde{\mathscr{S}_p} & := \big\{(x, t_s, t_e) \in \mathbb{R}^3 : -\infty < x < \kappa, \;\; 0 \leq t_s \leq T - D, \;\; t_e = 0\big\}. \end{cases} \tag{3.28}$$

Additionally, we define $\tilde{\mathscr{S}} := \tilde{\mathscr{S}}_c \cup \tilde{\mathscr{S}}_p$. EPUOP option price (3.17) becomes

$$\tilde{\pi}_{uo}(x, t_s, t_e) = \begin{cases} \tilde{\pi}^e_{uo}(x, t_e), & \text{if } (x, t_s, t_e) \in \tilde{\mathscr{E}}, \\ \tilde{\pi}^s_{uo}(x, t_s), & \text{if } (x, t_s, t_e) \in \tilde{\mathscr{S}}. \end{cases} \tag{3.29}$$

The PIDE system described by equations (3.20) and (3.18) is now given by

$$\begin{cases} \dfrac{\partial \tilde{\pi}^e_{uo}}{\partial t_e}(x, t_e) + \mathcal{L}\tilde{\pi}^e_{uo}(x, t_e) = r\tilde{\pi}^e_{uo}(x, t_e), & \text{if } (x, t_s, t_e) \in \tilde{\mathscr{E}}, \\ \dfrac{\partial \tilde{\pi}^s_{uo}}{\partial t_s}(x, t_s) + \mathcal{L}\tilde{\pi}^s_{uo}(x, t_s) = r\tilde{\pi}^s_{uo}(x, t_s), & \text{if } (x, t_s, t_e) \in \tilde{\mathscr{S}}. \end{cases} \tag{3.30}$$

The terminal and boundary conditions (3.19) in the excursion domain are now given by

$$\begin{aligned} \lim_{t_e \uparrow D} \tilde{\pi}^e_{uo}(x, t_e) &= 0, \\ \lim_{x \uparrow +\infty} \tilde{\pi}^e_{uo}(x, t_e) &= 0. \end{aligned} \tag{3.31}$$

In the standard region $\tilde{\mathscr{S}}$, the terminal and boundary conditions (3.21) and the high-contact condtions (3.22) become

$$\begin{aligned} \lim_{t_s \uparrow T-D} \tilde{\pi}^s_{uo}(x, t_s) &= \lim_{t_s \uparrow T-D} p(x, t_s + t_e; \kappa, T) = p(x, t_e; \kappa, D), \\ \lim_{x \downarrow -\infty} \tilde{\pi}^s_{uo}(x, t_s) &= e^{\kappa - r(T - t_s)}, \\ \lim_{x \uparrow \kappa} \tilde{\pi}^s_{uo}(x, t_s) &= \lim_{x \downarrow \kappa} \tilde{\pi}^s_{uo}(x, t_s), \\ \lim_{x \uparrow \kappa} \frac{\partial \tilde{\pi}^s_{uo}}{\partial x}(x, t_s) &= \lim_{x \downarrow \kappa} \frac{\partial \tilde{\pi}^s_{uo}}{\partial x}(x, t_s). \end{aligned} \tag{3.32}$$

Finally, the value-matching and smooth-pasting conditions (3.23) at the boundary between the standard and the excursion domains are now given by

$$\begin{aligned} \lim_{x \uparrow h} \tilde{\pi}^s_{uo}(x, t_s) &= \lim_{x \downarrow h} \tilde{\pi}^e_{uo}(x, 0), \\ \lim_{x \uparrow h} \frac{\partial \tilde{\pi}^s_{uo}}{\partial x}(x, t_s) &= \lim_{x \downarrow h} \frac{\partial \tilde{\pi}^e_{uo}}{\partial x}(x, 0). \end{aligned} \tag{3.33}$$

3.3.2 American Parisian up-and-out put

The early exercise feature of American-style options—which is also known in the literature as the free boundary problem (e.g., see Detemple 2005, Jeanblanc, Yor and Chesney 2009)—brings in an additional layer of complexity. Generally, a continuation domain (in which the option holder prefers to keep the contract), and an exercise domain (in which the option holder prefers to immediately exercise the contract and collect the proceeds thereupon) exist. The two regions are separated by a non-linear

boundary which is not known in advance and has to be computed jointly with the option price. Since the transformation (3.24) applies irrespectively of the option contract type, we introduce directly the transformed PIDE system for APUOP options.

First, we note that the excursion and corridor domains remain the same. On the other hand, the early exercise optionality divides the payoff domain into two subdomains:

(a) The *payoff continuation domain*

$$\tilde{\mathscr{S}}_{pc} := \big\{(x, t_s, t_e) \in \mathbb{R}^3 : b_{t_s} < x < \kappa, \;\; 0 \le t_s \le T - D, \;\; t_e = 0\big\}, \tag{3.34}$$

(b) The *payoff exercise domain*

$$\tilde{\mathscr{S}}_{pe} := \big\{(x, t_s, t_e) \in \mathbb{R}^3 : -\infty < x \le b_{t_s}, \;\; 0 \le t_s \le T - D, \;\; t_e = 0\big\}. \tag{3.35}$$

Furthermore, we denote the *standard continuation domain* (which includes the corridor and the payoff continuation subdomains) by $\tilde{\mathscr{S}}^* := \tilde{\mathscr{S}}_c \cup \tilde{\mathscr{S}}_{pc} = \tilde{\mathscr{S}} \setminus \tilde{\mathscr{S}}_{pe}$. Therefore, APUOP price can be decomposed in the form

$$\tilde{\Pi}_{uo}(x, t_s, t_e) = \begin{cases} \tilde{\Pi}^e_{uo}(x, t_e), & \text{if } \; (x, t_s, t_e) \in \tilde{\mathscr{E}}, \\ \tilde{\Pi}^s_{uo}(x, t_s), & \text{if } \; (x, t_s, t_e) \in \tilde{\mathscr{S}}^*, \\ e^{\kappa} - e^{x}, & \text{if } \; (x, t_s, t_e) \in \tilde{\mathscr{S}}_{pe}. \end{cases} \tag{3.36}$$

The early exercise boundary divides the payoff region into subregions (3.34) and (3.35), i.e.,

$$b_{t_s} := \sup\big\{x : \tilde{\Pi}^s_{uo}(x, t_s) = e^{\kappa} - e^{x}\big\}. \tag{3.37}$$

We note that the APUOP early exercise boundary is monotone in the barrier level H and in the Parisian window D.

APUOP option price dynamics are described by the PIDE system

$$\begin{cases} \dfrac{\partial \tilde{\Pi}^e_{uo}}{\partial t_e}(x, t_e) + \mathcal{L}\tilde{\Pi}^e_{uo}(x, t_e) = r\tilde{\Pi}^e_{uo}(x, t_e), & \text{if } \; (x, t_s, t_e) \in \tilde{\mathscr{E}}, \\ \dfrac{\partial \tilde{\Pi}^s_{uo}}{\partial t_s}(x, t_s) + \mathcal{L}\tilde{\Pi}^s_{uo}(x, t_s) = r\tilde{\Pi}^s_{uo}(x, t_s), & \text{if } \; (x, t_s, t_e) \in \tilde{\mathscr{S}}^*. \end{cases} \tag{3.38}$$

The value-matching and smooth-pasting conditions at the early exercise boundary are given by

$$\begin{aligned} \lim_{x \downarrow b_{t_s}} \tilde{\Pi}^s_{uo}(x, t_s) &= e^{\kappa} - e^{b_{t_s}}, \\ \lim_{x \downarrow b_{t_s}} \frac{\partial \tilde{\Pi}^s_{uo}}{\partial x}(x, t_s) &= -e^{b_{t_s}}. \end{aligned} \tag{3.39}$$

The terminal condition in the standard continuation domain is

$$\lim_{t_s \uparrow T-D} \tilde{\Pi}^s_{uo}(x, t_s) = P(x, t_e; \kappa, D), \tag{3.40}$$

where $P : \mathbb{R} \times \mathbb{R}^+ \mapsto \mathbb{R}^+$ represents the price of a vanilla American put option. The boundary conditions in this region are

$$\begin{aligned} \lim_{t_e \uparrow D} \tilde{\Pi}^e_{uo}(x, t_e) &= 0, \\ \lim_{x \uparrow +\infty} \tilde{\Pi}^e_{uo}(x, t_e) &= 0. \end{aligned} \tag{3.41}$$

Finally, the value-matching and smooth-pasting conditions at the boundary between the standard continuation domain and the excursion domain are

$$\begin{aligned} \lim_{x \uparrow h} \tilde{\Pi}^s(x, t_s) &= \lim_{x \downarrow h} \tilde{\Pi}^e(x, 0) \\ \lim_{x \uparrow h} \frac{\partial \tilde{\Pi}^s}{\partial x}(x, t_s) &= \lim_{x \downarrow h} \frac{\partial \tilde{\Pi}^e}{\partial x}(x, 0). \end{aligned} \tag{3.42}$$

3.4 Randomization approach for Parisian options

In this section, we first recall the definition of the (single) Laplace-Carson transform (LCT) and briefly explain the idea behind the canadization method for the pricing of vanilla and standard barrier options. Subsequently, we introduce the double Laplace-Carson transform (DLCT) and the québécoisation method for the pricing of Parisian options. To demonstrate our method, we derive closed-form solutions for randomized European and American Parisian up-and-out put options.

3.4.1 Canadization method: Maturity randomization

For any locally integrable function $f : \mathbb{R}^+ \to \mathbb{R}$ and for all $\alpha \in \mathbb{R}^+$, Laplace-Carson transform (LCT) is defined as

$$\check{f}(\alpha) := (\mathscr{LC})_z [f(z)](\alpha) := \alpha \int_0^{+\infty} e^{-\alpha z} f(z) dz. \tag{3.43}$$

Having computed the transform (either numerically or analytically), the original function can be evaluated using an inversion algorithm. One possible choice is the Gaver-Stehfest inversion algorithm (GS)

$$f_M(z) = \sum_{k=1}^{2M} \xi_{k,M} \check{f}\left(\frac{k \log(2)}{z}\right), \quad M \in \mathbb{N}, \tag{3.44}$$

where $\lfloor a \rfloor$ is defined as the greatest number $a' \in \mathbb{N}$ such that $a' \leq a$. This formula already includes the linear Salzer convergence acceleration scheme (e.g.,see Stehfest 1970). The summation coefficients are given by

$$\xi_{k,M} := \frac{(-1)^{M+k}}{k} \sum_{j=\lfloor (k+1)/2 \rfloor}^{\min\{k,M\}} \frac{j^{M+1}}{M!} \binom{M}{j} \binom{2j}{j} \binom{j}{k-j}. \tag{3.45}$$

For M large, the approximation (3.44) converges to the true value of the original function:

$$\lim_{M \to \infty} f_M(z) = f(z). \tag{3.46}$$

Formal proof of the convergence of the Gaver-Stehfest algorithm is provided in Kuznetsov (2013).[35]

Canadized options are defined as options whose time to maturity is an exponentially distributed random variable. Therefore, it follows from equation (3.43) that the price of a canadized option is an LCT of the original option price w.r.t. the time to maturity. Due to the memoryless property of the exponential class of distributions, an LCT of the PIDE describing the option price dynamics eliminates the time dependence. This implies that the original pricing problem reduces to the one of solving an OIDE, which is analytically tractable.

3.4.2 Québécoisation method: Maturity–excursion randomization

Equation (3.43) can be generalized to the two-dimensional case. For any $\alpha_1, \alpha_2 \in \mathbb{R}^+$ and a locally integrable function $g : \mathbb{R}^+ \times \mathbb{R}^+ \to \mathbb{R}$, double Laplace-Carson transform (DLCT) is defined as

$$\begin{aligned} \hat{g}(\alpha_1, \alpha_2) &:= (\mathscr{DLC})_{z_1,z_2} [g(z_1, z_2)](\alpha_1, \alpha_2) \\ &:= \alpha_1 \alpha_2 \int_0^{+\infty} e^{-\alpha_2 z_2} \int_0^{+\infty} e^{-\alpha_1 z_1} g(z_1, z_2) dz_1 dz_2. \end{aligned} \tag{3.47}$$

Following Abate and Whitt (2006), Section 3 and Section 4, pp. 413–414, a DLCT can be computed by successively applying two, one-dimensional LCTs:

$$\begin{aligned} \check{g}(\alpha_1, z_2) &:= \alpha_1 \int_0^{+\infty} e^{-\alpha_1 z_1} g(z_1, z_2) dz_1, \\ \hat{g}(\alpha_1, \alpha_2) &:= \alpha_2 \int_0^{+\infty} e^{-\alpha_2 z_2} \check{g}(\alpha_1, z_2) dz_2. \end{aligned} \tag{3.48}$$

Similarly, the inversion is carried through a two-step procedure. For given values of z_1 and z_2, we first invert the function $\hat{g}(\alpha_1, \alpha_2)$ w.r.t. the second argument (while we keep the first argument constant)

[35] Several authors propose using the GS method for option pricing (e.g., see Hofer and Mayer 2013, Kimura 2010, Leippold and Vasiljević 2017, Sepp 2004) and we follow this strand of literature.

and we obtain the function $\check{g}(\alpha_1, z_2)$. Subsequently, we invert the function $\check{g}(\alpha_1, z_2)$ w.r.t. the first argument. This two-step procedure can be summarized as follows:

$$\begin{aligned} \check{g}_N(\alpha_{1,m}, z_2) &:= \sum_{n=1}^{2N} \xi_{n,N} \hat{g}(\alpha_{1,m}, \alpha_{2,n}), \\ g_{M,N}(z_1, z_2) &:= \sum_{m=1}^{2M} \xi_{m,M} \check{g}_N(\alpha_{1,m}, z_2), \end{aligned} \tag{3.49}$$

where $\alpha_{1,m} := m \log(2)/z_1$ $(m = 1, 2, ..., 2M,\ M \in \mathbb{N})$ and $\alpha_{2,n} := n \log(2)/z_2$ $(n = 1, 2, ..., 2N,$ $N \in \mathbb{N})$. The coefficients $\xi_{m,M}$ and $\xi_{n,N}$ can be computed from equation (3.45). The two-dimensional Gaver-Stehfest inversion algorithm yields an approximation $g_{M,N}(z_1, z_2)$ of the original function's true value $g(z_1, z_2)$. When M and N become large, the following convergence result holds:

$$\lim_{M,N \to \infty} g_{M,N}(z_1, z_2) = g(z_1, z_2). \tag{3.50}$$

The convergence is a direct consequence of (3.46). In practice, the inner loop is crucial for the overall accuracy of the method. The intermediary function $\check{g}_N(\alpha_{1,m}, z_2)$ has to be computed with sufficient accuracy in order to obtain satisfactory results in the outer loop. Therefore, a general recommendation is to impose the condition $M < N$ (e.g., see Choudhury, Lucantoni and Whitt 1997, Section 8, pp. 461–462). However, Abate and Whitt (2006), Section 8, pp. 418–419, show that the case $M = N$ is good enough for many applications, and we follow their recommendation in our implementation.

DLCT plays a crucial role in our paper. First, assuming that the residual maturity $\tau_s := T - D - t_s$ and the residual hybrid excursion time $\tau_e := D - t_e$ are (independently) exponentially distributed, we can define a *québécoised Parisian option*. Essentially, this is a doubly canadized contract, and its price can be computed as a DLCT of the Parisian option price with fixed maturity and Parisian window. Similar to the discussion in Section 3.4.1, québécoisation of a Parisian option simplifies the pricing problem by transforming the PIDE system into an OIDE system, which can be solved in closed form. The price of the original (i.e. non-randomized) contract is then obtained via the two-dimensional GS inversion algorithm summarized above. Last but not least, in the case of American Parisian options, we emphasize that the randomized early exercise boundary is flat because the transformed option price is a time independent function.[36]

[36]Two comments are due. First, in the case of American Parisian options, the québécoised early exercise boundary is flat because the transformed option price is time-independent. This is another consequence of the memorylessness of exponential distributions. Second, the results in Appendix B.3 for the greeks of canadized vanilla European and American options can be easily generalized to the case of québécoised European and American Parisian greeks.

3.5 Québécoised EPUOP and APUOP options

We now consider the pricing of Parisian options in the hyper-exponential jump–diffusion model introduced in Section 3.2.1. The dynamics of an EPUOP option price are described by equations (3.28)–(3.33). By applying the québécoisation nmethod presented in the previous section, we obtain the price of the randomized EPUOP option in a closed form.

Theorem 3.5.1 (**Pricing of Québécoised EPUOP options**). *Assume that the asset price process* $\{S_u, t \leq u \leq T\}$ *is described by the hyper-exponential model* (3.1)–(3.2). *Consider an EPUOP option introduced in Section 3.3.1.*

(a) In the (hybrid) excursion domain, the québécoised option price is given by

$$\hat{\tilde{\pi}}^e_{uo}(x, \alpha^e_{k_e}) = \sum_{j=1}^{n+1} A^-_j e^{\gamma_{j,r+\alpha^e_{k_e}}(x-h)}. \tag{3.51}$$

(b) In the corridor domain, the québécoised option price is given by

$$\hat{\tilde{\pi}}^s_{uo}(x, \alpha^s_{k_s}) = \sum_{i=1}^{m+1} B^+_i e^{\beta_{i,r+\alpha^s_{k_s}}(x-h)} + \sum_{j=1}^{n+1} B^-_j e^{\gamma_{j,r+\alpha^s_{k_s}}(x-h)} + \sum_{j=1}^{n+1} \overline{\omega}'_j e^{\gamma_{j,r+\alpha^e_{k_e}}(x-\kappa)}. \tag{3.52}$$

(c) In the payoff domain, the québécoised option price is given by

$$\begin{aligned} \hat{\tilde{\pi}}^s_{uo}(x, \alpha^s_{k_s}) = &\sum_{i=1}^{m+1} C^+_i e^{\beta_{i,r+\alpha^s_{k_s}}(x-\kappa)} + \sum_{i=1}^{m+1} \underline{\omega}'_i e^{\beta_{i,r+\alpha^e_{k_e}}(x-\kappa)} \\ &+ \frac{\alpha^s_{k_s}}{\alpha^s_{k_s}+r}\frac{\alpha^e_{k_e}}{\alpha^e_{k_e}+r}e^{\kappa} - \frac{\alpha^s_{k_s}}{\alpha^s_{k_s}+\delta}\frac{\alpha^e_{k_e}}{\alpha^e_{k_e}+\delta}e^{x}. \end{aligned} \tag{3.53}$$

For $M_s, M_e \in \mathbb{N}$ *the parameters* $\{\alpha^s_{k_s}\}_{k_s=1,2,...,2M_s}$ *are* $\alpha^s_{k_s} := k_s \log(2)/(\tau_s - D)$, *and the parameters* $\{\alpha^e_{k_e}\}_{k_e=1,2,...,2M_e}$ *are and* $\alpha^s_{k_e} := k_e \log(2)/\tau_e$, *where* $\tau_s := T - t_s$ *and* $\tau_e := D - t_e$. *Positive and negative roots of the characteristic equation* $\Psi(u) = r + \alpha^\rho_{k_\rho}$, *where* $\rho \in \{e, s\}$, *are denoted by* $\{\beta_{i,r+\alpha^\rho_{k_\rho}}\}_{i=1,2,...,m+1}$ *and* $\{\gamma_{j,r+\alpha^\rho_{k_\rho}}\}_{j=1,2,...,n+1}$, *respectively. The Lévy exponent* $\Psi(\cdot)$ *is defined in* (3.6). *The coefficients* $\{A^-_j\}_{j=1,...,n+1}$, $\{B^+_i\}_{i=1,...,m+1}$, $\{B^-_j\}_{j=1,...,n+1}$, *and* $\{C^+_i\}_{i=1,...,m+1}$ *solve the system of linear equations*

$$\mathbf{P}\mathbf{u}_e = \mathbf{p}_e, \tag{3.54}$$

where $\mathbf{u}_e := (A^-_1, ..., A^-_{n+1}, B^+_1, ..., B^+_{m+1}, B^-_1, ..., B^-_{n+1}, C^+_1, ..., C^+_{m+1})'$, $\mathbf{p}_e$ *is a (2m+2n+4)-dimensional column vector, and* $\mathbf{P}$ *is a (2m+2n+4)-dimensional square matrix. Elements of the vector* $\mathbf{p}_e$ *and the matrix* $\mathbf{P}$ *are given in the appendix.*

Generally, the price of an American-style option can be written as a sum of the corresponding European-style option and the early exercise premium (EEP), e.g., see Kim (1990), Jacka (1991), and Carr, Jarrow and Myneni (1992). Therefore, an APUOP option value can be decomposed in the form

$$\tilde{\Pi}_{uo}(x,t_s,t_e) = \tilde{\pi}_{uo}(x,t_s,t_e) + \tilde{\epsilon}_{uo}(x,t_s,t_e). \tag{3.55}$$

From expressions (3.29), (3.36) and (3.55), it follows that the EEP of an APUOP option is given by

$$\tilde{\epsilon}_{uo}(x,t_s,t_e) = \begin{cases} \tilde{\epsilon}^e_{uo}(x,t_e), & \text{if } (x,t_s,t_e) \in \tilde{\mathscr{E}}, \\ \tilde{\epsilon}^s_{uo}(x,t_s), & \text{if } (x,t_s,t_e) \in \tilde{\mathscr{S}}^*, \\ e^{\kappa} - e^x - \tilde{\pi}^s_{uo}(x,t_s), & \text{if } (x,t_s,t_e) \in \tilde{\mathscr{S}}_{pe}. \end{cases} \tag{3.56}$$

Therefore, from the PIDE systems for EPUOP and APUOP options, we deduce the dynamics of the corresponding Parisian EEP in the form

$$\begin{cases} \dfrac{\partial \tilde{\epsilon}^e_{uo}}{\partial t_e}(x,t_e) + \mathcal{L}\tilde{\epsilon}^e_{uo}(x,t_e) = r\tilde{\epsilon}^e_{uo}(x,t_e), & \text{if } (x,t_s,t_e) \in \tilde{\mathscr{E}}, \\ \dfrac{\partial \tilde{\epsilon}^s_{uo}}{\partial t_s}(x,t_s) + \mathcal{L}\tilde{\epsilon}^s_{uo}(x,t_s) = r\tilde{\epsilon}^s_{uo}(x,t_s), & \text{if } (x,t_s,t_e) \in \tilde{\mathscr{S}}^*. \end{cases} \tag{3.57}$$

The value-matching and smooth-pasting conditions at the boundary between the standard continuation and the payoff domains are, respectively, given by

$$\begin{aligned} \lim_{x \downarrow b_{t_s}} \tilde{\epsilon}^s_{uo}(x,t_s) &= e^{\kappa} - e^{b_{t_s}} - \tilde{\pi}^s_{uo}(x,t_s)\big|_{x=b_{t_s}}, \\ \lim_{x \downarrow b_{t_s}} \frac{\partial \tilde{\epsilon}^s_{uo}}{\partial x}(x,t_s) &= -e^{b_{t_s}} - \frac{\partial \tilde{\pi}^s_{uo}}{\partial x}(x,t_s)\Big|_{x=b_{t_s}}. \end{aligned} \tag{3.58}$$

The terminal conditions for the Parisian EEP in the regions $\tilde{\mathscr{E}}$ and $\tilde{\mathscr{S}}^*$ are, respectively,

$$\begin{aligned} \lim_{t_e \uparrow D} \tilde{\epsilon}^e_{uo}(x,t_e) &= 0, \\ \lim_{t_s \uparrow T-D} \tilde{\epsilon}^s_{uo}(x,t_s) &= \lim_{t_s \uparrow T-D} \epsilon_p(x, t_s + t_e; \kappa, T) = \epsilon_p(x,t_e;\kappa,D), \end{aligned} \tag{3.59}$$

where $\epsilon_p : \mathbb{R} \times \mathbb{R}^+ \mapsto \mathbb{R}^+$ is the vanilla EEP, i.e., $\epsilon_p(x,t_e;\kappa,D) := P(x,t_e;\kappa,D) - p(x,t_e;\kappa,D)$. The boundary condition in the excursion region is

$$\lim_{x \uparrow +\infty} \tilde{\epsilon}^e_{uo}(x,t_e) = 0. \tag{3.60}$$

Finally, the value-matching and smooth-pasting conditions at the boundary between the standard continuation and the excursion domain are, respectively, given by

$$\begin{aligned}\lim_{x\uparrow h}\tilde{\epsilon}^s_{uo}(x,t_s) &= \lim_{x\downarrow h}\tilde{\epsilon}^e_{uo}(x,0),\\ \lim_{x\uparrow h}\frac{\partial\tilde{\epsilon}^s_{uo}}{\partial x}(x,t_s) &= \lim_{x\downarrow h}\frac{\partial\tilde{\epsilon}^e_{uo}}{\partial x}(x,0).\end{aligned} \tag{3.61}$$

Theorem 3.5.2 (**Pricing of Québécoised APUOP options**). *Assume that the asset price process* $\{S_u, t \le u \le T\}$ *is described by the hyper-exponential model* (3.1)–(3.2). *Consider an APUOP option introduced in Section 3.3.2.*

(a) In the (hybrid) excursion domain, the québécoised early exercise premium is given by

$$\hat{\tilde{\epsilon}}^e_{uo}(x,\alpha^e_{k_e}) = \sum_{j=1}^{n+1} D_j^- e^{\gamma_{j,r+\alpha^e_{k_e}}(x-h)}. \tag{3.62}$$

(b) In the standard continuation domain, the québécoised early exercise premium is given by

$$\hat{\tilde{\epsilon}}^s_{uo}(x,\alpha^s_{k_s}) = \sum_{i=1}^{m+1} F_i^+ e^{\beta_{i,r+\alpha^s_{k_s}}(x-h)} + \sum_{j=1}^{n+1} F_j^- e^{\gamma_{j,r+\alpha^s_{k_s}}(x-h)} + \sum_{j=1}^{n+1} v'_j e^{\gamma_{j,r+\alpha^e_{k_e}}(x-\hat{b})}. \tag{3.63}$$

(c) In the payoff exercise domain, the québécoised early exercise premium is given by

$$\hat{\tilde{\epsilon}}^s_{uo}(x,\alpha^s_{k_s}) = e^{\kappa} - e^x - \hat{\tilde{\pi}}^s_{uo}(x,\alpha^s_{k_s}). \tag{3.64}$$

The parameters $\{\alpha^s_{k_s}\}_{k_s=1,2,...,2M_s}$ *and* $\{\alpha^e_{k_e}\}_{k_e=1,2,...,2M_e}$, *and the coefficients* $\{\beta_{i,r+\alpha^\rho_{k_\rho}}\}_{i=1,2,...,m+1}$ *and* $\{\gamma_{j,r+\alpha^\rho_{k_\rho}}\}_{j=1,2,...,n+1}$ *for* $\rho \in \{e,s\}$ *are defined in Theorem 3.5.1. The coefficients* $\{D_j^-\}_{j=1,...,n+1}$, $\{F_i^+\}_{i=1,...,m+1}$, *and* $\{F_j^-\}_{j=1,...,n+1}$ *solve the system of linear equations*

$$\mathbf{Q}\mathbf{u}_a = \mathbf{q}_a, \tag{3.65}$$

where $\mathbf{u}_a := (D_1^-, ..., D_{n+1}^-, F_1^+, ..., F_{m+1}^+, F_1^-, ..., F_{n+1}^-)'$, $\mathbf{q}_a$ *is a (m+2n+3)-dimensional column vector, and* $\mathbf{Q}$ *is a (m+2n+3)-dimensional square matrix. Elements of the vector* $\mathbf{q}_a$ *and the matrix* $\mathbf{Q}$, *as well as the québécoised early exercise boundary* $\hat{b}$, *are given in the appendix.*

3.6 The impact of jumps on Parisian options

The vast majority of Parisian option pricing literature is related to the Black–Scholes model. The inclusion of jumps in the model naturally raises questions about their importance. In this section, we investigate the effects of jump risk on the European and American Parisian up-and-out put options prices and hedging parameters in the DEM framework—which is characterized with a diffusion parameter σ and a set of jump parameters $\{\lambda, p, \eta, \theta\}$. This model reduces to the Black–Scholes setting if the jump intensity is equal to zero ($\lambda = 0$). It is important to stress that Albrecher, Kortschak and Zhou (2012) studied European Parisian up-and-in call options (EPUIC) in a DEM setting. To the best of our knowledge, there is no known connection between EPUOP and EPUIC options. Therefore, our numerical investigation completes our financial knowledge and contributes to our understanding of Parisian options in a broader sense.

First, in Table 3.1, we provide numerical examples of vanilla, standard barrier and Parisian European and American option prices. For simplicity, we consider a set of double-exponential jump–diffusion model specifications. The computed option prices are monotone functions of the volatility, the jump intensity, and the average positive and negative jump size (the reciprocals of the respective jump parameter values). Second, in Figure 3.2, we plot EPUOP option price and APUOP EEP as functions of the underlying asset price S_t and the Parisian window D in a double-exponential jump–diffusion model. We observe that both EPUOP and APUOP EEP are increasing functions of the underlying asset price and the Parisian window (Panels A and B). Additionally, Parisian delta (gamma) is non-positive (non-negative). In the limiting case when the Parisian window is equal to zero (equal of greater than the option's time to maturity), Parisian option price, delta, and gamma converge to the values of their standard barrier (vanilla) counterparts. Hence, for $D = 0$, at $S_t = H$ Parisian delta is discontinuous and Parisian gamma diverges, whereas for $S_t > H$ both Parisian delta and gamma are equal to zero since options is knocked-out. Consequently, hedging standard barrier options is a difficult task because their greeks are not well-behaved functions around barrier level H. On the other hand, Parisian delta and gamma are smooth functions of the underlying asset price, which is demonstrated in Panels C and D, E and F.

Table 3.1: **Numerical examples.** Prices of ATM and OTM vanilla, standard barrier, and Parisian European and American options in a double-exponential jump-diffusion model using the québécoisation method. The time to maturity is $\tau = 1$ year, and the Parisian window D is assumed to be either one week (1w) or one month (1m). The risk-free rate is $r = 0.05$, the dividend yield is $\delta = 0.01$, and the conditional probabilities of positive and negative jumps are $p = q = 0.5$.

Panel A: ATM options ($S_t = 100$, $K = 100$, $H = 110$).

Parameters				Vanilla		Barrier		Parisian (1w)		Parisian (1m)	
σ	λ	η	θ	Euro.	Amer.	Euro.	Amer.	Euro.	Amer.	Euro.	Amer.
0.2	1	25	25	6.23	6.65	4.70	5.04	5.20	5.72	5.64	5.95
0.2	1	25	50	6.13	6.54	4.66	5.00	5.14	5.67	5.57	5.92
0.2	1	50	25	6.12	6.55	4.62	4.98	5.11	5.65	5.55	5.86
0.2	1	50	50	6.02	6.44	4.58	4.93	5.06	5.60	5.48	5.88
0.2	5	25	25	7.30	7.70	5.26	5.58	5.86	6.32	6.44	6.79
0.2	5	25	50	6.83	7.22	5.09	5.41	5.64	6.09	6.14	6.48
0.2	5	50	25	6.80	7.25	4.91	5.26	5.49	6.16	6.03	6.40
0.2	5	50	50	6.31	6.73	4.73	5.07	5.24	5.75	5.70	5.81
0.3	1	25	25	9.93	10.36	5.91	6.19	7.12	7.67	8.22	8.56
0.3	1	25	50	9.86	10.29	5.90	6.17	7.09	7.61	8.18	8.51
0.3	1	50	25	9.86	10.29	5.87	6.15	7.07	7.59	8.16	8.51
0.3	1	50	50	9.78	10.22	5.85	6.13	7.04	7.57	8.12	8.46
0.3	5	25	25	10.69	11.12	6.19	6.46	7.50	7.93	8.73	9.10
0.3	5	25	50	10.36	10.77	6.12	6.39	7.38	7.84	8.54	8.67
0.3	5	50	25	10.33	10.77	5.99	6.27	7.26	7.77	8.45	8.83
0.3	5	50	50	9.98	10.41	5.92	6.19	7.14	7.62	8.26	8.60

Panel B: OTM options ($S_t = 105$, $K = 100$, $H = 110$).

Parameters				Vanilla		Barrier		Parisian (1w)		Parisian (1m)	
σ	λ	η	θ	Euro.	Amer.	Euro.	Amer.	Euro.	Amer.	Euro.	Amer.
0.2	1	25	25	4.55	4.82	2.29	2.43	2.97	3.24	3.60	3.78
0.2	1	25	50	4.45	4.71	2.27	2.41	2.93	3.21	3.54	3.74
0.2	1	50	25	4.45	4.72	2.24	2.38	2.90	3.18	3.52	3.70
0.2	1	50	50	4.35	4.62	2.21	2.36	2.86	3.14	3.46	3.68
0.2	5	25	25	5.58	5.85	2.66	2.80	3.48	3.73	4.27	4.49
0.2	5	25	50	5.11	5.36	2.57	2.70	3.32	3.56	4.02	4.23
0.2	5	50	25	5.12	5.42	2.41	2.56	3.18	3.52	3.91	4.14
0.2	5	50	50	4.63	4.90	2.31	2.45	3.00	3.27	3.64	3.75
0.3	1	25	25	8.16	8.48	2.97	3.08	4.44	4.76	5.82	6.05
0.3	1	25	50	8.09	8.41	2.96	3.07	4.42	4.72	5.79	6.01
0.3	1	50	25	8.09	8.41	2.94	3.05	4.40	4.70	5.77	6.00
0.3	1	50	50	8.01	8.34	2.93	3.04	4.38	4.69	5.73	5.96
0.3	5	25	25	8.91	9.24	3.16	3.26	4.75	5.01	6.27	6.53
0.3	5	25	50	8.58	8.89	3.13	3.22	4.66	4.93	6.11	6.21
0.3	5	50	25	8.56	8.89	3.02	3.12	4.55	4.84	6.02	6.28
0.3	5	50	50	8.21	8.54	2.98	3.98	4.46	4.74	5.85	6.08

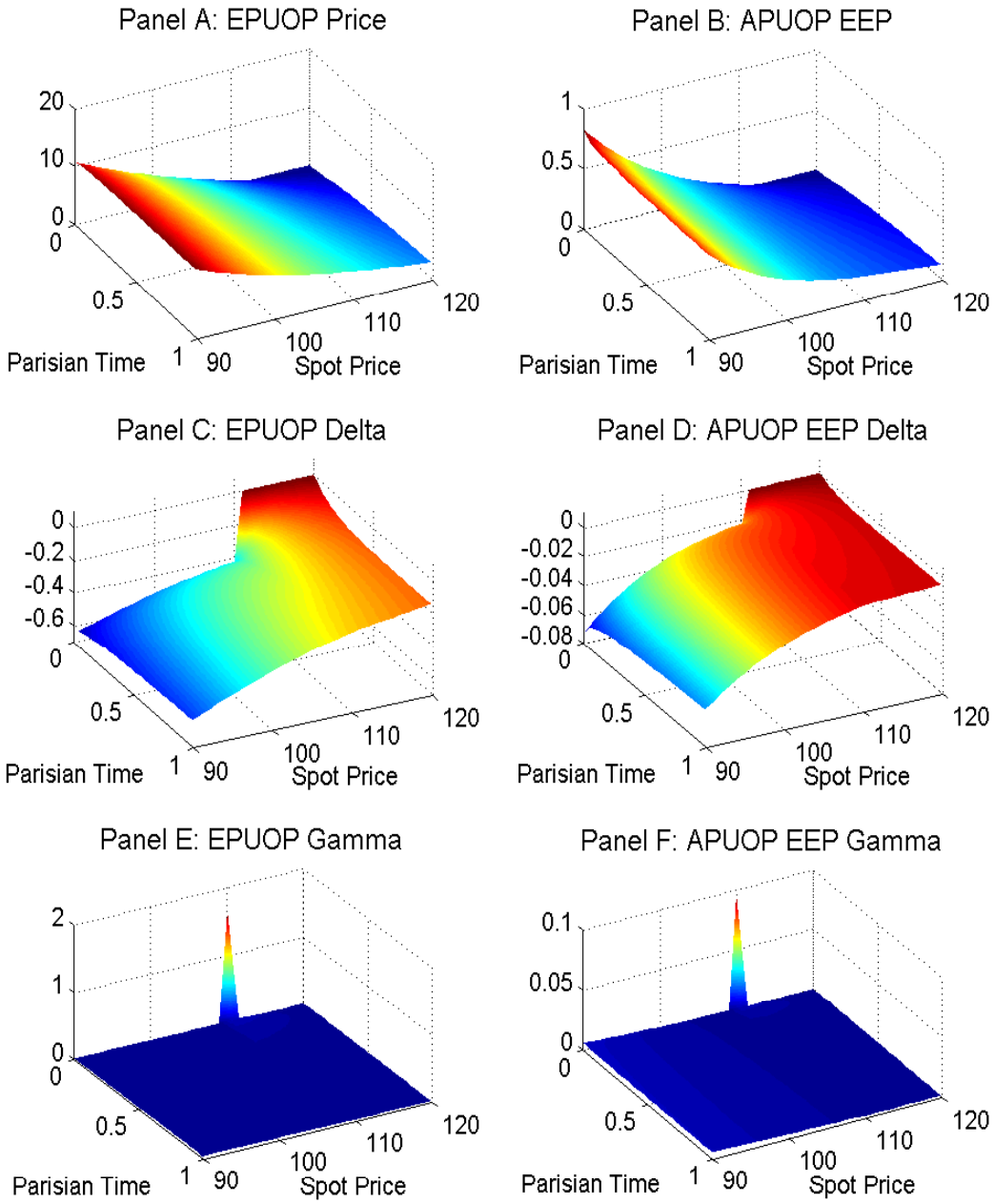

Figure 3.2: **The impact of the underlying asset price and the Parisian window on the option price and the greeks.** Prices and the Greeks (deltas and gammas) of European Parisian up-and-out put options (EPUOP) and early exercise premiums of American Parisian up-and-out put options (APUOP EEP) in a DEM model ($K = 100$, $H = 110$, $\tau = 1$ year, $r = 5\%$, $\delta = 1\%$, $\sigma = 20\%$, $p = q = 0.5$, $\lambda = 5$, $\eta = 50$, and $\theta = 25$) as a function of the underlying asset price $S_t \in [90, 120]$ and the Parisian window $D \in (0, 1)$.

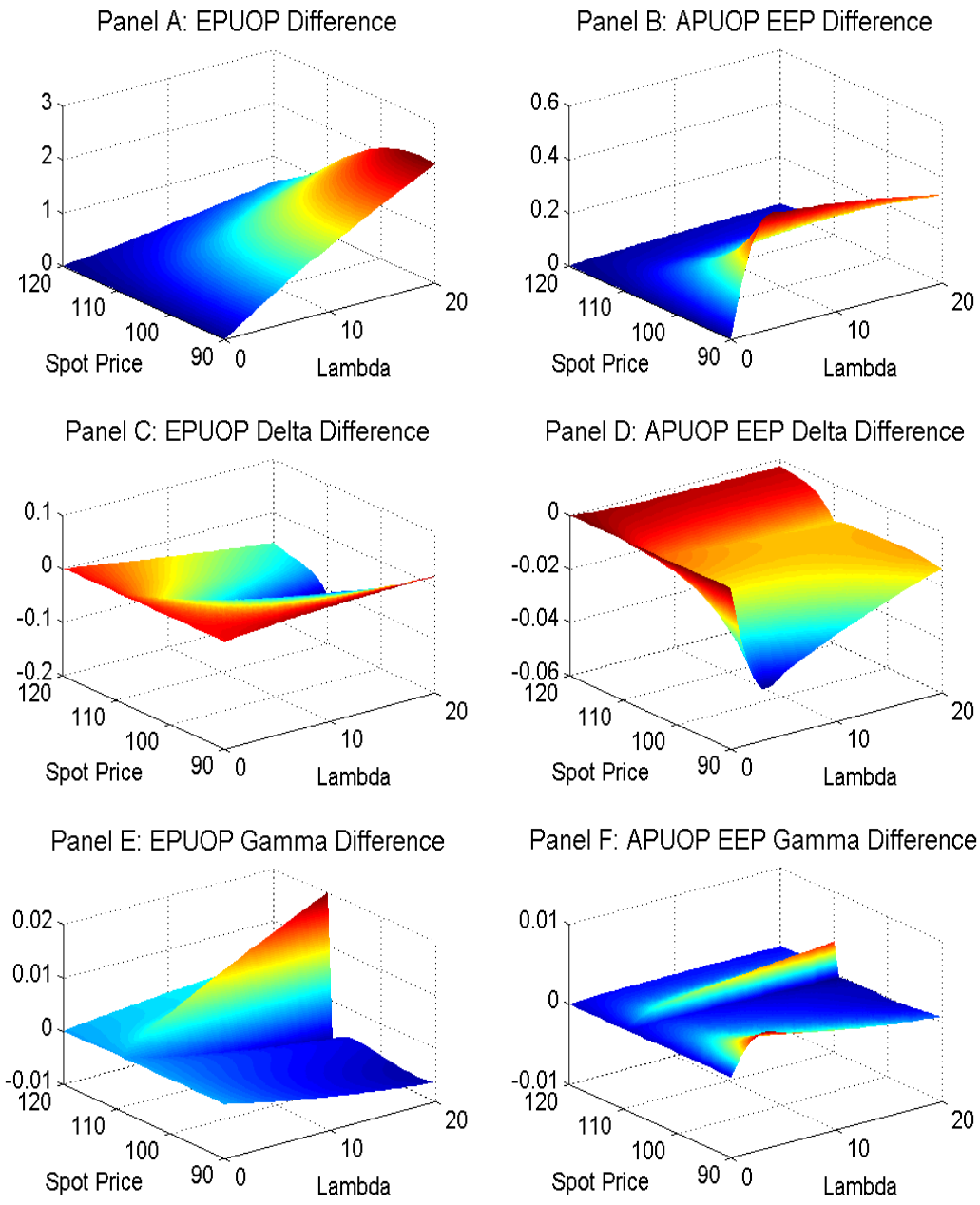

Figure 3.3: **The impact of the underlying asset price and the jump intensity parameter on the option price and the greeks.** The differences between prices, deltas, and gammas of the European Parisian up-and-out put options (EPUOP) and the early exercise premiums of American Parisian up-and-out put options (APUOP EEP) with and without jumps, in a DEM model ($K = 100$, $H = 110$, $\tau = 1$ year, $r = 5\%$, $\delta = 1\%$, $\sigma = 20\%$, $p = q = 0.5$, $\eta = 50$, and $\theta = 25$) as functions of the underlying asset price $S_t \in [90, 120]$ and the jump intensity $\lambda \in [0, 20]$.

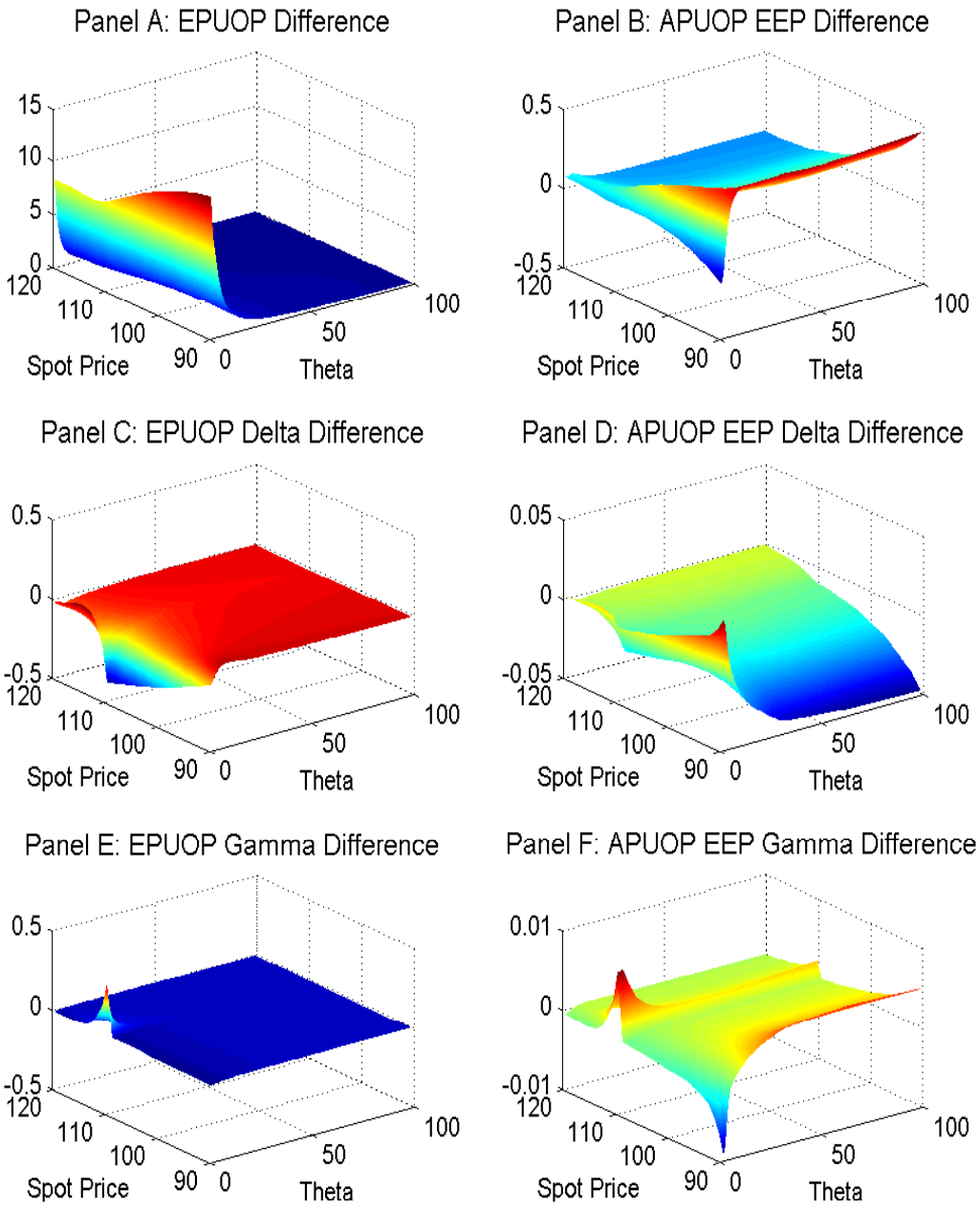

Figure 3.4: **The impact of the underlying price and the negative jump parameter on the option price and the greeks.** The differences between prices, deltas, and gammas of the European Parisian up-and-out put options (EPUOP) and the early exercise premiums of American Parisian up-and-out put options (APUOP EEP) with and without jumps, in a DEM model ($K = 100$, $H = 110$, $\tau = 1$ year, $r = 5\%$, $\delta = 1\%$, $\sigma = 20\%$, $\lambda = 5$, $p = q = 0.5$, and $\eta = 50$) as functions of the underlying asset price $S_t \in [90, 120]$ and the negative jump parameter $\theta \in [2, 100]$.

3.6.1 Jump intensity and magnitude effects

First, we quantify the impact of the jump intensity parameter λ on the prices and Greeks of an EPUOP option and APUOP early exercise premium. In Figure 3.3 we plot the dependence of the difference between the prices, deltas, and gammas with and without jumps on the underlying asset price S_t and the jump intensity λ. Other model parameters, i.e., p, η, and θ, are kept constant.

Expectedly, the differences vanish as the intensity parameter λ approaches zero. The impact of jumps on the EPUOP option price and APUOP EEP is always positive (Panels A and B). The existence of (negative) jumps increases the likelihood of the option exercise, hence it increases the prices. On the other hand, jumps decrease the EPUOP and APUOP EEP deltas (Panels C and D). Since the delta of a put option is always negative, it follows that EPUOP option price and APUOP EEP are more sensitive to changes in the underlying asset price if the model admits discontinuities. Finally, the impact on the gammas is relatively limited (Panels E and F). However, the gammas exhibit strongly non-linear behaviour across different spot price levels, with the most pronounced effect at barrier level.

Second, in Figure 3.4, we demonstrate the effects of the negative jump parameter θ on the prices and greeks of an EPUOP option and APUOP EEP. For a given spot price S_t, the EPUOP price difference increases with the average size of negative jumps (Panel A). The same conclusion holds for the APUOP EEP (Panel B), except in the payoff exercise domain where we observe an inverse relationship. The rationale for such behaviour lies in the fact that an APUOP EEP is equal to the difference between the intrinsic value (which does not depend on the model parameters) and the corresponding EPUOP option price (which increases with the average negative jump size). Therefore, the net effect in the payoff exercise domain displays an opposite trend to what is observed in the standard continuation and excursion domains. An increase in the average negative jump size leads to higher sensitivities of the EPUOP price and APUOP EEP (Panels B, D, E and F). However, we again observe the opposite effect in the payoff exercise domain for the APUOP EEP.

3.6.2 Non-monotonic effects of volatility and jump intensity

Vanilla options are monotonically increasing in volatility.However, depending on the drift of the underlying process, the vega of a standard barrier knock-out option can become negative if the underlying process is close to the barrier. This rather unusual pattern can be attributed to the increasing like-

lihood of a knock-out event with the rising volatility which offsets the probability of option exercise. On the other hand, standard barrier and vanilla options are merely special cases of Parisian options (as discussed in Section 3.1). Therefore, it is expected that non-monotonic behaviour might also be observed also in the case of Parisian knock-out options—albeit to a lesser extent—and especially for contracts with a relatively short Parisian window which are similar to standard barrier options.

Analogously, in the presence of jump risk, a similar effect might occur for Parisian knock-out option sensitivity w.r.t. the jump parameters. Motivated by these observations, we study the dependence of the EPUOP option price on volatility σ and jump intensity λ for different lengths of the Parisian window and different values of the risk-neutral drift.[37] To the best of our knowledge, this research question has not been previously addressed in the literature. Nevertheless, some interesting financial applications of the non-monotonic volatility effects on investment policy when the equity of a levered firm is modelled as a down-and-out call option are studied in Chesney and Gibson (1999, 2001). However, these papers focus on the Black–Scholes setting and do not entertain jumps.

We consider a DEM model. In particular, we are interested in the case when the underlying asset price S_t is in the standard domain and close to the barrier H. Furthermore, the drift is assumed to be non-positive. The results of our numerical experiments are summarized in Figure 3.5). In Panel A, we plot the price of a European UOP barrier option as a function of the drift and the volatility. Indeed, the option price is a non-monotonic function of the volatility for a wide range of drift values. Similar results are obtained for a European UOP barrier option as a function of the jump intensity parameter and the risk-neutral drift (Panel B). In both cases, a drift range exists in which the option price is a non-monotonic function of the volatility or the jump intensity.

To investigate potential non-monotonic effects in the case of Parisian option contracts, we compute the EPUOP option prices with Parisian windows of 1, 2 and 3 days. For each drift value, we record the 'critical volatility' and the 'critical jump intensity', i.e., the volatility and the jump intensity levels at which the respective option sensitivity changes sign. Our findings are summarized in Panels C and D. For comparison, we also include critical levels of the corresponding European UOP barrier options. The EPUOP option price indeed exhibits a non-monotonic behaviour. We observe two interesting effects. First, the drift ranges in which the critical volatility and the critical jump intensity levels exist shrink with increasing Parisian window. Second, the critical volatility and jump intensity levels increase for

[37] We only consider EPUOP options, however similar conclusions can be derived for their American counterparts.

longer Parisian windows. The observed pattern is consistent with the intuition that the probability of a knock-out event is inversely related to the Parisian window length. Therefore, our numerical results are in line with theoretical expectations.

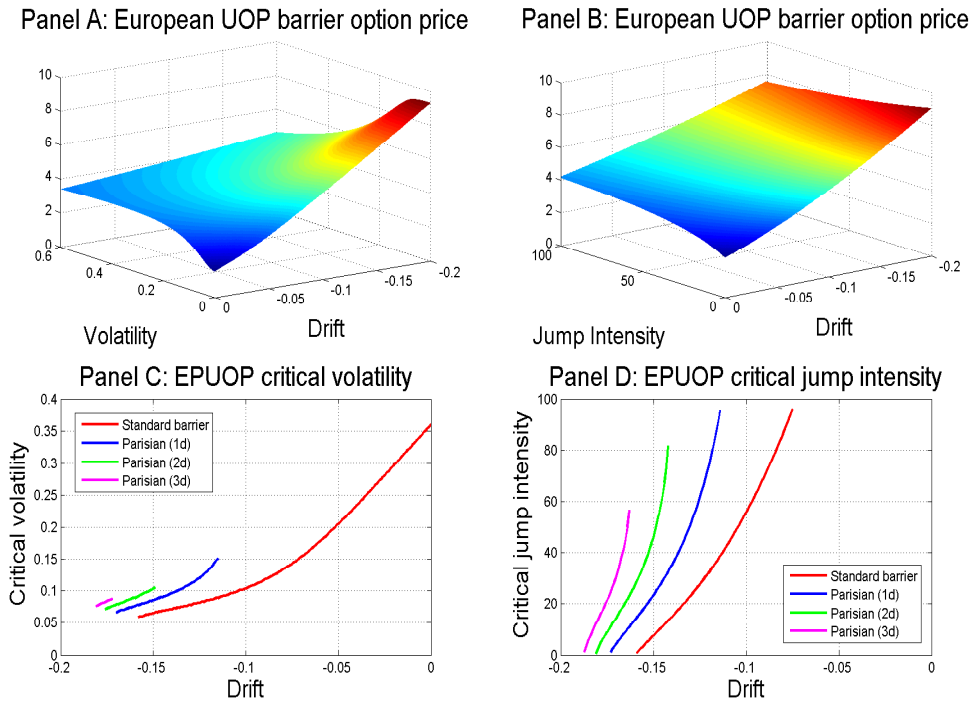

Figure 3.5: **Knock-out volatility and jump intensity effects.** Knock-out volatility and jump intensity effects for European Parisian up-and-out put option as a function of the drift and either the volatility or the jump intensity in a DEM model ($S_t = K = 100$, $H = 105$, $\tau = 6$ months, $r = 2\%$, $p = q = 0.5$, $\lambda = 5$ (if fixed), and $\eta = \theta = 50$). If fixed, volatility and the jump intensity are $\sigma = 10\%$ and $\lambda = 5$, otherwise $\sigma \in (0, 0.4)$ and $\lambda \in (0, 100)$, respectively. The drift term is $\mu \in (-0.2, 0)$.

3.7 Conclusion

In this paper,we introduce a new approach—québécoisation method—for the pricing of European and American Parisian options in a hyper-exponential jump–diffusion model. Using a double Laplace–Carson transform with respect to the option (hybrid) maturity and Parisian (excursion) time, we compute the randomized prices and greeks of European and American up-and-out put options in closed form. Results for other types of Parisian options can be derived by following a similar calculations procedure, and with the help of symmetry and parity relations discussed in the paper. To provide an intuition for our theoretical results, we numerically investigate the impact of jumps on the Parisian

option price and greeks. Finally, we examine and discuss conditions under which the standard barrier and Parisian options become non-monotonic functions of volatility and jump intensity—a feature inherent to path-dependent knock-out options.

Chapter 4

Option-Implied Intra-Horizon Risk and First-Passage Disentanglement

Nikola Vasiljević[38]

Abstract

In this paper, we study the intra-horizon value at risk (iVaR). We propose a new model of asset returns called displaced mixed-exponential model (D-MEM), which can arbitrarily closely approximate finite-activity jump–diffusions and completely monotone Lévy processes. We then derive analytical results for the iVaR and disentangle, in a theoretically consistent way, the contributions of jumps and diffusion to the intra-horizon risk. We estimate the iVaR for several popular jump models using two different S&P 100 index data sets, i.e., the historical returns and the American options spanning the period 2001–2014. Our backtesting results indicate that the option-implied estimates are much more responsive to market changes relative to their historical counterparts. Therefore, due to its forward-looking nature, the option-implied estimation approach represents a valuable source of information about the risk exposures, and should not be neglected in risk management practice. Finally, we empirically disentangle the contribution of jumps from diffusion to the iVaR, and conclude that jump account for about 90 percent on average.

Keywords: Value at risk, Intra-horizon risk, Displaced mixed-exponential model, First-passage disentanglement, Option-implied estimates.

JEL classification: G01 · G11 · G13 · C51 · C52.

[38]I thank Carol Alexander, Jérôme Detemple, Walter Farkas, Fulvia Fringuellotti, Markus Leippold, Rasmus Rousing, Davide Tedeschini, Adriano Tosi and the participants at the Brown Bag Lunch Seminar at the Department of Banking and Finance Institute at the University of Zürich and the Gerzensee Research Days 2015 for their valuable comments and suggestions. I gratefully acknowledge financial support from the Swiss Finance Institute (SFI) and Bank Vontobel.

4.1 Introduction

Value at risk (VaR) has been the most important market risk measure for two decades already. It is defined as a conditional quantile of the trading profit-and-loss (P&L) distribution at the end of a predefined time horizon. For example, a 10-day VaR at 99.0% confidence level is the loss that will *not* be exceeded at the end of the 10-day period with the probability of 99.0%. Although the VaR is widely used in practice, it does not perfectly describe the multifaceted nature of market risk. First, it is uninformative about the expected magnitude of losses beyond the calculated threshold level. To address this issue, Artzner et al. (1999), Acerbi and Tasche (2002a,b), and Rockafellar and Uryasev (2002) developed a new risk measure, i.e., the expected shortfall (ES), which represent the average loss beyond the VaR level. By construction, ES is a more conservative measure and it better captures tail risk than VaR, which is precisely what matters the most for the market risk management. The second important methodological issue inherent to VaR, which has been largely overlooked in the literature, is the fact that it captures only the end-of-horizon effects—it does not provide any information about the possible losses before the expiration of the monitoring period. Kritzman and Rich (2002), Boudoukh et al. (2004), Rossello (2008), Bhattacharyya, Misra and Kodase (2009) and Bakshi and Panayotov (2010) studied a risk measure called intra-horizon value at risk (iVaR), which captures the "time dimension" of the market risk.[39] In particular, the iVaR is defined as a conditional quantile of the first-passage distribution (FPD) over a given time horizon, hence it reflects the probability of incurring a loss of certain size at any point in time before (and including) the end of the monitoring period.

The intra-horizon risk was originally presented in Stulz (1996), pp. 20–22, in the context of cash flow risk in corporate risk management. Nevertheless, the notion of intra-horizon risk is much broader and has many potential applications in finance. Kritzman and Rich (2002), pp. 92–93, mention the following examples: fiduciary asset management (due to intra-horizon performance provisions), loan agreements (due to mandatory reserves covenant), hedge-fund solvency (due to possible within-horizon withdrawals), regulatory requirements (due to the maintenance of the capital account), and securities lending (due to the required collateral deposit). Therefore, the intra-horizon risk is very important in

[39] We emphasize that there is still no consensus in the literature regarding the name of the proposed risk measure. Boudoukh et al. (2004) and Bhattacharyya, Misra and Kodase (2009) use only the short name MaxVaR, and Bakshi and Panayotov (2010) call it the intra-horizon value at risk (abbreviated as VaR-I in their paper). We adopt the latter notation in our paper, but we propose a new short name, i.e., the iVaR.

a mark-to-mark environment where large trading losses in a short period of time can trigger margin calls and similar provisions.

In this paper, we consider the intra-horizon risk from a risk management perspective, and provide new important insights both from theoretical and empirical point of view. We build on the work of Bakshi and Panayotov (2010), who established a link between the VaR (iVaR) and the expectation of a European-style (one-touch) digital payoff, and subsequently studied the two risk measures for several Lévy models.[40] To facilitate the computations with digital payoffs, they rely on an explicit finite difference scheme.[41] One of the main reasons for such an approach is the lack of alternative techniques that would allow studying first-passage distributions—for a wide class of exponential Lévy processes, including both finite and infinite activity models—in a unified framework. The main theoretical contribution of our paper is to propose an alternative solution to this problem, which is analytical and provides important additional insights about the iVaR.

First, we introduce a new jump–diffusion model for the asset price dynamics, which generalizes the mixed-exponential model (MEM) studied in Cai and Kou (2011). Generally, MEM models are attractive because exponential mixtures are flexible enough to arbitrarily closely approximate any continuous function on $[0, +\infty)$; e.g., see Botta and Harris (1986).[42] Our model extends the standard setting by admitting the support in the form $[\mu, +\infty)$, with $\mu \in \mathbb{R}$, $|\mu| < +\infty$. For this reason we christen it the displaced mixed-exponential model (D-MEM). It can be verified that the D-MEM class is indeed very wide and flexible; it can approximate processes with completely monotone Lévy densities and jump–diffusion processes with arbitrary jump distributions. In the second step, following Leippold and Vasiljević (2017), we derive analytical results for the expectations of European and one-

[40] Other models are also considered the literature. Kritzman and Rich (2002) and Boudoukh et al. (2004) considered the Black–Scholes model and derived the closed-form expression for the probability of interim loss of a given magnitude. However, their modelling paradigm is overly simplistic as it does not capture the salient features of asset returns, e.g., volatility clustering, negative skewness and excess kurtosis. On the other hand, Rossello (2008) and Bhattacharyya, Misra and Kodase (2009) studied the first-passage distribution in the double-exponential jump–diffusion setting and a GARCH model with non-normal innovations, respectively, using Monte Carlo methods.

[41] A digital (or binary) payoff structure gives either one monetary unit or zero, conditionally on the occurrence of an event either at some specific date or within certain period of time in the future.

[42] The support can be extended to the whole real line by considering separately approximations on the positive and the negative real line. This is especially convenient for symmetric functions because it is enough to approximate only one half of the function, and obtain the other half by analogy. For example, Cai and Kou (2011) consider a MEM approximation of a normal distribution. However, their approximation procedure is directly applicable only to normal distributions with zero mean/mode.[43] In the case of a normal distribution with non-zero mean/mode ($\mu \neq 0$), the symmetry property cannot be exploited directly in the Botta and Harris (1986)'s framework because the support of the left and right half of the normal distribution, i.e., $(-\infty, \mu)$ and $[\mu, +\infty)$, do not coincide with the support of the approximation function, i.e., the positive and the negative real line. Therefore, the two halves of the distribution have to be treated separately, and the procedure is computationally more expensive.

touch digital payoffs in the D-MEM setting using the Laplace–Carson transform (LCT). Moreover, we analytically disentangle the contributions of jumps and diffusion to the iVaR by studying the LCT of the first-passage time and the overshoot of the barrier level for the expectations of one-touch digital payoffs.

In the empirical part of their study, Bakshi and Panayotov (2010) consider several popular Lévy models and stress the importance of the model risk (i.e., the uncertainty about the correct model specification). We argue that the estimation risk (i.e., the uncertainty about the model parameters) represents even a larger concern. In particular, Bakshi and Panayotov (2010) follow the financial industry standard and calculate VaR and iVaR using historical return time series. On the other hand, we estimate the two risk metrics using the options data, whereas the historical estimation serves as the benchmark in our empirical study. The rationale for our approach is the following. The existence of liquid options with different maturities and strikes makes it possible to study option-implied probability distributions and their statistical moments and quantiles for different investment horizons. Arguably, option-implied estimates are expected to exhibit superior forecasting performance than the historical estimates because they are more responsive to market changes due to their forward-looking nature.[44] Furthermore, the frequency of historical returns data very often does not match exactly the time horizon that we are interested in, hence the estimated statistics or model parameters have to be adjusted accordingly. One way to achieve this goal is to use the time scaling, however this is possible only in some specific cases, e.g., in the Black–Scholes model the drift term and the variance scale linearly with the time horizon. Nevertheless, the time scaling adjustment can be completely circumvented by computing the option-implied risk metrics. The term structure of option data makes it possible to closely match the option maturity with the target time horizon.

Although we argue that option-implied statistics and model parameters are more informative about the future asset price dynamics and do not require time scaling, we also stress that they are estimated under the risk-neutral measure. Using option-implied estimates as direct inputs in calculations under the historical measure would result in a theoretically inconsistent approach in risk management applications. The severity of this problem depends on the time horizon. Duffie and Pan (1997), pp. 10–11,

[44] Since the seminal work of Latané and Rendleman (1976) and Breeden and Litzenberger (1978) many researchers have studied the informational content of risk-neutral distributions of asset returns, their statistical moments and other relevant quantities. An excellent overview of applications of option-implied information in forecasting is provided in Christoffersen, Jacobs and Chang (2013).

claim that, in most markets, the distinction between the risk-neutral and the historical measure is negligible in the short term. On the other hand, Boudoukh et al. (2004), p. 4, and Bakshi and Panayotov (2010), p. 23, assume that the expected return is equal to zero under the historical measure over a short time horizon. We adopt the latter assumption in our study and incorporate a risk neutralization procedure. To this end, we derive results for the change of measure in a general D-MEM setting, which guarantee a unique translation of the option-implied model parameters into the risk-adjusted (ex-ante physical) parameters. Overall, we work with one historical measure and two forward-looking measures.

Finally, to make our empirical results comparable to those of Bakshi and Panayotov (2010), we study the Merton (1976)'s jump–diffusion model (MJD), the finite-moment log-stable model (FMLS) of Carr and Wu (2003), and the Carr-Geman-Madan-Yor model (CGMY) of Carr et al. (2002). Additionally, we consider the variance-gamma model of Madan and Seneta (1990). All these models can be approximated by the D-MEM class of processes, hence we are able to analyze them consistently in a unified framework using our theoretical results. The model parameters are estimated separately from the historical return time series and the short-term American put options on the S&P 100 index spanning the period from March 2001 until August 2014. Using a major index in an empirical study is particularly appealing because of the data availability, and due to the fact that broad indices are often used as proxies for risk factors. Our empirical findings for 10-day VaR and iVaR estimates at the confidence levels of 99.0% and 99.9% indicate significantly higher values under the forward-looking measures relative to the historical measure. A simple backtesting procedure shows that, irrespectively of the model used, the option-implied and the risk-adjusted VaR and iVaR are much more perceptive and responsive to asset price fluctuations, as they yield superior results to the estimates inferred from the historical return time series. We conclude that, at least within the scope of our study, the importance of estimation risk surpasses the importance of the model risk. For this reason, we believe that, whenever option data is available, the option-implied estimates of risk measures should be considered as well.

The paper is structured as follows. We introduce the displaced mixed-exponential model and the associated change of measures in Section 4.2. The connection between the European and one-touch digital payoffs the two risk metrics is thoroughly discussed in Section 4.3.1 and Section 4.3.2. Our theoretical results for the first-passage disentanglement of the jump contribution from the diffusion contribution to the iVaR are presented in Section 4.3.3. In Section 4.4, we describe the data treatment

and summarize the calibration and the model performance results. Our empirical findings for the VaR, the iVaR, and the FPD (under the historical and the risk-adjusted measure) are discussed in Section 4.5. We conclude in Section 4.6. All proofs, tables and figures are given in the Appendix.

4.2 Displaced mixed-exponential model (D-MEM)

4.2.1 The model set-up

Let $(\Omega, \mathcal{F}, \mathbb{F} = \{\mathcal{F}_t, t \geq 0\}, \mathbb{P})$ be a a filtered probability space which satisfies the usual assumptions, where $\mathcal{F}_t = \sigma(W_s, N_s; s \leq t, \{V_j\})$. The stochastic process $\{W_t, t \geq 0\}$ is a standard Brownian motion. The Poisson process $\{N_t, t \geq 0\}$ is characterized by jump intensity parameter $\lambda \in \mathbb{R}_0^+$, and $\{Y_i := \log(V_i) : i = 1, 2, ...\}$ represents a sequence of independent and identically distributed (i.i.d.) displaced mixed-exponential random variables. The Lévy density of D-MEM is

$$\nu(y) = \lambda_+ \sum_{i=1}^{m} p_i \eta_i e^{-\eta_i (y-\xi)} \mathbb{1}_{\{y \geq \xi\}} + \lambda_- \sum_{j=1}^{n} q_j \theta_j e^{\theta_j (y-\xi)} \mathbb{1}_{\{y < \xi\}}. \tag{4.1}$$

The displacement parameter ξ is the mode of the Lévy density. It represents the jump magnitude at which the mixture of standard exponential distributions (the right half of D-MEM distribution) is glued back-to-back to a mixture of "y-axis-mirrored" exponential distribution (the left half of D-MEM distribution), as graphically exemplified in Panels A and C in Figure 4.1. Henceforth we refer to the two types of jumps as ξ^+ and ξ^--jumps, respectively.

The parameters $\lambda_+ \in \mathbb{R}_0^+$ and $\lambda_- \in \mathbb{R}_0^+$ represent the respective (finite-activity) jump intensities of the two jump mixtures. The total jump activity is therefore given by $\lambda = \lambda_+ + \lambda_-$, and the jump size probability distribution function (p.d.f.) is defined as $f_Y(y) := \nu(y)/\lambda$. The parameters $\{\eta_i \in (1, +\infty) : i = 1, ..., m\}$ are the magnitude parameters of ξ^+-jumps. Similarly, the set $\{\theta_j \in (0, +\infty) : j = 1, ..., n\}$ represents the magnitude parameters of ξ^--jumps.[45] Without loss of generality we assume that $\eta_1 < \eta_2 < ... < \eta_m$ and $\theta_1 < \theta_2 < ... < \theta_n$. Finally, the mixing weights $\{p_i \in \mathbb{R} : i = 1, ..., m\}$ and $\{q_j \in \mathbb{R} : j = 1, ..., n\}$ satisfy equations: $\sum_{i=1}^{m} p_i = 1$ and $\sum_{j=1}^{n} q_j = 1$. Since we allow weights to be negative, certain conditions need to be satisfied to ensure that the function $f_Y(y)$ represents a p.d.f. In particular, Steutel (1967) showed that the necessary conditions are: $p_1 > 0$, $q_1 > 0$, $\sum_{i=1}^{m} p_i \eta_i \geq 0$,

[45] The average jump size of a given type is an inverse of the corresponding magnitude parameter.

and $\sum_{j=1}^{n} q_j\theta_j \geq 0$. On the other hand, Bartholomew (1969) showed that the sufficient conditions are: $\sum_{i=1}^{m'} p_i\eta_i \geq 0$ for all $m' = 1, 2, ..., m$, and $\sum_{j=1}^{n'} q_j\theta_j \geq 0$ for all $n' = 1, 2, ..., n$.

The asset price dynamics under the historical probability measure $\mathbb{P}$ follows a displaced mixed-exponential jump–diffusion process

$$\frac{dS_t}{S_{t^-}} = \mu dt + \sigma dW_t + d\left(\sum_{i=1}^{N_t}(V_i - 1)\right). \tag{4.2}$$

The drift $\mu \in \mathbb{R}$, and the volatility $\sigma \in \mathbb{R}^+$ are assumed to be constant. It follows from the Itô lemma that the log-price process $\{X_t := \log S_t, t \geq 0\}$ is given by

$$X_t = X_0 + \bar{\mu}t + \sigma W_t + \sum_{i=1}^{N_t} Y_i, \quad X_0 := \log S_0, \tag{4.3}$$

where $\bar{\mu} := \mu - \lambda\zeta - \frac{\sigma^2}{2}$ represents the compensated drift term. The average jump size is

$$\zeta := \mathbb{E}\left[e^{Y_1} - 1\right] = \left(\frac{\lambda_+}{\lambda}\sum_{i=1}^{m}\frac{p_i\eta_i}{\eta_i - 1} + \frac{\lambda_-}{\lambda}\sum_{j=1}^{n}\frac{q_j\theta_j}{\theta_j + 1}\right)e^{\xi} - 1. \tag{4.4}$$

The cumulant generating function (c.g.f.) of the log-price process $\{X_t, t \geq 0\}$ is defined for any $u \in (-\theta_1, \eta_1)$ as

$$\Psi(u) := \frac{1}{t}\log\mathbb{E}\left[e^{uX_t}\right] = \mu u + \frac{1}{2}\sigma^2u^2 + \lambda\left(\left(\frac{\lambda_+}{\lambda}\sum_{i=1}^{m}\frac{p_i\eta_i}{\eta_i - u} + \frac{\lambda_-}{\lambda}\sum_{j=1}^{n}\frac{q_j\theta_j}{\theta_j + u}\right)e^{u\xi} - 1\right). \tag{4.5}$$

Several popular jump-diffuson models can be nested in the D-MEM class. First, any MEM model can be interpreted as a D-MEM model without displacement ($\xi = 0$). Second, zero displacement parameter characterizes also the class of hyper-exponential models (HEM), with the additional constraint that the mixing weights $\{p_i\}_{i=1,...,m}$ and $\{q_j\}_{j=1,...,n}$ in (4.1) have to be strictly positive. Finally, double-exponential models (DEM) represent a subclass of HEM models (with $n = m = 1$), and therefore can also be nested in the D-MEM family.[46]

Cai (2009), Lemma 2.1, pp. 128–129, proved for the class of hyper-exponential models that the characteristic equation

$$\Psi(u) = \alpha, \ \alpha \in \mathbb{R}^+, \tag{4.6}$$

[46]HEM class of models was studied in the following papers: Lipton (2002), Cai (2009, 2011), Cai, Chen and Wan (2009), Crosby, Le Saux and Mijatović (2010), Jeannin and Pistorius (2010), Boyarchenko and Boyarchenko (2011), Cai and Kou (2012), Hofer and Mayer (2013), Yin, Shen and Wen (2013), Cai and Sun (2014). The main references for the DEM models are: Kou (2002), Kou and Wang (2003, 2004), Sepp (2004), Kou, Petrella and Wang (2005), AitSahlia and Runnemo (2007), Ramezani and Zeng (2007), Toivanen (2008), Wong and Lau (2008), Bayraktar and Xing (2009, 2011), Cai, Chen and Wan (2010), Albrecher, Kortschak and Zhou (2012) and Fuh, Luo and Yen (2013).

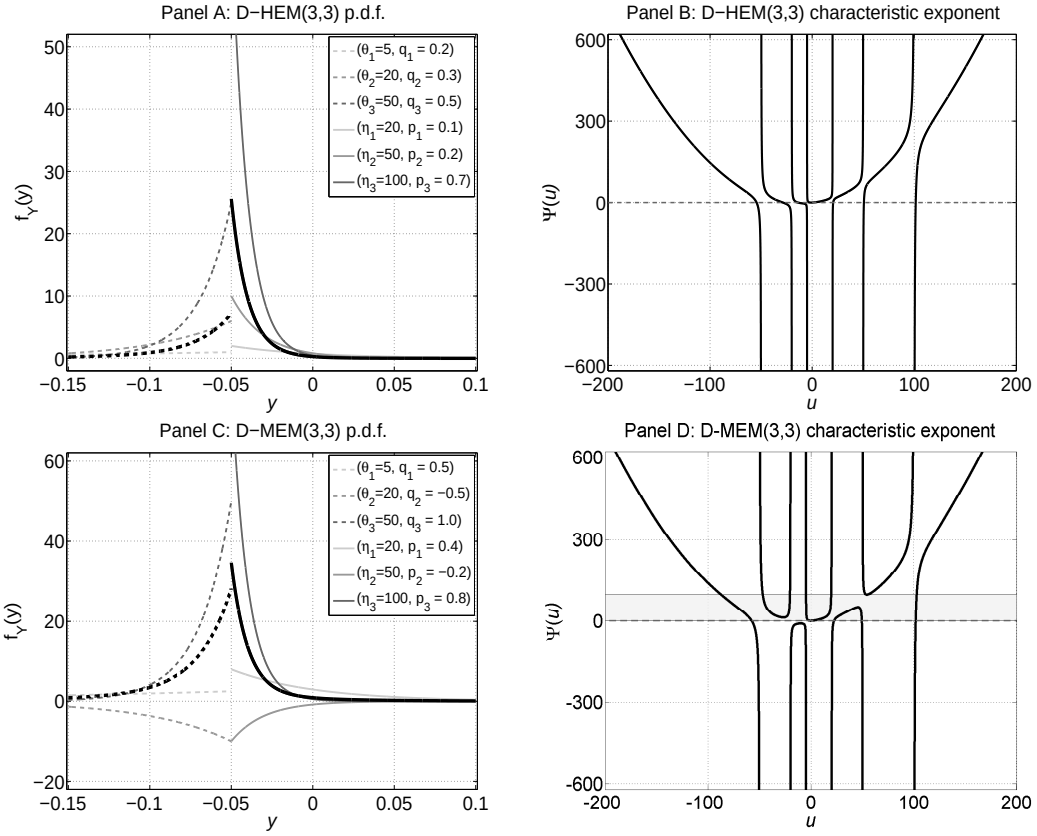

Figure 4.1: **D-MEM examples.** Two examples of displaced-mixed exponential models (D-MEM) are presented to illustrate the equations (4.1) and (4.5)–(E.14). We arbitrarily set the drift of the asset price process to $\mu = 0.02$. Both models have three types of ξ^+ and ξ^--jumps, and we assume the following parameter values. The displacement parameter is $\xi = -0.05$. The positive and the negative jump intensites are equal and set to $\lambda_+ = \lambda_- = 5$. The volatility parameter is $\sigma = 0.2$. The ξ^+-jump size parameters are $\eta = (20, 50, 100)$, and the ξ^--jump size parameters are $\theta = (5, 20, 50)$. However, the conditional probabilities of the occurence of different jump types are not the same for the two models. In the first model, ξ^+-jumps have probabilities $p = (0.1, 0.2, 0.7)$ and ξ^--jumps have probabilities $q = (0.2, 0.3, 0.5)$. Since all mixing weights are positive, this is a displaced *hyper*-exponential model, here denoted by D-HEM(3,3). In the second model, the ξ^+-jumps have probabilities $p = (0.4, -0.2, 0.8)$ and the ξ^--jumps have probabilities $q = (0.5, -0.5, 1.0)$. In this case, some of the mixing weights are negative, hence this is a displaced *mixed*-exponential model and we denote it by D-MEM(3,3). Panels A and B represent the p.d.f. and the characteristic exponent of the D-HEM(3,3) model, respectively. Similarly, Panels C and D represent respective plots of the p.d.f. and the characteristic exponent of the D-MEM(3,3) model. Shaded area in the Panel D is the subspace of the positive y-semiaxis where characteristic equation $\Psi(u) = \alpha$ (for $\alpha \in \mathbb{R}^+$) does not have $n+m+2 = 8$ distinct real roots. In fact, this is satisfied only for sufficiently large parameter α; see Theorem 3.1 in Cai and Kou (2011), pp. 2071–2072. On the other hand, Panel C does not display such a feature because any D-HEM(n, m) model (for $n, m \in \mathbb{N}$) has exactly $(n+m+2)$ distinct real roots if $\sigma > 0$; this statement can be proved by generalizing Lemma 2.1. in Cai (2009), pp. 128–129.

is a polynomial-type equation, and that it has exactly $(n+m+2)$ distinct real roots. Nevertheless, one cannot obtain the roots in analytic form for an arbitrary choice of m and n. Already in the case of double-exponential models one has to solve a quartic equation, and if we allow for additional types of positive and negative jumps the problem becomes analytically intractable. Furthermore, Cai and Kou (2011), Theorem 3.1, p. 2071, showed for the MEM class that the characteristic equation (4.5) has also $(n+m+2)$ real roots, but only for sufficiently large α. Similarly, the number of positive and negative characteristic roots in a D-MEM model depends on the constant α. However, any further generalization of the analytical results for HEM and MEM characteristic roots to the case of D-MEM class of jump–diffusion models is a much more challenging task. If the displacement parameter ξ is non-zero, the expression (4.5) becomes an exponential-polynomial equation, which is difficult to analyze and solve analytically in a general D-MEM setting. Even if some additional assumptions are imposed (e.g., the number of $\xi^{\pm}$-jumps is fixed in advance), one has to carefully investigate different model specifications. The most general statement that we can make regarding the roots of a D-MEM (exponential-polynomial) characteristic equation is that there exist $\hat{m} := \hat{m}(\alpha) \leq m+1$ positive roots $\{\beta_{i,\alpha}\}_{i=1,\dots,\hat{m}}$, and $\hat{n} := \hat{n}(\alpha) \leq n+1$ negative roots $\{\gamma_{i,\alpha}\}_{j=1,\dots,\hat{n}}$, which satisfy the ordering relation

$$-\infty < \gamma_{\hat{n},\alpha} < \cdots < \gamma_{2,\alpha} < \gamma_{1,\alpha} < 0 < \beta_{1,\alpha} < \beta_{2,\alpha} < \cdots < \beta_{\hat{m},\alpha} < +\infty. \tag{4.7}$$

Therefore, the characteristic root finding problem for a D-MEM model can only be tackled numerically. Some examples and intuition for the behavior of c.g.f. (4.5) and the roots of the equation (E.14) for different types of D-MEM models are presented in Panels B and D in Figure 4.1.

4.2.2 The change of measure

The market incompleteness of Lévy models represents one of the main challenges in practical applications. However, this problem can be solved by defining the change of measure via the Esscher (1932)'s transform, which can be interpreted as a generalization of the Cameron-Martin-Girsanov change of measure. Gerber and Shiu (1994) proved that the Esscher transform approach is justified in a rational expectations framework where the representative agent is characterized by a certain type of utility function. The main implication of this result for the option pricing is that there exists a risk-neutral measure such that, in equilibrium, options are priced as expectations of their discounted payoffs. Chan (1999) and Miyahara (1999) provided an alternative interpretation of the Esscher transform in terms

of the minimum entropy martingale measure.[47] We also adopt this approach and introduce the change of measure via the Esscher transform. The Radon-Nikodým derivative process is defined as

$$Z_t(\vartheta) := \frac{d\mathbb{Q}^\vartheta}{d\mathbb{P}}\bigg|_{\mathcal{F}_t} = \frac{e^{\vartheta X_t}}{\mathbb{E}\left[e^{\vartheta X_t}\right]}. \tag{4.8}$$

The expectation $\mathbb{E}[\cdot]$ is computed under the historical probability measure $\mathbb{P}$. The Esscher transform parameter is denoted by ϑ, and the process (4.8) is well defined for $\vartheta \in (-\theta_1, \eta_1)$. Theorem 4.2.1 proves that the Esscher transform admits a structure-preserving change of measure for D-MEM processes. Moreover, the risk-neutral probability measure $\mathbb{Q}^\vartheta$ is uniquely identified by choosing the value of ϑ such that the forward no-arbitrage constraint is satisfied, i.e., the discounted process $\left\{e^{-rt}S_t, t \geq 0\right\}$ is a $\mathbb{Q}^\vartheta$-martingale.

Theorem 4.2.1 (**Risk-netural dynamics**). *The risk-neutral dynamics of the log-price process in the displaced mixed-exponential model (4.1)–(4.3) is given by*

$$X_t = X_0 + \bar{r}t + \sigma W_t^* + \sum_{i=1}^{N_t^*} Y_i^*, \quad X_0 := \log S_0. \tag{4.9}$$

The processes $\{W_t^*, t \geq 0\}$ *and* $\{N_t^*, t \geq 0\}$ *represent the Brownian motion and the Poisson process under the risk-neutral measure* $\mathbb{Q}^\vartheta$*, respectively. The compensated drift term is* $\bar{r} := r - \frac{\sigma^2}{2} - \lambda^*\zeta^*$*, where parameter* r *denotes the risk-free rate, and* λ^* *and* $\zeta^* := \left(\frac{\lambda_+^*}{\lambda^*}\sum_{i=1}^m \frac{p_i^*\eta_i^*}{\eta_i^*-1} + \frac{\lambda_-^*}{\lambda^*}\sum_{j=1}^n \frac{q_j^*\theta_j^*}{\theta_j^*+1}\right)e^{\xi^*} - 1$ *represent the jump intensity and the expected jump size under the new measure, respectively. The* $\mathbb{Q}^\vartheta$*-parameters can be computed as follows:*

$$\begin{cases} \sigma^* = \sigma, \ \xi^* = \xi, \\ \lambda_+^* = \lambda_+ \displaystyle\sum_{i=1}^m \frac{p_i\eta_i}{\eta_i - \vartheta} e^{\vartheta\xi}, \quad \lambda_-^* = \lambda_- \sum_{j=1}^n \frac{q_j\theta_j}{\theta_j + \vartheta} e^{\vartheta\xi}, \ \lambda^* = \lambda_+^* + \lambda_-^*, \\ p_i^* = \dfrac{\frac{p_i\eta_i}{\eta_i - \vartheta}}{\sum_{i=1}^m \frac{p_i\eta_i}{\eta_i - \vartheta}}, \quad \eta_i^* = \eta_i - \vartheta, \quad \textit{for } i = 1, 2, ..., m, \\ q_j^* = \dfrac{\frac{q_j\theta_j}{\theta_j + \vartheta}}{\sum_{j=1}^n \frac{q_j\theta_j}{\theta_j + \vartheta}}, \quad \theta_j^* = \theta_j + \vartheta, \quad \textit{for } j = 1, 2, ..., n. \end{cases} \tag{4.10}$$

[47] For a detailed account on the Esscher transform in mathematical finance we refer an interested reader to Hubalek and Sgarra (2006) and the references therein. Additionally, some important examples of Esscher transform applications in option pricing with Lévy processes can be found in, e.g., Milne and Madan (1991), Eberlein and Keller (1995), Kou (2002), Kou and Wang (2004), Carr and Wu (2004), Kou, Petrella and Wang (2005), Wu (2006), Cai (2011), and Fabozzi, Leccadito and Tunaru (2014).

The Esscher transform parameter ϑ is the unique solution of the equation

$$\mu - r - \lambda\zeta + \vartheta\sigma^2 + \Psi_J(\vartheta + 1) - \Psi_J(\vartheta) = 0, \tag{4.11}$$

where $\Psi_J(a) := \mathbb{E}\left[e^{a\sum_{i=1}^{N_t} Y_i}\right] = \lambda\left(\left(\frac{\lambda_+}{\lambda}\sum_{i=1}^{m}\frac{p_i\eta_i}{\eta_i - a} + \frac{\lambda_-}{\lambda}\sum_{j=1}^{n}\frac{q_j\theta_j}{\theta_j + a}\right)e^{a\xi} - 1\right)$ *is the c.g.f. of the jump part (i.e., the compound Poisson process).*

Although we have introduced the Esscher transform for the D-MEM class following the standard approach in the literature and starting from the historical-world dynamics, it is actually the opposite direction of the change of measure which is of primary interest in our paper. The risk-adjusted parameters are computed by adopting the assumption of Boudoukh et al. (2004) and Bakshi and Panayotov (2010) that the risk-adjusted drift is equal to zero, and reversing the procedure for the change of measure in Theorem 4.2.1. We denote the risk-neutral measure by $\mathbb{Q}$ and the risk-adjusted measure by $\mathbb{Q}^\vartheta$, where ϑ now represents the Esscher transform parameter corresponding to the "backward" change of measure, i.e., from $\mathbb{Q}$ to $\mathbb{Q}^\vartheta$. Furthermore, we adjust accordingly the notation in the expression (4.10)—the $\mathbb{Q}^\vartheta$-parameters are henceforth designated by the asterisk sign in the superscript. It follows directly that the Esscher transform parameter ϑ is a function of the risk-neutral parameters, and it can be determined as the unique solution of the equation

$$r - \lambda\zeta + \vartheta\sigma^2 + \Psi_J(\vartheta + 1) - \Psi_J(\vartheta) = 0, \tag{4.12}$$

which, in turn, allows us to compute the risk-adjusted D-MEM parameters. Similarly to the characteristic equation (4.5), the equation (4.12) can be solved only numerically for more involved model specifications.

4.2.3 D-MEM approximations of exponential Lévy processes

In this section, we provide expressions for D-MEM approximations of several exponential Lévy models. They can be broadly classified in two groups: finite-activity jump–diffusion processes and completely monotone Lévy processes of infinite-activity. In particular, we focus on the models that are relevant for our empirical study: MJD, FMLS, VG, and CGMY.

Finite-activity jump–diffusion models: MJD

We have already mentioned in Section 4.2 that DEM, HEM, and MEM models can be nested within the D-MEM class, i.e., their respective D-MEM representations are exact. On the other hand, the D-MEM approximation is more involved for models with a "non-exponential" distribution of jump sizes. An important example is the well known jump–diffusion model of Merton (1976). The log-price dynamics is described by the equation (4.3), and jumps are assumed to be normally distributed, i.e., $Y \overset{\text{i.i.d.}}{\sim} \mathcal{N}(\mu_J, \sigma_J^2)$. Therefore, the Lévy density is given by

$$\nu_{\text{MJD}}(y) = \frac{\lambda}{\sqrt{2\pi\sigma_J^2}} \exp\left(-\frac{(y-\mu_J)^2}{2\sigma_J^2}\right), \tag{4.13}$$

and the characteristic function is

$$\begin{aligned} \varphi_{\text{MJD}}(u) :&= \mathbb{E}\left[\exp(iuX_t)\right] \\ &= \exp\left(iu\mu t - \frac{u^2\sigma^2 t}{2} + \lambda t\left(\exp\left(iu\mu_J - \frac{u^2\sigma_J^2}{2}\right) - 1\right)\right). \end{aligned} \tag{4.14}$$

Cai and Kou (2011), pp. 2077–2078, provided a MEM approximation for a normally distributed variable $Y \overset{\text{i.i.d.}}{\sim} \mathcal{N}(0, 0.01^2)$. We pointed out in Section 4.1 that displaced mixed-exponential distributions are better suited for approximations of normal distributions with non-zero mean/mode. Using a simple change of variables, we demonstrate below that a D-MEM approximation of a normal distribution can be transformed into a MEM approximation.

Let's assume that the MEM approximation of the p.d.f. of a normally distributed random variable $Y \overset{\text{i.i.d.}}{\sim} \mathcal{N}(0, \sigma_J^2)$ is given by

$$f_Y(y) \approx 0.5 \sum_{i=1}^{m} p_i \eta_i e^{-\eta_i |y|}. \tag{4.15}$$

The r.h.s. is a special case of the general expressions for MEM and D-MEM p.d.f.s given in equation (4.1). In addition to the zero displacement, the number of positive exponentials is equal to the number of negative exponentials ($m = n$), and the parameters of the positive and the negative exponential functions and their corresponding mixing weights are component-wise identical, i.e., $\theta_i = \eta_i$ and $p_i = q_i$ for all $i = 1, 2, ..., m$, respectively. Furthermore, the mixture of exponential distributions is pre-multiplied by a constant which can be translated in the condition $\lambda_+/\lambda = \lambda_-/\lambda = 0.5$, i.e., the activity rates of positive and negative jumps are equal. The reason for all these parameter restrictions is the symmetry property of normal distributions. Once the distribution of the random variable Y is fitted with desired accuracy, we can derive the approximation for any normally distributed variable

$\tilde{Y} \overset{\text{i.i.d.}}{\sim} \mathcal{N}(\tilde{\mu}_J, \tilde{\sigma}_J^2)$. The two random variables can be expressed in terms of a standard normal variable $Z \overset{\text{i.i.d.}}{\sim} \mathcal{N}(0,1)$, i.e., $Y = \sigma_J Z$ and $\tilde{Y} = \tilde{\mu}_J + \tilde{\sigma}_J Z$. Therefore, we have that $\tilde{Y} = \tilde{\mu}_J + \frac{\tilde{\sigma}_J}{\sigma_J} Y$. Simple algebra gives us the expression for the D-MEM approximation for the distribution of $\mathcal{N}(\tilde{\mu}_J, \tilde{\sigma}_J^2)$ via the MEM approximation (4.15):

$$f_{\tilde{Y}}(\tilde{y}) \approx 0.5 \sum_{i=1}^{m} \tilde{p}_i \tilde{\eta}_i e^{-\tilde{\eta}_i |\tilde{y} - \tilde{\mu}_J|}, \tag{4.16}$$

with $\tilde{\eta}_i = \frac{\sigma_J}{\tilde{\sigma}_J} \eta_i$ and $\tilde{p}_i = p_i$ for $i = 1, 2, ..., m$. Expectedly, the displacement parameter is $\xi = \tilde{\mu}_J$.[48]

Completely monotone Lévy processes: FMLS, VG, and CGMY

The Lévy processes considered in this paper (FMLS, VG, and CGMY) share a common feature—complete monotonicity. It is precisely this property that allows us to approximate the considered Lévy processes with hyper-exponential models. In particular, a Lévy density $\nu : (0, +\infty) \to \mathbb{R}$ is said to be completely monotone if it for all $k \in \mathbb{N}_0^+$ it is of class $\mathcal{C}^\infty$ and it holds that $(-1)^k d^k \nu(y)/dy^k > 0$ for all $y > 0$; e.g., see Sato (1999), p. 388.[49] Furthermore, Bernstein's theorem ensures that a Lévy density is completely monotone if and only if it can be decomposed as

$$\nu(y) = \mathbb{1}_{\{y<0\}} \int_{-\infty}^{0} e^{-vy} \rho_-(dv) + \mathbb{1}_{\{y>0\}} \int_{0}^{+\infty} e^{-vy} \rho_+(dv), \tag{4.17}$$

where $\rho_-(dv)$ and $\rho_+(dv)$ are Radon measures on intervals $(-\infty, 0)$ and $(0, +\infty)$, respectively, such that the two integrals are finite. In a nutshell, this means that the arrival rate of jumps is decreasing with the jump size. Upon discretization of the integrals on the r.h.s. of the equation (4.17), we obtain an approximation of a completely monotone Lévy density by a finite mixture of exponential densities. Moreover, jumps with expected size smaller then certain threshold, i.e., jumps with magnitudes close to zero, can be approximated by a diffusion process. Based on this approximation, Asmussen, Madan and Pistorius (2007) infer that completely monotone jump models can be approximated by hyper-exponential jump–diffusion models, which are a subset of the displaced mixed-exponential class.

As an example of a hyper-exponential approximation of a completely monotone Lévy model, we consider the CGMY process of Carr et al. (2002). It is a pure-jump process, and its Lévy density is

[48] The diffusion parameter σ and the jump intensity λ in Merton's jump–diffusion model remain unchanged, which is justified by the fact that the D-MEM approximation (4.16) affects only the distribution of jump sizes.

[49] This definition can be easily extended to the whole real line. The condition for the complete monotonicity then becomes $(-1)^k d^k \nu(|y|)/dy^k > 0$ for $y \in (-\infty, +\infty)$.

given by the exponentially dampened power law

$$\nu_{CGMY}(y) = C\left(\frac{e^{-G|y|}}{|y|^{1+Y}}\mathbb{1}_{\{y<0\}} + \frac{e^{-My}}{y^{1+Y}}\mathbb{1}_{\{y>0\}}\right), \tag{4.18}$$

and its characteristic function is

$$\begin{aligned}\varphi_{\text{CGMY}}(u) :&= \mathbb{E}\left[\exp(iuX_{\text{CGMY}}(t))\right] \\ &= \exp\left(iu\omega t + tC\Gamma(-Y)\left((M-iu)^Y - M^Y + (G+iu)^Y - G^Y\right)\right),\end{aligned} \tag{4.19}$$

where $\omega := -C\Gamma(-Y)((M-1)^Y - M^Y + (G+1)^Y - G^Y)$ represents the convexity adjustment, and $\Gamma(\cdot)$ denotes the mathematical gamma function. The parameter $C \in \mathbb{R}^+$ represents the jump intensity. The parameters $G \in \mathbb{R}_0^+$ and $M \in \mathbb{R}_0^+$ are exponential decay parameters of negative and positive jumps, respectively. Depending on their relative values, the model can generate positive, negative or zero skewness. The parameter Y is especially interesting because it characterizes the so-called fine structure of asset returns, i.e., it describes the behavior of the Lévy density in the neighborhood of zero.[50] Following the idea of Asmussen, Madan and Pistorius (2007), Section 2.1, pp. 85–87, and Jeannin and Pistorius (2010), Section 2, pp. 631–632, our starting point is the identity

$$\frac{1}{y^{1+Y}} = \frac{1}{\Gamma(1+Y)}\int_0^{+\infty} u^Y e^{-uy}du, \tag{4.20}$$

which holds for all $Y \in \mathbb{C}\setminus\{-2,-3,-4,...\}$. This expression follows directly from the definition of the gamma function. Discretization of the integral on the r.h.s. of (4.20) yields

$$\frac{1}{y^{1+Y}} \approx \frac{1}{\Gamma(1+Y)}\sum_{i=1}^{N-1} u_i^Y e^{-u_i y}(u_{i+1}-u_i). \tag{4.21}$$

The partitioning $\Pi(N) := (u_i)_{i=1,2,...,N-1}$ of the interval $(0,+\infty)$ is such that $\Delta_{\Pi(N)} \to 0$ when $N \to \infty$, with the norm defined as $\Delta_{\Pi(N)} = \max_{1\le i\le N-1}|u_{i+1}-u_i|$. Therefore, a completely monotone process can be approximated with arbitrary accuracy by choosing appropriate partition of the integration interval. For example, CGMY density (4.18) can be approximated in the form

$$\begin{aligned}\nu_{CGMY}(y) \approx &\frac{C}{\Gamma(1+Y)}\sum_{i=1}^{N^+-1} w_i^+ e^{-(M+u_i)y}\mathbb{1}_{\{y>0\}} \\ &+ \frac{C}{\Gamma(1+Y)}\sum_{j=1}^{N^--1} w_j^- e^{-(G+v_j)|y|}\mathbb{1}_{\{y<0\}},\end{aligned} \tag{4.22}$$

[50] A CGMY process is completely monotone if $Y \in (-1,2)$. Furthermore, for $Y<0$ the process is of finite activity; for $Y \in (0,1)$ it is characterized by infinite activity and finite variation, and for $Y \in (1,2)$ it has infinite variation, but finite quadratic variation. For more details about the CGMY process see, e.g., Koponen (1995), Boyarchenko and Levendorskiĭ (2000) and Carr et al. (2002).

where $w_i^+ := u_i^Y(u_{i+1} - u_i)$ for $i = 1, 2, ..., N^+$, and $w_j^- := v_j^Y(v_{j+1} - v_j)$ for $j = 1, 2, ..., N^-$. This scheme implicitly introduced the partitioning $U(N^+) := (u_i)_{i=1,2,...,N^+-1}$ of the interval $(0, +\infty)$, as well as the partition $V(N^-) := (v_j)_{j=1,2,...,N^--1}$ of the interval $(-\infty, 0)$. One can easily check that the r.h.s. of the expression (4.22) corresponds to the D-MEM Lévy density (4.1) with the following parameters: $m = N^+ - 1$, $n = N^- - 1$, $\eta_i = M + u_i$ and $p_i = w_i^+/\eta_i$ for $i = 1, 2, ..., m$, $\theta_j = G + v_j$ and $q_j = w_j^-/\theta_j$ for $j = 1, 2, ..., n$, $\lambda_+ = \tilde{C}\sum_{i=1}^{N^+-1} p_i$ and $\lambda_- = \tilde{C}\sum_{j=1}^{N^--1} q_j$, where $\tilde{C} = C/\Gamma(1+Y)$.[51] Therefore, depending on the discretization and the truncation error, which are determined by the choice of the partition of the positive and negative semi-axes, we can obtain an arbitrarily accurate approximation of the CGMY density.

In practical applications, Asmussen, Madan and Pistorius (2007) fix in advance the number of components in the mixture and their respective exponential decay parameters. Subsequently, they minimize a distance between the two Lévy densities by optimally choosing the partition of the integration intervals. Jeannin and Pistorius (2010) follow almost identical procedure, except that they optimize the mixing weights.[52] Nevertheless, the approximation derived in (4.22) implies that there exists a structural relation between the exponential decay parameters and the corresponding mixing weights. Hence, the total number of jumps and the values of the model parameters are in fact determined by the chosen partition. Consistently with the theoretical results presented in equations (4.20)–(4.22), and simultaneously avoiding a computationally burdensome numerical optimization without loss of accuracy, we make a trade-off by choosing a larger number of exponential terms.[53] However, for the remaining steps in our exercise, e.g., for the approximation of small jumps by a diffusion, we follow closely procedure outlined in Asmussen, Madan and Pistorius (2007) and Jeannin and Pistorius (2010) since it ensures the weak convergence of the constructed sequence of HEM processes to the target Lévy process.

[51] We note that, in the D-MEM approximation of a CGMY process, the displacement parameter is equal to zero. More generally, the displacement has to be zero for any model with infinite activity; otherwise, the integral of the Lévy density would not exist.

[52] The number of exponential terms in the mixture varies between 5 and 7 in Asmussen, Madan and Pistorius (2007) and Jeannin and Pistorius (2010).

[53] In particular, we use 50 (non-degenerate) exponential terms in the mixture. Our numerical tests show that the suggested procedure is generally fast and stable. It is important to stress out that a detailed investigation of the three approximation approaches described in this section is a separate research topic. The algorithms outlined here are by no means the major concern of our paper, and the sole purpose of this section is to briefly describe our approach and related it to the relevant papers. Admittedly, there also exist other approaches in the literature, e.g., Crosby, Le Saux and Mijatović (2010) and Hackmann and Kuznetsov (2016). Nonetheless, we find that our modification of Asmussen, Madan and Pistorius (2007) and Jeannin and Pistorius (2010) works sufficiently well for our application.

In addition to the CGMY model we consider two other popular pure-jump models, i.e., the VG model of Madan and Seneta (1990) and the FMLS model of Carr and Wu (2003). Both models are special cases of CGMY. The Lévy density of a VG process is obtained by setting the fine structure parameter to zero in the equation (4.18). On the other hand, the FMLS process is a spectrally negative Lévy process, i.e., positive jumps are completely excluded, and the exponential decay parameter of negative jumps is set to zero. We do not explicitly state the Lévy measures and the characteristic functions of VG and FMLS processes because they can be inferred directly from (4.18) using the aforementioned restrictions.

4.3 Theoretical results

4.3.1 VaR and iVaR: The connection with digital payoffs

Bakshi and Panayotov (2010) established a connection between the iVaR and an expectation of a one-touch digital payoff. In this section, we first summarize their finding and introduce our own notation to facilitate the discussion. Subsequently, we develop an analogous procedure to recover the VaR from an expectation of a European digital payoff.[54]

The iVaR is defined as a conditional quantile of the first-passage distribution (FPD) of the asset return process; see Section 3 in Bakshi and Panayotov (2010), p. 23. The cumulative distribution function (c.d.f.) of the FPD can be computed as the conditional expectation that the log-price process $\{X_u, t \leq u \leq T\}$ will drop below certain pre-specified level $\kappa := \log(K)$, i.e.,

$$P(X_t, \tau) := \mathbb{E}^x \left[\mathbb{1}_{\{X_u < \kappa\}}, t < u \leq T \right], \tag{4.23}$$

where $\tau := T - t$ represents the remaining time before the expiry of the monitoring period, and the value of the log-price process at time t is given by x. The iVaR calculations bring about the payoff structure of one-touch digital down-and-in put options.[55] However, the conditional expectation in the equation (4.23) is taken under the historical and not under the risk-neutral measure. Moreover, even if it were computed under the risk-neutral measure, there is no discounting (at the risk-free rate).

[54] Bakshi and Panayotov (2010), Section 6, p. 26, do not use the digital options framework to infer the VaR. They instead compute the conditional quantiles of the p.d.f. numerically using the Fourier inversion.

[55] Alternatively, one can study the case when the barrier level is above the current asset price level, i.e., the digital up-and-in call payoff structure. We focus in our study on the downside risk of the P&L distribution, i.e., we consider only long positions in the asset.

Therefore, we emphasize that the expression for the c.d.f. of the FPD resembles, but it is *not*, an option pricing problem.

To ease the notation, we first drop the adjective 'down-and-in', as this is the only type of digital payoffs that we consider in this paper. Second, we introduce the name *optionette* to designate the expectation (4.23) and alike.[56] We purposefully chose the name containing the word 'option' because, in our particular setting which assumes the zero expected return under the pricing measure, the c.d.f. of the FPD (as well as the c.d.f. of the end-of-horizon asset return distribution, as we will see in the case of VaR) is a martingale.[57] The differences with respect to the probability measure and the discounting create a wedge between options and optionettes. However, the martingale method is the underlying mathematical framework in both cases.

It follows from the Feynman-Kac theorem that the optionette price can be computed by solving the PIDE

$$-\frac{\partial P}{\partial \tau}(x,\tau)+\frac{\sigma^2}{2}\frac{\partial^2 P}{\partial x^2}(x,\tau)+\bar{\varrho}\frac{\partial P}{\partial x}(x,\tau)+\int_{-\infty}^{+\infty}[P(x+y,\tau)-P(x,\tau)]\nu(y)dy=0, \tag{4.24}$$

where $\bar{\varrho}$ denotes the compensated drift term of the log-price process under some pre-specified physical measure, and the Lévy measure $\nu(\cdot)$ is defined in the equation (4.1). The boundary and the initial conditions are

$$\begin{cases} \lim\limits_{x\uparrow+\infty} P(x,\tau) &= 0, \\ \lim\limits_{x\downarrow\kappa} P(x,\tau) &= 1, \\ \lim\limits_{\tau\downarrow 0} P(x,\tau) &= \mathbb{1}_{\{x<\kappa\}}. \end{cases} \tag{4.25}$$

The iVaR (with the monitoring horizon τ and the confidence level χ) can be computed as

$$\text{iVaR}(\tau,\chi)=e^{x}-e^{\underline{\kappa}}, \quad \text{given that} \quad P(x,\tau;\underline{\kappa})=1-\chi. \tag{4.26}$$

Therefore, the iVaR can be interpreted as the difference between the current asset price $S_t=\exp(x)$ and the implied $(1-\chi)$-quantile level $\underline{K}=\exp(\underline{\kappa})$ of the c.d.f. of the FPD estimated over the monitoring period τ.

[56] More specifically, we use the expressions 'to calculate the (undiscounted) expectation of the one-touch digital put payoff' and 'to price the one-touch digital put optionette' interchangeably.

[57] In the empirical part, we will look into two different physical-world measures, i.e., the historical measure $\mathbb{P}$ (which is obtained by calibrating the models to the historical returns data), and the risk-adjusted measure $\mathbb{Q}^{\vartheta}$ (which is obtained by calibrating the models to the options data, and subsequently applying the risk neutralization procedure).

On the other hand, the VaR is related to the c.d.f. of the asset price process at the end of the monitoring period τ, which can be computed as an expectation of the European digital put payoff:

$$p(X_t, \tau) = \mathbb{E}^x \left[\mathbb{1}_{\{X_T < \kappa\}} \right], \tag{4.27}$$

where κ should be interpreted as the strike price rather than the barrier level. Similarly to the case of one-touch digital put optionette, the dynamics of a European digital put optionette price satisfies the equation (E.30). However, the boundary and the initial conditions are

$$\begin{cases} \lim\limits_{x \uparrow +\infty} p(x, \tau) & = 0, \\ \lim\limits_{x \downarrow -\infty} p(x, \tau) & = 1, \\ \lim\limits_{\tau \downarrow 0} p(x, \tau) & = \mathbb{1}_{\{x < \kappa\}}. \end{cases} \tag{4.28}$$

Therefore, the VaR can be computed as the difference between the current asset price $S_t = \exp(x)$ and the implied $(1-\chi)$-quantile level $\overline{K} = \exp(\overline{\kappa})$ of the c.d.f. of the asset return distribution at the end of the monitoring period:

$$\mathrm{VaR}(\tau, \chi) = e^x - e^{\overline{\kappa}}, \quad \text{given that} \quad p(x, \tau; \overline{\kappa}) = 1 - \chi. \tag{4.29}$$

Equations (4.26) and (4.29) can be solved using, e.g., the bisection method.

Finally, we note that it can be verified that

$$\mathrm{VaR}(\tau, \chi) < \mathrm{iVaR}(\tau, \chi), \quad \text{a.s. for} \quad \tau \in \mathbb{R}^+, \ \chi \in (0, 1). \tag{4.30}$$

Intuitively, the probability of crossing a barrier (from above) at any point in time during the monitoring period is higher than the probability that the underlying process will end up below the barrier level at the expiration date. Indeed, the process which is in the stopping region at the end of the monitoring period has almost surely breached the barrier level before the expiration. Therefore, if a European and a one-touch digital put optionettes have identical prices, i.e., in our notation $p(x, \tau; \overline{\kappa}) = P(x, \tau; \underline{\kappa}) := 1 - \chi$, then almost surely the implied barrier level $\underline{\kappa}$ (the iVaR) has to be lower (greater) than the implied strike $\overline{\kappa}$ (the VaR).

4.3.2 Pricing digital optionettes

We solve the PIDE system (E.30)–(4.25) using the Laplace–Carson transform (LCT) approach. For any locally integrable function $f : \mathbb{R}^+ \to \mathbb{R}$ and for all $\alpha \in \mathbb{R}^+$, the LCT is defined as

$$(\mathscr{LC})_x [f(x)](\alpha) := \tilde{f}(\alpha) := \alpha \int_0^{+\infty} e^{-\alpha x} f(x) dx. \tag{4.31}$$

The main idea of our solution procedure is to compute the LCT of the optionette price with respect to the monitoring horizon τ. Applying the transformation to the PIDE (E.30) would eliminate the time dependence, hence effectively reducing the original pricing problem to an ordinary integro-differential equation (OIDE). Our results for European and one-touch digital put optionettes are summarized in Theorem 4.3.1 and Theorem 4.3.2, respectively.

The optionette prices in the time domain can be computed with the help of the Gaver-Stehfest inversion algorithm (GS):

$$f_M(x) = \sum_{k=1}^{M} \varsigma_k \tilde{f}\left(\frac{k \log(2)}{x}\right), \tag{4.32}$$

where

$$\varsigma_k = \frac{(-1)^{M+k}}{k} \sum_{j=\lfloor (k+1)/2 \rfloor}^{\min\{k,M\}} \frac{j^{M+1}}{M!} \binom{M}{j} \binom{2j}{j} \binom{j}{k-j}. \tag{4.33}$$

It holds that

$$\lim_{M \to \infty} f_M(x) = f(x). \tag{4.34}$$

In expression (4.33), $\lfloor a \rfloor$ is defined as the greatest number $a' \in \mathbb{N}$ such that $a' \leq a$. It is important to point out that the Gaver-Stehfest algorithm takes place on the real line. Morever, the linear Salzer convergence acceleration scheme is included in the formula. We refer to Valkó and Abate (2004), Abate and Whitt (2006) and Kuznetsov (2013) for technical details about the GS inversion algorithm.

Laplace–Carson transforms of option price functions w.r.t. the time to maturity have the meaning of canadized options, e.g., see Carr (1998). We borrow this notation for the pricing digital optionettes, and derive our main theoretical results along the lines of Leippold and Vasiljević (2017), Theorem 1 and Theorem 2, pp. 81, 90–93.

Theorem 4.3.1 (**Canadized European digital put optionette**). *Assume that the asset price process $\{S_u, t \leq u \leq T\}$ is described by the displaced mixed-exponential model (4.2). The price of a canadized European digital put optionette with the strike K and the monitoring horizon τ is thus given*

by

$$\tilde{p}(S_t,\alpha)=\begin{cases} 1+\displaystyle\sum_{i=1}^{\hat{m}}\underline{w}_i\left(\frac{S_t}{K}\right)^{\beta_{i,\alpha}} & \text{if } S_t<K,\\ \displaystyle\sum_{j=1}^{\hat{n}}\overline{w}_j\left(\frac{S_t}{K}\right)^{\gamma_{j,\alpha}} & \text{if } S_t\geq K. \end{cases} \tag{4.35}$$

The coefficients $\{\beta_{i,\alpha}\}_{i=1,\ldots,\hat{m}}$, *and* $\{\gamma_{j,\alpha}\}_{j=1,\ldots,\hat{n}}$ *are positive and negative roots of the characteristic equation* $\Psi(u)=\alpha$, *respectively, and the Lévy exponent* $\Psi(\cdot)$ *is defined in* (E.14). *The number of positive and negative characteristic roots depends on the LCT parameter* α, *i.e., it is equal to* $\hat{m}:=\hat{m}(\alpha)\leq m+1$ *and* $\hat{n}:=\hat{n}(\alpha)\leq n+1$, *respectively, where* $\hat{m},\hat{n}\in\mathbb{N}$. *The coefficients* $\{\underline{w}_i\}_{i=1,\ldots,\hat{m}}$ *and* $\{\overline{w}_j\}_{j=1,\ldots,\hat{n}}$ *can be computed by solving the system of linear equations*

$$\mathbf{A}\mathbf{w}=\mathbf{a}. \tag{4.36}$$

The $(\hat{m}+\hat{n})$*-dimensional column vector* $\mathbf{w}$ *and the* $(m+n+2)$*-dimensional column vector* $\mathbf{a}$ *are given in equations* (E.27) *and* (E.28), *respectively. The matrix* $\mathbf{A}$ *is an* $(m+n+2)\times(\hat{m}+\hat{n})$*-dimensional matrix given in equation* (E.29).

Theorem 4.3.2 (**Canadized one-touch digital put optionette**). *Assume that the asset price process* $\{S_u, t\leq u\leq T\}$ *is described by the displaced mixed-exponential model (4.2). The price of a canadized one-touch digital put optionette with the barrier level* K *and the monitoring horizon* τ *is thus given by*

$$\tilde{P}(S_t,\alpha)=\begin{cases} \displaystyle\sum_{j=1}^{\hat{n}}v_j\left(\frac{S_t}{K}\right)^{\gamma_{j,\alpha}} & \text{if } S_t>K,\\ 1 & \text{if } S_t\leq K, \end{cases} \tag{4.37}$$

using the same notation as in Theorem 4.3.1. The set of coefficients $\{\overline{v}_j\}_{j=1,\ldots,\hat{n}}$ *solve the system of linear equations*

$$\mathbf{B}\mathbf{v}=\mathbf{b}, \tag{4.38}$$

The $\hat{n}$*-dimensional column vector* $\mathbf{v}$ *and the* $(n+1)$*-dimensional column vector* $\mathbf{b}$ *are given in equations* (E.40) *and* (E.41), *respectively. The matrix* $\mathbf{B}$ *is an* $(n+1)\times\hat{n}$*-dimensional matrix given in equation* (E.42).

4.3.3 First-passage disentanglement (FPD)

A one-touch digital put optionette is exercised if the asset price directly hits or overshoots the barrier at any point in time before maturity. Due to the continuity of its paths, and conditionally on the stopping of the process, a Brownian motion almost surely hits the barrier separating the continuation from the stopping region; e.g., see Jeanblanc, Yor and Chesney (2009), Section 3, p. 135. On the other hand, an overshoot occurs if the asset price jumps over the barrier directly into the interior of the stopping region. More specifically, conditional on the stopping of the process due to a jump event, continuously distributed jumps almost surely induce an overshoot, i.e., the price process will almost surely not jump onto the barrier. Starting from the disentanglement results of Leippold and Vasiljević (2017), Theorem 3, pp. 81, 93–94, we show in Theorem 4.3.3 that precisely these properties allow us to quantify the first-passage disentanglement of the jump from the diffusion contribution to the stopping of the process, hence to the price of a one-touch digital put optionette and the iVaR value.

Theorem 4.3.3 (**Canadized first-passage disentanglement**). *Assume that the asset price process* $\{S_u, t \leq u \leq T\}$ *is described by the displaced mixed-exponential model (4.2). The price of a canadized one-touch digital put optionette with the barrier level* K *and the monitoring horizon* τ *can be decomposed as*

$$\tilde{P}(S_t, \alpha) = \tilde{P}_D(S_t, \alpha) + \tilde{P}_J(S_t, \alpha). \tag{4.39}$$

The function $\tilde{P}_D(\cdot, \cdot)$ *represents the contribution of the diffusion process, i.e., the Brownian motion, which is given by*

$$\tilde{P}_D(S_t, \alpha) = \begin{cases} \sum_{j=1}^{\hat{n}} \delta_j \left(\frac{S_t}{K}\right)^{\gamma_{j,\alpha}} & \text{if } S_t > K, \\ 1 & \text{if } S_t = K, \\ 0 & \text{if } S_t \leq K. \end{cases} \tag{4.40}$$

The function $\tilde{P}_J(\cdot, \cdot)$ *is the contribution of the jumps, i.e., the compound Poisson process, and it given by*

$$\tilde{P}_J(S_t, \alpha) = \begin{cases} \sum_{j=1}^{\hat{n}} \iota_j \left(\frac{S_t}{K}\right)^{\gamma_{j,\alpha}} & \text{if } S_t > K, \\ 0 & \text{if } S_t = K, \\ 1 & \text{if } S_t \leq K. \end{cases} \tag{4.41}$$

The sets of coefficients $\{\delta_j\}_{j=1,\dots,\hat{n}}$ *and* $\{\iota_j\}_{j=1,\dots,\hat{n}}$ *solve the systems of linear equations*

$$\begin{aligned} \mathbf{M}_D \boldsymbol{\delta} &= \boldsymbol{\epsilon}_D, \\ \mathbf{M}_J \boldsymbol{\iota} &= \boldsymbol{\epsilon}_J. \end{aligned} \tag{4.42}$$

The $\hat{n}$*-dimensional column vectors* $\boldsymbol{\delta}$ *and* $\boldsymbol{\iota}$ *are given in equations* (E.50) *and* (E.53)*, respectively. The* $(n+1)$*-dimensional column vectors* $\boldsymbol{\epsilon}_D$ *and* $\boldsymbol{\epsilon}_J$ *are given in equations* (E.51) *and* (E.54)*, respectively. The matrices* $\mathbf{M}_D$ *and* $\mathbf{M}_J$ *are identical* $(n+1) \times \hat{n}$*-dimensional matrices, which are equal to the matrix* $\mathbf{B}$ *defined for the one-touch digital put optionettes in equation* (E.42)*. The remaining notation is the same as in Theorem 4.3.1 and Theorem 4.3.2.*

4.4 Estimation of jump models

The first step in our empirical investigation is the calibration of the jump models introduced in Section 4.2.3 under the historical and the risk-neutral measure. To achieve this goal, we use two different data sets: historical returns of the S&P 100 index and OEX American option quotes (bid and ask prices for different strikes and maturities). Additionally, we use the zero-coupon curve for the calibration under the risk-neutral measure.[58] The data used in our study is obtained from OptionMetrics.

4.4.1 The data

Our first data set consists of 939 weekly historical returns of the S&P 100 index from January 1996 until August 2014, which are obtained by aggregating five successive daily return. It spans almost two decades and encompasses a broad spectrum of market conditions, including the Global financial crisis of 2008–2009. The data treatment for historical return time series closely follows Bakshi and Panayotov (2010), Section 5, pp. 25–26.[59] The ultimate goal of our study is to estimate 10-day VaR and iVaR levels. Ideally, the sampling frequency should match exactly the monitoring horizon. To achieve a reasonable level of accuracy, using biweekly returns requires long historical time series. However, if the

[58] Similarly to Bakshi and Panayotov (2010), the dividends are neglected in our study. The reason is that the digital optionette approach for the computation of the VaR and the iVaR, which is introduced in Section 4.3, is valid only if the drift term of the underlying asset process (4.2) is equal to zero. This means that both the expected return and the dividend yield are assumed to be zero in the short term.

[59] Bakshi and Panayotov (2010) investigate only the period 1995–2005 which does not include the most recent turbulent market conditions and the post-crisis period. On the other hand, our sample extends to the period 2005–2014. We believe that this is very important for our empirical study given that financial markets and the risk management practice have undergone a series of stupendous changes since 2008.

data were available, using observations from distant past might be misleading and irrelevant for the risk management. On the other hand, weekly returns are clearly a better candidate than daily returns. Therefore, we compromise by using weekly historical return time series, and we adopt the strategy of re-estimating models on monthly frequency based on rolling windows of 260 weekly returns. This implies that the first month for which we estimate our models will be January 2001 because we need 5 years of data to create a weekly time series of desired length.

The second data set used in our study contains option quotes exclusively. It comprises S&P 100 index American options data (ticker symbol: OEX) spanning the period from March 2001 until August 2014. The starting month of our option sample is chosen to coincide with the first month for which we are able to estimate the models based on the historical time series of S&P 100 index, conditional on the monthly re-calibration procedure and the choice of weekly sampling frequency. Overall, this leaves us with 162 dates on which we estimate the models on both historical and option data. For the re-calibration timestamps we choose those dates at the beginning of each month on which there exist liquid options maturing in exactly 10 trading days, hence matching the horizon which is recommended by the regulators for the computation of the risk measures.[60]

For each observation date in the sample, the option data treatment is conducted as follows. In the first step, we eliminate all calls because puts are much more informative about the downside risk in the underlying.[61] Second, we exclude illiquid in-the-money put options (ITM), i.e., puts with moneyness greater than 1.03.[62] Hence, our sample contains only liquid near-the-money (NTM) and out-of-the-money (OTM) put options. To match the 10-day horizon, we keep in our dataset only those options which have maturities equal or shorter than 10 days. We use mid-prices—which are computed as averages of the bid and ask market quotes—as a proxy for our market prices. Option quotes lower than 0.125 units are eliminated due to the minimum tick limitations. Additionally, we exclude the options with zero volume and/or zero open interest. Descriptive statistics of our option data sample are given in Table 4.1. The total number of option quotes in the dataset is 3,411. NTM put options ($0.97 < m < 1.03$) account for approximately 41.4 percent of the sample. OTM put options ($m < 0.97$)

[60] Our procedure for selection of re-calibration dates introduces a subtle modification of Bakshi and Panayotov (2010) where options bear no weight whatsoever. It turns out that most of the re-calibration dates chosen are first Mondays in each month. Sometimes re-calibration date is Tuesday or Wednesday if a national holiday happen to be on a Monday, e.g., the Independence Day or the Labor Day.

[61] For simplicity, we consider only the long position in the S&P 100 index.

[62] We define moneyness m as the ratio of the strike K and the futures price $F_{t,T} := S_t e^{r(T-t)}$, i.e., $m := K/F_{t,T}$.

Table 4.1: **S&P 100 index options data, March 2001–August 2014.** We report descriptive statistics for near-the-money (NTM) and out-of-the-money (OTM) S&P 100 American put options with maturities of up to 10 days. The data is obtained from OptionMetrics and filtered according to the standard criteria. Our option dataset comprises closing quotes of liquid put options sampled on monthly frequency. The data treatment and the monthly time-stamping procedure are described in Section 4.4.1. There are 162 observation dates in total. We report the number of option contracts traded (Panel A), the average quoted price (Panel B) and the average implied volatility (Panel C). Each statistic is computed for three different maturity bins and four different moneyness bins, as well as for the entire sample, i.e., aggregated across the maturity and the moneyness dimension. DTM stands for days to maturity.

Panel A: Number of contracts across moneyness and maturity

Moneyness	DTM≤5	5<DTM≤9	DTM=10	All
K/F < 0.94	78	81	1,207	1,366
0.94<K/F<0.97	173	22	437	632
0.97<K/F<1.00	311	26	450	787
1.00<K/F<1.03	164	27	435	626
All	726	156	2,529	3,411

Panel B: Average quoted price across moneyness and maturity

Moneyness	DTM≤5	5<DTM≤9	DTM=10	All
K/F < 0.94	0.39	0.42	0.65	0.62
0.94<K/F<0.97	0.70	1.51	1.97	1.60
0.97<K/F<1.00	2.16	3.54	4.90	3.77
1.00<K/F<1.03	8.78	11.84	13.02	11.86
All	3.11	3.07	3.76	3.59

Panel C: Average implied volatility across moneyness and maturity

Moneyness	DTM≤5	5<DTM≤9	DTM=10	All
K/F < 0.94	0.4985	0.3721	0.3930	0.3978
0.94<K/F<0.97	0.3444	0.2467	0.2452	0.2724
0.97<K/F<1.00	0.2343	0.1960	0.2088	0.2184
1.00<K/F<1.03	0.2475	0.1988	0.1987	0.2115
All	0.2920	0.2951	0.3014	0.2991

constitute approximately 58.6 percent of the dataset. The average implied volatility smile straddles the range from 21.15 percent (NTM puts) to 39.78 percent (OTM puts).

Before we present the empirical results, we provide a rationale for our particular choice of option data. The most actively traded types of derivative contracts in financial markets are European and American options. We use American options because they are path-dependent. Due to the early exercise feature, market quotes of American option prices embed the information about the set of events that might occur prior to the expiry. Therefore, market prices of American options reflect the first-passage probabilities and the intra-horizon risk. On the other hand, vanilla European options carry only information about the possible outcomes on a given future date (i.e., at the maturity). Since the pricing functional of an American option admits a decomposition into its European counterpart and the early exercise premium (e.g., see Detemple 2005, and references therein), which makes them informative about the end-of-horizon risk as well.

4.4.2 Calibration results

First, we estimate parameters for each considered model under the historical measure. In particular, we conduct a rolling-window maximum likelihood estimation (MLE) using the weekly historical returns.[63] Second, the calibration under the risk-neutral measure is conducted by minimizing a loss function in the form of a sequential weighted non-linear least squares (WNLLS) for each date in our sample. The weights are defined as the inverses of squared bid-ask spreads. Our objective function can be interpreted as a liquidity-weighted Euclidian distance between the market quotes and the corresponding model option prices.

The most important statistics for historical and option-based calibrations are summarized in Table 4.2. We report the average values and the standard deviations of model parameters over the whole sample. Several patterns can be observed. First, the option-implied estimates exhibit larger variation across time then the parameters obtained from the calibration based on the historical returns. Arguably, this is due to better responsiveness of option-implied model parameters to the changing market conditions.[64] Second, for our infinite activity Lévy processes, the jump arrival rate C is typically in-

[63] There are two notable differences in our estimation approach from that of Bakshi and Panayotov (2010). Namely, we use the Fourier cosine method of Fang and Oosterlee (2008) to compute the p.d.f. of the log-price process. Furthermore, we do not restrict the value of the fine structure parameter Y to 0.5 in the CGMY model. All values in the interval $Y \in (-1, 2)$ are allowed, which ensures an additional degree of freedom in the CGMY model.

[64] The instability of the risk-neutral parameters could partially be due to the non-convexity of the WNLLS loss function and the existence of multiple local minima; e.g., see Cont and Tankov (2004), Section 3.1, pp. 13–16.

Table 4.2: **Summary statistics for parameter estimates.** We estimate parameters of the Merton jump–diffusion (MJD), the finite-moment log-stable (FMLS), the variance gamma (VG), and the Carr-Geman-Madan-Yor (CGMY) model using the S&P 100 historical return time series data (Panel A) and the short-term S&P 100 American put options (Panel B). The total number of observations in our sample is 162 (monthly frequency). The table entries report the average values and the standard deviations (in parentheses) of the estimated parameters. Additionally, we include the values of the rolling-window negative log-likelihood based on the historical returns (MLE) and the weighted mean squared errors of the sequential option calibration (MSE). Detailed information about the data and the estimation techniques is provided in Section 4.4.1 and Section 4.4.2, respectively.

Panel A: Calibration under the historical measure					
Parameters	σ	λ	μ_J	σ_J	MLE
MJD	0.10	4.23	-0.32	0.14	4.62
	(0.03)	(5.56)	(0.49)	(0.18)	(0.18)
Parameters	C	G	M	Y	MLE
FMLS	0.09	_	_	1.88	4.65
	(0.01)			(0.07)	(0.17)
VG	549.78	110.48	184.40	_	4.63
	(5,102.29)	(289.99)	(408.29)		(0.17)
CGMY	14.22	2,144.64	3,033.41	1.24	4.68
	(77.36)	(1,003.31)	(876.54)	(0.27)	(0.18)
Panel B: Calibration under the risk-neutral measure					
Parameters	σ	λ	μ_J	σ_J	MSE
MJD	0.12	5.57	-0.05	0.07	3.11
	(0.09)	(13.86)	(0.06)	(0.04)	(3.49)
Parameters	C	G	M	Y	MSE
FMLS	0.13	_	_	1.85	4.04
	(0.08)			(0.08)	(4.00)
VG	17.78	66.00	1,711.59	_	3.50
	(41.06)	(374.41)	(7,982.77)		(3.53)
CGMY	254.39	14.92	715.62	0.95	2.90
	(991.68)	(22.43)	(1,526.60)	(0.95)	(3.45)

Table 4.3: **Model performance (pairwise comparison).** The table entries report the values of Vuong (1989)'s closeness test statistic for pairwise equivalence of non-nested models in terms of model performance. The statistics are computed for the pairwise combinations of the Merton jump–diffusion (MJD), the finite-moment log-stable (FMLS), the variance gamma (VG), and the Carr-Geman-Madan-Yor (CGMY) model. Panel A (Panel B) reports the pairwise statistics for the maximum likelihood estimation (weighted non-linear least squares estimation) under the historical (risk-neutral) measure. The null hypothesis is that there is no difference between the two models in terms of the closeness to the true data generating process, and the alternative is that one model is closer. Positive values of test statistic larger than 1.65 (2.32) imply, for the given pair of models, the domination of the first model over the second one at the confidence level of 95%(99%). Conversely, the negative values of test statistic smaller than -1.65 (-2.32) imply the domination of the second model over the first model at the confidence level of 95% (99%).

Panel A: Pairwise model comparison under the historical measure				
Model	MJD	FMLS	VG	CGMY
MJD	—	-1.80	-2.91	11.87
FMLS	—	—	-1.65	17.77
VG	—	—	—	16.68
Panel B: Pairwise model comparison under the risk-neutral measure				
Model	MJD	FMLS	VG	CGMY
MJD	—	7.19	6.05	-5.26
FMLS	—	—	-3.61	-8.80
VG	—	—	—	-8.60

versely proportional to the fine structure parameter Y. This result is plausible because higher values of the fine structure parameter indicate increased activity of the small jumps, which are effectively taking over some part of the variation of the stochastic process (that would otherwise be captured by the jump intensity parameter). Third, the exponential decay parameters M and G are positively correlated with the parameter C. The reason is that the reciprocal values of M and G represent the average sizes of large jumps, which are inversely related to the jump intensity parameter due to the property of complete monotonicity. Fourth, we observe across all models that the average jump size is negative.

4.4.3 Model performance

At first glance we observe similar performance for all models under the historical measure (MLE statistic in the Panel A of Table 4.2). The hierarchy among the four models is more apparent under the risk-neutral measure—CGMY model seems to provide the best fit to the option data (MSE statistic in the Panel B of Table 4.2). However, these values alone are not sufficiently informative about the model performance. To address this issue, we conduct Vuong (1989)'s closeness test (for non-nested models) for pairwise comparison of the model calibration performance; see Table 4.3). Panel A summarizes the Vuong test statistics for the historical estimation. The calibration performance ordering among the models is: VG $\succ$ FMLS $\succ$ MJD $\succ$ CGMY. On the other hand, the hierarchy of the models looks quite different for the option-based estimation (Panel B): (MJD $\sim$ CGMY) $\succ$ VG $\succ$ FMLS.[65] We therefore conclude that the model performance rankings are incoherent under the historical and the risk-neutral measure. This finding corroborates the argument that the informational content of the two probability measures are very different. Furthermore, it reinforces the importance of our research question regarding the relevance and the reliability of option-based estimates of risk measures—and more generally about the impact of the estimation risk—in the market risk management context.

[65] For two model (A and B) we write A $\succ$ B (B $\succ$ A) if the Vuong (1989)'s closeness test is rejected in favor of model A (B). We write A $\sim$ B if the test is not rejected.

4.5 Empirical results

4.5.1 VaR and iVaR estimates

To estimate VaR and iVaR we proceed as follows. First, we employ the approximation procedure given in Section 4.2.3, and obtain the historical and the risk-neutral D-MEM parameters corresponding to the calibrated Lévy models. Second, the risk-neutral D-MEM parameters are translated into the risk-adjusted parameters by applying the change of measure derived in Section 4.2.2. To demonstrate the outcome of the approximation concisely and instructively, the dynamics of the (diffusion) volatility and the average jump size of the respective D-MEM approximations are presented in Figure 4.2. We plot the time series of the average volatility and the average jump size with biweekly (10-day) horizon in view, which matches the regulatory monitoring period of of market risk measures.

Hinging on the approximation results, the VaR and iVaR estimates are computed—assuming 99.0% and 99.9% confidence levels, and 10-day monitoring horizon—via the digital optionette approach described in Section 4.3.1 and Section 4.3.2. Furthermore, for each observation date in the sample, we decompose the estimated iVaR into a diffusion and a jump component by applying the theoretical results for the first-passage disentanglement given in Section 4.3.3. The time evolution of the jump contribution to the iVaR (in the sense of Theorem 4.3.3) is presented in Figure 4.3. The results are striking: Irrespectively of the model and the estimation procedure, jumps typically account for more than 80% of the iVaR, with an average of about 90%. This means that potential reserve capital level breaches are most likely caused by a jump in the asset price process, which almost surely incurs an overshoot (i.e., the loss beyond the predetermined set-aside cash buffer).

In the next step, following the procedure presented in Bakshi and Panayotov (2010), we quantify the impact of jumps and intra-horizon risk by computing the ratios of our jump models' VaR and iVaR estimates to a benchmark VaR value.[66] The benchmark is defined as the $(1-\chi)$-quantile of the normal distribution $\mathcal{N}(\hat{\mu}, \hat{\sigma}^2)$, where χ is either 99.0% or 99.9%.

The parameter $\hat{\mu} = 0$ is the drift, and the parameter $\hat{\sigma}$ is the standard deviation of the of the (demeaned) return process under the historical measure. Therefore, assuming the aforementioned confidence levels, the benchmark VaR level is equal to $(2.32\hat{\sigma} - \hat{\mu})$ and $(3.09\hat{\sigma} - \hat{\mu})$, respectively. The

[66] Bakshi and Panayotov (2010) used the term 'multiple' for these ratios, and we adopt their notation. However, we note that Boudoukh et al. (2004) and Rossello (2008) used the term 'inflation factor' instead.

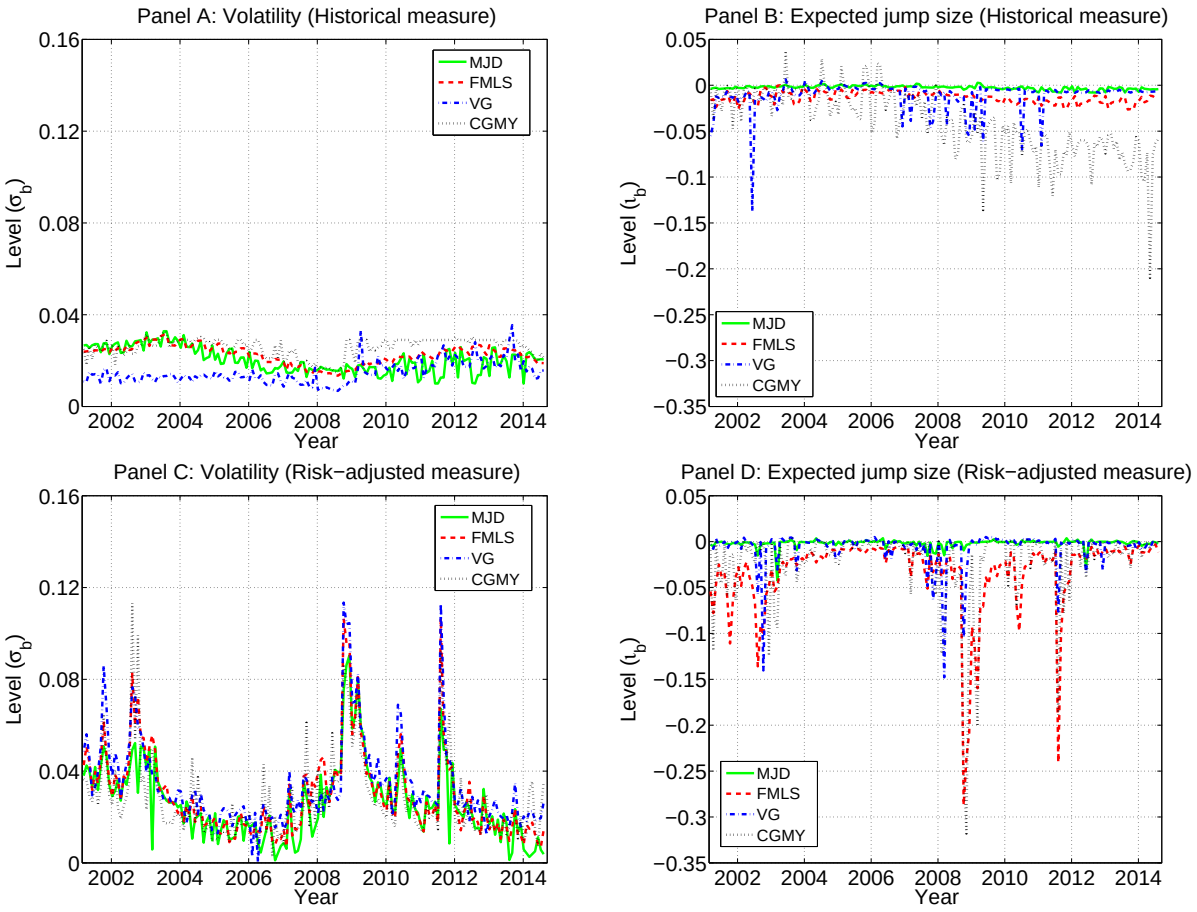

Figure 4.2: **Volatility and expected jumps size (D-MEM approximation).** The plots represent the time evolution (monthly frequency) of biweekly (diffusion) volatility $\sigma_b := \sigma\sqrt{\tau}$ and the expected jump size $\iota_b := \lambda\zeta\tau$ of log-price process over the time horizon of 10 days, i.e., $\tau = 10/252$. The parameter λ is the jump intensity, and the parameter ζ is defined in (4.4). The model parameters are estimated by approximating the Merton jump–diffusion (MJD), the finite-moment log-stable (FMLS), the variance gamma (VG), and the Carr-Geman-Madan-Yor (CGMY) model with displaced mixed-exponential models (D-MEM) under the historical and the risk-adjusted measure. Panels A and C (B and D) represent the evolution of the volatility (the expected jump sizes) for the considered models under the historical and the risk-adjusted measure, respectively.

second benchmark VaR is constructed using the filtered historical simulation (FHS) approach of Barone-Adesi, Giannopoulos and Vosper (1999) and Barone-Adesi, Engle and Mancini (2008).[67]

Our findings are summarized in Table 4.4. Panel A comprises average, median, and maximum values of the VaR and the iVaR multiples based on the estimation under the historical measure. Compared to the findings of Bakshi and Panayotov (2010), we estimate similar or lower (similar or higher) VaR and iVaR multiples at 99.0% (99.9%) confidence level. Almost uniformly, CGMY (FMLS) model has the lowest (highest) VaR and iVaR multiples. This results is stronger for the more stringent confidence level, i.e., the relative difference of the CGMY (FMLS) multiples w.r.t. the other two jump models is amplified. Elevated FMLS multiples can be explained by the fact that it is the only spectrally negative process, and the only one without exponentially dampened Lévy density, among the four considered jump models. Overall, at 99.0% (99.9%) confidence level, a historical VaR estimator and a historical iVaR estimator can increase the benchmark level by the factor 1.99 (3.43) and 2.16 (3.52), respectively. Using the alternative benchmark VaR, we obtain the same rankings among the models. However, the multiples are partially dampened; the maximum multiples are 1.24 (2.11) and 1.35 (2.17) at 99.0% (99.9%) confidence level for the respective risk measures.

Panel B reports the same descriptive statistics based on the multiples estimated under the risk-adjusted measure. We immediately observe that average, median, and maximum multiples are uniformly and significantly higher in this case. In other words, they are more conservative and thus provide a better protection against adverse market moves. Moreover, the forward-looking multiples exhibit larger variation across models, which can be interpreted as the model risk. However, the stupendous difference between the multiples estimated under the two probability measures (especially for the maximum iVaR multiples at 99.9% confidence level) strongly indicates that the estimation risk is probably even more important. In terms of rankings under the risk-adjusted measure, MJD (CGMY) model has the lowest (highest) VaR and iVaR multiples. A risk-adjusted VaR estimator and a risk-adjusted iVaR estimator can increase the benchmark level by the factor 7.61 (9.96) and 8.12 (9.96), respectively, at 99.0% (99.9%) confidence level. We note that the alternative benchmark VaR yields

[67] Our FHS exercise is based on an AR(1)-GARCH(1,1) model with leverage effect under the historical measure; see Monfort and Pegoraro (2012), Section 4.4.1, p. 1683. The algorithm is explained in detail in Barone-Adesi, Giannopoulos and Vosper (1999), pp. 585–587. We note that the GARCH model is estimated using 5 years of daily returns, i.e., 1,300 observations, and the FHS distributions of the cumulative returns and the running minima over 10-day horizon (from which we compute the VaR and the iVaR, respectively) arise from 10,000 replications of the filtered historical returns simulation.

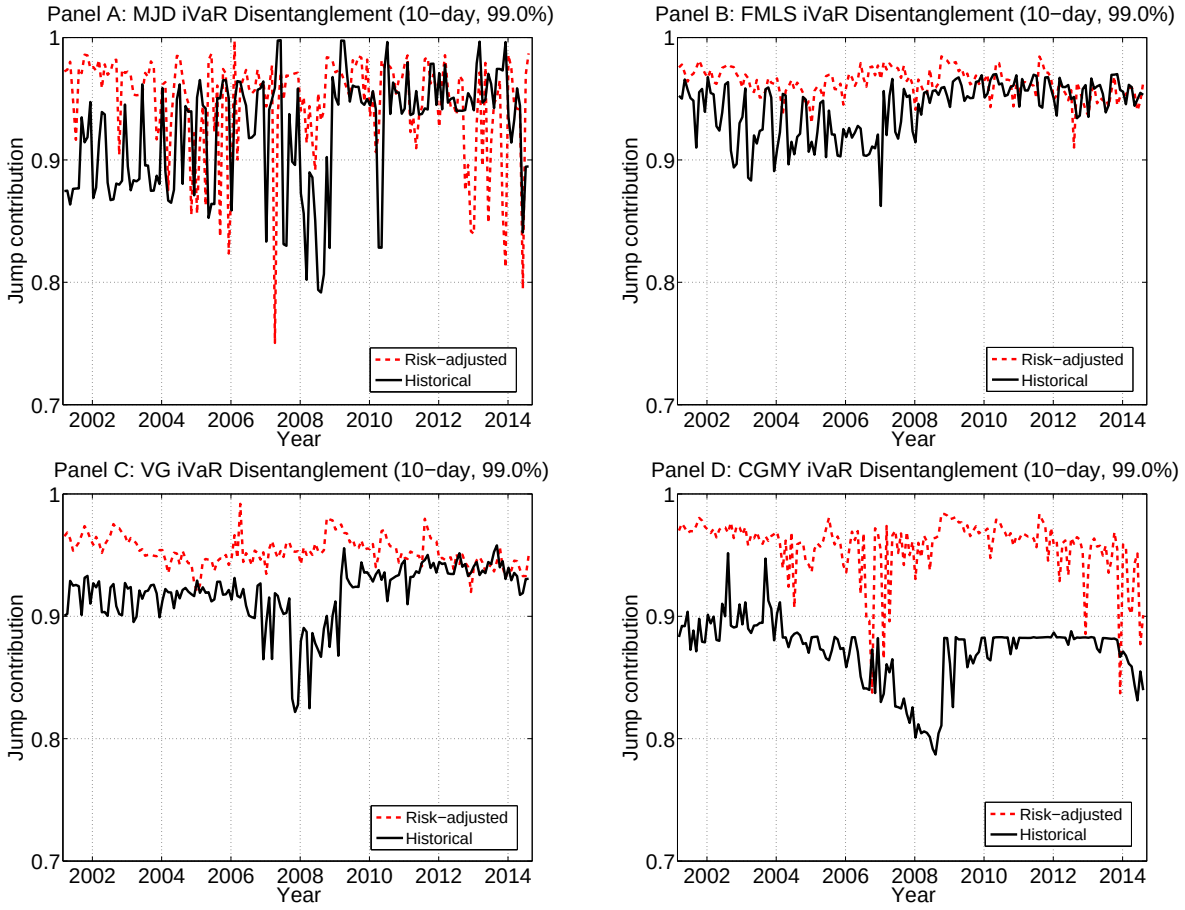

Figure 4.3: **First-passage disentanglement of the iVaR (10-day horizon, 99.0% confidence level).** For each considered model—the Merton jump–diffusion (MJD), the finite-moment log-stable (FMLS), the variance gamma (VG), and the Carr-Geman-Madan-Yor (CGMY) model, which are given in Panels A, B, C, and D, respectively—we plot the time evolution of the jump contribution to the 10-day intra-horizon value at risk (iVaR) calculated at the confidence level of 99.0%. Our results are based on the first-passage disentanglement (FPD) approach introduced in Section 4.3.3. For each of the four models, the jumps are contributing by approximately 90% to the iVaR. These findings hold under the historical and the risk-adjusted measure alike. Interestingly, the model and the estimation risk seem to have significantly smaller impact on the FPD results relative to the backtesting results presented in Figure 4.6 and Figure 4.7.

Table 4.4: **VaR and iVaR multiples.** The table reports average, median, and maximum multiples of the end-of-horizon value at risk (VaR) and the intra-horizon value at risk (iVaR)—computed for $\chi = 99.0\%$ and 99.9% confidence levels at 10-day monitoring horizon—for the Merton jump–diffusion (MJD), the finite-moment log-stable (FMLS), the variance gamma (VG), and the Carr-Geman-Madan-Yor (CGMY) model under the historical and the risk-adjusted measure. The analysis is based on the time series of S&P 100 historical returns and the short-term S&P 100 American put options over the period March 2001–August 2014. The estimation results are time-stamped monthly with total number of 162 dates in the sample. For each considered model, the multiples are computed as ratios of the respective VaR and iVaR estimates and the benchmark VaR value, which is given as either 1% or 0.1% quantile of the normal distribution $\mathcal{N}(\hat{\mu}, \hat{\sigma}^2)$. More precisely, the benchmark VaR is equal to $(2.32\hat{\sigma} - \hat{\mu})$ and $(3.09\hat{\sigma} - \hat{\mu})$ for the 99.0% and 99.9% confidence level, respectively. The parameter $\hat{\sigma}$ is the standard deviation of the (demeaned) time series of S&P 100 historical returns used for the estimation under the historical measure on a given day. The location parameter $\hat{\mu}$ is set to zero. We also report (in parentheses) the VaR and the iVaR multiples of our jump models w.r.t. the VaR estimates based on the filtered historical simulation (FHS) approach.

Panel A: Historical VaR & iVaR multiples

χ= **99.0**%	MJD	FMLS	VG	CGMY
Avg. VaR	1.11 (0.73)	1.20 (0.79)	1.20 (0.79)	1.00 (0.66)
Med. VaR	1.11 (0.73)	1.19 (0.76)	1.21 (0.77)	0.99 (0.65)
Max. VaR	1.99 (1.24)	1.70 (1.13)	1.85 (1.15)	1.26 (0.87)
Avg. iVaR	1.19 (0.79)	1.29 (0.85)	1.29 (0.85)	1.07 (0.71)
Med. iVaR	1.21 (0.78)	1.28 (0.82)	1.30 (0.83)	1.06 (0.70)
Max. iVaR	2.16 (1.35)	1.83 (1.22)	1.99 (1.24)	1.35 (0.93)
χ= **99.9**%	MJD	FMLS	VG	CGMY
Avg. VaR	1.38 (0.85)	1.99 (1.23)	1.32 (0.81)	1.00 (0.62)
Med. VaR	1.39 (0.81)	2.03 (1.20)	1.34 (0.80)	0.98 (0.61)
Max. VaR	2.47 (1.63)	3.43 (2.11)	2.09 (1.20)	2.65 (1.02)
Avg. iVaR	1.43 (0.88)	2.07 (1.28)	1.37 (0.85)	1.04 (0.65)
Med. iVaR	1.43 (0.84)	2.11 (1.25)	1.39 (0.83)	1.02 (0.64)
Max. iVaR	2.59 (1.71)	3.52 (2.17)	2.19 (1.25)	1.73 (1.08)

Panel B: Risk-adjusted VaR & iVaR multiples

χ= **99.0**%	MJD	FMLS	VG	CGMY
Avg. VaR	1.61 (1.06)	1.69 (1.11)	1.87 (1.23)	1.81 (1.19)
Med. VaR	1.37 (1.94)	1.35 (0.89)	1.51 (1.01)	1.49 (0.99)
Max. VaR	6.57 (3.93)	7.52 (4.50)	7.41 (4.43)	7.61 (4.55)
Avg. iVaR	1.69 (1.11)	1.83 (1.20)	2.02 (1.32)	1.95 (1.28)
Med. iVaR	1.42 (0.96)	1.46 (0.96)	1.65 (1.08)	1.61 (1.07)
Max. iVaR	6.82 (4.07)	8.04 (4.81)	7.90 (4.72)	8.12 (4.86)
χ= **99.9**%	MJD	FMLS	VG	CGMY
Avg. VaR	2.28 (1.40)	2.87 (1.77)	2.15 (1.31)	2.47 (1.51)
Med. VaR	2.15 (1.33)	2.58 (1.57)	1.82 (1.15)	2.27 (1.38)
Max. VaR	7.15 (3.28)	8.11 (4.19)	7.36 (3.38)	9.96 (5.63)
Avg. iVaR	2.35 (1.44)	2.99 (1.84)	2.25 (1.38)	2.57 (1.57)
Med. iVaR	2.22 (1.35)	2.69 (1.65)	1.92 (1.21)	2.36 (1.43)
Max. iVaR	7.29 (3.35)	8.48 (4.20)	7.62 (3.50)	9.96 (5.63)

again the same rankings. The maximum multiples with respect to the FHS VaR are 4.55 (5.64) and 4.86 (5.63) at 99.0% (99.9%) confidence level under the historical and the risk-adjusted measure, respectively.

To illustrate better the behavior of multiples, we plot the time evolution of each model's iVaR multiples under the historical and the risk-adjusted measure in Figure 4.4. The results are computed at 99.0% confidence level at 10-day monitoring horizon. In contrast to the analysis presented above, we use now the 10-day VaR estimates of each jump model for a given probability measure as the benchmark (instead of a quantile of a normal distribution or an FHS distribution) to compute the respective multiples. By construction, these "within-model" iVaR multiples are informative about the marginal contribution of the intra-horizon risk component to the iVaR; see equation (4.30). Our findings indicate that, under both probability measures, the iVaR exceeds the VaR estimate by 5–12% percent, with an average of about 7.5–8.0% (with a notable exception of the risk-adjusted MJD for which we obtain somewhat lower values). On the other hand, it can be easily verified that an iVaR of a normal distribution (with mean zero, and irrespectively of the standard deviation) exceeds the corresponding VaR level by 10.7%. Within the scope of their empirical study, Bakshi and Panayotov (2010), Section 6.4, pp. 29–30, report that the average marginal contribution of the intra-horizon component to iVaR multiple is larger than the benchmark number stated above. They conclude that jumps have a tendency to increase the marginal contribution of the intra-horizon risk to the iVaR. Our empirical results—which are qualitatively robust to the choice of probability measure—are pointing to the opposite effect, i.e., the expectation of jumps (on the top of the diffusion risk) typically elevates both risk metrics, but the VaR estimates seem to receive a stronger boost.

Finally, we plot in Figure 4.5 the dynamics of the ratio of the risk-adjusted and the historical iVaR estimates for each of the jump models separately.[68] The risk-adjusted iVaR estimates are lower than their historical counterparts in the periods of market calm. Conversely, the ratio sharply rises during the financial and economic crises, most notably during the Stock market downturn of 2002, the Global financial crisis of 2008–2009, the European debt crisis of 2009–2010, and the Stock market downturn of 2011. Therefore, the risk-adjusted iVaR is more sensitive and responsive to the market conditions. Indeed, this is a plausible result given the forward-looking nature of the risk metrics estimated under the risk-adjusted measure.

[68]The ratio of the risk-adjusted and the historical iVaR estimates follows almost identical pattern, hence we do not report it in Figure 4.5.

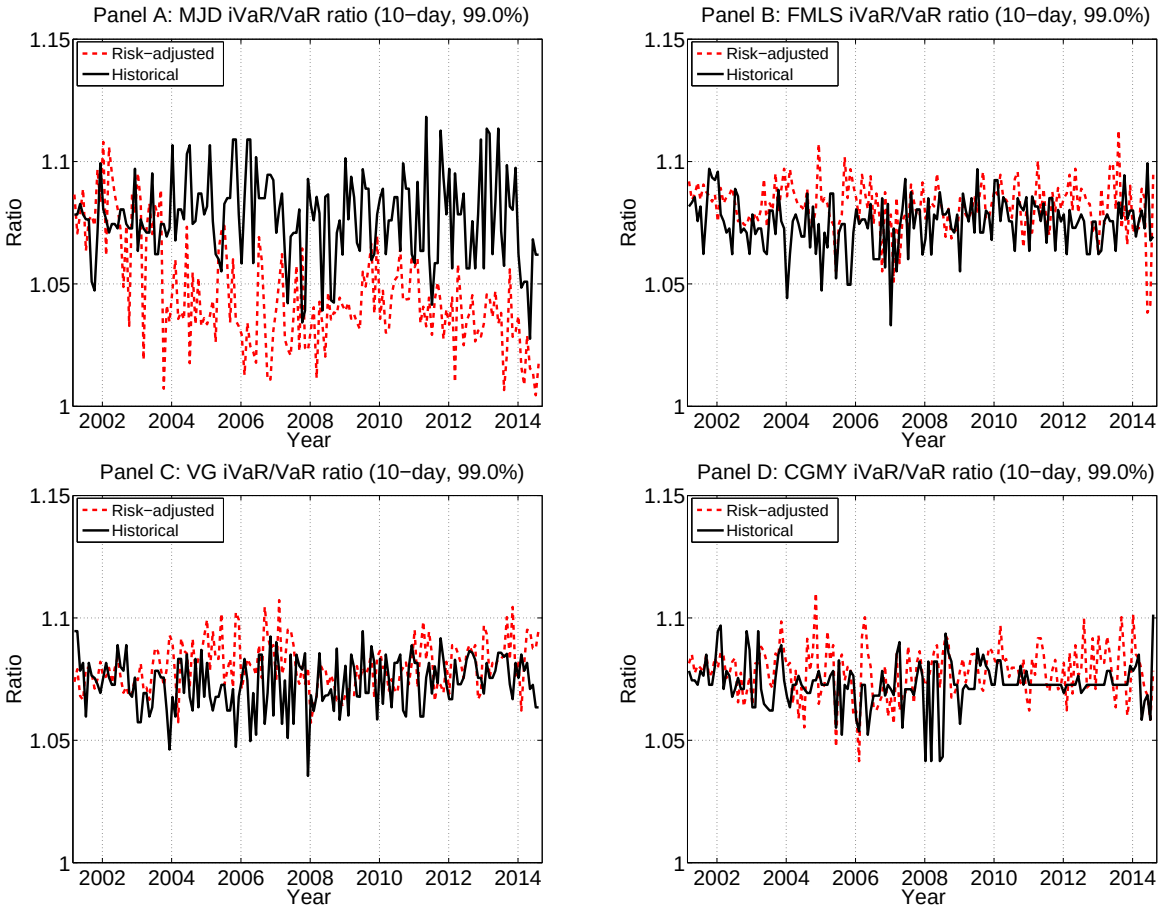

Figure 4.4: **iVaR multiples across models (10-day horizon, 99.0% confidence level).** For each considered model—the Merton jump–diffusion (MJD), the finite-moment log-stable (FMLS), the variance gamma (VG), and the Carr-Geman-Madan-Yor (CGMY) model, which are given in Panels A, B, C, and D, respectively—we plot the time evolution of the ratio of the intra-horizon value at risk (iVaR) to the end-of-horizon value at risk (VaR), estimated under the historical and the risk-adjusted measure at the confidence level of 99.0% and with the monitoring horizon of 10 days.

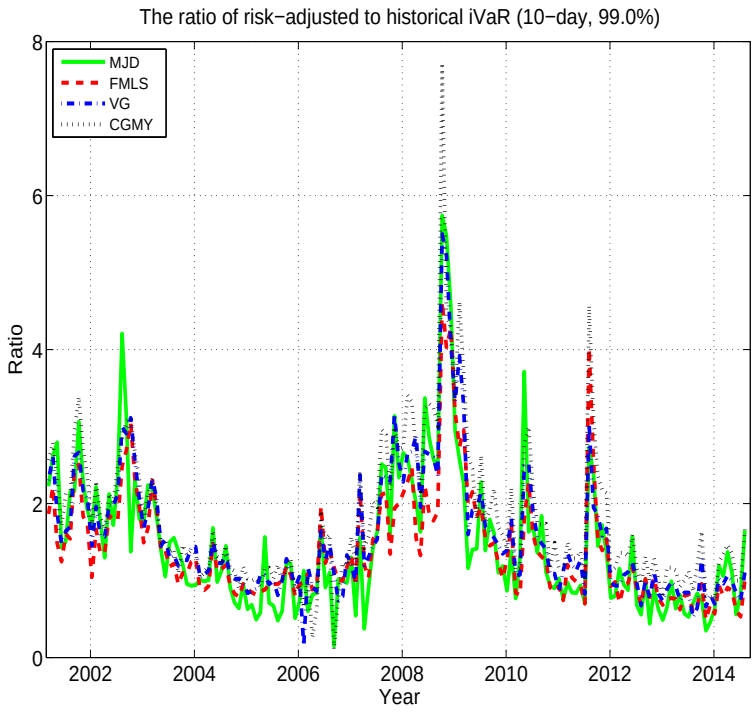

Figure 4.5: **The impact of the probability measure on iVaR (10-day horizon, 99.0% confidence level).** For each considered model—the Merton jump–diffusion (MJD), the finite-moment log-stable (FMLS), the variance gamma (VG), and the Carr-Geman-Madan-Yor (CGMY) model—we plot the time evolution of the ratio of the risk-adjusted to historical intra-horizon value at risk (iVaR) calculated at the confidence level of 99.0%, and with monitoring horizon of 10 days.

In summary, based on the empirical findings presented in this section, we conclude that the risk-adjusted iVaR estimates—with average (maximum) multiples in the range 1.69–2.02 (6.82–8.12)—can only partially explain the Basel multipliers, which are typically between 3 and 4. However, the results summarized in Table 4.4 and Figure 4.5 indicate that the Basel multipliers are often exaggerated in calm periods, thus unnecessarily inflating the risk metrics. On the other hand, historical estimates are not properly capturing the market sentiment when a crisis suddenly occurs. Moreover, it seems that the Basel multipliers do not provide a completely adequate compensation for the risk underestimation anomaly of VaR and iVaR estimates computed under the historical measure. Therefore, the implicit recommendation of the risk-adjusted approach to market risk management is to either use option-based estimates (whenever available) in addition to historical returns data, or to swiftly adjust, i.e., amplify, the current levels of Basel multipliers during imminent market turmoil periods (which is the time when their effectiveness is most needed).

4.5.2 Backtesting

To evaluate VaR (iVaR) forecasting performance of our jump models under the two probability measures, we retrieve the realized 10-day cumulative return (minimum interim cumulative return) for every observation date in the sample. In Figure 4.6 we compare the VaR estimates under the historical and the risk-adjusted measure with the realized returns. Additionally, we include the times series of FHS VaR estimates. An analogous plot for the iVaR is presented in Figure 4.7. In both cases, only the confidence level of 99.0% is considered.[69]

We observe VaR and iVaR violations across all models. However, the forecasting performance is markedly different under the two measures. In particular, under the historical measure, there are typically 6–7 VaR breaches and 8–11 iVaR breaches out of total number of 162 observations. On the other hand, under the risk-adjusted measure, there are either no violations at all or at most one violation of VaR and iVaR critical levels. Therefore, the risk-adjusted estimates are evidently giving better results in terms of the percentage of failures (up to 0.6% only for VaR and iVaR) relative to the historical estimates (3.7–4.3% for VaR and 4.9–6.8% for iVaR). At the confidence level of 99.9%, the number of VaR and iVaR violations is the same under the risk-adjusted measures, whereas the number of iVaR breaches is larger that the number of VaR breaches under the historical measure. These results imply that the historical approach is less effective in capturing the intra-horizon component of iVaR. Finally, we notice a clustering the behavior of VaR and iVaR violations in the months following the outbreak of the Global financial crisis of 2008, i.e., from October 2008 until February 2009. This finding strongly suggests that the assumption of the independence of VaR/iVaR violations does not hold.

To analyze our results within a proper theoretical and practical frame of reference, we consider a battery of statistical tests to evaluate model performance. In particular, we employ the backtesting procedures of Kupiec (1995), i.e., the Time Until First Failure test (TUFF) and the Proportion of Failures test (POF), which is also known as the Unconditional Coverage test (UC). Additionally, we include the Independence Coverage test (IC) and the Conditional Coverage test (CC) of Christoffersen (1998). The results are summarized in Table 4.5, and they reinforce our earlier conclusions. Irrespectively of the jump model, the historical VaR models provide relatively poor risk forecasts, and they are largely rejected by the standard statistical tests (Panel A). Moreover, their performance additionally

[69] We do not consider 99.9% confidence level because we have only 162 observations in our sample, which is not enough to make statistical inference on such a high confidence level.

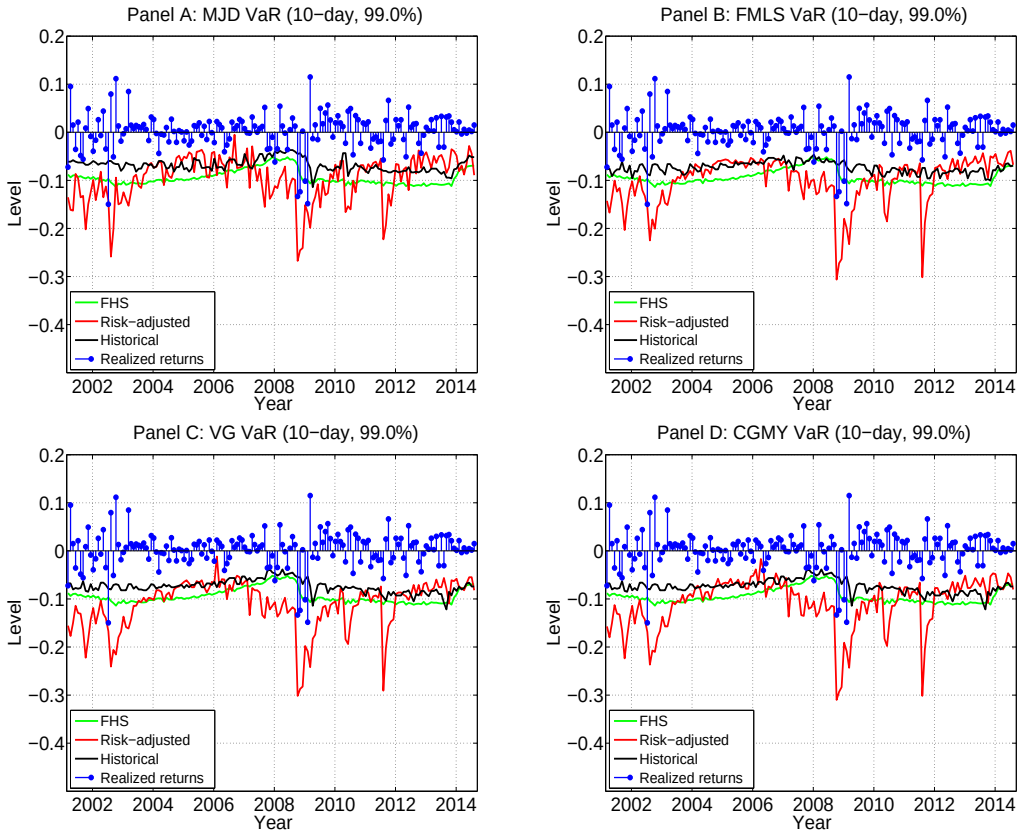

Figure 4.6: **VaR backtesting (10-day horizon, 99.0% confidence level).** For each considered model—the Merton jump–diffusion (MJD), the finite-moment log-stable (FMLS), the variance gamma (VG), and the Carr-Geman-Madan-Yor (CGMY) model, which are given in Panels A, B, C, and D, respectively—we graphically represent the time evolution of the 10-day end-of-horizon value at risk (VaR) calculated at the confidence level of 99.0% and the realized 10-day returns. We plot the estimates under both the historical and the risk-adjusted measure. Additionally, we include the VaR estimates based on a filtered historical simulation (FHS). The plots provide information about the ability of each model to forecast the VaR of the S&P 100 index *at the end* of the regulatory 10-day horizon. Although the model risk seems to be important, the results are particularly sensitive to the estimation risk, i.e., the risk-adjusted estimates better forecast market moves than the historical estimates.

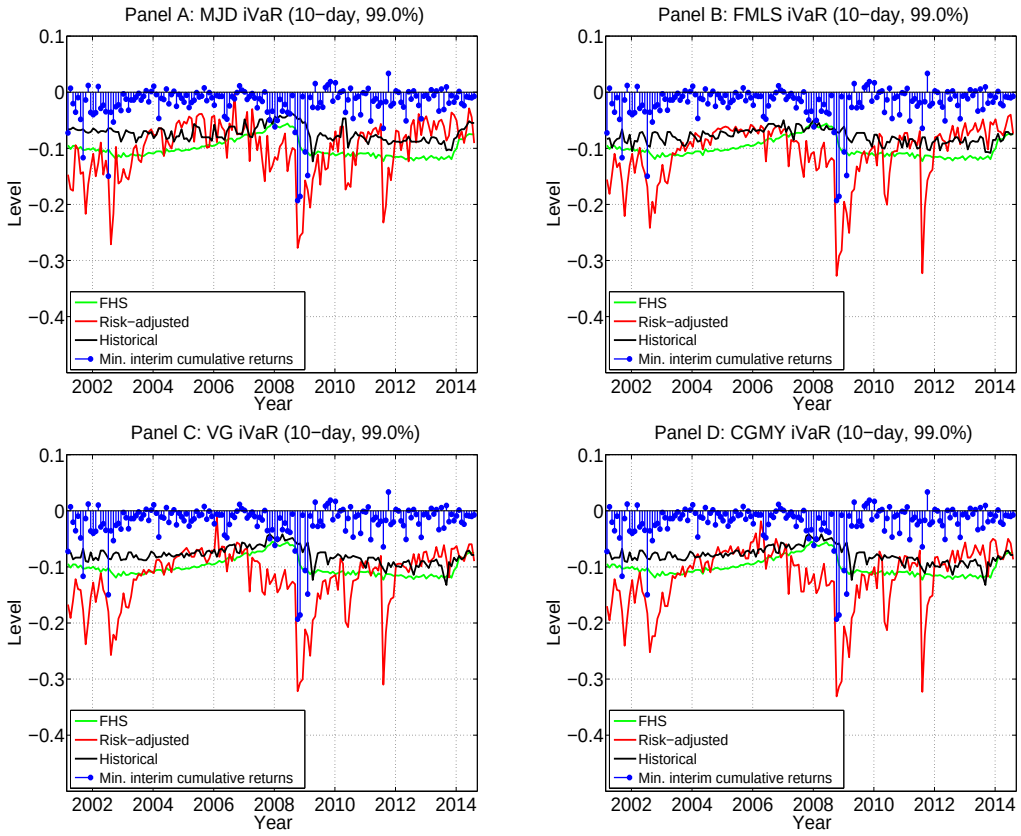

Figure 4.7: **iVaR backtesting (10-day horizon, 99.0% confidence level).** For each considered model—the Merton jump–diffusion (MJD), the finite-moment log-stable (FMLS), the variance gamma (VG), and the Carr-Geman-Madan-Yor (CGMY) model, which are given in Panels A, B, C, and D, respectively—we graphically represent the time evolution of the 10-day intra-horizon value at risk (iVaR) calculated at the confidence level of 99.0% and the realized minimal cumulative interim 10-day returns. We plot the estimates under the historical and the risk-adjusted measure. Additionally, we include the iVaR estimates based on a filtered historical simulation (FHS). The plots provide information about the ability of each model to forecast the iVaR of the S&P 100 index *within* the regulatory 10-day horizon. Similarly to the VaR case, we conclude that model risk matters also for the iVaR, but the results are again markedly more sensitive to the estimation risk.

Table 4.5: **VaR and iVaR backtesting.** The table summarizes the backtesting results for the end-of-horizon value at risk (VaR) and the intra-horizon value at risk (iVaR)—computed at the confidence level of $\chi = 99.0\%$, and for the regulatory 10-day monitoring period—for the Merton jump–diffusion (MJD), the finite-moment log-stable (FMLS), the variance gamma (VG), and the Carr-Geman-Madan-Yor (CGMY) model under the historical and the risk-adjusted measure. Additionally, we provide test statistics for the filtered historical simulation (FHS). The table reports the likelihood ration (LR) and the p-value (p-val.) for the following backtesting procedures: the Time Until First Failure test (TUFF), the Unconditional Coverage test (UC), the Independence Coverage test (IC), and the Conditional Coverage test (CC). Based on the test statistics, the historical (the risk-adjusted) approach to the estimation of VaR and iVaR is mostly rejected (mostly cannot be rejected) at the conventional confidence levels (i.e., 90%, 95%, and 99%).

Panel A: Historical VaR backtesting

Method	#	TUFF		UC		IC		CC	
		LR	p-val.	LR	p-val.	LR	p-val.	LR	p-val.
FHS	6	1.9225	0.1652	6.9087	0.0086	6.5286	0.0106	13.4370	0.0012
MJD	7	9.2103	0.0024	9.7092	0.0018	5.8424	0.0156	15.5525	0.0004
FMLS	6	1.9225	0.1652	6.9629	0.0083	6.5053	0.0108	13.4688	0.0012
VG	7	9.2103	0.0024	9.7762	0.0018	5.8195	0.0158	15.5951	0.0004
CGMY	7	9.2103	0.0024	9.7762	0.0018	5.8195	0.0158	15.5951	0.0004

Panel B: Risk-adjusted VaR backtesting

Method	#	TUFF		UC		IC		CC	
		LR	p-val.	LR	p-val.	LR	p-val.	LR	p-val.
MJD	1	1.9225	0.1652	0.3010	0.5832	0.0023	0.9621	0.3033	0.8593
FMLS	0	$<10^{-4}$	$\sim$1.0	$<10^{-4}$	$\sim$1.0	$<10^{-4}$	$\sim$1.0	$<10^{-4}$	$\sim$1.0
VG	0	$<10^{-4}$	$\sim$1.0	$<10^{-4}$	$\sim$1.0	$<10^{-4}$	$\sim$1.0	$<10^{-4}$	$\sim$1.0
CGMY	1	0.1863	0.6660	0.2931	0.5882	0.0023	0.9619	0.2954	0.8627

Panel C: Historical iVaR backtesting

Method	#	TUFF		UC		IC		CC	
		LR	p-val.	LR	p-val.	LR	p-val.	LR	p-val.
FHS	8	3.5893	0.0582	12.8099	0.0003	9.1029	0.0026	21.9123	$<10^{-4}$
MJD	11	9.2103	0.0024	23.5822	$<10^{-4}$	10.2772	0.0013	33.8590	$<10^{-4}$
FMLS	8	3.5893	0.0582	12.8885	0.0003	9.0679	0.0026	21.9566	$<10^{-4}$
VG	9	3.5893	0.0582	16.2644	0.0001	7.4684	0.0063	23.7332	$<10^{-4}$
CGMY	9	3.5893	0.0582	16.2644	0.0001	7.4684	0.0063	23.7332	$<10^{-4}$

Panel D: Risk-adjusted iVaR backtesting

Method	#	TUFF		UC		IC		CC	
		LR	p-val.	LR	p-val.	LR	p-val.	LR	p-val.
MJD	1	0.1426	0.7057	0.3010	0.5832	0.0023	0.9621	0.3033	0.8593
FMLS	0	$<10^{-4}$	$\sim$1.0	$<10^{-4}$	$\sim$1.0	$<10^{-4}$	$\sim$1.0	$<10^{-4}$	$\sim$1.0
VG	0	$<10^{-4}$	$\sim$1.0	$<10^{-4}$	$\sim$1.0	$<10^{-4}$	$\sim$1.0	$<10^{-4}$	$\sim$1.0
CGMY	1	0.1863	0.6660	0.2931	0.5882	0.0023	0.9619	0.2954	0.8627

worsens in the case of iVaR backtesting (Panel C). On the other hand, the risk-adjusted approach to the estimation of VaR and iVaR yields significantly better results (Panel B and Panel D, respectively). None of the models estimated under the risk-adjusted measure is rejected at any of the conventional confidence levels, i.e., 90%, 95% or 99%.[70] Nevertheless, despite the fact that our findings are strongly in favor of the risk-adjusted VaR and iVaR, it is important to recognize that our sample size is relatively small, and that a more comprehensive and statistically reliable study would require a larger set of VaR/iVaR estimates.

4.6 Conclusion

This paper studies the intra-horizon value at risk (iVaR), which has been considered previously in Boudoukh et al. (2004), Rossello (2008), Bhattacharyya, Misra and Kodase (2009) and Bakshi and Panayotov (2010). For completeness and comparison, our analysis includes the end-of-horizon value at risk (VaR), which has been the risk management industry standard for more than two decades now. We contribute to the current literature by developing a theoretical framework for the computation of VaR and iVaR. Our paper provides additional insights by applying our results in an empirical exercise using market data. In particular, we are interested in the implications of using option quotes instead of historical returns for the estimation of VaR and iVaR. Our data set is comprised of the historical return time series and the short-term American put options on S&P 100 index from March 2001 until August 2014, which are separately used for the calibration of several popular Lévy models, i.e., the Merton jump–diffusion model (MJD), the finite-moment log-stable model (FMLS), the variance-gamma model (VG), and the Carr-Geman-Madan-Yor model (CGMY). Our findings indicate that the option-implied VaR and iVaR multiples and significantly higher (lower) than the ones estimated using only the historical asset returns in times of crisis (during calm market periods). A set of standard statistical backtesting procedures implemented in our paper provides further evidence that the VaR and iVaR forecasting under the two probability measures produces vastly different results, and that the option-implied risk metrics are indeed more reliable. The rationale for such a result is that the option-based estimates provide a better protection against the market risk because they are more perceptive and responsive to asset price fluctuations due to their forward-looking nature. Within the scope of our study, we therefore conclude that the importance of the estimation risk seems to surpass the importance of the model risk. For this reason, the option-implied estimates of risk measures should not be neglected in practice whenever option data is available. Last but not least, we empirically

[70] These levels are not to be confused with the VaR/iVaR confidence level, which is set to $\chi = 99.0\%$.

disentangle the contribution of jumps from diffusion to the iVaR, and find that jumps are the main driver of the intra-horizon risk, accounting for about 90% on average.

Part III

Appendices

Appendix A

Proofs of results in Chapter 2

A.1 Proof of Theorem 2.2.1: Pricing of Canadized European put options

The price of a European put option with strike K (i.e., the log-strike is defined as $\kappa := \log(K)$) and time to maturity τ in a jump-diffusion model is the function $p := p(x, \tau)$, where x is the log-price process (2.4), which solves the partial integro-differential equation (PIDE)

$$-\frac{\partial p}{\partial \tau}(x,\tau) + \frac{\sigma^2}{2}\frac{\partial^2 p}{\partial x^2}(x,\tau) + \mu\frac{\partial p}{\partial x}(x,\tau) - rp(x,\tau) + \lambda\int_{-\infty}^{+\infty}[p(x+y,\tau) - p(x,\tau)]f_Y(y)dy = 0, \quad \text{(A.1)}$$

with the boundary conditions

$$\begin{aligned} \lim_{x\downarrow-\infty} p(x,\tau) &= e^{\kappa - r\tau}, \\ \lim_{x\uparrow+\infty} p(x,\tau) &= 0, \end{aligned} \quad \text{(A.2)}$$

and the initial condition

$$p(x,0) = (e^{\kappa} - e^{x})^{+} := \max(e^{\kappa} - e^{x}, 0). \quad \text{(A.3)}$$

Taking the Laplace-Carson transform (LCT) in (2.7) of the system (A.1)–(A.3), we obtain the ordinary integro-differential equation (OIDE) for the Canadized European put option $p^* := p^*(x, \alpha)$

$$\begin{aligned} \frac{\sigma^2}{2}\frac{d^2 p^*}{dx^2}(x,\alpha) + \mu\frac{dp^*}{dx}(x,\alpha) - (r+\alpha)p^*(x,\alpha) - \lambda p^*(x,\alpha) \\ + \alpha\left(e^{\kappa} - e^{x}\right)^{+} + \lambda\int_{-\infty}^{+\infty} p^*(x+y,\alpha)f_Y(y)dy = 0, \end{aligned} \quad \text{(A.4)}$$

with the transformed boundary conditions

$$\begin{aligned} \lim_{x\downarrow-\infty} p^*(x,\alpha) &= \frac{\alpha e^{\kappa}}{\alpha + r}, \\ \lim_{x\uparrow+\infty} p^*(x,\alpha) &= 0. \end{aligned} \quad \text{(A.5)}$$

The initial condition (A.3) is absorbed in the equation (A.4) due to the LCT. Assuming the solution to have the form

$$p^*(x,\alpha) = \begin{cases} \displaystyle\sum_{l=1}^{m+1} \underline{w}_l e^{\beta_{l,r+\alpha}(x-\kappa)} + \frac{\alpha e^{\kappa}}{\alpha+r} - \frac{\alpha e^{x}}{\alpha+\delta} & \text{if } \ x < \kappa, \\ \displaystyle\sum_{l=1}^{n+1} \overline{w}_l e^{\gamma_{l,r+\alpha}(x-\kappa)} & \text{if } \ x \geq \kappa, \end{cases} \tag{A.6}$$

we obtain the coefficients $\underline{w}_1, ..., \underline{w}_{m+1}$ and $\overline{w}_1, ..., \overline{w}_{n+1}$ by analyzing the solution in the two different regions, i.e., below and above the strike price.

- The case $x < \kappa$.

  First we need to compute each of the terms in the OIDE (A.4). The two derivative terms are

$$\begin{aligned} \frac{dp^*}{dx}(x,\alpha) &= \sum_{l=1}^{m+1} \underline{w}_l \beta_{l,r+\alpha} e^{\beta_{l,r+\alpha}(x-\kappa)} - \frac{\alpha e^{x}}{\alpha+\delta}, \ \text{ and} \\ \frac{d^2p^*}{dx^2}(x,\alpha) &= \sum_{l=1}^{m+1} \underline{w}_l \beta_{l,r+\alpha}^2 e^{\beta_{l,r+\alpha}(x-\kappa)} - \frac{\alpha e^{x}}{\alpha+\delta}. \end{aligned} \tag{A.7}$$

  The integral term is

$$\begin{aligned} \int_{-\infty}^{+\infty} p^*(x+y,\alpha) f_Y(y) dy = &\sum_{j=1}^{n}\sum_{l=1}^{m+1} \int_{-\infty}^{0} q_j \theta_j \underline{w}_l e^{\beta_{l,r+\alpha}(x-\kappa)} e^{(\beta_{l,r+\alpha}+\theta_j)y} dy \\ &+ \sum_{j=1}^{n} \int_{-\infty}^{0} \left(\frac{\alpha e^{\kappa}}{\alpha+r} - \frac{\alpha e^{x+y}}{\alpha+\delta} \right) q_j \theta_j e^{\theta_j y} dy \\ &+ \sum_{i=1}^{m}\sum_{l=1}^{m+1} \int_{0}^{\kappa-x} p_i \eta_i \underline{w}_l e^{\beta_{l,r+\alpha}(x-\kappa)} e^{(\beta_{l,r+\alpha}-\eta_i)y} dy \\ &+ \sum_{i=1}^{m} \int_{0}^{\kappa-x} \left(\frac{\alpha e^{\kappa}}{\alpha+r} - \frac{\alpha e^{x+y}}{\alpha+\delta} \right) p_i \eta_i e^{-\eta_i y} dy \\ &+ \sum_{i=1}^{m}\sum_{l=1}^{n+1} \int_{\kappa-x}^{+\infty} p_i \eta_i \overline{w}_l e^{\gamma_{l,r+\alpha}(x-\kappa)} e^{(\gamma_{l,r+\alpha}-\eta_i)y} dy. \end{aligned} \tag{A.8}$$

  After some algebra, the OIDE (A.4) yields the following conditions

$$\begin{aligned} &\sum_{l=1}^{m+1} \underline{w}_l e^{\beta_{l,r+\alpha}(x-\kappa)} \left(\frac{\sigma^2}{2}\beta_{l,r+\alpha}^2 + \mu\beta_{l,r+\alpha} + \lambda \left(\sum_{i=1}^{m} \frac{p_i\eta_i}{\eta_i - \beta_{l,r+\alpha}} + \sum_{j=1}^{n} \frac{q_j\theta_j}{\theta_j + \beta_{j,r+\alpha}} - 1 \right) - (\alpha+r) \right) \\ &- \sum_{l=1}^{m} \lambda p_l \eta_l e^{\eta_l(x-\kappa)} \left(\sum_{i=1}^{m+1} \frac{\underline{w}_i}{\eta_l - \beta_{i,r+\alpha}} - \sum_{j=1}^{n+1} \frac{\overline{w}_j}{\eta_l - \gamma_{j,r+\alpha}} + \frac{1}{\eta_l}\frac{\alpha e^{\kappa}}{\alpha+r} - \frac{1}{\eta_l - 1}\frac{\alpha e^{\kappa}}{\alpha+\delta} \right) = 0. \end{aligned} \tag{A.9}$$

Using the definition of the cumulant generating function (2.5) and the characteristic equation, the first sum in (A.9) vanishes. Therefore, we obtain m conditions (for $l = 1, 2, ..., m$) on the coefficients $\underline{w}_1, ..., \underline{w}_{m+1}$ and $\overline{w}_1, ..., \overline{w}_{n+1}$ as a system of linear equations

$$\sum_{i=1}^{m+1} \frac{\underline{w}_i}{\eta_l - \beta_{i,r+\alpha}} - \sum_{j=1}^{n+1} \frac{\overline{w}_j}{\eta_l - \gamma_{j,r+\alpha}} = \frac{1}{\eta_l - 1} \frac{\alpha e^{\kappa}}{\alpha + \delta} - \frac{1}{\eta_l} \frac{\alpha e^{\kappa}}{\alpha + r}. \tag{A.10}$$

- The case $x \geq \kappa$.

We proceed in the same way as in the previous case. The derivative terms are

$$\begin{aligned} \frac{dp^*}{dx}(x, \alpha) &= \sum_{l=1}^{n+1} \overline{w}_l \gamma_{l,r+\alpha} e^{\gamma_{l,r+\alpha}(x-\kappa)}, \\ \frac{d^2p^*}{dx^2}(x, \alpha) &= \sum_{l=1}^{n+1} \overline{w}_l \gamma_{l,r+\alpha}^2 e^{\gamma_{l,r+\alpha}(x-\kappa)}. \end{aligned} \tag{A.11}$$

The integral term is

$$\begin{aligned} \int_{-\infty}^{+\infty} p^*(x+y, \alpha) f_Y(y) dy = &\sum_{i=1}^{m} \sum_{l=1}^{n+1} \int_0^{+\infty} p_i \eta_i \overline{w}_l e^{\gamma_{l,r+\alpha}(x-\kappa)} e^{(\gamma_{l,r+\alpha} - \eta_i)y} dy \\ &+ \sum_{j=1}^{n} \sum_{l=1}^{n+1} \int_{\kappa-x}^{0} q_j \theta_j \overline{w}_l e^{\gamma_{l,r+\alpha}(x-\kappa)} e^{(\gamma_{l,r+\alpha} + \theta_j)y} dy \\ &+ \sum_{j=1}^{n} \sum_{l=1}^{m+1} \int_{-\infty}^{\kappa-x} q_j \theta_j \underline{w}_l e^{\beta_{l,r+\alpha}(x-\kappa)} e^{(\beta_{l,r+\alpha} + \theta_j)y} dy \\ &+ \sum_{j=1}^{n} \int_{-\infty}^{\kappa-x} \left(\frac{\alpha e^{\kappa}}{\alpha + r} - \frac{\alpha e^{x+y}}{\alpha + \delta} \right) q_j \theta_j e^{\theta_j y} dy. \end{aligned} \tag{A.12}$$

Therefore, we obtain

$$\begin{aligned} &\sum_{l=1}^{n+1} \overline{w}_l e^{\gamma_{l,r+\alpha}(x-\kappa)} \left(\frac{\sigma^2}{2} \gamma_{l,r+\alpha}^2 + \mu \gamma_{l,r+\alpha} + \lambda \left(\sum_{i=1}^{m} \frac{p_i \eta_i}{\eta_i - \gamma_{l,r+\alpha}} + \sum_{j=1}^{n} \frac{q_j \theta_j}{\theta_j + \gamma_{l,r+\alpha}} - 1 \right) - (\alpha + r) \right) \\ &+ \sum_{l=1}^{n} \lambda q_l \theta_l e^{\theta_l(x-\kappa)} \left(\sum_{i=1}^{m+1} \frac{\underline{w}_i}{\theta_l + \beta_{i,r+\alpha}} - \sum_{j=1}^{n+1} \frac{\overline{w}_j}{\theta_l + \gamma_{j,r+\alpha}} + \frac{1}{\theta_l} \frac{\alpha e^{\kappa}}{\alpha + r} - \frac{1}{\theta_l + 1} \frac{\alpha e^{\kappa}}{\alpha + \delta} \right) = 0, \end{aligned} \tag{A.13}$$

which yields n conditions (for $l = 1, ..., n$) on coefficients $\underline{w}_1, ..., \underline{w}_{m+1}$ and $\overline{w}_1, ..., \overline{w}_{n+1}$

$$\sum_{i=1}^{m+1} \frac{\underline{w}_i}{\theta_l + \beta_{i,r+\alpha}} - \sum_{j=1}^{n+1} \frac{\overline{w}_j}{\theta_l + \gamma_{j,r+\alpha}} = \frac{1}{\theta_l + 1} \frac{\alpha e^{\kappa}}{\alpha + \delta} - \frac{1}{\theta_l} \frac{\alpha e^{\kappa}}{\alpha + r}. \tag{A.14}$$

Finally, we impose one Dirichlet condition, i.e., the value matching, and one Neumann condition, i.e., the smooth pasting, at the boundary of the two regions ($x = \kappa$):

$$\begin{aligned} \lim_{x\uparrow\kappa} p^*(x,\alpha) &= \lim_{x\downarrow\kappa} p^*(x,\alpha), \quad \text{and} \\ \lim_{x\uparrow\kappa} \frac{dp^*}{dx}(x,\alpha) &= \lim_{x\downarrow\kappa} \frac{dp^*}{dx}(x,\alpha), \end{aligned} \tag{A.15}$$

resulting in the following two conditions:

$$\begin{aligned} \sum_{i=1}^{m+1} \underline{w}_i - \sum_{j=1}^{n+1} \overline{w}_j &= \frac{\alpha e^\kappa}{\alpha+\delta} - \frac{\alpha e^\kappa}{\alpha+r}, \\ \sum_{i=1}^{m+1} \beta_{i,r+\alpha} \underline{w}_i - \sum_{j=1}^{n+1} \gamma_{j,r+\alpha} \overline{w}_j &= \frac{\alpha e^\kappa}{\alpha+\delta}. \end{aligned} \tag{A.16}$$

Finally, the conditions (A.10), (A.14), and (A.16) can be jointly summarized in a matrix equation

$$\mathbf{A}\mathbf{w} = \mathbf{J}, \tag{A.17}$$

where

$$\mathbf{w} := \left(\underline{w}_1, ..., \underline{w}_{m+1}, \overline{w}_1, ..., \overline{w}_{n+1}\right)' \tag{A.18}$$

and

$$\mathbf{J} := \left(\kappa_\delta - \kappa_r, \kappa_\delta, \frac{\kappa_\delta}{\eta_1 - 1} - \frac{\kappa_r}{\eta_1}, ..., \frac{\kappa_\delta}{\eta_m - 1} - \frac{\kappa_r}{\eta_m}, \frac{\kappa_\delta}{\theta_1 + 1} - \frac{\kappa_r}{\theta_1}, ..., \frac{\kappa_\delta}{\theta_n + 1} - \frac{\kappa_r}{\theta_n}\right)' \tag{A.19}$$

are a $(n+m+2)$-dimensional column vector, and $\kappa_\rho := \frac{\alpha e^\kappa}{\alpha+\rho}$ for $\rho = \{r, \delta\}$.

The matrix $\mathbf{A}$ is given by

$$\mathbf{A} := \begin{pmatrix} 1 & \cdots & 1 & -1 & \cdots & -1 \\ \beta_{1,r+\alpha} & \cdots & \beta_{m+1,r+\alpha} & -\gamma_{1,r+\alpha} & \cdots & -\gamma_{n+1,r+\alpha} \\ \frac{1}{\eta_1-\beta_{1,r+\alpha}} & \cdots & \frac{1}{\eta_1-\beta_{m+1,r+\alpha}} & -\frac{1}{\eta_1-\gamma_{1,r+\alpha}} & \cdots & -\frac{1}{\eta_1-\gamma_{n+1,r+\alpha}} \\ \vdots & \ddots & \vdots & \vdots & \ddots & \vdots \\ \frac{1}{\eta_m-\beta_{1,r+\alpha}} & \cdots & \frac{1}{\eta_m-\beta_{m+1,r+\alpha}} & -\frac{1}{\eta_m-\gamma_{1,r+\alpha}} & \cdots & -\frac{1}{\eta_m-\gamma_{n+1,r+\alpha}} \\ \frac{1}{\theta_1+\beta_{1,r+\alpha}} & \cdots & \frac{1}{\theta_1+\beta_{m+1,r+\alpha}} & -\frac{1}{\theta_1+\gamma_{1,r+\alpha}} & \cdots & -\frac{1}{\theta_1+\gamma_{n+1,r+\alpha}} \\ \vdots & \ddots & \vdots & \vdots & \ddots & \vdots \\ \frac{1}{\theta_n+\beta_{1,r+\alpha}} & \cdots & \frac{1}{\theta_n+\beta_{m+1,r+\alpha}} & -\frac{1}{\theta_n+\gamma_{1,r+\alpha}} & \cdots & -\frac{1}{\theta_n+\gamma_{n+1,r+\alpha}} \end{pmatrix}. \tag{A.20}$$

This concludes the proof. ■

A.2 Proof of Theorem 2.2.2: Pricing of Canadized American put options

The price of an American put option with strike K (i.e., the log-strike is defined as $\kappa := \log(K)$) and time to maturity τ in a jump-diffusion model is the function $P := P(x,\tau)$, where x is the log-return (2.4), which solves the free boundary problem

$$-\frac{\partial P}{\partial \tau}(x,\tau)+\frac{\sigma^2}{2}\frac{\partial^2 P}{\partial x^2}(x,\tau)+\mu\frac{\partial P}{\partial x}(x,\tau)-rP(x,\tau)+\lambda\int_{-\infty}^{+\infty}[P(x+y,\tau)-P(x,\tau)]f_Y(y)dy=0, \quad \text{(A.21)}$$

with the boundary conditions

$$\begin{aligned}\lim_{x\uparrow+\infty} P(x,\tau) &= 0,\\ \lim_{x\downarrow b_p} P(x,\tau) &= e^{\kappa}-e^{b_p},\\ \lim_{x\downarrow b_p}\frac{\partial P}{\partial x}(x,\tau) &= -e^{b_p},\end{aligned} \quad \text{(A.22)}$$

and the initial condition

$$P(x,0) := p(x,0) = (e^{\kappa}-e^{x})^{+}. \quad \text{(A.23)}$$

Since we work in log-returns, the early exercise boundary B_p is expressed as the log-boundary $b_p := \log(B_p)$. Taking the LCT of the American option PIDE we obtain the OIDE:

$$\begin{aligned}\frac{\sigma^2}{2}\frac{d^2P^*}{dx^2}(x,\alpha)+\mu\frac{dP^*}{dx}(x,\alpha)-(r+\alpha)P^*(x,\alpha)-\lambda P^*(x,\alpha)\\ +\alpha\,(e^{\kappa}-e^{x})^{+}+\lambda\int_{-\infty}^{+\infty}P^*(x+y,\alpha)f_Y(y)dy=0,\end{aligned} \quad \text{(A.24)}$$

with the new boundary conditions:

$$\begin{aligned}\lim_{x\uparrow+\infty} P^*(x,\tau) &= 0,\\ \lim_{x\downarrow b_p^*} P^*(x,\alpha) &= e^{\kappa}-e^{b_p^*},\\ \lim_{x\downarrow b_p^*}\frac{dP^*}{dx}(x,\alpha) &= -e^{b_p^*}.\end{aligned} \quad \text{(A.25)}$$

It is important to recognize that the transformed early exercise boundary is not a non-linear function any more. Since we have applied the LCT with respect to the residual maturity τ, the time dependence disappears and b_p^* becomes a flat boundary. For more details on the time-independence of the early exercise boundary of a Canadized American option we refer to Carr (1998).

Given that an American option can be decomposed into its European counterpart and the early exercise premium, price of an American option in the Laplace-Carson domain can be conjectured in the form

$$P^*(x,\alpha) = \begin{cases} p^*(x,\alpha) + e_p^*(x,\alpha) & \text{if } \ x > b_p^*, \\ e^\kappa - e^x & \text{if } \ x \le b_p^*, \end{cases} \tag{A.26}$$

where $e_p^* := e_p(x,\alpha)$ represents the transformed early exercise premium. Furthermore, since the dynamics of the corresponding European/Canadized European and American/Canadized American options can be described by the same PIDE/OIDE, then the early exercise premium which is a difference between the two, satisfies the same equation as well. Thus, one can price American options by solving the early exercise premium OIDE

$$\frac{\sigma^2}{2}\frac{d^2e_p^*}{dx^2}(x,\alpha) + \mu\frac{de_p^*}{dx}(x,\alpha) - (r+\alpha)e_p^*(x,\alpha) + \lambda\int_{-\infty}^{+\infty}[e_p^*(x+y,\alpha) - e_p^*(x,\alpha)]f_Y(y)dy = 0, \tag{A.27}$$

and using the expression (A.26) in connection with the boundary conditions (A.25). Equations (A.6), (A.26), and (A.27) allow us to conjecture the EEP in the form:

$$e_p^*(x,\alpha) = \begin{cases} \displaystyle\sum_{l=1}^{n+1} v_l e^{\gamma_{l,r+\alpha}(x-b_p^*)} & \text{if } \ x > b_p^*, \\ e^\kappa - e^x - p^*(x,\alpha) & \text{if } \ x \le b_p^*. \end{cases} \tag{A.28}$$

The OIDE (A.24) holds in the region $x > b_p^*$. Therefore, we have the following expressions for the derivative and integral terms in the equation (A.27)

$$\begin{aligned} \frac{de_p^*}{dx}(x,\alpha) &= \sum_{l=1}^{n+1} v_l\gamma_{l,r+\alpha}e^{\gamma_{l,r+\alpha}(x-b_p^*)}, \\ \frac{d^2e_p^*}{dx^2}(x,\alpha) &= \sum_{l=1}^{n+1} v_l\gamma_{l,r+\alpha}^2e^{\gamma_{l,r+\alpha}(x-b_p^*)}, \end{aligned} \tag{A.29}$$

and

$$\begin{aligned} \int_{-\infty}^{+\infty} e_p^*(x+y,\alpha)f_Y(y)dy = &\sum_{i=1}^{m}\sum_{l=1}^{n+1}\int_0^{+\infty} p_i\eta_i v_l e^{\gamma_{l,r+\alpha}(x-b_p^*)}e^{(\gamma_{l,r+\alpha}-\eta_i)y}dy \\ &+ \sum_{j=1}^{n}\sum_{l=1}^{n+1}\int_{b_p^*-x}^{0} q_j\theta_j v_l e^{\gamma_{l,r+\alpha}(x-b_p^*)}e^{(\gamma_{l,r+\alpha}+\theta_j)y}dy \\ &- \sum_{j=1}^{n}\sum_{l=1}^{m+1}\int_{-\infty}^{b_p^*-x} q_j\theta_j\underline{w}_l e^{\beta_{l,r+\alpha}(x-\kappa)}e^{(\beta_{l,r+\alpha}+\theta_j)y}dy \\ &+ \sum_{j=1}^{n}\int_{-\infty}^{b_p^*-x}\left(\frac{re^\kappa}{\alpha+r} - \frac{\delta e^{x+y}}{\alpha+\delta}\right)q_j\theta_j e^{\theta_j y}dy. \end{aligned} \tag{A.30}$$

Solving the integrals yields

$$\sum_{l=1}^{n+1} v_l e^{\gamma_{l,r+\alpha}(x-b_p^*)} \left(\frac{\sigma^2}{2}\gamma_{l,r+\alpha}^2 + \mu\gamma_{l,r+\alpha} + \lambda \left(\sum_{i=1}^{m} \frac{p_i\eta_i}{\eta_i - \beta_{l,r+\alpha}} + \sum_{j=1}^{n} \frac{q_j\theta_j}{\theta_j + \beta_{j,r+\alpha}} - 1 \right) - (\alpha + r) \right)$$
$$+ \sum_{l=1}^{n} \lambda q_l \theta_l e^{\theta_l(b_p^*-x)} \left(\sum_{i=1}^{m+1} \frac{\underline{w}_i e^{\beta_{i,r+\alpha}(b_p^*-k)}}{\theta_l + \beta_{i,r+\alpha}} + \sum_{j=1}^{n+1} \frac{v_j}{\theta_l + \gamma_{j,r+\alpha}} - \frac{1}{\theta_l}\frac{re^{\kappa}}{\alpha + r} + \frac{1}{\theta_l + 1}\frac{\delta e^{\kappa}}{\alpha + \delta} \right) = 0. \tag{A.31}$$

From this equation we obtain n conditions (for $l = 1, ..., n$) as a system of linear equations

$$\sum_{j=1}^{n+1} \frac{v_j}{\theta_l + \gamma_{j,r+\alpha}} = \frac{1}{\theta_l}\frac{re^{\kappa}}{\alpha + r} - \frac{1}{\theta_l + 1}\frac{\delta e^{\kappa}}{\alpha + \delta} - \sum_{i=1}^{m+1} \frac{\underline{w}_i e^{\beta_{i,r+\alpha}(b_p^*-k)}}{\theta_l + \beta_{i,r+\alpha}}. \tag{A.32}$$

Finally, by collecting the results for European put and the early exercise premium, and applying the conditions (A.25), i.e., the value matching and the smooth pasting conditions at the boundary in the HEJD framework, yields

$$\begin{aligned} \sum_{j=1}^{n+1} v_j &= \frac{re^{\kappa}}{\alpha + r} - \frac{\delta e^{\kappa}}{\alpha + \delta} e^{(b_p^*-\kappa)} - \sum_{i=1}^{m+1} \underline{w}_i e^{\beta i, r+\alpha(b_p^*-\kappa)}, \\ \sum_{j=1}^{n+1} \gamma_{j,r+\alpha} v_j &= -\frac{\delta e^{\kappa}}{\alpha + \delta} e^{(b_p^*-\kappa)} - \sum_{i=1}^{m+1} \beta_{i,r+\alpha}\underline{w}_i e^{\beta i, r+\alpha(b_p^*-\kappa)}. \end{aligned} \tag{A.33}$$

The vector $\mathbf{v} := (v_1, ..., v_{n+1})'$ can be obtained by solving the matrix equation

$$\tilde{\mathbf{A}}\mathbf{v} = \tilde{\mathbf{J}}. \tag{A.34}$$

The $(n+1)$-dimensional column vector $\tilde{\mathbf{J}}$ is defined as

$$\tilde{\mathbf{J}} = -\mathbf{\Omega}\mathbf{b}_\beta + e^{(b_p^*-\kappa)}\boldsymbol{\omega} + \boldsymbol{\xi}, \tag{A.35}$$

where $\mathbf{\Omega}$ is $(n+1) \times (m+1)$-dimensional matrix

$$\mathbf{\Omega} = \begin{pmatrix} \underline{w}_1 & \underline{w}_2 & \cdots & \underline{w}_{m+1} \\ \frac{\underline{w}_1}{\theta_1+\beta_{1,r+\alpha}} & \frac{\underline{w}_2}{\theta_1+\beta_{2,r+\alpha}} & \cdots & \frac{\underline{w}_{m+1}}{\theta_1+\beta_{m+1,r+\alpha}} \\ \vdots & \vdots & \ddots & \vdots \\ \frac{\underline{w}_1}{\theta_n+\beta_{1,r+\alpha}} & \frac{\underline{w}_2}{\theta_n+\beta_{2,r+\alpha}} & \cdots & \frac{\underline{w}_{m+1}}{\theta_n+\beta_{m+1,r+\alpha}} \end{pmatrix}, \tag{A.36}$$

and $\mathbf{b}_\beta$, $\boldsymbol{\omega}$, and $\boldsymbol{\xi}$ are $(n+1)$-dimensional column vectors given by

$$\begin{aligned}
\mathbf{b}_\beta &= \left(e^{\beta_{1,r+\alpha}(b_p^*-\kappa)}, ..., e^{\beta_{m+1,r+\alpha}(b_p^*-\kappa)}\right)', \\
\boldsymbol{\omega} &= \left(-\frac{\delta e^\kappa}{\alpha+\delta}, -\frac{1}{\theta_1+1}\frac{\delta e^\kappa}{\alpha+\delta}, ..., -\frac{1}{\theta_n+1}\frac{\delta e^\kappa}{\alpha+\delta}\right)', \quad \text{and} \\
\boldsymbol{\xi} &= \left(\frac{re^\kappa}{\alpha+r}, \frac{1}{\theta_1}\frac{re^\kappa}{\alpha+r}, ..., \frac{1}{\theta_n}\frac{re^\kappa}{\alpha+r}\right)'.
\end{aligned} \tag{A.37}$$

The matrix $\tilde{\mathbf{A}}$ is specified as

$$\tilde{\mathbf{A}} := \begin{pmatrix}
1 & 1 & \cdots & 1 \\
\frac{1}{\theta_1+\gamma_{1,r+\alpha}} & \frac{1}{\theta_1+\gamma_{2,r+\alpha}} & \cdots & \frac{1}{\theta_1+\gamma_{n+1,r+\alpha}} \\
\frac{1}{\theta_2+\gamma_{1,r+\alpha}} & \frac{1}{\theta_2+\gamma_{2,r+\alpha}} & \cdots & \frac{1}{\theta_2+\gamma_{n+1,r+\alpha}} \\
\vdots & \vdots & \ddots & \vdots \\
\frac{1}{\theta_n+\gamma_{1,r+\alpha}} & \frac{1}{\theta_n+\gamma_{2,r+\alpha}} & \cdots & \frac{1}{\theta_n+\gamma_{n+1,r+\alpha}}
\end{pmatrix}. \tag{A.38}$$

Notice that we have used only $(n+1)$ conditions so far, i.e., the value matching condition given in the first equation in (A.33) and the conditions (A.32). However, the elements of the vector $\mathbf{v}$ depend on the early exercise boundary b_p^* and we have to obtain their functional form before we apply the smooth pasting condition.

The remaining smooth pasting condition given in the second equation in (A.33) can be rewritten in the matrix form

$$\left(\boldsymbol{\gamma}'\tilde{\mathbf{A}}^{-1}\boldsymbol{\Omega} - \boldsymbol{\beta}' \odot \underline{\mathbf{w}}'\right)\mathbf{b}_\beta - e^{(b_p^*-\kappa)}\left(\boldsymbol{\gamma}'\tilde{\mathbf{A}}^{-1} - \mathbf{e}_1'\right)\boldsymbol{\omega} - \boldsymbol{\gamma}'\tilde{\mathbf{A}}^{-1}\boldsymbol{\xi} = 0, \tag{A.39}$$

where $\underline{\mathbf{w}} := (\underline{w}_1, ..., \underline{w}_{m+1})'$ and $\boldsymbol{\beta} := (\beta_{1,r+\alpha}, ..., \beta_{m+1,r+\alpha})'$ are $(m+1)$-dimensional column vectors, and $\mathbf{e}_1 := (1, 0, ..., 0)'$ and $\boldsymbol{\gamma} := (\gamma_{1,r+\alpha}, ..., \gamma_{n+1,r+\alpha})'$ are $(n+1)$-dimensional column vectors. The symbol $\odot$ denotes the Hadamard (element-wise) product.

The critical stock price can be computed numerically via, e.g., bisection method or a similar technique. ■

A.3 Proof of Theorem 2.2.3: Disentangling jumps from diffusion

The early exercise premium of a Canadized American put solves the OIDE in the continuation region, i.e., for $x > b_p^*$,

$$\frac{\sigma^2}{2}\frac{d^2e_p^*}{dx^2}(x,\alpha) + \mu\frac{de_p^*}{dx}(x,\alpha) - (r+\alpha)e_p^*(x,\alpha) + \lambda\int_{-\infty}^{+\infty}[e_p^*(x+y,\alpha) - e_p^*(x,\alpha)]f_Y(y)dy = 0, \quad \text{(A.40)}$$

with the boundary conditions

$$\begin{aligned} &\lim_{x\uparrow+\infty} e_p^*(x,\alpha) = 0, \\ &\lim_{x\downarrow b_p^*} e_p^*(x,\alpha) = e^{\kappa} - e^{b_p^*} - p^*(b_p^*,\alpha), \quad \text{and} \\ &\lim_{x\downarrow b_p^*} \frac{\partial e_p^*}{\partial x}(x,\alpha) = -e^{b_p^*} - \frac{\partial p^*}{\partial x}\Big|_{x=b_p^*}. \end{aligned} \quad \text{(A.41)}$$

Using the Feynman-Kac formula and the result (2.13) for Canadized European put options, we can express the value of the early exercise premium for an Canadized American put option as

$$e_p^*(x,\alpha) = \mathbb{E}_x\left[e^{-(r+\alpha)(\tau_{b_p^*}-t)}\left(\frac{re^{\kappa}}{\alpha+r} - \frac{\delta e^{X_{\tau_{b_p^*}}}}{\alpha+\delta} - \sum_{i=1}^{m+1}\underline{w}_i e^{\beta_{i,r+\alpha}(X_{\tau_{b_p^*}}-\kappa)}\right)\right], \quad \text{(A.42)}$$

where $\tau_{b_p^*}$ is the first hitting time of the flat boundary $b_p^* < \kappa$ from above for the process X_t given by (2.4). Therefore, we have

$$\begin{aligned} e_p^*(x,\alpha) = &\frac{re^{\kappa}}{\alpha+r}\mathbb{E}_x\left[e^{-(r+\alpha)(\tau_{b_p^*}-t)}\right] \\ &+ \frac{\delta e^{b_p^*}}{\alpha+\delta}\mathbb{E}_x\left[e^{-(r+\alpha)(\tau_{b_p^*}-t)+(X_{\tau_{b_p^*}}-b_p^*)}\right] \\ &- \sum_{i=1}^{m+1}\underline{w}_i e^{\beta_{i,r+\alpha}(b_p^*-\kappa)}\mathbb{E}_x\left[e^{-(r+\alpha)(\tau_{b_p^*}-t)+\beta_{i,r+\alpha}(X_{\tau_{b_p^*}}-b_p^*)}\right]. \end{aligned} \quad \text{(A.43)}$$

At this point, we introduce a notation which will help us distinguish whether the stopping of the process X_t is due to the diffusion or the jumps. The events $\mathscr{E}_0 := \{X_{\tau_{b_p^*}} = b_p^*\}$ correspond to the stopping of the process X_t due to the hitting of the flat boundary b_p^*. On the other hand, we define for all $j = 1, ..., n$ the events $\mathscr{E}_j := \{X_{\tau_{b_p^*}} < b_p^* \big| \text{the overshoot is due to the jump of type } j\}$ which represent the stopping of the process X_t due to the overshoot of the flat boundary b_p^*.

Due to the conditional memorylessness of the hyper-exponential distribution (e.g., see Cai (2009) and Yin, Shen and Wen (2013)), the following result holds in the continuation region for any $\rho \in \mathbb{R}_+$:

$$\mathbb{E}_x\left[e^{-(\alpha+r)(\tau_{b_p^*}-t)+\rho(X_{\tau_{b_p^*}}-b_p^*)}\right] = \mathbb{E}_x\left[e^{-(\alpha+r)(\tau_{b_p^*}-t)}\mathbb{1}_{\mathscr{E}_0}\right] + \sum_{j=1}^{n}\frac{\theta_j}{\theta_j+\rho}\mathbb{E}_x\left[e^{-(\alpha+r)(\tau_{b_p^*}-t)}\mathbb{1}_{\mathscr{E}_j}\right]. \quad \text{(A.44)}$$

Using the Lemma 2.2 of Yin, Shen and Wen (2013), we obtain the matrix equation

$$\mathbf{M}\boldsymbol{\epsilon} = \mathbf{b}_\gamma, \tag{A.45}$$

where $(n+1)$-dimensional column vectors $\boldsymbol{\epsilon}$ and $\mathbf{b}_\gamma$ are respectively given by

$$\boldsymbol{\epsilon} := \left(\mathbb{E}_x\left[e^{-(\alpha+r)(\tau_{b_p^*}-t)}\mathbb{1}_{\mathscr{E}_0}\right], \mathbb{E}_x\left[e^{-(\alpha+r)(\tau_{b_p^*}-t)}\mathbb{1}_{\mathscr{E}_1}\right], ..., \mathbb{E}_x\left[e^{-(\alpha+r)(\tau_{b_p^*}-t)}\mathbb{1}_{\mathscr{E}_n}\right]\right)', \tag{A.46}$$

$$\mathbf{b}_\gamma := \left(e^{\gamma_{1,r+\alpha}(x-b_p^*)}, e^{\gamma_{2,r+\alpha}(x-b_p^*)}, ..., e^{\gamma_{n+1,r+\alpha}(x-b_p^*)}\right)'. \tag{A.47}$$

Finally, $(n+1)$-dimensional square matrix $\mathbf{M}$ is defined as

$$\mathbf{M} := \begin{pmatrix} 1 & \frac{\theta_1}{\theta_1+\gamma_{1,r+\alpha}} & \frac{\theta_2}{\theta_2+\gamma_{1,r+\alpha}} & \cdots & \frac{\theta_n}{\theta_n+\gamma_{1,r+\alpha}} \\ 1 & \frac{\theta_1}{\theta_1+\gamma_{2,r+\alpha}} & \frac{\theta_2}{\theta_2+\gamma_{2,r+\alpha}} & \cdots & \frac{\theta_n}{\theta_n+\gamma_{2,r+\alpha}} \\ \vdots & \vdots & \vdots & \vdots & \vdots \\ 1 & \frac{\theta_1}{\theta_1+\gamma_{n+1,r+\alpha}} & \frac{\theta_2}{\theta_2+\gamma_{n+1,r+\alpha}} & \cdots & \frac{\theta_n}{\theta_n+\gamma_{n+1,r+\alpha}}. \end{pmatrix}. \tag{A.48}$$

Therefore, by calculating the vector $\boldsymbol{\epsilon}$ and by decomposition (A.44), we can disentangle diffusion and jump for the Canadized early exercise premium as in (A.43). The diffusion component is given by

$$e_{p,d}^*(x,\alpha) = \left(\frac{re^\kappa}{\alpha+r} - \frac{\delta e^\kappa}{\alpha+\delta}e^{(b_p^*-\kappa)} - \sum_{i=1}^{m+1}\underline{w}_i e^{\beta i,r+\alpha(b_p^*-\kappa)}\right)\mathbb{E}_x\left[e^{-(\alpha+r)(\tau_{b_p^*}-t)}\mathbb{1}_{\mathscr{E}_0}\right], \tag{A.49}$$

and the jump component can be represented as a sum of individual contribution of all jump types to the early exercise premium

$$e_{p,j}^*(x,\alpha) = \sum_{l=1}^{n} e_{p,j,l}^*(S_t,\alpha), \tag{A.50}$$

where[71]

$$\begin{aligned} e_{p,j,l}^*(S_t,\alpha) &= \left(\frac{re^\kappa}{\alpha+r} - \frac{\theta_l\delta e^\kappa}{(\theta_l+1)(\alpha+\delta)}e^{(b_p^*-\kappa)} - \sum_{i=1}^{m+1}\frac{\theta_l}{\theta_l+\beta_{i,r+\alpha}}\underline{w}_i e^{\beta i,r+\alpha(b_p^*-\kappa)}\right) \\ &\quad \times\mathbb{E}_x\left[e^{-(\alpha+r)(\tau_{b_p^*}-t)}\mathbb{1}_{\mathscr{E}_l}\right]. \end{aligned} \tag{A.51}$$

This concludes the proof. ■

[71] Note that the expectations in (A.49) and (A.51) are computed by solving matrix equation (A.45).

Appendix B

Supplementary results for Chapter 2

B.1 Addendum to Appendix A.1: Proof of non-singularity

We follow the idea of Cai and Kou (2011), Theorem 3.3, p. 2072, and prove by contradiction the non-singularity of the matrix $\mathbf{A}$ given in equation (A.20). Let's assume that the matrix $\mathbf{A}$ is singular. Therefore, there exist non-zero constants a, b, $\{c_i\}_{i=1,\dots,m}$, and $\{d_j\}_{i=1,\dots,n}$ such that

$$\begin{cases} a + b\beta_{l,r+\alpha} + \sum_{i=1}^{m} \frac{c_i}{\eta_i - \beta_{l,r+\alpha}} + \sum_{j=1}^{m} \frac{d_j}{\theta_j + \beta_{l,r+\alpha}} = 0, \quad \text{for } l = 1, ..., m+1, \\ a + b\gamma_{l,r+\alpha} + \sum_{i=1}^{m} \frac{c_i}{\eta_i - \gamma_{l,r+\alpha}} + \sum_{j=1}^{m} \frac{d_j}{\theta_j + \gamma_{l,r+\alpha}} = 0, \quad \text{for } l = 1, ..., n+1. \end{cases} \tag{B.1}$$

From these equations we conclude that the function

$$f_{\mathbf{A}}(z) := a + bz + \sum_{i=1}^{m} \frac{c_i}{\eta_i - z} + \sum_{j=1}^{m} \frac{d_j}{\theta_j + z} \tag{B.2}$$

has at least $(m + n + 2)$ roots. Nevertheless, the order of the polynomial

$$p_{\mathbf{A}}(z) := f_{\mathbf{A}}(z) \prod_{i=1}^{m} (\eta_i - z) \prod_{j=1}^{n} (\theta_j + z) \tag{B.3}$$

is at most $(m + n + 1)$. This implies that the polynomial (B.2), and thus the function (B.1), has at most $(m + n + 1)$ roots. This is a contradiction, therefore the matrix $\mathbf{A}$ is non-singular.[72] ■

B.2 Addendum to Appendix A.3: Verification of the proof

The analytical disentanglement obtained in (2.18) and (2.19) can be verified as follows. By adopting the notation introduced in Appendix A.2 and Appendix A.3, from equations (A.28) and (A.34) we

[72] The non-singularity of the matrices $\tilde{\mathbf{A}}$ and $\mathbf{M}$ given in (A.38) and (A.48), respectively, can be proved by following the arguments presented in this section.

obtain the expression for the early exercise premium in the matrix form

$$e_p^*(x,\alpha) = \mathbf{b}'_\gamma \tilde{\mathbf{A}}^{-1} \tilde{\mathbf{J}}. \tag{B.4}$$

On the other hand, the disentanglement of the early exercise premium can be written as

$$\begin{aligned} e_p^*(x,\alpha) &= e_{p,d}^*(x,\alpha) + \sum_{l=1}^{n} e_{p,j,l}^*(x,\alpha;l) \\ &= \boldsymbol{\epsilon}_0 \tilde{\mathbf{J}}_0 + \sum_{l=1}^{n} \boldsymbol{\epsilon}_l \boldsymbol{\theta}_l \tilde{\mathbf{J}}_l \\ &= \boldsymbol{\epsilon}'(\boldsymbol{\theta} \odot \tilde{\mathbf{J}}), \end{aligned} \tag{B.5}$$

where $\boldsymbol{\theta} := (1, \theta_1, ..., \theta_n)'$ is $(n+1)$–dimensional column vector. Furthermore, we establish the connection between the matrices defined in (A.38) and (A.48):

$$\mathbf{M}' = \boldsymbol{\Theta} \odot \tilde{\mathbf{A}}, \tag{B.6}$$

where $\boldsymbol{\Theta}$ is $(n+1)$ –dimensional square matrix defined as

$$\boldsymbol{\Theta} := \begin{pmatrix} 1 & 1 & \cdots & 1 \\ \theta_1 & \theta_1 & \cdots & \theta_1 \\ \theta_2 & \theta_2 & \cdots & \theta_2 \\ \vdots & \vdots & \ddots & \vdots \\ \theta_n & \theta_n & \cdots & \theta_n \end{pmatrix}. \tag{B.7}$$

Combining the results (A.45) and (B.6) in the equation (B.5) we obtain

$$\begin{aligned} e_p^*(x,\alpha) &= \mathbf{b}'_\gamma (\mathbf{M}^{-1})' (\boldsymbol{\theta} \odot \tilde{\mathbf{J}}) \\ &= \mathbf{b}'_\gamma (\boldsymbol{\Theta} \odot \tilde{\mathbf{A}})^{-1} (\boldsymbol{\theta} \odot \tilde{\mathbf{J}}). \end{aligned} \tag{B.8}$$

After some algebra, we compute the following result:

$$(\boldsymbol{\Theta} \odot \tilde{\mathbf{A}})^{-1} = \frac{1}{\det \tilde{\mathbf{A}} \cdot \prod_{l=1}^{n} \theta_l} \begin{pmatrix} (\boldsymbol{\Theta} \odot \tilde{\mathbf{A}})^{\mathrm{c}}_{1,1} & (\boldsymbol{\Theta} \odot \tilde{\mathbf{A}})^{\mathrm{c}}_{2,1} & \cdots & (\boldsymbol{\Theta} \odot \tilde{\mathbf{A}})^{\mathrm{c}}_{n+1,1} \\ (\boldsymbol{\Theta} \odot \tilde{\mathbf{A}})^{\mathrm{c}}_{1,2} & (\boldsymbol{\Theta} \odot \tilde{\mathbf{A}})^{\mathrm{c}}_{2,2} & \cdots & (\boldsymbol{\Theta} \odot \tilde{\mathbf{A}})^{\mathrm{c}}_{n+1,2} \\ \vdots & \vdots & \ddots & \vdots \\ (\boldsymbol{\Theta} \odot \tilde{\mathbf{A}})^{\mathrm{c}}_{1,n+1} & (\boldsymbol{\Theta} \odot \tilde{\mathbf{A}})^{\mathrm{c}}_{2,n+1} & \cdots & (\boldsymbol{\Theta} \odot \tilde{\mathbf{A}})^{\mathrm{c}}_{n+1,n+1} \end{pmatrix}. \tag{B.9}$$

Cofactors $(\boldsymbol{\Theta} \odot \tilde{\mathbf{A}})^{\mathrm{c}}_{i,j}$ for $i, j = 1, 2, ..., n+1$ can be expressed via cofactors of the matrix $\tilde{\mathbf{A}}$ as

$$(\boldsymbol{\Theta} \odot \tilde{\mathbf{A}})^{\mathrm{c}}_{i,j} = \begin{cases} \tilde{\mathbf{A}}^{\mathrm{c}}_{i,j} & \text{for } \; i = 1, 2, ..., n+1, \;\; \text{and } \; j = 1, \\ \tilde{\mathbf{A}}^{\mathrm{c}}_{i,j} \cdot \prod\limits_{\substack{l=1 \\ l \neq j}}^{n} \theta_l & \text{for } \; i = 1, 2, 3, ..., n+1, \;\; \text{and } \; j = 2, ..., n+1, \end{cases} \tag{B.10}$$

hence yielding the following representation

$$(\boldsymbol{\Theta} \odot \tilde{\mathbf{A}})^{-1} = \hat{\boldsymbol{\Theta}} \odot \tilde{\mathbf{A}}^{-1}. \tag{B.11}$$

The matrix $\hat{\boldsymbol{\Theta}} = (\boldsymbol{\Theta}')^{\odot -1}$ which represents the Hadamard inverse of the matrix $\boldsymbol{\Theta}'$, i.e., $\hat{\boldsymbol{\Theta}} \odot \boldsymbol{\Theta}' = \mathbb{1}$ with $\mathbb{1} := \mathrm{diag}(1, 1, ..., 1)$ being $(n+1)$–dimensional unit matrix, is given by

$$\hat{\boldsymbol{\Theta}} = \begin{pmatrix} 1 & \frac{1}{\theta_1} & \frac{1}{\theta_2} & \cdots & \frac{1}{\theta_n} \\ 1 & \frac{1}{\theta_1} & \frac{1}{\theta_2} & \cdots & \frac{1}{\theta_n} \\ \vdots & \vdots & \vdots & \ddots & \vdots \\ 1 & \frac{1}{\theta_1} & \frac{1}{\theta_2} & \cdots & \frac{1}{\theta_n} \end{pmatrix}. \tag{B.12}$$

Lastly, one can show that the following equation holds for an arbitrary $(n+1) \times (n+1)$-dimensional matrix $\mathbf{C}$ and $(n+1)$–dimensional column vector $\mathbf{u}$:

$$\mathbf{C}(\boldsymbol{\theta} \odot \mathbf{u}) = (\boldsymbol{\Theta}' \odot \mathbf{C})\mathbf{u}. \tag{B.13}$$

Plugging the expressions (B.11) and (B.13) back into the equation (B.8) and using the Hadamard inverse (B.12) yields the final result:

$$\begin{aligned} e^*_p(x, \alpha) &= \mathbf{b}'_\gamma(\hat{\boldsymbol{\Theta}} \odot \tilde{\mathbf{A}}^{-1})(\boldsymbol{\theta} \odot \tilde{\mathbf{J}}) \\ &= \mathbf{b}'_\gamma(\hat{\boldsymbol{\Theta}} \odot \boldsymbol{\Theta}' \odot \tilde{\mathbf{A}}^{-1})\tilde{\mathbf{J}} \\ &= \mathbf{b}'_\gamma \tilde{\mathbf{A}}^{-1} \tilde{\mathbf{J}}, \end{aligned} \tag{B.14}$$

which is exactly the same expression as in (B.4). ■

B.3 Addendum to Section 2.2.2: Canadized European and American Greeks

The Laplace–Carson transform of the delta and gamma of a European option can be computed in a closed form by taking the first and second-order derivatives of the European-Canadian option price

(see Theorem 2.2.1 and Appendix A.1) with respect to the underlying price,respectively. The theta of a European option can be computed using the Laplace–Carson transform of a derivative of the option price with respect to the time. The computations are straightforward, hence we omit the algebraic calculations and provide only the final expressions.

The delta, gamma and theta of a Canadized European put are respectively given by

$$\Delta_p^*(S_t,\alpha)=\frac{\partial p^*}{\partial S_t}(S_t,\alpha)=\begin{cases}\dfrac{1}{S_t}\displaystyle\sum_{i=1}^{m+1}\beta_{i,r+\alpha}\underline{w}_i\left(\frac{S_t}{K}\right)^{\beta_{i,r+\alpha}}-\frac{\alpha}{\alpha+\delta} & \text{if } S_t<K,\\ \dfrac{1}{S_t}\displaystyle\sum_{j=1}^{n+1}\gamma_{j,r+\alpha}\overline{w}_j\left(\frac{S_t}{K}\right)^{\gamma_{j,r+\alpha}} & \text{if } S_t\geq K,\end{cases} \tag{B.15}$$

$$\Gamma_p^*(S_t,\alpha)=\frac{\partial^2 p^*}{\partial S_t^2}(S_t,\alpha)=\begin{cases}\dfrac{1}{S_t^2}\displaystyle\sum_{i=1}^{m+1}\beta_{i,r+\alpha}(\beta_{i,r+\alpha}-1)\underline{w}_i\left(\frac{S_t}{K}\right)^{\beta_{i,r+\alpha}} & \text{if } S_t<K,\\ \dfrac{1}{S_t^2}\displaystyle\sum_{j=1}^{n+1}\gamma_{j,r+\alpha}(\gamma_{j,r+\alpha}-1)\overline{w}_j\left(\frac{S_t}{K}\right)^{\gamma_{j,r+\alpha}} & \text{if } S_t\geq K,\end{cases} \tag{B.16}$$

and

$$\Theta_p^*(S_t,\alpha)=\alpha\left((K-S_t)^+-p^*(S_t,\alpha)\right)=\begin{cases}\alpha\left(\dfrac{rK}{\alpha+r}-\dfrac{\delta S_t}{\alpha+\delta}-\displaystyle\sum_{i=1}^{m+1}\underline{w}_i\left(\frac{S_t}{K}\right)^{\beta_{i,r+\alpha}}\right) & \text{if } S_t<K,\\ -\alpha\displaystyle\sum_{j=1}^{n+1}\overline{w}_j\left(\frac{S_t}{K}\right)^{\gamma_{j,r+\alpha}} & \text{if } S_t\geq K.\end{cases} \tag{B.17}$$

On the other hand, the early exercise premium delta, gamma, and theta are, respectively,

$$\Delta_{e_p}^*(S_t,\alpha)=\frac{\partial e_p^*}{\partial S_t}(S_t,\alpha)=\begin{cases}\dfrac{1}{S_t}\displaystyle\sum_{j=1}^{n+1}\gamma_{j,r+\alpha}v_j\left(\frac{S_t}{B_p^*}\right)^{\gamma_{j,r+\alpha}} & \text{if } S_t>B_p^*,\\ -1-\Delta_p^*(S_t,\alpha) & \text{if } S_t\leq B_p^*,\end{cases} \tag{B.18}$$

$$\Gamma_{e_p}^*(S_t,\alpha)=\frac{\partial^2 e_p^*}{\partial S_t^2}(S_t,\alpha)=\begin{cases}\dfrac{1}{S_t^2}\displaystyle\sum_{j=1}^{n+1}\gamma_{j,r+\alpha}(\gamma_{j,r+\alpha}-1)v_j\left(\frac{S_t}{B_p^*}\right)^{\gamma_{j,r+\alpha}} & \text{if } S_t>B_p^*,\\ -\Gamma_p^*(S_t,\alpha) & \text{if } S_t\leq B_p^*,\end{cases} \tag{B.19}$$

and

$$\Theta_{e_p}^*(S_t,\alpha)=-\alpha e_p^*(S_t,\alpha)=\begin{cases}-\alpha\displaystyle\sum_{j=1}^{n+1}v_j\left(\frac{S_t}{B_p^*}\right)^{\gamma_{j,r+\alpha}} & \text{if } S_t>B_p^*,\\ -\alpha(K-S_t-p^*(S_t,\alpha)) & \text{if } S_t\leq B_p^*.\end{cases} \tag{B.20}$$

Therefore, based on the early exercise premium decomposition, and given the results (B.15)–(B.17) and (B.18)–(B.20), we can compute the American-Canadian put greeks as the sum of the corresponding European-Canadian put and early exercise premium greeks. ■

B.4 Addendum to Section 2.3.1: Calibration procedure

In this section we provide additional information about the calibration procedure for the estimation of model parameters which are consistent with observed market option prices. We emphasize that our approach is sequential, i.e., it involves daily re-calibration of the model parameters, which is well suited for a dynamic analysis of the early exercise premium disentanglement.

First, we introduce the (daily) weighted non-linear least squares (WNLLS) objective function in the form

$$\mathcal{E}(\boldsymbol{\xi}_{t_j}) := \frac{1}{N_{t_j}} \sum_{i=1}^{N_{t_j}} \omega_{t_j,i} \left(F(\boldsymbol{\xi}_{t_j}; \tau_{t_j,i}, K_{t_j}, i, S_{t_j}, r_{t_j,i}, \delta_{t_j}) - F^{\text{mkt}}(\tau_{t_j,i}, K_{t_j,i}) \right)^2, \tag{B.21}$$

where sample dates are indexed by $j = 1, 2, ..., M$, and the observed market quotes of option prices on a given day j are indexed by $i = 1, 2, ..., N_{t_j}$. Function $F^{\text{mkt}}(\cdot)$ represents the market option price, whereas $F(\cdot)$ is the corresponding model option price. Time to maturity and strike price are denoted by $\tau_{t_j,i}$ and $K_{t_j,i}$, respectively. The set of HEJD(m, n) model parameters on a given day j is given by $\boldsymbol{\xi}_{t_j} := \left\{ \sigma^{(j)}, \lambda^{(j)}, p_1^{(j)}, ..., p_m^{(j)}, q_1^{(j)}, ..., q_n^{(j)}, \eta_1^{(j)}, ..., \eta_m^{(j)}, \theta_1^{(j)}, ..., \theta_n^{(j)} \right\} \in \boldsymbol{\Xi} := \mathbb{R}_+ \times \mathbb{R}_+ \times [0,1]^m \times [0,1]^n \times \mathbb{R}_+^m \times \mathbb{R}_+^n$. The spot price of the underlying instrument is S_{t_j}. The risk-free interest rate $r_{t_j,i}$ corresponds to the zero-coupon bond maturing on date $t_j + \tau_{t_j,i}$. The dividend yield is denoted as δ_{t_j}. Following Lindström et al. (2008), p. 2881, the objective-function weights are given by the inverse of the squared bid-ask spread:

$$\omega_{t_j,i} := \frac{1}{\left| \text{Ask}_{t_j}^{\text{mkt}}(\tau_{t_j,i}, K_{t_j,i}) - \text{Bid}_{t_j}^{\text{mkt}}(\tau_{t_j,i}, K_{t_j,i}) \right|^2}. \tag{B.22}$$

Inverse problems are generally ill-posed since small data perturbation could result in an abrupt change of the basin of attraction in the optimization space, which in turn could result in unstable parameter estimates. In particular, non-convexity of a multidimensional loss function implies existence of multiple local minima. Moreover, the "landscape" of such an objective function is characterized by wide flat regions. For these reasons, any empirical option pricing problem involving a re-calibration of

model parameters via minimization of an objective function that takes form (B.21) or similar is likely to suffer from instability. Therefore, it can have adverse effects on the P&L via sharply fluctuating hedging ratios. However, robustness of a sequential calibration procedure can be achieved by introducing a regularization method. The main idea is to circumvent the difficulties associated with the non-convexity by adding a positive and locally convex penalty term to the loss function, hence recasting the original problem into a series of minimizations of the regularized WNLLS objective function.

In general, there are many different ways to define the penalty function for the regularization method. For example, Cont and Tankov (2004) use the relative entropy. However, this approach is based on the Kullback–Leibler divergence with respect to a prior model in the path space, In continuous-time framework, it implies that the volatility parameter remains constant to insure the non-singularity (equivalence) of probability measures. Therefore, the choice of the penalty term defined as the relative entropy function would make it impossible to obtain dynamic diffusion parameter. For this reason we follow Hellmich, Kassberger and Schmidt (2013) instead, and define the penalty function as the Kulback-Leibler divergence between the probability distributions on a given point in time, as opposed to the Cont and Tankov (2004)'s path-space approach. For every $j = 2, 3, ..., M$ we define the penalty function as

$$\mathcal{P}(\boldsymbol{\xi}_{t_j}; \hat{\boldsymbol{\xi}}_{t_{j-1}}) = \mathcal{D}_{\mathcal{KL}}(\Phi(\boldsymbol{\xi}_{t_j})||\Phi(\hat{\boldsymbol{\xi}}_{t_{j-1}})) := \int_{-\infty}^{+\infty} \phi\left(x; \boldsymbol{\xi}_{t_j}\right) \left(\ln \phi\left(x; \boldsymbol{\xi}_{t_j}\right) - \ln \phi(x; \hat{\boldsymbol{\xi}}_{t_{j-1}})\right) dx, \quad \text{(B.23)}$$

where $\phi(x; \boldsymbol{\xi}_{t_j})$ and $\phi(x; \hat{\boldsymbol{\xi}}_{t_{j-1}})$ are the probability density functions of the probability distribution $\Phi(\boldsymbol{\xi}_{t_j})$ and the probability distribution $\Phi(\hat{\boldsymbol{\xi}}_{t_{j-1}})$, respectively. The set of parameters $\hat{\boldsymbol{\xi}}_{t_{j-1}} := \left\{\hat{\sigma}^{(j-1)}, \hat{\lambda}^{(j-1)}, \hat{p}_1^{(j-1)}, ..., \hat{p}_m^{(j-1)}, \hat{q}_1^{(j-1)}, ..., \hat{q}_n^{(j-1)}, \hat{\eta}_1^{(j-1)}, ..., \hat{\eta}_m^{(j-1)}, \hat{\theta}_1^{(j-1)}, ..., \hat{\theta}_n^{(j-1)}\right\}$ is the product of the calibration at time t_{j-1}. Essentially, by adding the penalty term defined in (B.23) to the objective function (B.21) we are imposing a dependence of the optimal model parameters for a given date on the optimal model parameters obtained for the previous date via the Kullback-Leibler measure of divergence between the corresponding risk-neutral density functions. Therefore, our sequential regularized calibration procedure uses the data through the WNLLS function, and the penalty term addresses the issue of ill-posedness and overfitting by dampening the oscillations of the estimated model parameters.

We employ the regularization technique described above at every point in time except for the first observation date, since no prior information is available. Therefore, the loss function at time t_1 is

identical to the WNLLS objective function given in (B.21):

$$\mathcal{J}\left(\boldsymbol{\xi}_{t_1}\right) := \mathcal{E}\left(\boldsymbol{\xi}_{t_1}\right), \tag{B.24}$$

and the model parameters are computed by solving the minimization problem

$$\hat{\boldsymbol{\xi}}_{t_1} = \underset{\boldsymbol{\xi}_{t_1} \in \boldsymbol{\Xi}}{\arg\min}\ \mathcal{J}\left(\boldsymbol{\xi}_{t_1}\right). \tag{B.25}$$

Similarly to Cai and Kou (2011), Section 4.2, pp. 2073–2074, we tackle the optimization problem (B.25) by randomly generating 20,000 values for the set of model parameters and by choosing 100 starting points with the smallest objective function values. Subsequently, we run an optimization algorithm for each of the chosen sets of parameters. The calibrated model parameters resulting in the smallest value of the loss function represent the optimal set of parameters for the first date in out sample.

For observation dates $t_j (j = 2, 3, ..., M)$ the regularized loss function takes the form

$$\mathcal{J}(\boldsymbol{\xi}_{t_j}; \hat{\boldsymbol{\xi}}_{t_{j-1}}, \psi_{t_j}) := \mathcal{E}(\boldsymbol{\xi}_{t_j}) + \psi_{t_j} \cdot \mathcal{P}(\boldsymbol{\xi}_{t_j}; \hat{\boldsymbol{\xi}}_{t_{j-1}}). \tag{B.26}$$

The optimal model parameters are obtained as

$$\hat{\boldsymbol{\xi}}_{t_j} = \underset{\boldsymbol{\xi}_{t_j} \in \boldsymbol{\Xi}}{\arg\min}\ \mathcal{J}(\boldsymbol{\xi}_{t_j}; \hat{\boldsymbol{\xi}}_{t_{j-1}}, \psi_{t_j}), \tag{B.27}$$

where ψ_{t_j} represents the regularization parameter which provides information about the importance of the penalty term (which captures the difference between the model parameters on two consecutive days) relative to the the standard WNLLS term (which minimizes the distance between the model and market option prices on a given day). The regularization parameter is not known a priori; it is data-dependent and its value changes with every re-calibration step.

The solution to the problem (B.27) is based on Cont and Tankov (2004), Section 4.2 and Section 4.3, pp. 23–26. First, we solve the optimization problem for the case $\psi_{t_j} = 0$, i.e., we minimize the unregularized objective function (B.21):

$$\hat{\boldsymbol{\xi}}^{(0)}_{t_j} = \underset{\boldsymbol{\xi}_{t_j} \in \boldsymbol{\Xi}}{\arg\min}\ \mathcal{E}(\boldsymbol{\xi}_{t_j}). \tag{B.28}$$

Second, we use the Morozov discrepancy principle in order to choose a plausible value for the regularization parameter. The main idea is to choose the value of ψ_{t_j} in such a way that the error induced by the regularization is of the same order of magnitude as the model error:

$$\mathcal{J}(\hat{\boldsymbol{\xi}}^{(1)}_{t_j}; \hat{\boldsymbol{\xi}}_{t_{j-1}}, \psi_{t_j}) = (1 + \epsilon) \cdot \mathcal{E}(\hat{\boldsymbol{\xi}}^{(0)}_{t_j}), \tag{B.29}$$

where ϵ is a small number, e.g., $\epsilon = 0.1$. This step typically does not require high precision computation. Finally, once the regularization parameter—which gives us the desired trade-off between the data and the calibration stability—is estimated, we can perform the high-precision optimization given in (B.27).

♣

B.5 Addendum to Section 2.3.2: Model selection

In this section we provide additional information about the model selection procedure. Theoretically, the HEJD modelling framework admits any number of distinct positive and negative jump types to be used. Increasing the number of positive and negative jump types results in a richer model structure, and naturally improves the quality of the in-sample fit. On the other hand, it is suboptimal to overfit a mode (e.g., see Burnham and Anderson 2002, Section 1.4, pp. 29–37). Information theory tackles model selection problems by balancing out the goodness-of-fit and the number of degrees of freedom.

The sequential regularized WNLLS procedure (B.21)–(B.29) can be represented as a series of maximum a posteriori (MAP) problems which can be interpreted as a regularized maximum likelihood. The equivalence between the two methods can be demonstrated as follows. For a given sample date $t_j (j = 2, 3, ..., M)$, the observed market prices $F^{\text{mkt}}(\tau_{t_j,i}, K_{t_j,i})$ for $i = 1, 2, ..., N_{t_j}$ can be expressed as a regression model:

$$F^{\text{mkt}}(\tau_{t_j,i}, K_{t_j,i}) = F(\boldsymbol{\xi}_{t_j}; \tau_{t_j,i}, K_{t_j,i}, S_{t_j}, r_{t_j,i}, \delta_{t_j}) + \varepsilon_{t_j,i}. \tag{B.30}$$

The error terms $\varepsilon_{t_j,i} \sim \mathcal{N}(0, \varsigma^2_{t_j,i})$ are assumed to be normally distributed and heteroskedastic. We define the variance of the error term as

$$\varsigma^2_{t_j,i} := \frac{\varsigma^2}{\omega_{t_j,i}}, \tag{B.31}$$

with $\varsigma \in \mathbb{R}_+$ being a nuisance parameter and $\varsigma_{t_j,i}$ being defined in (B.22). We denote the collection of error variances on observation date t_j as $\boldsymbol{\varsigma}^2_{t_j} := (\varsigma^2_{t_j,1}, \varsigma^2_{t_j,2}, ..., \varsigma^2_{t_j,N_{t_j}})$. Moneyness $\boldsymbol{\tau}_{t_j} := (\tau_{t_j,1}, \tau_{t_j,2}, ..., \tau_{t_j,N_{t_j}})$ and strike price $\mathbf{K}_{t_j} := (K_{t_j,1}, K_{t_j,2}, ..., K_{t_j,N_{t_j}})$, defined for each sample date t_j, are exogenous variables in this model. The Gaussian log-likelihood for the non-linear regression

(B.30) is given by

$$\begin{aligned}\ell(\boldsymbol{\xi}_{t_j}, \varsigma_{t_j}^2; \boldsymbol{\tau}_{t_j}, \mathbf{K}_{t_j}) = &- N_{t_j} \ln \sqrt{2\pi} - \frac{1}{2} \sum_{i=1}^{N_{t_j}} \ln \varsigma_{t_j,i}^2 \\ &- \frac{1}{2} \sum_{i=1}^{N_{t_j}} \frac{1}{\varsigma_{t_j,i}^2} \left(F^{\text{mkt}}(\tau_{t_j,i}, K_{t_j,i}) - F(\boldsymbol{\xi}_{t_j}; \tau_{t_j,i}, K_{t_j,i}, S_{t_j}, r_{t_j,i}, \delta_{t_j}) \right)^2.\end{aligned} \tag{B.32}$$

It is straightforward to verify that the maximization of the log-likelihood function is equivalent to the minimization of the WNLLS objective function (B.21). In the presence of the (scaled) Kullback–Leibler penalty term (B.23), the regularized log-likelihood function is

$$\begin{aligned}\ell_{\text{reg}}(\boldsymbol{\xi}_{t_j}, \varsigma_{t_j}^2; \boldsymbol{\tau}_{t_j}, \mathbf{K}_{t_j}, \hat{\boldsymbol{\xi}}_{t_{j-1}}) = &- N_{t_j} \ln \sqrt{2\pi} - \frac{1}{2} \sum_{i=1}^{N_{t_j}} \ln \varsigma_{t_j,i}^2 \\ &- \frac{1}{2} \sum_{i=1}^{N_{t_j}} \frac{1}{\varsigma_{t_j,i}^2} \left(F^{\text{mkt}}(\tau_{t_j,i}, K_{t_j,i}) - F(\boldsymbol{\xi}_{t_j}; \tau_{t_j,i}, K_{t_j,i}, S_{t_j}, r_{t_j,i}, \delta_{t_j}) \right)^2 \\ &- \psi_{t_j}^* \cdot \mathcal{P}(\boldsymbol{\xi}_{t_j}; \hat{\boldsymbol{\xi}}_{t_{j-1}}).\end{aligned} \tag{B.33}$$

The choice of the modified regularization parameter as $\psi_{t_j}^* := \frac{N_{t_j}}{2\varsigma^2} \psi_{t_j}$ results in a regularized log-likelihood whose maximization is equivalent to the minimization given in (B.27). The model parameters can be estimated by solving the optimization problem

$$\hat{\boldsymbol{\xi}}_{t_j} = \underset{\boldsymbol{\xi}_{t_j} \in \boldsymbol{\Xi}}{\arg\min}\ \ell \left(\boldsymbol{\xi}_{t_j}, \varsigma_{t_j}^2; \boldsymbol{\tau}_{t_j}, \mathbf{K}_{t_j} \right) + \ln \left(\phi_{\exp}(\mathcal{P}(\boldsymbol{\xi}_{t_j}; \hat{\boldsymbol{\xi}}_{t_{j-1}}); \psi_{t_j}^*) \right), \tag{B.34}$$

where $\phi_{\exp}(y; \nu)$ is a (positive) exponential probability distribution function with parameter $\nu \in \mathbb{R}_+$. Finally, by switching from the "log-likelihood space" to the "likelihood space" we obtain the MAP interpretation of our regularized WNLLS objective function. Therefore, our calibration procedure is equivalent to the maximization of the ordinary Gaussian likelihood with an indirect prior on parameters $\boldsymbol{\xi}_{t_j}$ specified via an exponential prior on the Kullback–Leibler divergence, which satisfies the positivity and the convexity requirements. The augmented likelihood function can be written as the product of standard maximum likelihood and the prior distribution on the model parameters (Kullback–Leibler divergence):

$$\begin{aligned}\mathcal{L}_{\text{MAP}}(\boldsymbol{\xi}_{t_j}, \varsigma_{t_j}^2; \boldsymbol{\tau}_{t_j}, \mathbf{K}_{t_j}, \hat{\boldsymbol{\xi}}_{t_{j-1}}) &= \mathcal{L}_{\text{ML}}(\boldsymbol{\xi}_{t_j}, \varsigma_{t_j}^2; \boldsymbol{\tau}_{t_j}, \mathbf{K}_{t_j}) \cdot \phi_{\exp}(\mathcal{P}(\boldsymbol{\xi}_{t_j}; \hat{\boldsymbol{\xi}}_{t_{j-1}}); \psi_{t_j}^*) \\ &= \phi_{\text{normal}}(\boldsymbol{\tau}_{t_j}, \mathbf{K}_{t_j}; \boldsymbol{\xi}_{t_j}, \varsigma_{t_j}^2) \cdot \phi_{\exp}(\mathcal{P}(\boldsymbol{\xi}_{t_j}; \hat{\boldsymbol{\xi}}_{t_{j-1}}); \psi_{t_j}^*),\end{aligned} \tag{B.35}$$

where $\mathcal{L}_{\mathrm{ML}}(\boldsymbol{\xi}_{t_j}, \varsigma^2_{t_j}; \boldsymbol{\tau}_{t_j}, \mathbf{K}_{t_j}) := \exp(\ell(\boldsymbol{\xi}_{t_j}, \varsigma^2_{t_j}; \boldsymbol{\tau}_{t_j}, \mathbf{K}_{t_j}))$ is the Gaussian likelihood function, and the probability density function $\phi_{\mathrm{normal}}(\boldsymbol{\tau}_{t_j}, \mathbf{K}_{t_j}; \boldsymbol{\xi}_{t_j}, \varsigma^2_{t_j}) := \prod_{i=1}^{N_{t_j}} \phi_{\mathrm{normal}}(\tau_{t_j,i}, K_{t_j,i}; \boldsymbol{\xi}_{t_j}, \varsigma^2_{t_j,i})$ corresponds to the joint normal distribution of the error terms on a given observation date.

We note that alternative approaches to the penalty functions based on the Kullback–Leibler information divergences considered in Cont and Tankov (2004) and Hellmich, Kassberger and Schmidt (2013) include least absolute deviations ($\mathcal{L}_1$-distance) or least squares ($\mathcal{L}_2$-distance) between the two sets of parameters. These two methods are also know as LASSO and ridge regressions, respectively. In the MAP framework they can be interpreted as an ordinary Gaussian likelihood with a Laplace (for LASSO regressions) or a Gaussian prior (for ridge regressions) on the parameters $\boldsymbol{\xi}_{t_j}$. Since our model parameters are defined on the space $\boldsymbol{\Xi} = \mathbb{R}_+ \times \mathbb{R}_+ \times [0,1]^m \times [0,1]^n \times \mathbb{R}_+^m \times \mathbb{R}_+^n$, a Laplace or a Gaussian prior—which can assume negative values—would be inconsistent with the domain of our parameter set. Therefore, in our opinion, an indirect prior via the Kullback–Liebler divergence between the risk-neutral distribution functions on two consecutive observation dates is a better choice than LASSO and ridge regression from both mathematical and financial point of view.

Finally, in addition to the MAP objective function, we compare the in-sample performance of the considered models in terms of the Akaike (AIC), the corrected Akaike (AICc) and the Bayesian (BIC) information criterion, all of which are valid for non-nested models. The corresponding weights based on the relative likelihood of the models are also computed. We also compute the pairwise evidence ratios. The number of parameters for the HEJD(m,n) model is $N_{\mathrm{par}} = 2(m+n)+1$. Hence, for a given observation date $t_j (j = 2, 3, ..., M)$ and a chosen jump structure, i.e., fixed m and n, the information criteria can be computed as

$$\begin{aligned}
\mathrm{AIC}_{t_j}(m,n) &= -2\ell_{\mathrm{reg}}(\boldsymbol{\xi}_{t_j}, \varsigma^2_{t_j}; \boldsymbol{\tau}_{t_j}, \mathbf{K}_{t_j}, \hat{\boldsymbol{\xi}}_{t_{j-1}}) + 2N_{\mathrm{par}}, \\
\mathrm{AICc}_{t_j}(m,n) &= \mathrm{AIC}_{t_j}(m,n) + 2\frac{N_{\mathrm{par}}(N_{\mathrm{par}}+1)}{N_{t_j} - N_{\mathrm{par}} - 1}, \\
\mathrm{BIC}_{t_j}(m,n) &= -2\ell_{\mathrm{reg}}(\boldsymbol{\xi}_{t_j}, \varsigma^2_{t_j}; \boldsymbol{\tau}_{t_j}, \mathbf{K}_{t_j}, \hat{\boldsymbol{\xi}}_{t_{j-1}}) + 2N_{\mathrm{par}} \ln N_{t_j}.
\end{aligned} \tag{B.36}$$

The AIC, AICc, and BIC weights are given by:

$$
\begin{aligned}
W_{t_j}^{\mathrm{AIC}}(m,n) &= \frac{\exp\left(-\frac{1}{2}\Delta\mathrm{AIC}_{t_j}(m,n)\right)}{\sum\limits_{\substack{i_1,i_2=0\\ i_1+i_2\leq 4}}^{4}\exp\left(-\frac{1}{2}\Delta\mathrm{AIC}_{t_j}(i_1,i_2)\right)},\\
W_{t_j}^{\mathrm{AICc}}(m,n) &= \frac{\exp\left(-\frac{1}{2}\Delta\mathrm{AICc}_{t_j}(m,n)\right)}{\sum\limits_{\substack{i_1,i_2=0\\ i_1+i_2\leq 4}}^{4}\exp\left(-\frac{1}{2}\Delta\mathrm{AICc}_{t_j}(i_1,i_2)\right)},\\
W_{t_j}^{\mathrm{BIC}}(m,n) &= \frac{\exp\left(-\frac{1}{2}\Delta\mathrm{BIC}_{t_j}(m,n)\right)}{\sum\limits_{\substack{i_1,i_2=0\\ i_1+i_2\leq 4}}^{4}\exp\left(-\frac{1}{2}\Delta\mathrm{BIC}_{t_j}(i_1,i_2)\right)}.
\end{aligned}
\tag{B.37}
$$

♣

Appendix C

Supplementary graphs for Chapter 2

C.1 S&P 100 index and the OEX ATM impled volatility

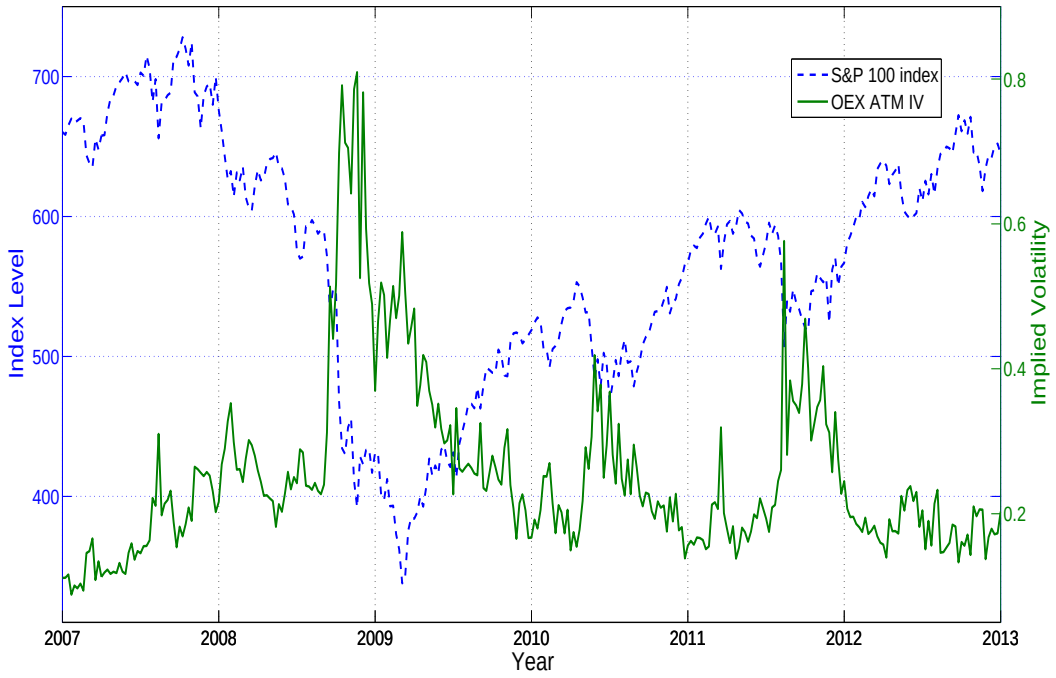

Figure C.1: **S&P 100 index and the OEX ATM impled volatility.** Joint plot of the weekly S&P 100 closing index level (dashed blue line, scale given on the left y-axis) and the corresponding weekly average ATM implied volatility on S&P 100 obtained from the closing option prices on the chosen observation dates (solid green line, scale given on the right y-axis).

C.2 Number of OEX call and put contracts per day

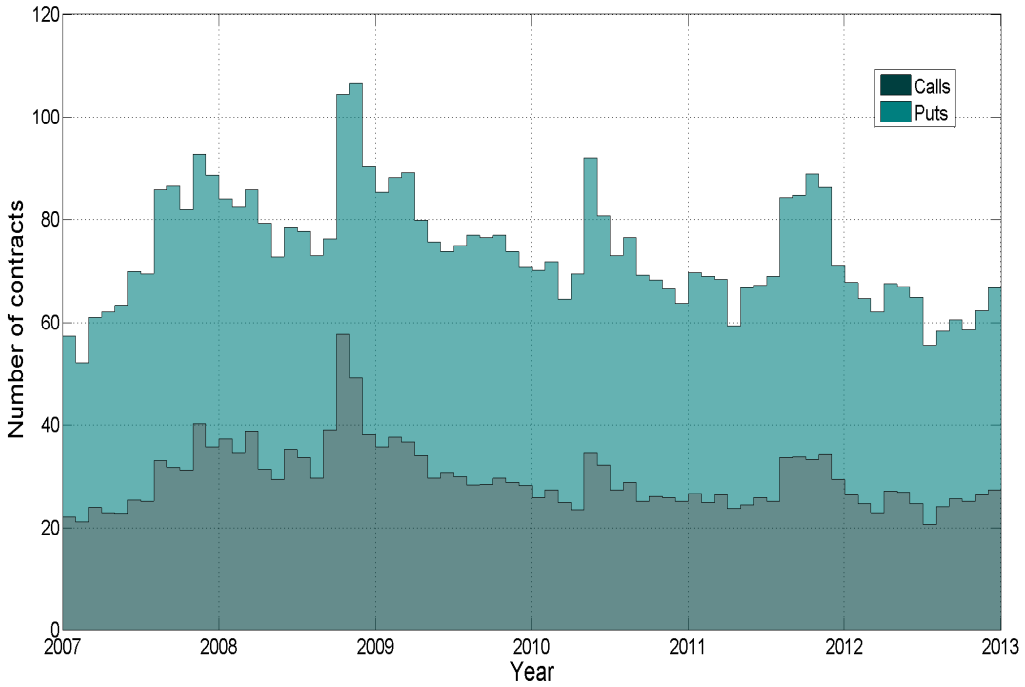

Figure C.2: **Number of OEX call and put contracts per day.** The average number of OEX (American) call and put options per day is computed based on the number of traded contracts within a given calendar month.

C.3 OEX liquidity metrics

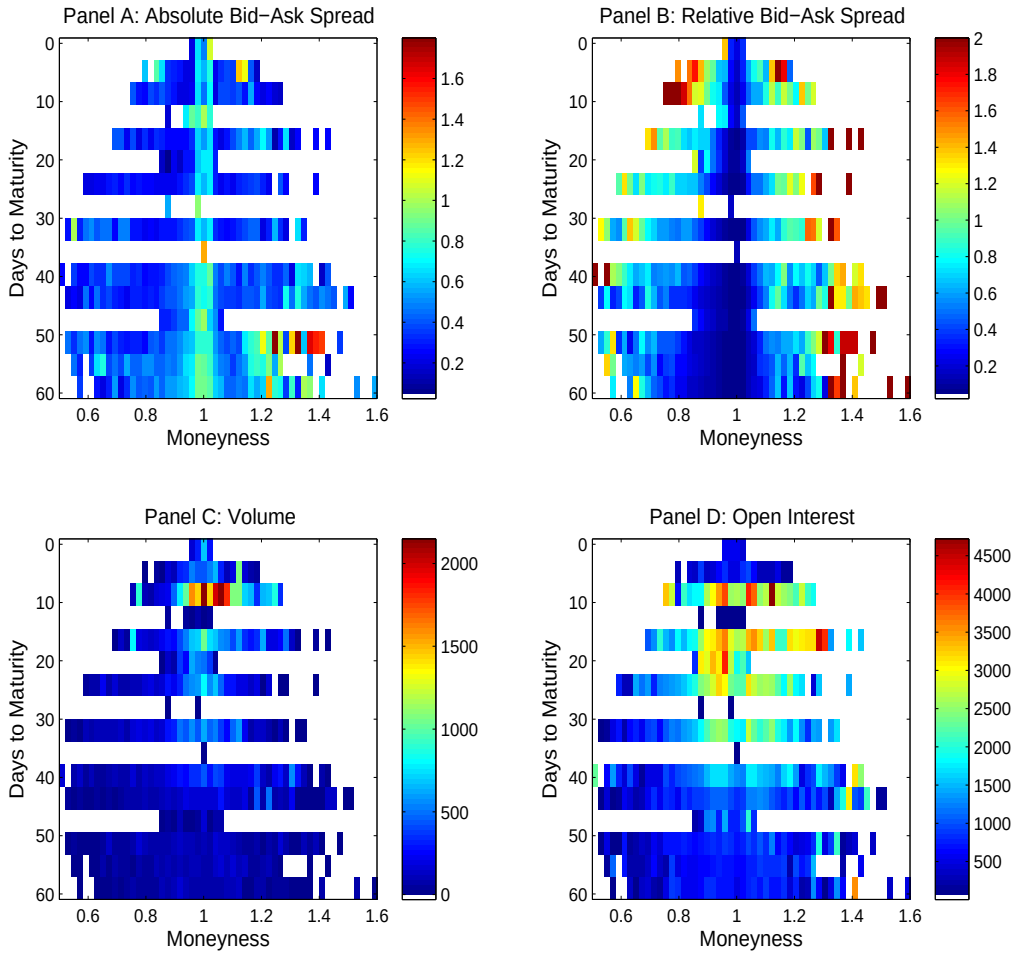

Figure C.3: **OEX liquidity metrics.** The plots summarize four liquidity metrics across moneyness and time to maturity (in days) for the S&P 100 index options data with maturity of up to 2 months in the period from January 3, 2007 until December 31, 2012. In total, there are 16 different observed maturities: 1, 2, 3, 9, 10, 16, 17, 23, 24, 30, 31, 38, 44, 45, 52 and 59 days. The moneyness ($m_t := K/F_t$) is between 0.51 and 1.59. The full moneyness range is divided into 54 segments of width equal to 0.02. In each panel, the average value for a given liquidity metric is computed for all available moneyness–maturity buckets. Panels A and B represent the absolute and the relative bid–ask spreads, respectively. Dark blue (red) values corresponds to tighter (wider) absolute and relative bid–ask spreads, hence more (less) liquid OEX contracts. Panels C and D represent the volume and the open interest, respectively. Dark blue (red) values represent lower (higher) volume and open interest, hence less (more) liquid OEX contracts.

C.4 Pricing errors for the HEJD$(1, 2)$ model

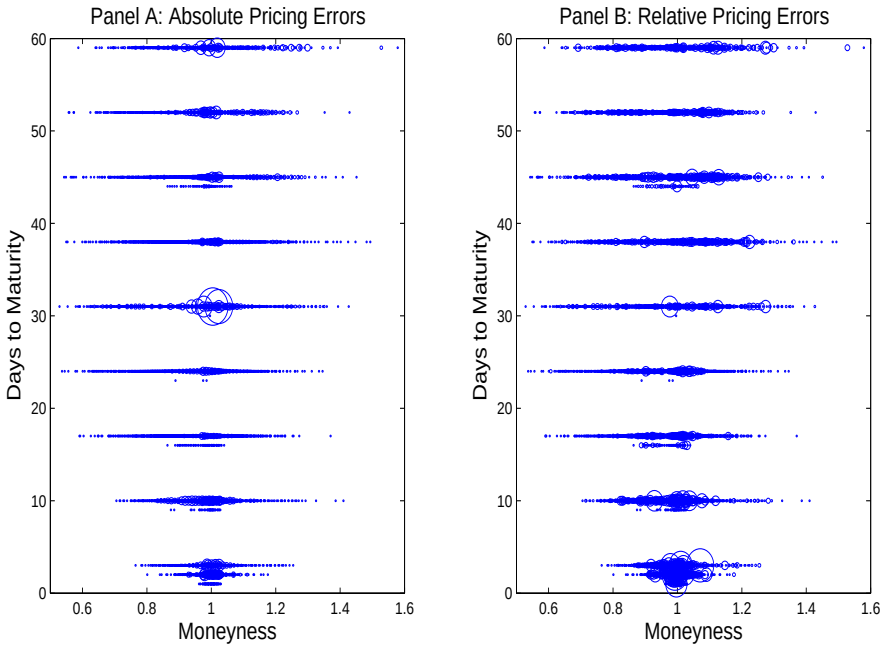

Figure C.4: **Pricing errors for the HEJD$(1, 2)$ model.** The pricing errors for the HEJD$(1, 2)$ model applied to the S&P 100 index options data with maturity of up to 2 months in the period from January 3, 2007 until December 31, 2012. Pricing errors are presented for all moneyness–maturity combinations corresponding to the observations in the dataset. Panel A represents the absolute (dollar) pricing errors, and the Panel B represents the relative (percentage) pricing errors, i.e., absolute pricing errors are scaled by the corresponding bid-ask spreads.

C.5 Calibrated risk-neutral density for the HEJD$(1,2)$ model

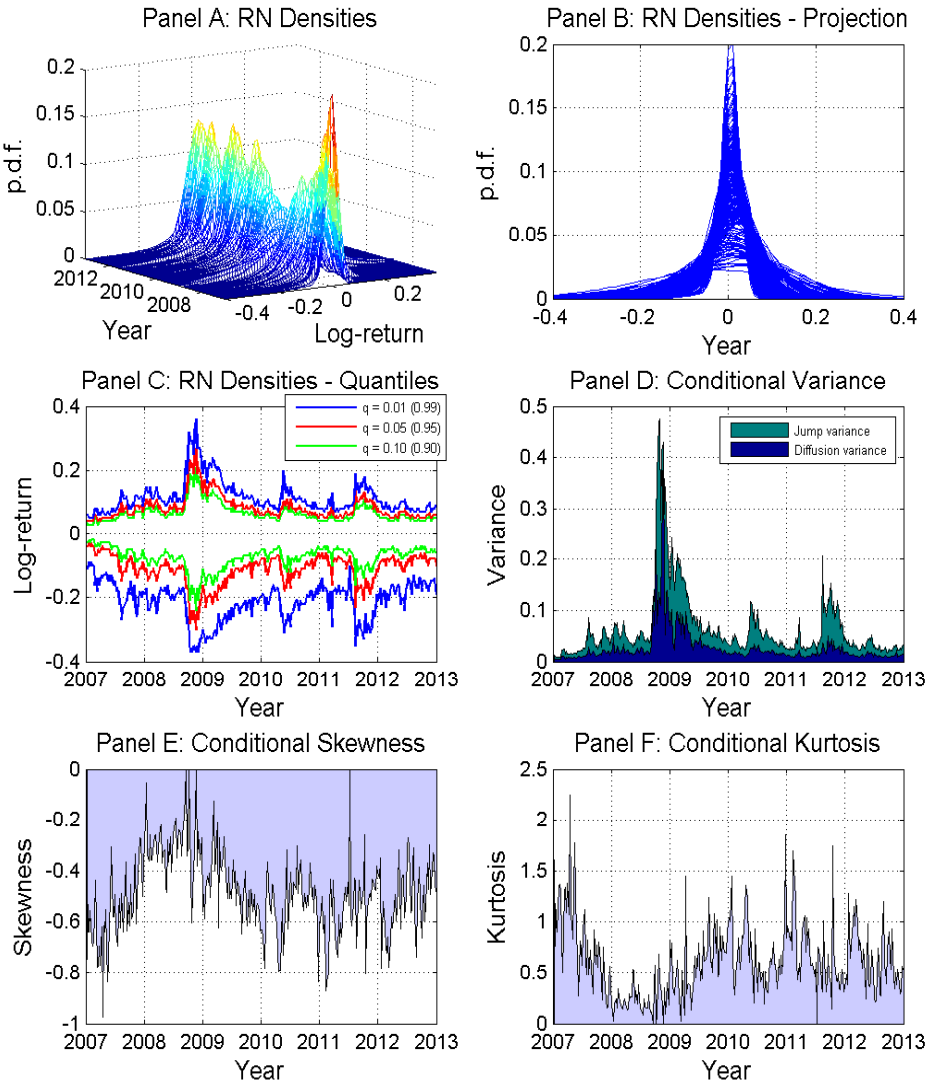

Figure C.5: **Calibrated risk-neutral density for the HEJD$(1,2)$ model.** The evolution of the risk-neutral (RN) density and the main statistics for the HEJD(1,2) model over horizon of 1 month (i.e., the average option maturity in the sample). Panels A and B depict the the dynamics of the RN density and its pooled projections, respectively. In Panel C we represent 1 and 99-percentiles (blue line), 5 and 95 percentiles (red line), and 10 and 90 (green line). Panel D gives the decomposition of the conditional variance into diffusion and jump part. Panels E and F present conditional skewness and excess kurtosis over the given time horizon, respectively.

C.6 OEX implied volatility

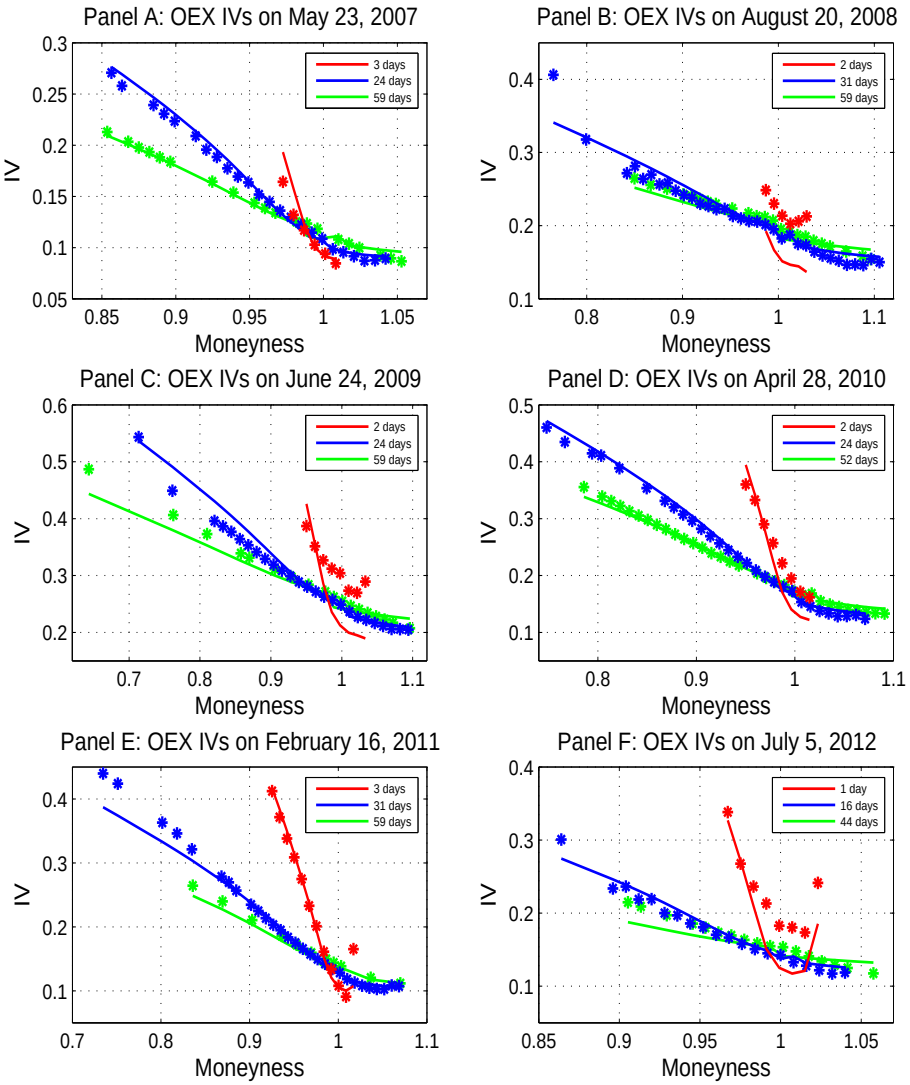

Figure C.6: **OEX implied volatility.** The implied volatility skews and smirks of short-maturity American options on S&P 100 index for arbitrarily selected six dates (as a function of moneyness $m_t := K/F_t$). Each panel features market and model implied volatilities for three different maturities ranging from 1 day to 59 days. The market implied volatilities are represented by asterisk-style markers, whereas the HEJD(1,2) model implied volatilities are depicted by solid lines. The shortest maturity options are represented in red color, mid-maturity options are given in blue, and the longest maturity is indicated in green.

Appendix D

Proofs of results in Chapter 3

D.1 Proof of Theorem 3.5.1: Québécoised EPUOP option

Step 1: DLCT. We start by introducing the change of variables, i.e., instead of the standard time t_s and the hybrid excursion time t_e we define $\tau_s := T - D - t_s$ and $\tau_e := D - t_e$, respectively. The PIDE system (3.30) becomes

$$\begin{cases} -\dfrac{\partial \tilde{\pi}^e_{uo}}{\partial \tau_e}(x,\tau_e) + \mathcal{L}\tilde{\pi}^e_{uo}(x,\tau_e) = r\tilde{\pi}^e_{uo}(x,\tau_e), & \text{if } (x,t_s,t_e) \in \tilde{\mathscr{E}}, \\ -\dfrac{\partial \tilde{\pi}^s_{uo}}{\partial \tau_s}(x,\tau_s) + \mathcal{L}\tilde{\pi}^s_{uo}(x,\tau_s) = r\tilde{\pi}^s_{uo}(x,\tau_s), & \text{if } (x,t_s,t_e) \in \tilde{\mathscr{S}}. \end{cases} \tag{D.1}$$

The notation in the equations (3.32)–(3.33) is adjusted accordingly. Applying the DLCT to our PIDE system results in two coupled OIDEs. The OIDE describing the dynamics of the québécoised EPUOP in the standard domain $\tilde{\mathscr{S}}$ is

$$\begin{aligned} \frac{\sigma^2}{2}\frac{d^2\hat{\tilde{\pi}}^s_{uo}}{dx^2}(x,\alpha^s_{k_s}) + \mu\frac{d\hat{\tilde{\pi}}^s_{uo}}{dx}(x,\alpha^s_{k_s}) - (r+\alpha^s_{k_s}+\lambda)\hat{\tilde{\pi}}^s_{uo}(x,\alpha^s_{k_s}) \\ + \alpha^s_{k_s}\hat{p}(x,\alpha^e_{k_e};\kappa,D) + \lambda\int_{-\infty}^{+\infty}\hat{\tilde{\pi}}_{uo}(x+y,\alpha^s_{k_s},\alpha^e_{k_e})\varphi_Y(y)dy = 0, \end{aligned} \tag{D.2}$$

and in the excursion region $\tilde{\mathscr{E}}$ we have

$$\begin{aligned} \frac{\sigma^2}{2}\frac{d^2\hat{\tilde{\pi}}^e_{uo}}{dx^2}(x,\alpha^e_{k_e}) + \mu\frac{d\hat{\tilde{\pi}}^e_{uo}}{dx}(x,\alpha^e_{k_e}) - (r+\alpha^e_{k_e}+\lambda)\hat{\tilde{\pi}}^e_{uo}(x,\alpha^e_{k_e}) \\ + \lambda\int_{-\infty}^{+\infty}\hat{\tilde{\pi}}_{uo}(x+y,\alpha^s_{k_s},\alpha^e_{k_e})\varphi_Y(y)dy = 0. \end{aligned} \tag{D.3}$$

The québécoised initial conditions in the standard and excursion domains are absorbed in the system of OIDEs. The québécoised boundary condition in the standard domain is

$$\lim_{x\downarrow-\infty}\hat{\tilde{\pi}}^s_{uo}(x,\alpha^s_{k_s}) = \frac{\alpha^s_{k_s}}{\alpha^s_{k_s}+r}\lim_{x\downarrow-\infty}\hat{p}(x,\alpha^e_{k_e};\kappa,D) = \frac{\alpha^s_{k_s}}{\alpha^s_{k_s}+r}\frac{\alpha^e_{k_e}}{\alpha^s_{k_e}+r}e^{\kappa}, \tag{D.4}$$

and the québécoised boundary condition in the excursion domain is given by

$$\lim_{x\uparrow+\infty} \hat{\tilde{\pi}}^e_{uo}(x, \alpha^e_{k_e}) = 0. \tag{D.5}$$

The transformed value-matching and smooth-pasting conditions at the boundary between the corridor and the payoff subdomains—which can be obtained from the third and the fourth equation in (3.32)—are

$$\begin{aligned} \lim_{x\uparrow\kappa} \hat{\tilde{\pi}}^s_{uo}(x, \alpha^s_{k_s}) &= \lim_{x\downarrow\kappa} \hat{\tilde{\pi}}^s_{uo}(x, \alpha^s_{k_s}), \\ \lim_{x\uparrow\kappa} \frac{d\hat{\tilde{\pi}}^s_{uo}}{dx}(x, \alpha^s_{k_s}) &= \lim_{x\downarrow\kappa} \frac{d\hat{\tilde{\pi}}^s_{uo}}{dx}(x, \alpha^s_{k_s}). \end{aligned} \tag{D.6}$$

Finally, the québécoisation procedure transforms the high-contact conditions at the boundary between the standard and excursion domains to

$$\begin{aligned} \lim_{x\uparrow h} \hat{\tilde{\pi}}^s_{uo}(x, \alpha^s_{k_s}) &= \lim_{x\downarrow h} \hat{\tilde{\pi}}^e_{uo}(x, \alpha^e_{k_e}), \\ \lim_{x\uparrow h} \frac{d\hat{\tilde{\pi}}^s_{uo}}{dx}(x, \alpha^s_{k_s}) &= \lim_{x\downarrow h} \frac{d\hat{\tilde{\pi}}^e_{uo}}{dx}(x, \alpha^e_{k_e}). \end{aligned} \tag{D.7}$$

To solve the system of two-dimensional OIDEs (D.2)–(D.3) we study the problem separately in each domain. Subsequently, we add the boundary and terminal conditions (D.4)–(D.7).

Step 2: Excursion domain OIDE. Let's assume that the québécoised option price in the excursion domain takes the form (3.51). The two derivative terms in the OIDE (D.3) are

$$\begin{aligned} \frac{d\hat{\tilde{\pi}}^e_{uo}}{dx}(x, \alpha^e_{k_e}) &= \sum_{j=1}^{n+1} A^-_j \gamma_{j,r+\alpha^e_{k_e}} e^{\gamma_{j,r+\alpha^e_{k_e}}(x-h)}, \\ \frac{d^2\hat{\tilde{\pi}}^e_{uo}}{dx^2}(x, \alpha^e_{k_e}) &= \sum_{j=1}^{n+1} A^-_j \gamma^2_{j,r+\alpha^e_{k_e}} e^{\gamma_{j,r+\alpha^e_{k_e}}(x-h)}. \end{aligned} \tag{D.8}$$

We denote the integral term in (D.3) by $\mathscr{I}(\tilde{\mathscr{E}}) := \int_{-\infty}^{+\infty} \hat{\tilde{\pi}}_{uo}(x+y, \alpha^s_{k_s}, \alpha^e_{k_e})\varphi_Y(y)dy$, and obtain the following decomposition:

$$\mathscr{I}(\tilde{\mathscr{E}}) = \mathscr{I}(\tilde{\mathscr{E}}\big|\tilde{\mathscr{E}}^+) + \mathscr{I}(\tilde{\mathscr{E}}\big|\tilde{\mathscr{E}}^-) + \mathscr{I}(\tilde{\mathscr{E}}\big|\tilde{\mathscr{S}}_c) + \mathscr{I}(\tilde{\mathscr{E}}\big|\tilde{\mathscr{S}}_p). \tag{D.9}$$

The term $\mathscr{I}(\tilde{\mathscr{E}}\big|\tilde{\mathscr{E}}^+)$ describes the positive jumps within the excursion domain, and is given by

$$\mathscr{I}(\tilde{\mathscr{E}}\big|\tilde{\mathscr{E}}^+) = \int_0^{+\infty} \sum_{k=1}^{m} p_k \eta_k e^{-\eta_k y} \sum_{j=1}^{n+1} A^-_j e^{\gamma_{j,r+\alpha^e_{k_e}}(x+y-h)} dy, \tag{D.10}$$

whereas the term $\mathscr{I}(\tilde{\mathscr{E}}\big|\tilde{\mathscr{E}}^{-})$ describes the negative jumps within the excursion domain, and it takes the form

$$\mathscr{I}(\tilde{\mathscr{E}}\big|\tilde{\mathscr{E}}^{-}) = \int_{h-x}^{0} \sum_{l=1}^{n} q_l \theta_l e^{\theta_l y} \sum_{j=1}^{n+1} A_j^{-} e^{\gamma_{j,r+\alpha_{k_e}^e}(x+y-h)} dy. \tag{D.11}$$

The (negative) jumps from the excursion domain to the corridor domain are captured by the term

$$\begin{aligned}\mathscr{I}(\tilde{\mathscr{E}}\big|\tilde{\mathscr{S}}_c) = &\int_{\kappa-x}^{h-x} \sum_{l=1}^{n} q_l \theta_l e^{\theta_l y} \left(\sum_{i=1}^{m+1} B_i^{+} e^{\beta_{i,r+\alpha_{k_s}^s}(x+y-h)} + \sum_{j=1}^{n+1} B_j^{-} e^{\gamma_{j,r+\alpha_{k_s}^s}(x+y-h)} \right) dy \\ &+ \int_{\kappa-x}^{h-x} \sum_{l=1}^{n} q_l \theta_l e^{\theta_l y} \sum_{j=1}^{n+1} \overline{\omega}_j' e^{\gamma_{j,r+\alpha_{k_e}^e}(x+y-\kappa)} dy.\end{aligned} \tag{D.12}$$

The remaining term quantifies the effect of the (negative) jumps from the excursion domain to the payoff domain, i.e.,

$$\begin{aligned}\mathscr{I}(\tilde{\mathscr{E}}\big|\tilde{\mathscr{S}}_p) = &\int_{-\infty}^{\kappa-x} \sum_{l=1}^{n} q_l \theta_l e^{\theta_l y} \sum_{i=1}^{m+1} \underline{\omega}_i' e^{\beta_{i,r+\alpha_{k_e}^e}(x+y-\kappa)} dy + \int_{-\infty}^{\kappa-x} \sum_{l=1}^{n} q_l \theta_l e^{\theta_l y} \sum_{i=1}^{m+1} C_i^{+} e^{\beta_{i,r+\alpha_{k_s}^s}(x+y-\kappa)} dy \\ &+ \int_{-\infty}^{\kappa-x} \sum_{l=1}^{n} q_l \theta_l e^{\theta_l y} \left(\frac{\alpha_{k_s}^s}{\alpha_{k_s}^s + r} \frac{\alpha_{k_e}^e}{\alpha_{k_e}^e + r} e^{\kappa} - \frac{\alpha_{k_s}^s}{\alpha_{k_s}^s + \delta} \frac{\alpha_{k_e}^e}{\alpha_{k_e}^e + \delta} e^{x+y} \right) dy.\end{aligned} \tag{D.13}$$

After some algebra, the equation (D.3) can be transformed into

$$\sum_{j=1}^{n+1} A_j^{-} e^{\gamma_{j,r+\alpha_{k_e}^e}(x-h)} \left(\Psi(\gamma_{j,r+\alpha_{k_e}^e}) - (\alpha_{k_e}^e + r) \right) + \sum_{l=1}^{n} \lambda q_l \theta_l e^{\theta_l (h-x)} \Phi_l(\tilde{\mathscr{E}}) = 0, \tag{D.14}$$

where $\Phi_l(\tilde{\mathscr{E}})$ $(l = 1, 2, ..., n)$ is given by

$$\begin{aligned}\Phi_l(\tilde{\mathscr{E}}) := &\sum_{j=1}^{n+1} \frac{A_j^{-}}{\theta_l + \gamma_{j,r+\alpha_{k_e}^e}} - \sum_{i=1}^{m+1} \frac{B_i^{-} \left(1 - e^{(\theta_l + \beta_{i,r+\alpha_{k_s}^s})(\kappa-h)} \right)}{\theta_l + \beta_{i,r+\alpha_{k_s}^s}} \\ &- \sum_{j=1}^{n+1} \frac{B_j^{-} \left(1 - e^{(\theta_l + \gamma_{j,r+\alpha_{k_s}^s})(\kappa-h)} \right)}{\theta_l + \gamma_{j,r+\alpha_{k_s}^s}} - \sum_{i=1}^{m+1} \frac{C_i^{+} e^{\theta_l(\kappa-h)}}{\theta_l + \beta_{i,r+\alpha_{k_s}^s}} \\ &- \sum_{i=1}^{m+1} \frac{\underline{\omega}_i' e^{\theta_l(\kappa-h)}}{\theta_l + \beta_{i,r+\alpha_{k_e}^e}} - \sum_{j=1}^{n+1} \frac{\overline{\omega}_j' \left(e^{\gamma_{j,r+\alpha_{k_e}^e}(h-\kappa)} - e^{\theta_l(\kappa-h)} \right)}{\theta_l + \gamma_{j,r+\alpha_{k_e}^e}} \\ &- e^{\theta_l(\kappa-h)} \left(\frac{e^{\kappa}}{\theta_l} \frac{\alpha_{k_s}^s}{\alpha_{k_s}^s + r} \frac{\alpha_{k_e}^e}{\alpha_{k_e}^e + r} - \frac{e^{\kappa}}{\theta_l + 1} \frac{\alpha_{k_s}^s}{\alpha_{k_s}^s + \delta} \frac{\alpha_{k_e}^e}{\alpha_{k_e}^e + \delta} \right).\end{aligned} \tag{D.15}$$

The first term on the l.h.s. of the equation (D.14) is equal to zero (by construction of the HEM Lévy exponent). For strictly positive jump intensity λ, the second term yields the set of conditions

$$\Phi_l(\tilde{\mathscr{E}}) = 0, \quad \text{for} \quad l = 1, 2, ..., n. \tag{D.16}$$

Step 3: Corridor domain OIDE. Assuming the québécoised option price in the form (3.52), the two derivative terms in the OIDE (D.2) are

$$\begin{aligned}\frac{d\hat{\tilde{\pi}}^s_{uo}}{dx}(x,\alpha^s_{k_s}) &= \sum_{i=1}^{m+1}\beta_{i,r+\alpha^s_{k_s}}B_i^+ e^{\beta_{i,r+\alpha^s_{k_s}}(x-h)} + \sum_{j=1}^{n+1}\gamma_{j,r+\alpha^s_{k_s}}B_j^- e^{\gamma_{j,r+\alpha^s_{k_s}}(x-h)} \\ &\quad + \sum_{j=1}^{n+1}\gamma_{j,r+\alpha^e_{k_e}}\overline{\omega}'_j e^{\gamma_{j,r+\alpha^e_{k_e}}(x-\kappa)}, \\ \frac{d^2\hat{\tilde{\pi}}^s_{uo}}{dx^2}(x,\alpha^s_{k_s}) &= \sum_{i=1}^{m+1}\beta^2_{i,r+\alpha^s_{k_s}}B_i^+ e^{\beta_{i,r+\alpha^s_{k_s}}(x-h)} + \sum_{j=1}^{n+1}\gamma^2_{j,r+\alpha^s_{k_s}}B_j^- e^{\gamma_{j,r+\alpha^s_{k_s}}(x-h)} \\ &\quad + \sum_{j=1}^{n+1}\gamma^2_{j,r+\alpha^e_{k_e}}\overline{\omega}'_j e^{\gamma_{j,r+\alpha^e_{k_e}}(x-\kappa)}.\end{aligned} \tag{D.17}$$

The integral term in the equation (D.2), defined as $\mathscr{I}(\tilde{\mathscr{S}_c}) := \int_{-\infty}^{+\infty}\hat{\tilde{\pi}}_{uo}(x+y,\alpha^s_{k_s},\alpha^e_{k_e})\varphi_Y(y)dy$ can be decomposed as

$$\mathscr{I}(\tilde{\mathscr{S}_c}) = \mathscr{I}(\tilde{\mathscr{S}_c}\big|\tilde{\mathscr{E}}) + \mathscr{I}(\tilde{\mathscr{S}_c}\big|\tilde{\mathscr{S}_c^+}) + \mathscr{I}(\tilde{\mathscr{S}_c}\big|\tilde{\mathscr{S}_c^-}) + \mathscr{I}(\tilde{\mathscr{S}_c}\big|\tilde{\mathscr{S}_p}). \tag{D.18}$$

The first term on the r.h.s. of equation (D.18) describes the effect of the (positive) jumps from the corridor region to the excursion domain:

$$\mathscr{I}(\tilde{\mathscr{S}_c}\big|\tilde{\mathscr{E}}) = \int_{h-x}^{+\infty}\sum_{k=1}^{m}p_k\eta_k e^{-\eta_k y}\sum_{j=1}^{n+1}A_j^- e^{\gamma_{j,r+\alpha^e_{k_e}}(x+y-h)}dy. \tag{D.19}$$

The second and the third term on the r.h.s. of equation (D.18) capture the positive and negative jumps within the corridor domain, respectively, and they are given as follows

$$\begin{aligned}\mathscr{I}(\tilde{\mathscr{S}_c}\big|\tilde{\mathscr{S}_c^+}) &= \int_0^{h-x}\sum_{k=1}^{m}p_k\eta_k e^{-\eta_k y}\left(\sum_{i=1}^{m+1}B_i^+ e^{\beta_{i,r+\alpha^s_{k_s}}(x+y-h)} + \sum_{j=1}^{n+1}B_j^- e^{\gamma_{j,r+\alpha^s_{k_s}}(x+y-h)}\right)dy \\ &\quad + \int_0^{h-x}\sum_{k=1}^{m}p_k\eta_k e^{-\eta_k y}\sum_{j=1}^{n+1}\overline{\omega}'_j e^{\gamma_{j,r+\alpha^e_{k_e}}(x+y-\kappa)}dy,\end{aligned} \tag{D.20}$$

and

$$\begin{aligned}\mathscr{I}(\tilde{\mathscr{S}_c}\big|\tilde{\mathscr{S}_c^-}) &= \int_{\kappa-x}^{0}\sum_{l=1}^{n}q_l\theta_l e^{\theta_l y}\left(\sum_{i=1}^{m+1}B_i^+ e^{\beta_{i,r+\alpha^s_{k_s}}(x+y-h)} + \sum_{j=1}^{n+1}B_j^- e^{\gamma_{j,r+\alpha^s_{k_s}}(x+y-h)}\right)dy \\ &\quad + \int_{\kappa-x}^{0}\sum_{l=1}^{n}q_l\theta_l e^{\theta_l y}\sum_{j=1}^{n+1}\overline{\omega}'_j e^{\gamma_{j,r+\alpha^e_{k_e}}(x+y-\kappa)}dy.\end{aligned} \tag{D.21}$$

Finally, the last term on the r.h.s. of equation (D.18) captures the (negative) jumps from the corridor region to the payoff region is denoted by $\mathscr{I}(\tilde{\mathscr{S}_c}|\tilde{\mathscr{S}_p})$, and it can be computed as

$$\begin{aligned}\mathscr{I}(\tilde{\mathscr{S}_c}\big|\tilde{\mathscr{S}_p}) = &\int_{-\infty}^{\kappa-x}\sum_{l=1}^{n} q_l\theta_l e^{\theta_l y}\sum_{i=1}^{m+1} C_i^+ e^{\beta_{i,r+\alpha_{k_s}^s}(x+y-\kappa)}dy + \int_{-\infty}^{\kappa-x}\sum_{l=1}^{n} q_l\theta_l e^{\theta_l y}\sum_{i=1}^{m+1}\underline{\omega}_i' e^{\beta_{i,r+\alpha_{k_e}^e}(x+y-\kappa)}dy\\ &+\int_{-\infty}^{\kappa-x}\sum_{l=1}^{n} q_l\theta_l e^{\theta_l y}\left(\frac{\alpha_{k_s}^s}{\alpha_{k_s}^s+r}\frac{\alpha_{k_e}^e}{\alpha_{k_e}^e+r}e^{\kappa} - \frac{\alpha_{k_s}^s}{\alpha_{k_s}^s+\delta}\frac{\alpha_{k_e}^e}{\alpha_{k_e}^e+\delta}e^{x+y}\right)dy.\end{aligned} \tag{D.22}$$

By plugging the results for the two derivative terms and the jump integral back to (D.2), we obtain the equation

$$\begin{aligned}&\sum_{i=1}^{m+1} B_i^+ e^{\beta_{i,r+\alpha_{k_s}^s}(x-h)}\Big(\Psi(\beta_{i,r+\alpha_{k_s}^s}) - (\alpha_{k_s}^s+r)\Big)\\ &+\sum_{j=1}^{n+1} B_j^- e^{\gamma_{j,r+\alpha_{k_s}^s}(x-h)}\Big(\Psi(\gamma_{j,r+\alpha_{k_s}^s}) - (\alpha_{k_s}^s+r)\Big)\\ &+\sum_{j=1}^{n+1}\overline{\omega}_j' e^{\gamma_{j,r+\alpha_{k_e}^e}(x-\kappa)}\Big(\Psi(\gamma_{j,r+\alpha_{k_e}^e}) - (\alpha_{k_e}^e+r)\Big)\\ &+\sum_{j=1}^{n+1} e^{\gamma_{j,r+\alpha_{k_e}^e}(x-\kappa)}\left(\alpha_{k_s}^s\overline{\omega}_j - (\alpha_{k_s}^s-\alpha_{k_e}^e)\overline{\omega}_j'\right)\\ &+\sum_{k=1}^{m}\lambda p_k\eta_k e^{\eta_k(x-h)}\Xi_k(\tilde{\mathscr{S}_c}) + \sum_{l=1}^{n}\lambda q_l\theta_l e^{\theta_l(\kappa-x)}\Phi_l(\tilde{\mathscr{S}_c}) = 0,\end{aligned} \tag{D.23}$$

where for all $k = 1, 2, ..., m$:

$$\Xi_k(\tilde{\mathscr{S}_c}) := \sum_{j=1}^{n+1}\frac{A_j^-}{\eta_k - \gamma_{j,r+\alpha_{k_e}^e}} - \sum_{i=1}^{m+1}\frac{B_i^+}{\eta_k - \beta_{i,r+\alpha_{k_s}^s}} - \sum_{j=1}^{n+1}\frac{B_j^-}{\eta_k - \gamma_{j,r+\alpha_{k_s}^s}} - \sum_{j=1}^{n+1}\frac{\overline{\omega}_j' e^{\gamma_{j,r+\alpha_{k_e}^e}(h-\kappa)}}{\eta_k - \gamma_{j,r+\alpha_{k_e}^e}}, \tag{D.24}$$

and for $l = 1, 2, ..., n$:

$$\begin{aligned}\Phi_l(\tilde{\mathscr{S}_c}) := &\sum_{i=1}^{m+1}\frac{B_i^+ e^{\beta_{i,r+\alpha_{k_s}^s}(\kappa-h)}}{\theta_l + \beta_{i,r+\alpha_{k_s}^s}} + \sum_{j=1}^{n+1}\frac{B_j^- e^{\gamma_{j,r+\alpha_{k_s}^s}(\kappa-h)}}{\theta_l + \gamma_{j,r+\alpha_{k_s}^s}} - \sum_{i=1}^{m+1}\frac{C_i^+}{\theta_l + \beta_{i,r+\alpha_{k_s}^s}}\\ &-\left(\sum_{i=1}^{m+1}\frac{\underline{\omega}_i'}{\theta_l + \beta_{i,r+\alpha_{k_e}^e}} - \sum_{j=1}^{n+1}\frac{\overline{\omega}_j'}{\theta_l + \gamma_{j,r+\alpha_{k_e}^e}}\right) - \left(\frac{e^{\kappa}}{\theta_l}\frac{\alpha_{k_s}^s}{\alpha_{k_s}^s+r}\frac{\alpha_{k_e}^e}{\alpha_{k_e}^e+r} - \frac{e^{\kappa}}{\theta_l+1}\frac{\alpha_{k_s}^s}{\alpha_{k_s}^s+\delta}\frac{\alpha_{k_e}^e}{\alpha_{k_e}^e+\delta}\right).\end{aligned} \tag{D.25}$$

Equation (D.23) is satisfied if the following conditions hold:

$$\begin{cases}\Xi_k(\tilde{\mathscr{S}_c}) = 0, & \text{for } k = 1, 2, ..., m,\\ \Phi_l(\tilde{\mathscr{S}_c}) = 0, & \text{for } l = 1, 2, ..., n,\end{cases} \tag{D.26}$$

and also if it holds that

$$\overline{\omega}'_j = \frac{\alpha^s_{k_s}\overline{\omega}_j}{\alpha^s_{k_s} - \alpha^e_{k_e}}, \quad \text{for} \quad j = 1, ..., n. \tag{D.27}$$

It is important to stress out that this expression imposes a restriction on the Parisian window D, i.e., $D \neq k_e T/(k_s + k_e)$, where $k_s, k_e \in \mathbb{N}$.[73]

Step 4: Payoff domain OIDE. Using the ansatz (3.53) we first compute the derivative terms

$$\begin{aligned}
\frac{d\hat{\tilde{\pi}}^s_{uo}}{dx}(x, \alpha^s_{k_s}) &= \sum_{i=1}^{m+1} \beta_{i,r+\alpha^s_{k_s}} C^+_i e^{\beta_{i,r+\alpha^s_{k_s}}(x-\kappa)} \\
&\quad + \sum_{i=1}^{m+1} \beta_{i,r+\alpha^e_{k_e}} \underline{\omega}'_i e^{\beta_{i,r+\alpha^e_{k_e}}(x-\kappa)} - \frac{\alpha^s_{k_s}}{\alpha^s_{k_s}+\delta}\frac{\alpha^e_{k_e}}{\alpha^e_{k_e}+\delta} e^x, \\
\frac{d^2\hat{\tilde{\pi}}^s_{uo}}{dx^2}(x, \alpha^s_{k_s}) &= \sum_{i=1}^{m+1} \beta^2_{i,r+\alpha^s_{k_s}} C^+_i e^{\beta_{i,r+\alpha^s_{k_s}}(x-\kappa)} \\
&\quad + \sum_{i=1}^{m+1} \beta^2_{i,r+\alpha^e_{k_e}} \underline{\omega}'_i e^{\beta_{i,r+\alpha^e_{k_e}}(x-\kappa)} - \frac{\alpha^s_{k_s}}{\alpha^s_{k_s}+\delta}\frac{\alpha^e_{k_e}}{\alpha^e_{k_e}+\delta} e^x.
\end{aligned} \tag{D.28}$$

The integral term in the standard payoff domain $\mathscr{I}(\tilde{\mathscr{S}}_p) := \int_{-\infty}^{+\infty} \hat{\tilde{\pi}}_{uo}(x+y, \alpha^s_{k_s}, \alpha^e_{k_e})\varphi_Y(y)dy$ can be decomposed as

$$\mathscr{I}(\tilde{\mathscr{S}}_p) = \mathscr{I}(\tilde{\mathscr{S}}_p|\tilde{\mathscr{E}}) + \mathscr{I}(\tilde{\mathscr{S}}_p|\tilde{\mathscr{S}}_c) + \mathscr{I}(\tilde{\mathscr{S}}_p|\tilde{\mathscr{S}}^+_p) + \mathscr{I}(\tilde{\mathscr{S}}_p|\tilde{\mathscr{S}}^-_p). \tag{D.29}$$

The first term on the r.h.s. of equation (D.29) describes the effect of the (positive) jumps from the payoff region to the excursion region:

$$\mathscr{I}(\tilde{\mathscr{S}}_p|\tilde{\mathscr{E}}) = \int_{h-x}^{+\infty} \sum_{k=1}^{m} p_k \eta_k e^{-\eta_k y} \sum_{j=1}^{n+1} A^-_j e^{\gamma_{j,r+\alpha^e_{k_e}}(x+y-h)} dy. \tag{D.30}$$

The effect of the (positive) jumps from the payoff region to the corridor region is captured by the second term on the r.h.s. of equation (D.29):

$$\begin{aligned}
\mathscr{I}(\tilde{\mathscr{S}}_p|\tilde{\mathscr{S}}_c) &= \int_{\kappa-x}^{h-x} \sum_{k=1}^{m} p_k \eta_k e^{-\eta_k y} \left(\sum_{i=1}^{m+1} B^+_i e^{\beta_{i,r+\alpha^s_{k_s}}(x+y-h)} + \sum_{j=1}^{n+1} B^-_j e^{\gamma_{j,r+\alpha^s_{k_s}}(x+y-h)} \right) dy \\
&\quad + \int_{\kappa-x}^{h-x} \sum_{k=1}^{m} p_k \eta_k e^{-\eta_k y} \sum_{j=1}^{n+1} \overline{\omega}'_j e^{\gamma_{j,r+\alpha^e_{k_e}}(x+y-\kappa)} dy.
\end{aligned} \tag{D.31}$$

[73] The expressions for $\underline{\omega}_i$ $(i = 1, 2, \ldots, m)$ and $\overline{\omega}_j$ $(j = 1, 2, \ldots, n)$ can be computed using the results in Leippold and Vasiljević (2017), equation (36), pp. 91–92.

Finally, the last two terms on the r.h.s. in equation (D.29) are related to the positive and negative jumps within the payoff domain, respectively:

$$\begin{aligned}\mathscr{I}(\tilde{\mathscr{S}}_p|\tilde{\mathscr{S}}_p^+) = &\int_0^{\kappa-x}\sum_{k=1}^{m} p_k\eta_k e^{-\eta_k y}\sum_{i=1}^{m+1} C_i^+ e^{\beta_{i,r+\alpha_{k_s}^s}(x+y-\kappa)}dy + \int_0^{\kappa-x}\sum_{k=1}^{m} p_k\eta_k e^{-\eta_k y}\sum_{i=1}^{m+1}\underline{\omega}_i' e^{\beta_{i,r+\alpha_{k_e}^e}(x+y-\kappa)}dy\\ &+\int_0^{\kappa-x}\sum_{k=1}^{m} p_k\eta_k e^{-\eta_k y}\left(\frac{\alpha_{k_s}^s}{\alpha_{k_s}^s+r}\frac{\alpha_{k_v}^v}{\alpha_{k_v}^v+r}e^{\kappa} - \frac{\alpha_{k_s}^s}{\alpha_{k_s}^s+\delta}\frac{\alpha_{k_v}^v}{\alpha_{k_v}^v+\delta}e^{x+y}\right)dy,\end{aligned} \tag{D.32}$$

and

$$\begin{aligned}\mathscr{I}(\tilde{\mathscr{S}}_p|\tilde{\mathscr{S}}_p^-) = &\int_{-\infty}^{0}\sum_{l=1}^{n} q_l\theta_l e^{\theta_l y}\sum_{i=1}^{m+1} C_i^+ e^{\beta_{i,r+\alpha_{k_s}^s}(x+y-\kappa)}dy + \int_{-\infty}^{0}\sum_{l=1}^{n} q_l\theta_l e^{\theta_l y}\sum_{i=1}^{m+1}\underline{\omega}_i' e^{\beta_{i,r+\alpha_{k_e}^e}(x+y-\kappa)}dy\\ &+\int_{-\infty}^{0}\sum_{l=1}^{n} q_l\theta_l e^{\theta_l y}\left(\frac{\alpha_{k_s}^s}{\alpha_{k_s}^s+r}\frac{\alpha_{k_e}^e}{\alpha_{k_e}^e+r}e^{\kappa} - \frac{\alpha_{k_s}^s}{\alpha_{k_s}^s+\delta}\frac{\alpha_{k_e}^e}{\alpha_{k_e}^e+\delta}e^{x+y}\right)dy.\end{aligned} \tag{D.33}$$

After some algebra, we obtain the following equation

$$\begin{aligned}&\sum_{i=1}^{m+1} C_i^+ e^{\beta_{i,r+\alpha_{k_s}^s}(x-\kappa)}\left(\Psi(\beta_{i,r+\alpha_{k_s}^s}) - (\alpha_{k_s}^s+r)\right)\\ &+\sum_{i=1}^{m+1}\underline{\omega}_i' e^{\beta_{i,r+\alpha_{k_e}^e}(x-\kappa)}\left(\Psi(\beta_{i,r+\alpha_{k_e}^e}) - (\alpha_{k_e}^e+r)\right)\\ &+\sum_{i=1}^{m+1} e^{\beta_{i,r+\alpha_{k_e}^e}(x-\kappa)}\left(\alpha_{k_s}^s\underline{\omega}_i - (\alpha_{k_s}^s-\alpha_{k_e}^e)\underline{\omega}_i'\right)\\ &+\sum_{k=1}^{m}\lambda p_k\eta_k e^{\eta_k(x-h)}\Xi_k(\tilde{\mathscr{S}}_c) = 0,\end{aligned} \tag{D.34}$$

where for all $k = 1, 2, ..., m$:

$$\begin{aligned}\Xi_k(\tilde{\mathscr{S}}_p) := &\sum_{j=1}^{n+1}\frac{A_j^-}{\eta_k-\gamma_{j,r+\alpha_{k_e}^e}} - \sum_{i=1}^{m+1}\frac{B_i^+\left(1-e^{(\eta_k-\beta_{i,r+\alpha_{k_s}^s})(h-\kappa)}\right)}{\eta_k-\beta_{i,r+\alpha_{k_s}^s}}\\ &-\sum_{j=1}^{n+1}\frac{B_j^-\left(1-e^{(\eta_k-\gamma_{j,r+\alpha_{k_s}^s})(h-\kappa)}\right)}{\eta_k-\gamma_{j,r+\alpha_{k_s}^s}} - \sum_{i=1}^{m+1}\frac{C_i^+ e^{\eta_k(h-\kappa)}}{\eta_k-\beta_{i,r+\alpha_{k_s}^s}}\\ &-\left(\sum_{i=1}^{m+1}\frac{\underline{\omega}_i' e^{\eta_k(h-\kappa)}}{\eta_k-\beta_{i,r+\alpha_{k_e}^e}} + \sum_{j=1}^{n+1}\frac{\overline{\omega}_j'\left(e^{\gamma_{j,r+\alpha_{k_e}^e}(h-\kappa)} - e^{\eta_k(h-\kappa)}\right)}{\eta_k-\gamma_{j,r+\alpha_{k_e}^e}}\right)\\ &-e^{\eta_k(h-\kappa)}\left(\frac{e^{\kappa}}{\eta_k}\frac{\alpha_{k_s}^s}{\alpha_{k_s}^s+r}\frac{\alpha_{k_e}^e}{\alpha_{k_v}^v+r} - \frac{e^{\kappa}}{\eta_k-1}\frac{\alpha_{k_s}^s}{\alpha_{k_s}^s+\delta}\frac{\alpha_{k_e}^e}{\alpha_{k_e}^e+\delta}\right).\end{aligned} \tag{D.35}$$

The equation (D.34) is satisfied if

$$\Xi_k(\tilde{\mathscr{S}}_p) = 0, \quad \text{for} \quad k = 1, 2, ..., m. \tag{D.36}$$

In addition, the following condition has to hold

$$\underline{\omega}'_i = \frac{\alpha^s_{k_s}\underline{\omega}_i}{\alpha^s_{k_s} - \alpha^e_{k_e}}, \quad \text{for} \quad i = 1, ..., m. \tag{D.37}$$

Step 5: Transformed boundary conditions. The value-matching and smooth-pasting conditions at $x = h$ are, respectively,

$$\begin{aligned}
\sum_{j=1}^{n+1} A_j^- - \sum_{i=1}^{m+1} B_i^+ - \sum_{j=1}^{n+1} B_j^- &= \sum_{j=1}^{n+1} \overline{\omega}'_j e^{\gamma_{j,r+\alpha^e_{k_e}}(h-\kappa)}, \\
\sum_{j=1}^{n+1} \gamma_{j,r+\alpha^e_{k_e}} A_j^- - \sum_{i=1}^{m+1} \beta_{i,r+\alpha^s_{k_s}} B_i^+ - \sum_{j=1}^{n+1} \gamma_{j,r+\alpha^s_{k_s}} B_j^- &= \sum_{j=1}^{n+1} \gamma_{j,r+\alpha^e_{k_e}} \overline{\omega}'_j e^{\gamma_{j,r+\alpha^e_{k_e}}(h-\kappa)}.
\end{aligned} \tag{D.38}$$

At $x = \kappa$ we obtain two additional linear conditions:

$$\begin{aligned}
&\sum_{i=1}^{m+1} B_i^+ e^{\beta_{i,r+\alpha^s_{k_s}}(\kappa-h)} + \sum_{j=1}^{n+1} B_j^+ e^{\gamma_{j,r+\alpha^s_{k_s}}(\kappa-h)} - \sum_{i=1}^{m+1} C_i^+ \\
&= \sum_{i=1}^{m+1} \underline{\omega}'_i - \sum_{j=1}^{n+1} \overline{\omega}'_j + \frac{\alpha^s_{k_s}}{\alpha^s_{k_s}+r}\frac{\alpha^e_{k_e}}{\alpha^e_{k_e}+r} e^{\kappa} - \frac{\alpha^s_{k_s}}{\alpha^s_{k_s}+\delta}\frac{\alpha^e_{k_e}}{\alpha^e_{k_e}+\delta} e^{\kappa}, \\
&\sum_{i=1}^{m+1} \beta_{i,r+\alpha^s_{k_s}} B_i^+ e^{\beta_{i,r+\alpha^s_{k_s}}(\kappa-h)} + \sum_{j=1}^{n+1} \gamma_{j,r+\alpha^s_{k_s}} B_j^+ e^{\gamma_{j,r+\alpha^s_{k_s}}(\kappa-h)} - \sum_{i=1}^{m+1} \beta_{i,r+\alpha^s_{k_s}} C_i^+ \\
&= \sum_{i=1}^{m+1} \beta_{i,r+\alpha^e_{k_e}} \underline{\omega}'_i - \sum_{j=1}^{n+1} \gamma_{j,r+\alpha^e_{k_e}} \overline{\omega}'_j - \frac{\alpha^s_{k_s}}{\alpha^s_{k_s}+\delta}\frac{\alpha^e_{k_e}}{\alpha^e_{k_e}+\delta} e^{\kappa}.
\end{aligned} \tag{D.39}$$

Step 6: System of linear equations. The unknown coefficients solve the system of linear equations

$$\mathbf{P}\mathbf{u}_e = \mathbf{p}_e, \tag{D.40}$$

where $\mathbf{u}_e := (\mathbf{a}^-, \mathbf{b}^+, \mathbf{b}^-, \mathbf{c}^+)'$, with the elements are defined as $\mathbf{a}^- := (A_1^-, ..., A_{n+1}^-)'$, $\mathbf{b}^+ := (B_1^+, ..., B_{m+1}^+)'$, $\mathbf{b}^- := (B_1^-, ..., B_{n+1}^-)'$, and $\mathbf{c}^+ := (C_1^+, ..., C_{m+1}^+)'$. The $(2n + 2m + 4)$-dimensional column vector $\mathbf{p}_e$ is defined as $\mathbf{p}_e := (\mathbf{p}_{e,1}, \mathbf{p}_{e,2}, \mathbf{p}_{e,3}, \mathbf{p}_{e,4}, \mathbf{p}_{e,5}, \mathbf{p}_{e,6}, \mathbf{p}_{e,7}, \mathbf{p}_{e,8})'$.

The elements $\mathbf{p}_{e,1}, \mathbf{p}_{e,2}, \mathbf{p}_{e,4}, \mathbf{p}_{e,5} \in \mathbb{R}^{1\times 1}$ are given by

$$\begin{aligned}
\mathbf{p}_{e,1} &= \sum_{j=1}^{n+1} \overline{\omega}'_j e^{\gamma_{j,r+\alpha^e_{k_e}}(h-\kappa)}, \\
\mathbf{p}_{e,2} &= \sum_{j=1}^{n+1} \gamma_{j,r+\alpha^e_{k_e}} \overline{\omega}'_j e^{\gamma_{j,r+\alpha^e_{k_e}}(h-\kappa)}, \\
\mathbf{p}_{e,4} &= \sum_{i=1}^{m+1} \underline{\omega}'_i - \sum_{j=1}^{n+1} \overline{\omega}'_j + \frac{\alpha^s_{k_s}}{\alpha^s_{k_s}+r}\frac{\alpha^e_{k_e}}{\alpha^e_{k_e}+r}e^{\kappa} - \frac{\alpha^s_{k_s}}{\alpha^s_{k_s}+\delta}\frac{\alpha^e_{k_e}}{\alpha^e_{k_e}+\delta}e^{\kappa}, \\
\mathbf{p}_{e,5} &= \sum_{i=1}^{m+1} \beta_{i,r+\alpha^e_{k_e}} \underline{\omega}'_i - \sum_{j=1}^{n+1} \gamma_{j,r+\alpha^e_{k_e}} \overline{\omega}'_j - \frac{\alpha^s_{k_s}}{\alpha^s_{k_s}+\delta}\frac{\alpha^e_{k_e}}{\alpha^e_{k_e}+\delta}e^{\kappa}.
\end{aligned} \tag{D.41}$$

The elements $\mathbf{p}_{e,3}, \mathbf{p}_{e,7} \in \mathbb{R}^{1\times m}$ are defined (for $k = 1, .., m$) as

$$\begin{aligned}
(\mathbf{p}_{e,3})_{1k} &= \sum_{j=1}^{n+1} \frac{\overline{\omega}'_j e^{\gamma_{j,r+\alpha^e_{k_e}}(h-\kappa)}}{\eta_k - \gamma_{j,r+\alpha^e_{k_e}}}, \\
(\mathbf{p}_{e,7})_{1k} &= \sum_{i=1}^{m+1} \frac{\underline{\omega}'_i e^{\eta_k(h-\kappa)}}{\eta_k - \beta_{i,r+\alpha^e_{k_e}}} + \sum_{j=1}^{n+1} \frac{\overline{\omega}'_j \left(e^{\gamma_{j,r+\alpha^e_{k_e}}(h-\kappa)} - e^{\eta_k(h-\kappa)}\right)}{\eta_k - \gamma_{j,r+\alpha^e_{k_e}}} \\
&\quad + e^{\eta_k(h-\kappa)} \left(\frac{e^{\kappa}}{\eta_k}\frac{\alpha^s_{k_s}}{\alpha^s_{k_s}+r}\frac{\alpha^e_{k_e}}{\alpha^e_{k_e}+r} - \frac{e^{\kappa}}{\eta_k - 1}\frac{\alpha^s_{k_s}}{\alpha^s_{k_s}+\delta}\frac{\alpha^e_{k_e}}{\alpha^e_{k_e}+\delta} \right).
\end{aligned} \tag{D.42}$$

The elements $\mathbf{p}_{e,6}, \mathbf{p}_{e,8} \in \mathbb{R}^{1\times n}$ are defined (for $l = 1, .., n$) as

$$\begin{aligned}
(\mathbf{p}_{e,6})_{1l} &= \sum_{i=1}^{m+1} \frac{\underline{\omega}'_i}{\theta_l + \beta_{i,r+\alpha^e_{k_e}}} - \sum_{j=1}^{n+1} \frac{\overline{\omega}'_j}{\theta_l + \gamma_{j,r+\alpha^e_{k_e}}} \\
&\quad + \frac{e^{\kappa}}{\theta_l}\frac{\alpha^s_{k_s}}{\alpha^s_{k_s}+r}\frac{\alpha^e_{k_e}}{\alpha^e_{k_e}+r} - \frac{e^{\kappa}}{\theta_l+1}\frac{\alpha^s_{k_s}}{\alpha^s_{k_s}+\delta}\frac{\alpha^e_{k_e}}{\alpha^e_{k_e}+\delta}, \\
(\mathbf{p}_{e,8})_{1l} &= \sum_{i=1}^{m+1} \frac{\underline{\omega}'_i e^{\theta_l(\kappa-h)}}{\theta_l + \beta_{i,r+\alpha^e_{k_e}}} + \sum_{j=1}^{n+1} \frac{\overline{\omega}'_j \left(e^{\gamma_{j,r+\alpha^s_{k_s}}(h-\kappa)} - e^{\theta_l(\kappa-h)}\right)}{\theta_l + \gamma_{j,r+\alpha^e_{k_e}}} \\
&\quad + e^{\theta_l(\kappa-h)} \left(\frac{e^{\kappa}}{\theta_l}\frac{\alpha^s_{k_s}}{\alpha^s_{k_s}+r}\frac{\alpha^e_{k_e}}{\alpha^e_{k_e}+r} - \frac{e^{\kappa}}{\theta_l+1}\frac{\alpha^s_{k_s}}{\alpha^s_{k_s}+\delta}\frac{\alpha^e_{k_e}}{\alpha^e_{k_e}+\delta} \right).
\end{aligned} \tag{D.43}$$

Finally, the $(2n+2m+4)$-dimensional square matrix $\mathbf{P}$ is given by

$$\mathbf{P} := \begin{pmatrix} \mathbf{P}_{11} & \mathbf{P}_{12} & \mathbf{P}_{13} & \mathbf{P}_{14} \\ \mathbf{P}_{21} & \mathbf{P}_{22} & \mathbf{P}_{23} & \mathbf{P}_{24} \\ \mathbf{P}_{31} & \mathbf{P}_{32} & \mathbf{P}_{33} & \mathbf{P}_{34} \\ \mathbf{P}_{41} & \mathbf{P}_{42} & \mathbf{P}_{43} & \mathbf{P}_{44} \\ \mathbf{P}_{51} & \mathbf{P}_{52} & \mathbf{P}_{53} & \mathbf{P}_{54} \\ \mathbf{P}_{61} & \mathbf{P}_{62} & \mathbf{P}_{63} & \mathbf{P}_{64} \\ \mathbf{P}_{71} & \mathbf{P}_{72} & \mathbf{P}_{73} & \mathbf{P}_{74} \\ \mathbf{P}_{81} & \mathbf{P}_{82} & \mathbf{P}_{83} & \mathbf{P}_{84} \end{pmatrix}, \tag{D.44}$$

where the elements of the matrix $\mathbf{P}$, i.e., the sub-matrices $\mathbf{P}_{kl}$ with $k = 1, ..., 8$ and $l = 1, ..., 4$, are given as follows.

1. For all $j = 1, ..., n+1$, $\mathbf{P}_{11}, \mathbf{P}_{13}, \mathbf{P}_{21}, \mathbf{P}_{23}, \mathbf{P}_{41}, \mathbf{P}_{43}, \mathbf{P}_{51}, \mathbf{P}_{53} \in \mathbb{R}^{1\times(n+1)}$ are:

   $(\mathbf{P}_{11})_{1j} = -(\mathbf{P}_{13})_{1j} = 1$, $(\mathbf{P}_{21})_{1j} = \gamma_{j,r+\alpha^e_{ke}}$, $(\mathbf{P}_{23})_{1j} = -\gamma_{j,r+\alpha^s_{ks}}$, $(\mathbf{P}_{41})_{1j} = (\mathbf{P}_{51})_{1j} = 0$, $(\mathbf{P}_{43})_{1j} = e^{\gamma_{j,r+\alpha^s_{ks}}(\kappa-h)}$, and $(\mathbf{P}_{53})_{1j} = \gamma_{j,r+\alpha^s_{ks}} e^{\gamma_{j,r+\alpha^s_{ks}}(\kappa-h)}$.

2. For all $j = 1, ..., m+1$, $\mathbf{P}_{12}, \mathbf{P}_{14}, \mathbf{P}_{22}, \mathbf{P}_{24}, \mathbf{P}_{42}, \mathbf{P}_{44}, \mathbf{P}_{52}, \mathbf{P}_{54} \in \mathbb{R}^{1\times(m+1)}$ are:

   $(\mathbf{P}_{12})_{1j} = (\mathbf{P}_{44})_{1j} = -1$, $(\mathbf{P}_{14})_{1j} = (\mathbf{P}_{24})_{1j} = 0$, $(\mathbf{P}_{22})_{1j} = -\beta_{j,r+\alpha^s_{ks}}$, $(\mathbf{P}_{42})_{1j} = e^{\beta_{j,r+\alpha^s_{ks}}(\kappa-h)}$, $(\mathbf{P}_{52})_{1j} = \beta_{j,r+\alpha^s_{ks}} e^{\beta_{j,r+\alpha^s_{ks}}(\kappa-h)}$, and $(\mathbf{P}_{54})_{1j} = -\beta_{j,r+\alpha^s_{ks}}$.

3. For $i = 1, ..., m$ and $j = 1, ..., n+1$, $\mathbf{P}_{31}, \mathbf{P}_{33}, \mathbf{P}_{71}, \mathbf{P}_{73} \in \mathbb{R}^{m\times(n+1)}$ are:

   $(\mathbf{P}_{31})_{ij} = (\mathbf{P}_{71})_{ij} = 1/(\eta_i - \gamma_{j,r+\alpha^e_{ke}})$, $(\mathbf{P}_{33})_{ij} = -1/(\eta_i - \gamma_{j,r+\alpha^s_{ks}})$, and $(\mathbf{P}_{73})_{ij} = -\left(1 - e^{(\eta_i-\gamma_{j,r+\alpha^s_{ks}})(h-\kappa)}\right)/(\eta_i - \gamma_{j,r+\alpha^s_{ks}})$.

4. For $i = 1, ..., m$ and $j = 1, ..., m+1$, $\mathbf{P}_{32}, \mathbf{P}_{34}, \mathbf{P}_{72}, \mathbf{P}_{74} \in \mathbb{R}^{m\times(m+1)}$ are:

   $(\mathbf{P}_{32})_{ij} = -1/(\eta_i - \beta_{j,r+\alpha^s_{ks}})$, $(\mathbf{P}_{34})_{ij} = 0$, $(\mathbf{P}_{72})_{ij} = -\left(1 - e^{(\eta_i-\beta_{j,r+\alpha^s_{ks}})(h-\kappa)}\right)/(\eta_i - \beta_{j,r+\alpha^s_{ks}})$, and $(\mathbf{P}_{74})_{ij} = -e^{\eta_i(h-\kappa)}/(\eta_i - \beta_{j,r+\alpha^s_{ks}})$.

5. For $i = 1, ..., n$ and $j = 1, ..., n+1$, $\mathbf{P}_{61}, \mathbf{P}_{63}, \mathbf{P}_{81}, \mathbf{P}_{83} \in \mathbb{R}^{n\times(n+1)}$ are:

   $(\mathbf{P}_{61})_{ij} = 0$, $(\mathbf{P}_{63})_{ij} = e^{\gamma_{j,r+\alpha^s_{ks}}(\kappa-h)}/(\theta_i + \gamma_{j,r+\alpha^s_{ks}})$, $(\mathbf{P}_{81})_{ij} = 1/(\theta_i + \gamma_{j,r+\alpha^e_{ke}})$, and $(\mathbf{P}_{83})_{ij} = -\left(1 - e^{(\theta_i+\gamma_{j,r+\alpha^s_{ks}})(\kappa-h)}\right)/(\theta_i + \gamma_{j,r+\alpha^s_{ks}})$.

6. For $i = 1, ..., n$ and $j = 1, ..., m+1$, $\mathbf{P}_{62}, \mathbf{P}_{64}, \mathbf{P}_{82}, \mathbf{P}_{84} \in \mathbb{R}^{n\times(m+1)}$ are:

$$(\mathbf{P}_{62})_{ij} = e^{\beta_{j,r+\alpha^s_{k_s}}(\kappa-h)}/(\theta_i + \beta_{j,r+\alpha^s_{k_s}}),\ (\mathbf{P}_{64})_{ij} = -1/(\theta_i + \beta_{j,r+\alpha^s_{k_s}}),$$
$$(\mathbf{P}_{82})_{ij} = -\left(1 - e^{(\theta_i+\beta_{j,r+\alpha^s_{k_s}})(\kappa-h)}\right)/(\theta_i + \beta_{j,r+\alpha^s_{k_s}}),\text{ and } (\mathbf{P}_{84})_{ij} = -e^{\theta_i(\kappa-h)}/(\theta_i + \beta_{j,r+\alpha^s_{k_s}}).$$

■

D.2 Proof of Theorem 3.5.2: Québécoised APUOP option

Step 1: DLCT. Using the same change of variables as in Appendix D.1 the equation (3.57) becomes

$$\begin{cases} -\dfrac{\partial\tilde{\epsilon}^e_{uo}}{\partial\tau_e}(x,\tau_e) + \mathcal{L}\tilde{\epsilon}^e_{uo}(x,\tau_e) = r\tilde{\epsilon}^e_{uo}(x,\tau_e), & \text{if } (x,t_s,t_e) \in \tilde{\mathscr{E}}, \\ -\dfrac{\partial\tilde{\epsilon}^s_{uo}}{\partial\tau_s}(x,\tau_s) + \mathcal{L}\tilde{\epsilon}^s_{uo}(x,\tau_s) = r\tilde{\epsilon}^s_{uo}(x,t_s), & \text{if } (x,\tau_s,\tau_e) \in \tilde{\mathscr{S}}^*. \end{cases} \tag{D.45}$$

Similarly, we adjust the notation in the equations (3.58)–(3.61). The DLCT of the PIDE system (D.45) for the APUOP EEP results in two coupled OIDEs, which can be solved analytically.

Step 2: Standard continuation domain OIDE. In the standard continuation domain $\tilde{\mathscr{S}}^*$, the OIDE describing the dynamics of the québécoised APUOP EEP is

$$\begin{aligned} \frac{\sigma^2}{2}\frac{d^2\hat{\tilde{\epsilon}}^s_{uo}}{dx^2}(x,\alpha^s_{k_s}) + \mu\frac{d\hat{\tilde{\epsilon}}^s_{uo}}{dx}(x,\alpha^s_{k_s}) - (r+\alpha^s_{k_s}+\lambda)\hat{\tilde{\epsilon}}^s_{uo}(x,\alpha^s_{k_s}) \\ + \alpha^s_{k_s}\hat{\epsilon}_p(x,\alpha^e_{k_e};\kappa,D) + \lambda\int_{-\infty}^{+\infty}\hat{\tilde{\epsilon}}_{uo}(x+y,\alpha^s_{k_s},\alpha^e_{k_e})\varphi_Y(y)dy = 0, \end{aligned} \tag{D.46}$$

where $\hat{\epsilon}_p(x,\alpha^e_{k_e};\kappa,D)$ is the LCT of the vanilla American EEP w.r.t. the residual hybrid excursion time $\tau_e := D - t_e$ (with parameter $\alpha^e_{k_e} = k_e\log(2)/\tau_e$).

Step 3: Excursion domain OIDE. In the excursion region $\tilde{\mathscr{E}}$, we have

$$\begin{aligned} \frac{\sigma^2}{2}\frac{d^2\hat{\tilde{\epsilon}}^e_{uo}}{dx^2}(x,\alpha^e_{k_e}) + \mu\frac{d\hat{\tilde{\epsilon}}^e_{uo}}{dx}(x,\alpha^e_{k_e}) - (r+\alpha^e_{k_e}+\lambda)\hat{\tilde{\epsilon}}^e_{uo}(x,\alpha^e_{k_e}) \\ + \lambda\int_{-\infty}^{+\infty}\hat{\tilde{\epsilon}}_{uo}(x+y,\alpha^s_{k_s},\alpha^e_{k_e})\varphi_Y(y)dy = 0. \end{aligned} \tag{D.47}$$

The initial conditions in the standard continuation and the excursion domains are incorporated in the OIDEs. The boundary condition in the excursion domain (after québécoisation is applied) is

$$\lim_{x\uparrow+\infty}\hat{\tilde{\epsilon}}^e_{uo}(x,\alpha^e_{k_e}) = 0, \tag{D.48}$$

whereas the transformed boundary conditions between the excursion and the standard continuation domain are

$$\begin{aligned}\lim_{x\uparrow h}\hat{\tilde{\epsilon}}^s_{uo}(x,\alpha^s_{k_s}) &= \lim_{x\downarrow h}\hat{\tilde{\epsilon}}^e_{uo}(x,\alpha^e_{k_e}),\\ \lim_{x\uparrow h}\frac{\partial\hat{\tilde{\epsilon}}^s_{uo}}{\partial x}(x,\alpha^s_{k_s}) &= \lim_{x\downarrow h}\frac{\partial\hat{\tilde{\epsilon}}^e_{uo}}{\partial x}(x,\alpha^e_{k_e}).\end{aligned} \tag{D.49}$$

Step 4: Transformed boundary conditions. Transformed value-matching and smooth-pasting conditions at the boundary between the standard continuation and the exercise domain are

$$\begin{aligned}\lim_{x\downarrow\hat{b}}\hat{\tilde{\epsilon}}^s_{uo}(x,\alpha^s_{k_s}) &= e^{\kappa}-e^{\hat{b}}-\hat{\tilde{\pi}}^s_{uo}(x,\alpha^s_{k_s})\big|_{x=\hat{b}},\\ \lim_{x\downarrow\hat{b}}\frac{\partial\hat{\tilde{\epsilon}}^s_{uo}}{\partial x}(x,\alpha^s_{k_s}) &= -e^{\hat{b}}-\frac{\partial\hat{\tilde{\pi}}^s_{uo}}{\partial x}(x,\alpha^s_{k_s})\Big|_{x=\hat{b}}.\end{aligned} \tag{D.50}$$

Using the ansatz (3.62)–(3.64) to solve our system of OIDEs given above and by following the same steps as in the case of EPUOP options—which we omit here for brevity—we obtain the following matrix equation for the unknown coefficients

$$\mathbf{Q}\mathbf{u}_a = \mathbf{q}_a. \tag{D.51}$$

The vector $\mathbf{u}_a$ is given by $\mathbf{u}_a := (\mathbf{d}^-, \mathbf{f}^+, \mathbf{f}^-)'$ where $\mathbf{d}^- := (D_1^-, ..., D_{n+1}^-)'$, $\mathbf{f}^+ := (F_1^+, ..., F_{m+1}^+)'$, and $\mathbf{f}^- := (F_1^-, ..., F_{n+1}^-)'$. The $(m+2n+3)$-dimensional column vector $\mathbf{q}_a$ is defined as $\mathbf{q}_a := (\mathbf{q}_{a,1}, \mathbf{q}_{a,2}, \mathbf{q}_{a,3}, \mathbf{q}_{a,4}, \mathbf{q}_{a,5}, \mathbf{q}_{a,6})'$.

The elements $\mathbf{q}_{a,1}, \mathbf{q}_{a,2}, \mathbf{q}_{a,4} \in \mathbb{R}^{1\times 1}$ are

$$\begin{aligned}\mathbf{q}_{a,1} &= \sum_{j=1}^{n+1} v'_j e^{\gamma_{j,r+\alpha^e_{k_e}}(h-\hat{b})},\\ \mathbf{q}_{a,2} &= \sum_{j=1}^{n+1} \gamma_{j,r+\alpha^e_{k_e}} v'_j e^{\gamma_{j,r+\alpha^e_{k_e}}(h-\hat{b})},\\ \mathbf{q}_{a,4} &= \sum_{j=1}^{n+1} v'_j + \sum_{i=1}^{m+1} C_i^+ e^{\beta_{i,r+\alpha^s_{k_s}}(\hat{b}-\kappa)} + \sum_{i=1}^{m+1} \underline{\omega}'_i e^{\beta_{i,r+\alpha^e_{k_e}}(\hat{b}-\kappa)}\\ &\quad - \left(1-\frac{\alpha^s_{k_s}}{\alpha^s_{k_s}+r}\frac{\alpha^e_{k_e}}{\alpha^e_{k_e}+r}\right)e^{\kappa} + \left(1-\frac{\alpha^s_{k_s}}{\alpha^s_{k_s}+\delta}\frac{\alpha^e_{k_e}}{\alpha^e_{k_e}+\delta}\right)e^{\hat{b}}.\end{aligned} \tag{D.52}$$

The element $\mathbf{q}_{a,5} \in \mathbb{R}^{1\times m}$ (for $k = 1, .., m$) is given by

$$(\mathbf{q}_{a,5})_{1k} = \sum_{j=1}^{n+1} \frac{\underline{\omega}'_j e^{\gamma_{j,r+\alpha^e_{k_e}}(h-\hat{b})}}{\eta_k - \gamma_{j,r+\alpha^e_{r+k_e}}}. \tag{D.53}$$

The elements $\mathbf{q}_{a,3}, \mathbf{q}_{a,6} \in \mathbb{R}^{1\times n}$ (for $l = 1, .., n$) are defined as

$$
\begin{aligned}
(\mathbf{q}_{a,3})_{1l} = & \sum_{j=1}^{n+1} \frac{v'_j \left(e^{\gamma_{j,r+\alpha^e_{k_e}}(h-\hat{b})} - e^{\theta_l(\hat{b}-h)} \right)}{\theta_l + \gamma_{j,r+\alpha^e_{r+k_e}}} - \sum_{i=1}^{m+1} \frac{C_i^+ e^{\beta_{i,r+\alpha^s_{k_s}}(\hat{b}-\kappa)+\theta_l(\hat{b}-h)}}{\theta_l + \beta_{i,r+\alpha^s_{k_s}}} \\
& - \sum_{i=1}^{m+1} \frac{\underline{\omega}'_i e^{\beta_{i,r+\alpha^e_{k_e}}(\hat{b}-\kappa)+\theta_l(\hat{b}-h)}}{\theta_l + \beta_{i,r+\alpha^e_{k_e}}} \\
& + e^{\theta_l(\hat{b}-h)} \left(1 - \frac{\alpha^s_{k_s}}{\alpha^s_{k_s}+r} \frac{\alpha^e_{k_e}}{\alpha^e_{k_e}+r} \right) \frac{e^{\kappa}}{\theta_l} - e^{\theta_l(\hat{b}-h)} \left(1 - \frac{\alpha^s_{k_s}}{\alpha^s_{k_s}+\delta} \frac{\alpha^e_{k_e}}{\alpha^e_{k_e}+\delta} \right) \frac{e^{\hat{b}}}{\theta_l + 1}, \\
(\mathbf{q}_{a,6})_{1l} = & (\mathbf{p}_{a,3})_{1l} - \sum_{j=1}^{n+1} \frac{v'_j e^{\gamma_{j,r+\alpha^e_{k_e}}(h-\hat{b})}}{\theta_l + \gamma_{j,r+\alpha^e_{r+k_e}}}.
\end{aligned}
\tag{D.54}
$$

Finally, the $(m + 2n + 3)$-dimensional square matrix $\mathbf{Q}$ is given by

$$
\mathbf{Q} := \begin{pmatrix}
\mathbf{Q}_{11} & \mathbf{Q}_{12} & \mathbf{Q}_{13} \\
\mathbf{Q}_{21} & \mathbf{Q}_{22} & \mathbf{Q}_{23} \\
\mathbf{Q}_{31} & \mathbf{Q}_{32} & \mathbf{Q}_{33} \\
\mathbf{Q}_{41} & \mathbf{Q}_{42} & \mathbf{Q}_{43} \\
\mathbf{Q}_{51} & \mathbf{Q}_{52} & \mathbf{Q}_{53} \\
\mathbf{Q}_{61} & \mathbf{Q}_{62} & \mathbf{Q}_{63}
\end{pmatrix},
\tag{D.55}
$$

where the elements of the matrix $\mathbf{Q}$, i.e., the sub-matrices $\mathbf{Q}_{kl}$ with $k = 1, ..., 6$ and $l = 1, 2, 3$, are given as follows:

1. For all $j = 1, ..., n + 1$, $\mathbf{Q}_{11}, \mathbf{Q}_{13}, \mathbf{Q}_{21}, \mathbf{Q}_{23}, \mathbf{Q}_{41}, \mathbf{Q}_{43} \in \mathbb{R}^{1\times(n+1)}$ are:

   $(\mathbf{Q}_{11})_{1j} = -(\mathbf{Q}_{13})_{1j} = 1$, $(\mathbf{Q}_{21})_{1j} = \gamma_{j,r+\alpha^e_{k_e}}$, $(\mathbf{P}_{23})_{1j} = -\gamma_{j,r+\alpha^s_{k_s}}$, $(\mathbf{Q}_{41})_{1j} = 0$, and $(\mathbf{Q}_{43})_{1j} = -e^{\gamma_{j,r+\alpha^s_{k_s}}(\hat{b}-\kappa)}$.

2. For all $j = 1, ..., m + 1$, $\mathbf{Q}_{12}, \mathbf{Q}_{22}, \mathbf{Q}_{42} \in \mathbb{R}^{1\times(m+1)}$ are:

   $(\mathbf{Q}_{12})_{1j} = -1$, $(\mathbf{Q}_{22})_{1j} = -\beta_{j,r+\alpha^s_{k_s}}$, and $(\mathbf{Q}_{42})_{1j} = -e^{\beta_{j,r+\alpha^s_{k_s}}(\hat{b}-\kappa)}$.

3. For $i = 1, ..., m$ and $j = 1, ..., n + 1$, $\mathbf{Q}_{51}, \mathbf{Q}_{53} \in \mathbb{R}^{m\times(n+1)}$ are:

   $(\mathbf{Q}_{51})_{ij} = 1/(\eta_i - \gamma_{j,r+\alpha^e_{k_e}})$, and $(\mathbf{Q}_{53})_{ij} = -1/(\eta_i - \gamma_{j,r+\alpha^s_{k_s}})$.

4. For $i = 1, ..., m$ and $j = 1, ..., m + 1$, $\mathbf{Q}_{52} \in \mathbb{R}^{m\times(m+1)}$ are:

   $(\mathbf{Q}_{52})_{ij} = -1/(\eta_i - \beta_{j,r+\alpha^s_{k_s}})$.

5. For $i = 1, ..., n$ and $j = 1, ..., n+1$, $\mathbf{Q}_{31}, \mathbf{Q}_{33}, \mathbf{Q}_{61}, \mathbf{Q}_{63} \in \mathbb{R}^{n\times(n+1)}$ are:

   $(\mathbf{Q}_{31})_{ij} = 1/(\theta_i + \gamma_{j,r+\alpha^e_{k_e}})$, $(\mathbf{Q}_{33})_{ij} = -\left(1 - e^{(\theta_i+\gamma_{j,r+\alpha^s_{k_s}})(\hat{b}-h)}\right)/(\theta_i + \gamma_{j,r+\alpha^s_{k_s}})$, $(\mathbf{Q}_{63})_{ij} = e^{(\theta_i+\gamma_{j,r+\alpha^s_{k_s}})(\hat{b}-h)}/(\theta_i + \gamma_{j,r+\alpha^s_{k_s}})$ and $(\mathbf{Q}_{61})_{ij} = 0$.

6. For $i = 1, ..., n$ and $j = 1, ..., m+1$, $\mathbf{Q}_{32}, \mathbf{Q}_{62} \in \mathbb{R}^{n\times(m+1)}$ are:

   $(\mathbf{Q}_{32})_{ij} = -\left(1 - e^{(\theta_i+\beta_{j,r+\alpha^s_{k_s}})(\hat{b}-h)}\right)/(\theta_i + \beta_{j,r+\alpha^s_{k_s}})$, and $(\mathbf{Q}_{62})_{ij} = e^{(\theta_i+\beta_{j,r+\alpha^s_{k_s}})(\hat{b}-h)}/(\theta_i + \beta_{j,r+\alpha^s_{k_s}})$.

   The québécoised early exercise boundary can be computed using the second equation in (D.50).

■

Appendix E

Proofs of results in Chapter 4

E.1 Proof of Theorem 4.2.1: Risk-neutral dynamics

The Esscher transform of D-MEM process is

$$Z_t(\vartheta) := \left.\frac{d\mathbb{Q}^\vartheta}{d\mathbb{P}}\right|_{\mathcal{F}_t} = \underbrace{e^{\vartheta\sigma W_t - \frac{1}{2}\vartheta^2\sigma^2 t}}_{Z_t^D(\vartheta)} \underbrace{e^{\vartheta\sum_{i=1}^{N_t} Y_i - t\Psi_J(\vartheta)}}_{Z_t^J(\vartheta)}. \tag{E.1}$$

First, it follows from the Girsanov theorem that the $\mathbb{Q}^\vartheta$-Brownian motion is $W_t^* = W_t - [W, \vartheta\sigma W]_t = W_t - \vartheta\sigma t$. The volatility parameter remains the same after the change of measure, i.e., $\sigma^* = \sigma$. Second, it can be shown that the cumulant generating function (c.g.f.) of the jump part is given by

$$\Psi_J(a) = \lambda\left(\left(\frac{\lambda_+}{\lambda}\sum_{i=1}^{m}\frac{p_i\eta_i}{\eta_i - a} + \frac{\lambda_-}{\lambda}\sum_{j=1}^{n}\frac{q_j\theta_j}{\theta_j + a}\right)e^{a\xi} - 1\right), \tag{E.2}$$

for every $a \in (-\theta_1, \eta_1)$. The jump c.g.f. under the new measure is

$$\Psi_J^*(\varkappa) := \frac{1}{t}\log\mathbb{E}\left[Z_t^J(\vartheta)e^{\varkappa\sum_{i=1}^{N_t} Y_i}\right] = \Psi_J(\varkappa + \vartheta) - \Psi_J(\vartheta), \tag{E.3}$$

for every $\varkappa \in (-\theta_1, \eta_1)$. This equation can be written in the form

$$\begin{aligned}\Psi_J^*(\varkappa) &= \lambda\int_{-\infty}^{+\infty}(e^{\varkappa y} - 1)\, e^{\vartheta y} f_Y(y)dy \\ &= \lambda^*\int_{-\infty}^{+\infty}(e^{\varkappa y} - 1)\,\frac{e^{\vartheta y} f_Y(y)}{\int_{-\infty}^{+\infty} e^{\vartheta y} f_Y(y)dy}dy,\end{aligned} \tag{E.4}$$

where the jump intensity under the new measure is given by

$$\lambda^* := \lambda\int_{-\infty}^{+\infty} e^{\vartheta y} f_Y(y)dy = \underbrace{\lambda_+\sum_{i=1}^{m}\frac{p_i\eta_i}{\eta_i - \vartheta}e^{\vartheta\xi}}_{\lambda_+^*} + \underbrace{\lambda_-\sum_{j=1}^{n}\frac{q_j\theta_j}{\theta_j + \vartheta}e^{\vartheta\xi}}_{\lambda_-^*}, \tag{E.5}$$

and the exponentially tilted jump size distribution under the new measure is defined as

$$f_Y^*(y) := \frac{e^{\vartheta y} f_Y(y)}{\int_{-\infty}^{+\infty} e^{\vartheta y} f_Y(y) dy}. \tag{E.6}$$

After some algebraic calculation, we obtain the expression for the jump c.g.f. under risk-neutral measure

$$\Psi_J^*(\varkappa) = \lambda^* \left(\left(\frac{\lambda_+^*}{\lambda^*} \sum_{i=1}^{m} \frac{p_i^* \eta_i^*}{\eta_i^* - \varkappa} + \frac{\lambda_-^*}{\lambda^*} \sum_{j=1}^{n} \frac{q_j^* \theta_j^*}{\theta_j^* + \varkappa} \right) e^{\varkappa \xi^*} - 1 \right). \tag{E.7}$$

The coefficients λ_+^* and λ_-^* are defined in equation (E.5). Furthermore, for all $i = 1, 2, ..., m$ we have that $\eta_i^* = \eta_i - \vartheta$ and $p_i^* = p_i \frac{\eta_i}{\eta_i - \vartheta} \frac{1}{\upsilon_+(\vartheta)}$, and for all $j = 1, 2, ..., n$ the adjusted coefficients are $\theta_j^* = \theta_j + \vartheta$ and $q_j^* = q_j \frac{\theta_j}{\theta_j + \vartheta} \frac{1}{\upsilon_-(\vartheta)}$. The introduced υ-coefficients are: $\upsilon_+(\vartheta) = \sum_{i=1}^{m} \frac{p_i \eta_i}{\eta_i - \vartheta}$ and $\upsilon_-(\vartheta) = \sum_{j=1}^{n} \frac{q_j \theta_j}{\theta_j + \vartheta}$. The displacement parameter ξ remain unchanged, i.e., $\xi^* = \xi$. Thus, we conclude that the log-price process under the measure $\mathbb{Q}^\vartheta$ is described by (4.9).

It remains to find the value of the Esscher transform parameter ϑ which guarantees that the new probability measure is indeed the risk-neutral measure. We require that the discounted process $\left\{ e^{-rt} S_t, t \geq 0 \right\}$ is a $\mathbb{Q}^\vartheta$-martingale, i.e.,

$$\mathbb{E}^* \left[e^{-rt + X_t} \right] = e^{(\bar{\mu} - r)t} e^{\frac{1}{2}(2\vartheta + 1)\sigma^2 t} e^{(\Psi_J(\vartheta + 1) - \Psi_J(\vartheta))t} = 1. \tag{E.8}$$

Therefore, our equivalent martingale measure $\mathbb{Q}^\vartheta$ is indeed the risk-neutral measure if the Esscher transform parameter solves computed the equation

$$\bar{\mu} - r + \left(\vartheta + \frac{1}{2} \right) \sigma^2 + \Psi_J(\vartheta + 1) - \Psi_J(\vartheta) = 0. \tag{E.9}$$

It can be easily verified that this equation can be reduced to the form (4.11). This The proof of existence and uniqueness of ϑ for the change of measure via Esscher transform is given in Thul and Zhang (2014), Proposition 2, pp. 12–13. ■

E.2 Proof of Theorem 4.3.1: Canadized European digital put optionettes in D-MEM framework

First, for computational convenience, we recast the original problem in the log-space, i.e., we define the log-price $x := \log S_t$ and the log-strike $\kappa := \log K$. Second, we note that the Feynman–Kac theorem allows us to compute the European digital option price in Equation (4.27) by solving the

partial integro-differential equation (PIDE)

$$-\frac{\partial p}{\partial \tau}(x,\tau)+\frac{\sigma^2}{2}\frac{\partial^2 p}{\partial x^2}(x,\tau)+\bar{\mu}\frac{\partial p}{\partial x}(x,\tau)+\int_{-\infty}^{+\infty}[p(x+y,\tau)-p(x,\tau)]\nu(y)dy=0, \tag{E.10}$$

where $\bar{\mu}$ denotes the compensated drift term of the log-price process under the physical measure, and the Lévy measure $\nu(\cdot)$ is defined in Equation (4.1). The boundary and initial conditions are: $\lim_{x\uparrow+\infty} p(x,\tau)=0$, $\lim_{x\downarrow-\infty} p(x,\tau)=1$, and $\lim_{\tau\downarrow 0} p(x,\tau)=\mathbb{1}_{\{x<\kappa\}}$.

To solve this equation, we first introduce the change of variables $y\mapsto y':=y-\xi$. Therefore, the transformed jump distribution takes the form

$$f_Y(y')=\frac{\lambda_+}{\lambda}\sum_{i=1}^{m}p_i\eta_i e^{-\eta_i y'}\mathbb{1}_{\{y'\geq 0\}}+\frac{\lambda_-}{\lambda}\sum_{j=1}^{n}q_j\theta_j e^{\theta_j y'}\mathbb{1}_{\{y'<0\}}. \tag{E.11}$$

Third, taking the Laplace–Carson transform (LCT) of the PIDE (E.10), we obtain the ordinary integro-differential equation (OIDE) for the Canadized European digital put $\tilde{p}:=\tilde{p}(x,\alpha)$:

$$\frac{\sigma^2}{2}\frac{d^2\tilde{p}}{dx^2}(x,\alpha)+\bar{\mu}\frac{d\tilde{p}}{dx}(x,\alpha)-(\lambda+\alpha)\tilde{p}(x,\alpha)+\alpha\mathbb{1}_{\{x<\kappa\}}+\lambda\int_{-\infty}^{+\infty}\tilde{p}(x+\xi+y',\alpha)f_Y(y')dy'=0. \tag{E.12}$$

The initial condition is absorbed into Equation (E.12) due to the LCT. On the other hand, the transformed boundary conditions are: $\lim_{x\downarrow-\infty}\tilde{p}(x,\alpha)=1$ and $\lim_{x\uparrow+\infty}\tilde{p}(x,\alpha)=0$.

We conjecture the solution in the form[74]

$$\tilde{p}(x,\alpha)=\begin{cases}1+\displaystyle\sum_{l=1}^{\hat{m}}\underline{w}'_l e^{\beta_{l,\alpha}(x-\kappa-\xi)} & \text{if } x<\kappa,\\ \displaystyle\sum_{l=1}^{\hat{n}}\overline{w}'_l e^{\gamma_{l,\alpha}(x-\kappa-\xi)} & \text{if } x\geq\kappa.\end{cases} \tag{E.13}$$

The coefficients $\{\beta_{i,\alpha}\}_{i=1,\ldots,\hat{m}}$ and $\{\gamma_{j,\alpha}\}_{j=1,\ldots,\hat{n}}$ represent the positive and negative roots, respectively, of the characteristic equation

$$\Psi'(u)=\alpha,\ \alpha\in\mathbb{R}^+. \tag{E.14}$$

where $\Psi'(u):=\bar{\mu}u+\frac{1}{2}\sigma^2u^2+\lambda\left(\frac{\lambda_+}{\lambda}\sum_{i=1}^{m}\frac{p_i\eta_i}{\eta_i-u}+\frac{\lambda_-}{\lambda}\sum_{j=1}^{n}\frac{q_j\theta_j}{\theta_j+u}-1\right)$.[75] The roots, which can be computed numerically, satisfy the ordering relation

$$-\infty<\gamma_{\hat{n},\alpha}<\cdots<\gamma_{2,\alpha}<\gamma_{1,\alpha}<0<\beta_{1,\alpha}<\beta_{2,\alpha}<\cdots<\beta_{\hat{m},\alpha}<+\infty, \tag{E.15}$$

[74] We note that the Equation (E.13) is equivalent to the Equation (4.35). The difference is that the former represents a "displaced" version of the latter (i.e., the displacement parameter ξ is explicitly included in the exponential terms, and we defined $\underline{w}'_l:=\underline{w}_l e^{\beta_{l,\alpha}\xi}$ for $l=1,\cdots,\hat{m}$ and $\overline{w}'_l:=\overline{w}_l e^{\gamma_{l,\alpha}\xi}$ for $l=1,\cdots,\hat{n}$). The introduction of expression (E.13) is a merely formal and intermediate step, however it is necessary to analytically solve the OIDE (E.12).

[75] It can be verified that $\Psi'(u)=\Psi(u)|_{\xi=0}+\lambda\left(\frac{\lambda_+}{\lambda}\sum_{i=1}^{m}\frac{p_i\eta_i}{\eta_i-1}+\frac{\lambda_-}{\lambda}\sum_{j=1}^{n}\frac{q_j\theta_j}{\theta_j+1}\right)(1-e^{\xi})$.

where $\hat{m} := \hat{m}(\alpha) \leq m+1$ and $\hat{n} := \hat{n}(\alpha) \leq n+1$. The coefficients $\{\underline{w}_i\}_{i=1,...,\hat{m}}$ and $\{\overline{w}_j\}_{j=1,...,\hat{n}}$ can be calculated by analyzing the solution in the two different regions, i.e., below and above the strike price, respectively.

First, we consider the case $x < \kappa$. It is straightforward to compute the two derivative terms in (E.12), i.e.,

$$\begin{aligned}\frac{d\tilde{p}}{dx}(x,\alpha) &= \sum_{l=1}^{\hat{m}} \underline{w}'_l \beta_{l,\alpha} e^{\beta_{l,\alpha}(x-\kappa-\xi)},\\ \frac{d^2\tilde{p}}{dx^2}(x,\alpha) &= \sum_{l=1}^{\hat{n}} \underline{w}'_l \beta_{l,\alpha}^2 e^{\beta_{l,\alpha}(x-\kappa-\xi)}.\end{aligned} \tag{E.16}$$

On the other hand, the integral term is much more involved. It can be decomposed in the form:

$$\begin{aligned}\mathscr{I} &= \frac{\lambda^-}{\lambda}\sum_{l=1}^{\hat{m}}\sum_{j=1}^{n}\int_{-\infty}^{0} q_j\theta_j\underline{w}'_l e^{\beta_{l,\alpha}(x-\kappa)}e^{(\beta_{l,\alpha}+\theta_j)y'}dy'\\ &+ \frac{\lambda^-}{\lambda}\sum_{j=1}^{n}\int_{-\infty}^{0} q_j\theta_j e^{\theta_j y'}dy'\\ &+ \frac{\lambda^+}{\lambda}\sum_{l=1}^{\hat{m}}\sum_{i=1}^{m}\int_{0}^{\kappa-x} p_i\eta_i\underline{w}'_l e^{\beta_{l,\alpha}(x-\kappa)}e^{(\beta_{l,\alpha}-\eta_i)y'}dy'\\ &+ \frac{\lambda^+}{\lambda}\sum_{l=1}^{m}\int_{0}^{\kappa-x} p_l\eta_l e^{-\eta_l y'}dy'\\ &+ \frac{\lambda^+}{\lambda}\sum_{i=1}^{m}\sum_{l=1}^{\hat{n}}\int_{\kappa-x}^{+\infty} p_i\eta_i\overline{w}'_l e^{\gamma_{l,\alpha}(x-\kappa)}e^{(\gamma_{l,\alpha}-\eta_i)y'}dy'.\end{aligned} \tag{E.17}$$

After some algebra, the OIDE (E.12) yields the following condition

$$\sum_{l=1}^{\hat{m}}\underline{w}_l e^{\beta_{l,\alpha}(x-\kappa)}\left(\Psi'(\beta_{l,\alpha})-\alpha\right) - \sum_{l=1}^{m}\lambda^+ p_l\eta_l e^{\eta_l(x-\kappa)}\left(\sum_{i=1}^{\hat{m}}\frac{\underline{w}_i}{\eta_l-\beta_{i,\alpha}} - \sum_{j=1}^{\hat{n}}\frac{\overline{w}_j}{\eta_l-\gamma_{j,\alpha}} + \frac{1}{\eta_l}\right) = 0, \tag{E.18}$$

for all $l = 1, 2, ..., m$. Using the characteristic equation (E.14), we conclude that the first sum in (E.18) is equal to zero. Therefore, we obtain a system of m linear equations for the coefficients $\{\underline{w}_i\}_{i=1,...,\hat{m}}$ and $\{\overline{w}_j\}_{j=1,...,\hat{n}}$, i.e.,

$$\sum_{i=1}^{\hat{m}}\frac{\underline{w}_i}{\eta_l-\beta_{i,\alpha}} - \sum_{j=1}^{\hat{n}}\frac{\overline{w}_j}{\eta_l-\gamma_{j,\alpha}} = -\frac{1}{\eta_l}, \quad \text{for } l = 1, ..., m. \tag{E.19}$$

Now we study the case $x \geq \kappa$. First, the derivative terms are given by

$$\begin{aligned}\frac{d\tilde{p}}{dx}(x,\alpha) &= \sum_{l=1}^{\hat{n}}\overline{w}'_l\gamma_{l,\alpha}e^{\gamma_{l,\alpha}(x-\kappa-\xi)},\\ \frac{d^2\tilde{p}}{dx^2}(x,\alpha) &= \sum_{l=1}^{\hat{n}}\overline{w}'_l\gamma_{l,\alpha}^2 e^{\gamma_{l,\alpha}(x-\kappa-\xi)}.\end{aligned} \tag{E.20}$$

The integral term can be decomposed as

$$\begin{aligned}\mathscr{I} = &\frac{\lambda^+}{\lambda}\sum_{l=1}^{\hat{n}}\sum_{i=1}^{m}\int_0^{+\infty} p_i\eta_i\overline{w}_l' e^{\gamma_{l,\alpha}(x-\kappa)}e^{(\gamma_{l,\alpha}-\eta_i)y'}dy' \\ &+\frac{\lambda^-}{\lambda}\sum_{j=1}^{n}\int_{-\infty}^{\kappa-x} q_j\theta_j e^{\theta_j y'}dy' \\ &+\frac{\lambda^-}{\lambda}\sum_{l=1}^{\hat{n}}\sum_{j=1}^{n}\int_{\kappa-x}^{0} q_j\theta_j\overline{w}_l' e^{\gamma_{l,\alpha}(x-\kappa)}e^{(\gamma_{l,\alpha}+\theta_j)y'}dy' \\ &+\frac{\lambda^-}{\lambda}\sum_{j=1}^{n}\sum_{l=1}^{\hat{m}}\int_{-\infty}^{\kappa-x} q_j\theta_j\underline{w}_l' e^{\beta_{l,\alpha}(x-\kappa)}e^{(\beta_{l,\alpha}+\theta_j)y'}dy'.\end{aligned} \tag{E.21}$$

Again, after some lengthy calculations we obtain the condition

$$\sum_{l=1}^{\hat{n}}\overline{w}_l e^{\gamma_{l,\alpha}(x-\kappa)}\left(\Psi'(\gamma_{l,\alpha})-\alpha\right)+\sum_{l=1}^{n}\lambda^- q_l\theta_l e^{\theta_l(x-\kappa)}\left(\sum_{i=1}^{\hat{m}}\frac{\underline{w}_i}{\theta_l+\beta_{i,\alpha}}-\sum_{j=1}^{\hat{n}}\frac{\overline{w}_j}{\theta_l+\gamma_{j,\alpha}}+\frac{1}{\theta_l}\right)=0. \tag{E.22}$$

Using the same arguments as in the case $x<\kappa$, we get the following set of conditions:

$$\sum_{i=1}^{\hat{m}}\frac{\underline{w}_i}{\theta_l+\beta_{i,\alpha}}-\sum_{j=1}^{\hat{n}}\frac{\overline{w}_j}{\theta_l+\gamma_{j,\alpha}}=-\frac{1}{\theta_l},\quad \text{for } l=1,...,n. \tag{E.23}$$

To close the system of equations we use the value matching and the smooth pasting conditions at $x=\kappa$:

$$\begin{aligned}\lim_{x\uparrow\kappa}\tilde{p}(x,\alpha)&=\lim_{x\downarrow\kappa}\tilde{p}(x,\alpha),\\ \lim_{x\uparrow\kappa}\frac{d\tilde{p}}{dx}(x,\alpha)&=\lim_{x\downarrow\kappa}\frac{d\tilde{p}}{dx}(x,\alpha).\end{aligned} \tag{E.24}$$

Therefore, we have

$$\begin{aligned}\sum_{i=1}^{\hat{m}}\underline{w}_i-\sum_{j=1}^{\hat{n}}\overline{w}_j&=-1,\\ \sum_{i=1}^{\hat{m}}\beta_{i,\alpha}\underline{w}_i-\sum_{j=1}^{\hat{n}}\gamma_{j,\alpha}\overline{w}_j&=0.\end{aligned} \tag{E.25}$$

After collecting the conditions (E.19), (E.23), and (E.25) we obtain the following system of linear equations:

$$\mathbf{A}\mathbf{w}=\mathbf{a}, \tag{E.26}$$

where

$$\mathbf{w}:=(\underline{w}_1,...,\underline{w}_{\hat{m}},\overline{w}_1,...,\overline{w}_{\hat{n}})' \tag{E.27}$$

is an $(\hat{n}+\hat{m})$-dimensional column vector, and

$$\mathbf{a}:=\left(-1,0,-\frac{1}{\eta_1},...,-\frac{1}{\eta_m},-\frac{1}{\theta_1},...,-\frac{1}{\theta_n}\right)' \tag{E.28}$$

is an $(m+n+2)$-dimensional column vectors. Lastly, the matrix $\mathbf{A}$ is defined as

$$\mathbf{A} := \begin{pmatrix} 1 & \cdots & 1 & -1 & \cdots & -1 \\ \beta_{1,\alpha} & \cdots & \beta_{\hat{m},\alpha} & -\gamma_{1,\alpha} & \cdots & -\gamma_{\hat{n},\alpha} \\ \frac{1}{\eta_1-\beta_{1,\alpha}} & \cdots & \frac{1}{\eta_1-\beta_{\hat{m},\alpha}} & -\frac{1}{\eta_1-\gamma_{1,\alpha}} & \cdots & -\frac{1}{\eta_1-\gamma_{\hat{n},\alpha}} \\ \vdots & \ddots & \vdots & \vdots & \ddots & \vdots \\ \frac{1}{\eta_m-\beta_{1,\alpha}} & \cdots & \frac{1}{\eta_m-\beta_{\hat{m},\alpha}} & -\frac{1}{\eta_m-\gamma_{1,\alpha}} & \cdots & -\frac{1}{\eta_m-\gamma_{\hat{n},\alpha}} \\ \frac{1}{\theta_1+\beta_{1,\alpha}} & \cdots & \frac{1}{\theta_1+\beta_{\hat{m},\alpha}} & -\frac{1}{\theta_1+\gamma_{1,\alpha}} & \cdots & -\frac{1}{\theta_1+\gamma_{\hat{n},\alpha}} \\ \vdots & \ddots & \vdots & \vdots & \ddots & \vdots \\ \frac{1}{\theta_n+\beta_{1,\alpha}} & \cdots & \frac{1}{\theta_n+\beta_{\hat{m},\alpha}} & -\frac{1}{\theta_n+\gamma_{1,\alpha}} & \cdots & -\frac{1}{\theta_n+\gamma_{\hat{n},\alpha}} \end{pmatrix}. \tag{E.29}$$

This concludes the proof. ■

E.3 Proof of Theorem 4.3.2: Canadized one-touch digital put optionettes in D-MEM framework

Following the same line of arguments as in Appendix E.2, we compute the price of the one-touch digital put in Equation (4.23) by solving the PIDE

$$-\frac{\partial P}{\partial \tau}(x,\tau) + \frac{\sigma^2}{2}\frac{\partial^2 P}{\partial x^2}(x,\tau) + \bar{\mu}\frac{\partial P}{\partial x}(x,\tau) + \int_{-\infty}^{+\infty}[P(x+y,\tau) - P(x,\tau)]\nu(y)dy = 0. \tag{E.30}$$

The boundary and initial conditions are: $\lim_{x\uparrow+\infty} P(x,\tau) = 0$, $\lim_{x\downarrow\kappa} P(x,\tau) = 1$, and $\lim_{\tau\downarrow 0} P(x,\tau) = \mathbb{1}_{\{x<\kappa\}}$. Unless otherwise stated, we keep the same notation as in Appendix E.2. The proof is similar to the one provided for Canadized European digital puts. First, we introduce the displaced variable $y \mapsto y' := y - \xi$. In a second step, we apply the LCT. A notable difference is that, due to a path-dependent payoff, we have two different regions in the case of one-touch digital puts: the continuation region ($x > \kappa$) and the stopping region ($x \leq \kappa$).

The LCT of the PIDE (E.30) yields the following OIDE in the continuation region

$$\frac{\sigma^2}{2}\frac{d^2\tilde{P}}{dx^2}(x,\alpha) + \bar{\mu}\frac{d\tilde{P}}{dx}(x,\alpha) - (\lambda+\alpha)\tilde{P}(x,\alpha) + \lambda\int_{-\infty}^{+\infty}\tilde{P}(x+\xi+y',\alpha)f_Y(y')dy' = 0. \tag{E.31}$$

The initial condition is again absorbed into the resulting OIDE. The boundary conditions are given by

$$\begin{aligned} \lim_{x\downarrow\kappa}\tilde{P}(x,\alpha) &= 1, \\ \lim_{x\uparrow+\infty}\tilde{P}(x,\alpha) &= 0. \end{aligned} \tag{E.32}$$

We follow the same steps as in the case of digital puts and introduce the ansatz

$$\tilde{P}(x,\alpha) = \begin{cases} 1 & \text{if } \ x \leq \kappa, \\ \sum_{l=1}^{\hat{n}} v_l' e^{\gamma_{l,\alpha}(x-\kappa-\xi)} & \text{if } \ x > \kappa, \end{cases} \tag{E.33}$$

where $v_l' := v_l e^{\gamma_{l,\alpha}\xi}$, for $l = 1, \cdots, \hat{n}$.

The two derivative terms in (E.31) are

$$\begin{aligned} \frac{d\tilde{P}}{dx}(x,\alpha) &= \sum_{l=1}^{\hat{n}} v_l' \gamma_{l,\alpha} e^{\gamma_{l,\alpha}(x-\kappa-\xi)}, \\ \frac{d^2\tilde{P}}{dx^2}(x,\alpha) &= \sum_{l=1}^{\hat{n}} v_l' \gamma_{l,\alpha}^2 e^{\gamma_{l,\alpha}(x-\kappa-\xi)}. \end{aligned} \tag{E.34}$$

After applying the same change of jump size variable that is applied in the proof for European digital put optionettes, the integral term in equation (E.31) becomes

$$\begin{aligned} \mathscr{J} :&= \int_{-\infty}^{+\infty} \tilde{P}(x+\xi+y',\alpha) f_Y(y') dy' \\ &= \frac{\lambda^+}{\lambda} \sum_{l=1}^{\hat{n}} \sum_{i=1}^{m} \int_0^{+\infty} p_i \eta_i v_l' e^{\gamma_{l,\alpha}(x-\kappa)} e^{(\gamma_{l,\alpha}-\eta_i)y'} dy' \\ &+ \frac{\lambda^-}{\lambda} \sum_{j=1}^{n} \int_{-\infty}^{\kappa-x} q_j \theta_j e^{\theta_j y'} dy' \\ &+ \frac{\lambda^-}{\lambda} \sum_{l=1}^{\hat{n}} \sum_{j=1}^{n} \int_{\kappa-x}^{0} q_j \theta_j v_l' e^{\gamma_{l,\alpha}(x-\kappa)} e^{(\gamma_{l,\alpha}+\theta_j)y'} dy'. \end{aligned} \tag{E.35}$$

Solving the integrals on the r.h.s. gives us the condition

$$\sum_{l=1}^{\hat{n}} v_l e^{\gamma_{l,\alpha}(x-\kappa)} \left(\Psi'(\gamma_{l,\alpha}) - \alpha\right) - \sum_{l=1}^{n} \lambda^- q_l \theta_l e^{\theta_l(\kappa-x)} \left(\sum_{j=1}^{\hat{n}} \frac{v_j}{\theta_l + \gamma_{j,\alpha}} - \frac{1}{\theta_l} \right) = 0. \tag{E.36}$$

Following the same logic as in the previous proof, the following n linear conditions emerge:

$$\sum_{j=1}^{\hat{n}} \frac{v_j}{\theta_l + \gamma_{j,\alpha}} = \frac{1}{\theta_l}, \quad \text{for } l = 1, ..., n. \tag{E.37}$$

We close the system with the value matching condition at the boundary between the exercise and the continuation region, which reads

$$\sum_{j=1}^{\hat{n}} v_j = 1. \tag{E.38}$$

Finally, we collect the conditions (E.37) and (E.38), and obtain the matrix equation

$$\mathbf{B}\mathbf{v} = \mathbf{b}, \tag{E.39}$$

where

$$\mathbf{v} := (v_1, v_2, ..., v_{\hat{n}})' \tag{E.40}$$

is $\hat{n}$-dimensional column vector, and

$$\mathbf{b} := \left(1, \frac{1}{\theta_1}, ..., \frac{1}{\theta_n}\right)' \tag{E.41}$$

is $(n+1)$-dimensional column vectors. Finally, the matrix $\mathbf{B}$ is $(n+1) \times \hat{n}$-dimensional matrix which is given by

$$\mathbf{B} := \begin{pmatrix} 1 & \cdots & 1 \\ \frac{1}{\theta_1+\gamma_{1,\alpha}} & \cdots & \frac{1}{\theta_1+\gamma_{\hat{n},\alpha}} \\ \vdots & \ddots & \vdots \\ \frac{1}{\theta_n+\gamma_{1,\alpha}} & \cdots & \frac{1}{\theta_n+\gamma_{\hat{n},\alpha}} \end{pmatrix}. \tag{E.42}$$

This completes the proof. ■

E.4 Proof of Theorem 4.3.3: First-passage disentanglement of canadized one-touch digital put optionettes in D-MEM framework

We showed in Theorem 4.3.2 that a canadized one-touch digital put optionette solves the OIDE (E.31) with the boundary conditions (E.32). It follows from the Feynman-Kac formula that we can express the price of a canadized one-touch digital put optionette as

$$\tilde{P}(x, \alpha) = \mathbb{E}^x \left[e^{-\alpha(\tau_\kappa - t)} \right], \tag{E.43}$$

where τ_κ is the first-passage time (from above) of the barrier level κ for the log-price process X_t:

$$\tau_\kappa := \inf\{u \geq t : X_u \leq \kappa\}. \tag{E.44}$$

The mathematical formalism of the relationship between the OIDE system (E.31)–(E.32) and the expectation (E.43) can be derived by closely following the proof of Theorem 3.1 in Kou and Wang (2003), pp. 509–512, and Theorem 3.3 in Cai and Kou (2011), p. 2072. Since we are studying the Laplace transform of the first-passage time to a lower boundary, and the aforementioned papers study the Laplace transform of the first-passage time to an upper boundary, the formal proof is omitted in our paper.

Following the notation in Theorem 3 in Leippold and Vasiljević (2017), pp. 81, 93–94, the set $\mathscr{E}_{\mathcal{D}} := \{X_{\tau_\kappa} = \kappa\}$ represents all the possible events of the stopping of the process X_t exactly at the barrier κ, i.e., the stopping due to the diffusion. Similarly, we denote by $\mathscr{E}_{\mathcal{J}} := \{X_{\tau_\kappa} < \kappa\}$ the set of all possible events of the stopping due to overshooting of the barrier level κ by the process X_t, i.e., the stopping due to the jumps. The price of the canadized one-touch digital put optionette given in equation (E.43) can be orthogonally decomposed as

$$\tilde{P}(x,\alpha) = \mathbb{E}^x\left[e^{-\alpha(\tau_\kappa - t)}\mathbb{1}_{\mathscr{E}_{\mathcal{D}}}\right] + \sum_{j=1}^{n}\mathbb{E}^x\left[e^{-\alpha(\tau_\kappa - t)}\mathbb{1}_{\mathscr{E}_{\mathcal{J}}}\right]. \tag{E.45}$$

It will therefore suffice to compute either diffusion or jump contribution, since $\tilde{P}(x,\alpha) = \tilde{P}_D(x,\alpha) + \tilde{P}_J(x,\alpha)$, and the (total) price of a one-touch digital put optionette is given in Theorem 4.3.2.

Following the solution procedure in Appendix E.2 and Appendix E.3, we introduce the substitution $y \mapsto y' := y - \xi$. Subsequently, we apply the LCT. Therefore, to compute, e.g., the diffusion contribution $\tilde{P}_D(x,\alpha)$, we have to solve the OIDE

$$\frac{\sigma^2}{2}\frac{d^2\tilde{P}_D}{dx^2}(x,\alpha) + \bar{\mu}\frac{d\tilde{P}_D}{dx}(x,\alpha) - (\lambda+\alpha)\tilde{P}_D(x,\alpha) + \lambda\int_{-\infty}^{+\infty}\tilde{P}_D(x+y',\alpha)f_Y(y')dy' = 0, \tag{E.46}$$

which is the same as Equation (E.31). The boundary conditions (E.32) remain unchanged as well. However, the diffusion contribution in the interior of the stopping region, i.e., for $x < \kappa$ is zero. This is a consequence of the fact that stopping due to diffusion can happen only at the boundary, i.e., almost surely a diffusion will not generate an overshoot. Therefore, we use the following ansatz:

$$\tilde{P}_D(S_t,\alpha) = \begin{cases} \displaystyle\sum_{j=1}^{\hat{n}}\delta_j\left(\frac{S_t}{K}\right)^{\gamma_{j,\alpha}} & \text{if } S_t > K, \\ 1 & \text{if } S_t = K, \\ 0 & \text{if } S_t \leq K. \end{cases} \tag{E.47}$$

Following the same procedure as in Appendix E.2 and Appendix E.3, we obtain the conditions that summations coefficients $\{\delta_j\}_{j=1,\dots,\hat{n}}$ have to satisfy:

$$\begin{cases} \displaystyle\sum_{j=1}^{\hat{n}}\frac{\delta_j}{\theta_l + \gamma_{j,\alpha}} = 0, & \text{for } l = 1,\dots,n, \\ \displaystyle\sum_{j=1}^{\hat{n}}\delta_j = 1. \end{cases} \tag{E.48}$$

We rewrite these conditions in the matrix form

$$\mathbf{M}_D \boldsymbol{\delta} = \boldsymbol{\epsilon}_D, \tag{E.49}$$

where

$$\boldsymbol{\delta} := (\delta_1, \delta_2, ..., \delta_{\hat{n}})' \tag{E.50}$$

is $\hat{n}$-dimensional column vector, and

$$\boldsymbol{\epsilon}_D := \left(1, \underbrace{0, ..., 0}_{n \text{ times}}\right)' \tag{E.51}$$

is $(n+1)$-dimensional column vectors. The matrix $\mathbf{M}_D$ is $(n+1) \times \hat{n}$-dimensional matrix which is the same as the matrix $\mathbf{B}$, which is given in (E.42).

By analogy, it can be shown the summation coefficients $\{\iota_i\}_{j=1,...,\hat{m}}$ can be computed as the solution of the matrix equation

$$\mathbf{M}_J \boldsymbol{\iota} = \boldsymbol{\epsilon}_J, \tag{E.52}$$

where

$$\boldsymbol{\iota} := (\iota_1, \iota_2, ..., \iota_{\hat{m}})' \tag{E.53}$$

is $\hat{n}$-dimensional column vector, and

$$\boldsymbol{\epsilon}_J := \left(0, \frac{1}{\theta_1}, ..., \frac{1}{\theta_n}\right)' \tag{E.54}$$

is $(n+1)$-dimensional column vectors. The matrix $\mathbf{M}_J$ is $(n+1) \times \hat{n}$-dimensional matrix which is identical to the matrix $\mathbf{M}_D$.

This concludes the proof. ■

Bibliography

Abate, J., W. Whitt. 2006. A unified framework for numerically inverting Laplace transforms. *INFORMS Journal on Computing* **18** 408–421. doi: https://doi.org/10.1287/ijoc.1050.0137

Acerbi, C., D. Tasche. 2002a. On the coherence of expected shortfall. *Journal of Banking & Finance* **26** 1487–1503. doi: https://doi.org/10.1016/S0378-4266(02)00283-2

Acerbi, C., D. Tasche. 2002b. Expected shortfall: A natural coherent alternative to value at risk. *Economic Notes* **26** 379–388. doi: https://doi.org/10.1111/1468-0300.00091

Ait Aoudia, D., J. F. Renaud. 2016. Pricing occupation-time options in a mixed-exponential jump-diffusion model. *Applied Mathematical Finance* **23** 1–21. doi: https://doi.org/10.1080/1350486X.2016.1145066

AitSahlia, F., A. Runnemo. 2007. A canonical optimal stopping problem for American options under a double exponential jump-diffusion model. *Journal of Risk* **10** 85–100.

Aït-Sahalia, Y. 2004. Disentangling diffusion from jumps. *Journal of Financial Economics* **74** 487–528. doi: https://doi.org/10.1016/j.jfineco.2003.09.005

Albrecher, H., D. Kortschak, X. Zhou. 2012. Pricing of Parisian options for a jump-diffusion model with two-sided jumps. *Applied Mathematical Finance* **19** 97–129. doi: https://doi.org/10.1080/1350486X.2011.599976

Alili, L., A. E. Kyprianou. 2005. Some remarks on first passage of Lévy processes, the American put, and pasting principles. *The Annals of Applied Probability* **15** 2062–2080. doi: https://doi.org/10.1214/105051605000000377

Anderluh, J. H. M. 2008. Pricing Parisians and barriers by hitting time simulation. *The European Journal of Finance* **14** 137–156. doi: https://doi.org/10.1080/13518470701705595

Anderluh, J. H. M., J. A. M. van der Weide. 2009. Double-sided Parisian option pricing. *Finance and Stochastics* **13** 205–238. doi: https://doi.org/10.1007/s00780-009-0090-3

Andrews, D. 1991. Heteroskedasticity and autocorrelation consistent covariance matrix estimation. *Econometrica* **59** 817–858. doi: https://doi.org/10.2307/2938229

Artzner, P., F. Delbaen, J. M. Eber, D. Heath. 1999. Coherent measures of risk. *Mathematical Finance* **9** 203–228. doi: https://doi.org/10.1111/1467-9965.00068

Asmussen, S., D. Madan, M. Pistorius. 2007. Pricing equity default swaps under an approximation to the CGMY Lévy model. *Journal of Computational Finance* **11** 79–93.

Avellaneda, M., L. Wu. 1999. Pricing Parisian-style options with a lattice method. *International Journal of Theoretical and Applied Finance* **2** 1–16. doi: https://doi.org/10.1142/S0219024999000029

Avram, F., T. Chan, M. Usabel. 2002. On the valuation of constant barrier options under spectrally one-sided exponential Lévy models and Carr's approximation for American puts. *Stochastic Processes and their Applications* **100** 75–107. doi: https://doi.org/10.1016/S0304-4149(02)00104-7

Bakshi, G., G. Panayotov. 2010. First-passage probability, jump models, and intra-horizon risk. *Journal of Financial Economics* **95** 20–40. doi: https://doi.org/10.1016/j.jfineco.2009.01.003

Barone-Adesi, G., R. E. Whaley. 1987. Efficient analytic approximation of American option values. *The Journal of Finance* **42** 301–320. doi: https://doi.org/10.1111/j.1540-6261.1987.tb02569.x

Barone-Adesi, G., K. Giannopoulos, L. Vosper. 1999. VaR without correlations for portfolios of derivative securities. *Journal of Futures Markets* **19** 583–602.doi: https://doi.org/10.1002/(SICI)1096-9934(199908)19:5%3C583::AID-FUT5%3E3.0.CO;2-S

Barone-Adesi, G., R. F. Engle, L. Mancini. 2008. A GARCH option pricing model with filtered historical simulation. *Review of Financial Studies* **21** 1223–1258. doi: https://doi.org/10.1093/rfs/hhn031

Bayraktar, E., H. Xing. 2009. Pricing American options for jump diffusions by iterating optimal stopping problems for diffusions. *Mathematical Methods of Operations Research* **70** 505–525. doi: https://doi.org/10.1007/s00186-008-0282-1

Bayraktar, E., H. Xing. 2011. Pricing Asian options for jump diffusion. *Mathematical Finance* **21** 117–143. doi: https://doi.org/10.1111/j.1467-9965.2010.00426.x

Bernard, C., O. Le Courtois, F. Quitard-Pinon. 2005. A new procedure for pricing Parisian options. *The Journal of Derivatives* **12** 45–54. doi: https://doi.org/10.3905/jod.2005.517185

Bartholomew, D. J. 1969. Sufficient conditions for a mixture of exponentials to be a probability density function. *The Annals of Mathematical Statistics* **40** 2183–2188. Stable URL: http://www.jstor.org/stable/2239531

Bhattacharyya, M., N. Misra, B. Kodase. 2009. MaxVaR for non-normal and heteroskedastic returns. *Quantitative Finance* **9** 925–935. doi: https://doi.org/10.1080/14697680802595684

Black, F., M. S. Scholes. 1973. The pricing of options and corporate liabilities. *Journal of Political Economy* **81** 637–654. doi: https://doi.org/10.1086/260062

Botta, R. F., C. M. Harris. 1986. Approximation with generalized hyperexponential distributions: Weak convergence results.*Queueing Systems* **1** 169–190. doi: https://doi.org/10.1007/BF01536187

Boudoukh, J., M. Richardson, R. Stanton, R. F. Whitelaw. 2004. MaxVaR: Long-horizon value at risk in a mark-to-market environment. *Journal of Investment Management* **2** 1–6.

Boyarcheko, M., S. Boyarchenko. 2011. Double barrier options in regime-switching hyper-exponential jump-diffusion models. *International Journal of Theoretical and Applied Finance* **14** 1005–1043. doi: https://doi.org/10.1142/S0219024911006620

Boyarchenko, S. I., S. Z. Levendorskiĭ. 2000. Option pricing for Truncated Lévy processes. *International Journal of Theoretical and Applied Finance* **3** 549–552. doi: https://doi.org/10.1142/S0219024900000541

Boyarchenko, S. I., S. Z. Levendorskiĭ. 2002. Non-Gaussian Merton-Black-Scholes theory. Vol. 9. Singapore: World Scientific.

Breeden, D. T., R. H. Litzenberger. 1978. Prices of state-contingent claims implicit in option prices. *Journal of Business* **51** 621–651. Stable URL: http://www.jstor.org/stable/2352653

Broadie, M., J. B. Detemple. 2004. Option pricing: Valuation models and applications. *Management Science* **50** 1145–1177. doi: https://doi.org/10.1287/mnsc.1040.0275

Burnham, K.P., D. R. Anderson. 2002. Model selection and multimodel inference: A practical information-theoretic approach. Springer.

Cai, N. 2009. On first passage times of a hyper-exponential jump diffusion process. *Operations Research Letters* **37** 127–134. doi: https://doi.org/10.1016/j.orl.2009.01.002

Cai, N., N. Chen, X. Wan. 2009. Pricing double-barrier options under a flexible jump diffusion model. *Operations Research Letters* **37** 163–167. doi: https://doi.org/10.1016/j.orl.2009.02.006

Cai, N., N. Chen, X. Wan. 2010. Occupation times of jump-diffusion processes with double-exponential jumps and the pricing of options. *Mathematics of Operations Research* **35** 412–437. doi: https://doi.org/10.1287/moor.1100.0447

Cai, N. 2011. Pricing and hedging of quantile options in a flexible jump diffusion model. *Journal of Applied Probability* **48** 637–656. doi: https://doi.org/10.1239/jap/1316796904

Cai, N., S. Kou. 2011. Option pricing under a mixed-exponential jump diffusion model. *Management Science* **57** 2067–2081. doi: https://doi.org/10.1287/mnsc.1110.1393

Cai, N., S. Kou. 2012. Pricing Asian options under a hyper-exponential jump-diffusion model. *Operations Research* **60** 64–77. doi: https://doi.org/10.1287/opre.1110.1006

Cai, N., L. Sun. 2014. Valuation of stock loans with jump risk. *Journal of Economic Dynamics & Control* **40** 213–241. doi: https://doi.org/10.1016/j.jedc.2014.01.004

Carr, P., R. Jarrow, R. Myneni. 1992. Alternative characterizations of American put options. *Mathematical Finance* **2** 87–106. doi: https://doi.org/10.1111/j.1467-9965.1992.tb00040.x

Carr, P., M. Chesney. 1996. American put call symmetry. *HEC Preprint* **70** 85–112.

Carr, P. 1998. Randomization and the American put. *The Review of Financial Studies* **11** 597–626. doi: https://doi.org/10.1093/rfs/11.3.597

Carr, P., H. Geman, D. B. Madan, M. Yor. 2002. The fine structure of asset returns: An empirical investigation. *Journal of Business* **75** 305–332. doi: https://doi.org/10.1086/338705

Carr, P., L. Wu. 2003. The finite moment log stable process and option pricing. *The Journal of Finance* **58** 753–778. doi: https://doi.org/10.1111/1540-6261.00544

Carr, P., L. Wu. 2004. Time-changed Lévy processes and option pricing. *Journal of Financial Economics* **71** 113–141. doi: https://doi.org/10.1016/S0304-405X(03)00171-5

Chan, T. 1999. Pricing contingent claims on stocks driven by Lévy processes. *Annals of Applied Probability* **9** 504–528. Stable URL: http://www.jstor.org/stable/2667343

Chesney, M., M. Jeanblanc, M. Yor. 1997. Brownian excursions and Parisian barrier options. *Advances in Applied Probability* **29**, 165–184. doi: https://doi.org/10.2307/1427865

Chesney, M., J. Cornwall, M. Jeanblanc, G. Kentwall, M. Yor. 1997. Parisian pricing. Risk **10** 77–79.

Chesney, M., R. Gibson. 1999. The investment policy and the pricing of equity in a levered ÂŽfirm: A re-examination of the 'contingent claims' valuation approach. *The European Journal of Finance*. **5**, 95–107. doi: http://dx.doi.org/10.1080/135184799337118

Chesney, M., R. Gibson. 2001. Reducing asset substitution with warrant and convertible debt issue. *The Journal of Derivatives*. **9**, 39–52. doi: https://doi.org/10.3905/jod.2001.319168

Chesney, M., M. Jeanblanc. 2004. Pricing American currency options in an exponential Lévy model. *Applied Mathematical Finance* **3** 207–225. doi: https://doi.org/10.1080/1350486042000249336

Chesney, M., L. Gauthier. 2006. American Parisian options. *Finance and Stochastics*. **10** 475–506. doi: https://doi.org/10.1007/s00780-006-0015-3

Chiarella, C., A. Ziogas. 2009. American call options under jump-diffusion processes - A Fourier transform approach. *Applied Mathematical Finance* **16** 37–79. doi: https://doi.org/10.1080/13504860802221672

Choudhury, G. L., D. M. Lucantoni, W. Whitt. 1997. Numerical solution of piecewise-stationary $M_t/G_t/1$ queues. *Operations Research* **45** 451–463. doi: https://doi.org/10.1287/opre.45.3.451

Christoffersen, P., 1998. Evaluating interval forecasts. *International Economic Review* **39** 841–862. doi: https://doi.org/10.2307/2527341

Christoffersen, P., K. Jacobs, B. Y. Chang. 2013. Forecasting with option-implied information. *Handbook of Economic Forecasting* Vol. 2A 581–656. Elsevier.

Cont, R., P. Tankov. 2004. Non-parametric calibration of jump-diffusion option pricing models. *Journal of Computational Finance* **7** 1–50.

Costabile, M. 2002. A combinatorial approach for pricing Parisian options. *Decisions in Economics and Finance***25** 111–125. doi: https://doi.org/10.1007/s102030200007

Czarna, I., Z. Palmowski. 2011. Ruin probability with Parisian delay for a spectrally negative Lévy risk process. *Journal of Applied Probability*. **48** 984–1002. doi: https://doi.org/10.1239/jap/1324046014

Crosby, J., N. Le Saux, A. Mijatović. 2010. Approximating Lévy processes with a view to option prices. *International Journal of Theoretical and Applied Finance* **13** 63–91. doi: https://doi.org/10.1142/S0219024910005681

Dassios, A., S. Wu. 2010. Perturbed Brownian motion and its application to Parisian option pricing. *Finance and Stochastics*. **14** 473–494. doi: https://doi.org/10.1007/s00780-009-0113-0

Dassios, A., S. Wu. 2011. Double-barrier Parisian Options. *Journal of Applied Probability*. **48** 1–20. doi: https://doi.org/10.1239/jap/1300198132

Dassios, A., J. W. Lim. 2013. Parisian option pricing: A recursive solution for the density of the Parisian stopping time. *SIAM Journal of Financial Mathematics*. **4** 599–615. doi: https://doi.org/10.1137/120875466

Detemple, J. 2005. American-style derivatives: Valuation and computation. CRC Press.

Diebold, F., R. S. Mariano. 1995. Comparing predictive accuracy. *Journal of Business and Economic Statistics*. **13** 253–265.doi: https://doi.org/10.1198/073500102753410444

Duffie, D., J. Pan. 1997. An overview of value at risk. *The Journal of Derivatives* **4** 7–49. doi: https://doi.org/10.3905/jod.1997.407971

Eberlein, E., U. Keller. 1995. Hyperbolic distributions in finance. *Bernoulli* **1** 281–299. doi: https://doi.org/10.3150/bj/1193667819

Esscher, F. 1932. On the probability function in the collective theory of risk. *Skandinavisk Aktuarietidskrift* **15** 175–195.

Fabozzi, F. J., A. Leccadito, R. S. Tunaru. 2014. Extracting market information from equity options with exponential Lévy processes. *Journal of Economic Dynamics & Control* **38** 125–141. doi: https://doi.org/10.1016/j.jedc.2013.10.001

Fang, F., C. W. Oosterlee. 2008. A novel pricing method for European options based on Fourier-cosine series expansions. *SIAM Journal of Scientific Computating* **31** 826–848. doi: https://doi.org/10.1137/080718061

Fang, F., C. W. Oosterlee. 2009. Pricing early-exercise and discrete barrier options by Fourier-cosine series expansions. *Numerische Mathematik* **114** 27–62. doi: https://doi.org/10.1007/s00211-009-0252-4

Fuh, C.-D., S.-F. Luo, J.-F. Yen. 2013. Pricing discrete path-dependent options under a double exponential jump-diffusion model. *Journal of Banking & Finance* **37** 2702–2713. doi: https://doi.org/10.1016/j.jbankfin.2013.03.023

Fujita, T., R. Miura. 2002. Edokko options: A new framework for barrier options. *Asia-Pacific Financial Markets*. **9** 141–151. doi: https://doi.org/10.1023/A:1022294204470

Gaver, D. P. Jr. 1966. Observing stochastic processes, and approximate transform inversion. *Operations Research* **15** 444–459. doi: https://doi.org/10.1287/opre.14.3.444

Gerber, H. U., E. S. W. Shiu. 1994. Option prices by Esscher transforms. *Transactions of Society of Actuaries* **46** 99–191.

Haber, R. J., P. J. Schönbucher, P. Wilmott. 1999. Pricing Parisian options. *The Journal of Derivatives* **6** 71–79. doi: https://doi.org/10.3905/jod.1999.319120

Hackmann, D., A. Kuznetsov. 2016. Approximating Lévy processes with completely monotone jumps. *Annals of Applied Probability* **26** 328–359. Permanent link: https://projecteuclid.org/euclid.aoap/1452003241

Hellmich, M., S. Kassberger, W. M. Schmidt. 2013. Credit modeling under jump-diffusion with exponentially distributed jumps — Stable calibration, dynamics and gap risk. *International Journal of Theoretical and Applied Finance* **16** 1–26.doi: https://doi.org/10.1142/S0219024913500210

Hofer, M., P. Mayer. 2013. Pricing and hedging of lookback options in hyper-exponential jump-diffusion model. *Applied Mathematical Finance* **20** 489–511. doi: https://doi.org/10.1080/1350486X.2013.774985

Hubalek, F., C. Sgarra. 2006. Esscher transforms and the minimal entropy martingale measure for exponential Lévy models. *Quantitative Finance* **6** 125–145. doi: https://doi.org/10.1080/14697680600573099

Huber, P. J. Robust Statistics. Hoboken, NJ: John Wiley & Sons, Inc., 1981.

Hugonnier, J. 1999. The Feynman-Kac formula and pricing occupation time derivatives. *International Journal of Theoretical and Applied Finance* **2** 153–178.doi:https://doi.org/10.1142/S021902499900011X

Jacka, S. D. 1991. Optimal stopping and the American put. *Mathematical Finance* **1** 1–14. doi: https://doi.org/10.1111/j.1467-9965.1991.tb00007.x

Jackson, K. R., S. Jaimungal, V. Surkov. 2008. Fourier space time-stepping for option pricing with Lévy models. *Journal of Computational Finance* **12** 1–29.

Jeanblanc, M., M. Yor, M. Chesney. 2009. Mathematical methods for financial markets. Springer.

Jeannin, M., M. Pistorius. 2010. A transform approach to compute prices and Greeks of barrier options driven by a class of Lévy processes. *Quantitative Finance* **10** 629–644. doi: http://dx.doi.org/10.1080/14697680902896057

Kim, I. J. 1990. The analytic valuation of American options. *Review of Financial Studies* **3** 547–572.doi: https://doi.org/10.1093/rfs/3.4.547

Kimura, T. 2010. Alternative randomization for valuing American options. *Asia-Pacific Journal of Operational Research* **27** 167–187. doi: https://doi.org/10.1142/S0217595910002624

Koponen, I. 1995. Analytic approach to the problem of convergence of truncated Lévy flights towards the Gaussian stochastic process. *Physical Review E* **52** 1197–1199. doi: https://doi.org/10.1103/PhysRevE.52.1197

Kou, S. G. 2002. A jump-diffusion model for option pricing. *Management Science* **48** 1086–1101. doi: https://doi.org/10.1287/mnsc.48.8.1086.166

Kou, S. G., H. Wang. 2003. First passage times of a jump diffusion process. *Advances in Applied Probability* **35** 504–531. doi: https://doi.org/10.1239/aap/1051201658

Kou, S. G., H. Wang. 2004. Option pricing under a double exponential jump diffusion model. *Management Science* **35** 1178–1192.doi: https://doi.org/10.1287/mnsc.1030.0163

Kou, S. G., G. Petrella, H. Wang. 2005. Pricing path-dependent options with jump risk via Laplace transforms. *The Kyoto Economic Review* **74** 1–23. doi: https://doi.org/10.11179/ker.74.1

Kritzman, M., D. Rich. 2002. The mismeasurement of risk. *Financial Analysts Journal* **58** 91–99. doi: https://doi.org/10.2469/faj.v58.n3.2541

Kupiec, P. H., 1995. Techniques for verifying the accuracy of risk measurement models. *The Journal of Derivatives* **3** 73–84. doi: https://doi.org/10.3905/jod.1995.407942

Kuznetsov, A. 2013. On the convergence of the Gaver-Stehfest algorithm. *SIAM Journal of Numerical Analysis* **51** 2984–2998. doi: https://doi.org/10.1137/13091974X

Labart, C., J. Lelong. 2009. Pricing double Parisian options using Laplace tranforms. *International Journal of Theoretical and Applied Finance* **12** 19–44. doi: https://doi.org/10.1142/S0219024909005154

Landriault, D., J.-F. Renaud, X. Zhou. 2011. Occupation times of spectrally negative Lévy processes with applications. *Stochastic Processes and their Applications* **121** 2629–2641. doi: https://doi.org/10.1016/j.spa.2011.07.008

Latané, H. A., R. J. Rendleman. 1976. Standard deviations of stock price ratios implied in option prices. *The Journal of Finance* **31** 369–381. doi: https://doi.org/10.1111/j.1540-6261.1976.tb01892.x

Leippold, M., N. Vasiljević. 2017. Pricing and disentanglement of American puts in the hyper-exponential jump-diffusion model. *Journal of Banking & Finance* **77** 78–94. doi: https://doi.org/10.1016/j.jbankfin.2017.01.014

Levendorskiĭ, S. Z. 2004a. Pricing of the American put under Lévy processes. *International Journal of Theoretical and Applied Finance* **7** 303–335. doi: https://doi.org/10.1142/S0219024904002463

Levendorskiĭ, S. Z. 2004b. Early exercise boundary and option prices in Lévy driven models. *Quantitative Finance* **4** 525–547.doi: https://doi.org/10.1080/14697680400023295

Li, B. Q., H. J. Zhao. 2009. Pricing Parisian options by generating functions. *The Journal of Derivatives* **16** 72–81. doi: https://doi.org/10.3905/JOD.2009.16.4.072

Lindström, E., J. Ströjby, M. Brodén, M. Wiktorsson, J. Holst. 2008. Sequential calibration of options. *Computational Statistics & Data Analysis* **52** 2877–2891. doi: https://doi.org/10.1016/j.csda.2007.08.009

Lipton, A. 2002. Assets with jumps. *Risk* **15** 149–153.

Loeffen, R. L., J.-F. Renaud, X. Zhou. 2014. Occupation times of intervals until first passage times for spectrally negative Lévy processes. *Stochastic Processes and their Applications* **124** 1408–1435. doi: https://doi.org/10.1016/j.spa.2013.11.005

Lord, R., F. Fang, F. Bervoets, C. W. Oosterlee. 2008. A fast and accurate FFT-based method for pricing early-exercise options under Lévy processes. *SIAM Journal of Scientific Computating* **30** 1678–1705. doi: https://doi.org/10.1137/070683878

Madan, D. B., E. Seneta. 1990. The variance gamma (V.G.) model for share market returns. *Journal of Business* **63** 511–524. Stable URL: www.jstor.org/stable/2353303

Merton, R. C. 1976. Option pricing when underlying stock returns are discontinuous. *Journal of Financial Economics* **3** 125–144. doi: https://doi.org/10.1016/0304-405X(76)90022-2

Milne, F., D. B. Madan. 1991. Option pricing with V.G. martingale components. *Mathematical Finance* **1** 39–55. doi: https://doi.org/10.1111/j.1467-9965.1991.tb00018.x

Miyahara, Y. 1999. Minimal entropy martingale measures of jump type price processes in incomplete assets markets. *Asia-Pacific Financial Markets* **6** 97–113. doi: https://doi.org/10.1023/A:1010062625672

Monfort, A., F. Pegoraro. 2012. Asset pricing with second-order Esscher transforms. *Journal of Banking & Finance* **36** 1678–1687. doi: https://doi.org/10.1016/j.jbankfin.2012.01.014

Mordecki, E. 2002. Optimal stopping and perpetual options for Lévy processes. *Finance and Stochastics* **6** 473–493. doi: https://doi.org/10.1007/s007800200070

Ramezani, C. A., Y. Zeng. 2007. Maximum likelihood estimation of the double exponential jump-diffusion process. *Annals of Finance* **3** 487–507.doi: https://doi.org/10.1007/s10436-006-0062-y

Rockafellar, R. T., S. Uryasev. 2002. Conditional value-at-risk for general loss distributions. *Journal of Banking & Finance* **26** 1443–1471. doi: https://doi.org/10.1016/S0378-4266(02)00271-6

Rossello, D. 2008. MaxVaR with non-Gaussian distributed returns. *European Journal of Operational Research* **189** 159–171. doi: https://doi.org/10.1016/j.ejor.2007.05.021

Sato, K.-I. 1999. *Lévy processes and infinitely divisible distributions*. Cambridge Studies in Advanced Mathematics Vol. 68 (Cambridge University Press).

Schroder, M. 1999. Changes of numeraire for pricing futures, forwards, and options. *The Review of Financial Studies* **12** 1143–1163. doi: https://doi.org/10.1093/rfs/12.5.1143

Schröder, M. 2003. Brownian excursions and Parisian barrier options: A note. *Journal of Applied Probability* **40** 855–864. doi: https://doi.org/10.1239/jap/1067436086

Sepp, A. 2004. Analytical pricing of double-barrier options under a double-exponential jump diffusion process — Applications of Laplace transform. *International Journal of Theoretical and Applied Finance* **7** 151–175. doi: https://doi.org/10.1142/S0219024904002402

Sepp, A. 2012. An Approximate distribution of delta-hedging Errors in a jump-diffusion model with discrete trading and transaction costs. *Quantitative Finance* **12** 1119–1141. doi: https://doi.org/10.1080/14697688.2010.494613

Stehfest, H. 1970. Algorithm 368: Numerical inversion of Laplace transforms. *Communications of the ACM* **13** 47–49. doi: https://doi.org/10.1145/361953.361969

Steutel, F. W. 1967. Note on the infinite divisibility of exponential mixtures. *The Annals of Mathematical Statistics* **38** 1303–1305. Stable URL: http://www.jstor.org/stable/2238856

Stulz, R. 1996. Rethinking risk management. *Journal of Applied Corporate Finance* **9** 8–24. doi: https://doi.org/10.1111/j.1745-6622.1996.tb00295.x

Thul, M., A. Q. Zhang. 2014. Analytical option pricing under an asymmetrically displaced double gamma jump-diffusion model. 26th Australasian Finance and Banking Conference 2013. Available at SSRN. doi: https://dx.doi.org/10.2139/ssrn.2311673

Toivanen, J. 2008. Numerical valuation of European and American options under Kou's jump-diffusion model. *SIAM Journal of Scientific Computing* **30** 1949–1970. doi: https://doi.org/10.1137/060674697

Valkó, P. P., J. Abate. 2004. Comparison of sequence accelerators for the Gaver method of numerical Laplace transform inversion. *Computers and Mathematics with Applications* **48** 629–636. doi: https://doi.org/10.1016/j.camwa.2002.10.017

Vetzal, K. R., P. A. Forsyth. 1999. Discrete Parisian and delayed barrier options: A general numerical approach. *Advances in Futures and Options Research* **10** 1–16.

Vuong, Q. H. 1989. Likelihood ratio tests for model selection and non-nested hypotheses. *Econometrica* **57** 307–333. doi: https://doi.org/10.2307/1912557

Wong, H. Y., K. Y. Lau. 2008. Analytical valuation of turbo warrants under double exponential jump diffusion. *The Journal of Derivatives* **9** 61–73. doi: https://doi.org/10.3905/jod.2008.707211

Wu, L. 2006. Dampened power law: Reconciling the tail behavior of financial security returns. *The Journal of Business* **79** 1445–1473. doi: https://doi.org/10.1086/500681

Wu, L., J. Zhou. 2016. Occupation times of hyper-exponential jump diffusion processes with application to price step options. *Journal of Computational and Applied Mathematics* **294** 251–274. doi: https://doi.org/10.1016/j.cam.2015.09.001

Yin, C., Y. Shen, Y. Wen. 2013. Exit problems for jump processes with applications to dividend problems. *Journal of Computational and Applied Mathematics* **245** 30–52. doi: https://doi.org/10.1016/j.cam.2012.12.004

Zhu, Z., N. Stokes. 1998. A finite element platform for pricing path dependent exotic options. CSIRO Working Paper.

Zhu, S.-P., W.-T. Chen. 2013. Pricing Parisian and *Parasian* options analytically. *Journal of Economic Dynamics and Control* **37** 875–896. doi: https://doi.org/10.1016/j.jedc.2012.12.005

Zhu, S.–P., N.–T. Le, W. Chen, X. Lu. 2015. Pricing Parisian down-and-in options. *Applied Mathematics Letters* **43** 15–24. doi: https://doi.org/10.1016/j.aml.2014.10.019

Nikola Vasiljević

Curriculum Vitae

Personal Information

Date of Birth: 14 November 1983
Nationality: Serbian

Education

University of Zurich and Swiss Finance Institute — Zurich, Switzerland
Ph.D. Studies in Finance (*summa cum laude*) — 09/2010 – 07/2016

- *Dissertation*: "Option pricing and market risk management in the presence of jump risk".
- *Committee*: Markus Leippold (advisor), Marc Chesney, Walter Farkas, Loriano Mancini.

University of Belgrade, Faculty of Economics — Belgrade, Serbia
M.Sc. in Quantitative Finance (*summa cum laude*) — 10/2008 – 06/2011

- *Thesis*: "Jump fears make volatility smiles".
- *Advisor*: Branko Urošević.
- National Bank of Serbia 2011 Award for the Best Master's Thesis.

University of Belgrade, Faculty of Physics — Belgrade, Serbia
M.Sc. in Theoretical Physics (*summa cum laude*) — 10/2002 – 06/2008

- *Thesis*: "Thallium detectors of solar neutrinos".
- *Advisor*: Ivan Aničin.
- CERN Summer School and Internship (ECAL, CMS) — Geneva, Switzerland, 06/2008 – 08/2008

Professional Experience

Credit Suisse, International Wealth Management — Zurich, Switzerland
Investment Strategist – Quantitative Analyst (Assistant Vice President) — 03/2016 – Present

Credit Suisse, International Wealth Management — Zurich, Switzerland
Investment Strategist – Quantitative Analyst (part-time position) — 05/2013 – 02/2016

University of Zurich, Department of Banking and Finance — Zurich, Switzerland
Research and Teaching Assistant — 10/2011 – 02/2016

Unicredit Bank, Controlling and Market Risk — Belgrade, Serbia
Quantitative Analyst — 03/2010 – 08/2010